Effects of the neurotrophic factors CNTF and IGF-1 in mouse models for spinal muscular atrophy and diabetic neuropathy

Effekte der neurotrophen Faktoren CNTF und IGF-1 in Mausmodellen für spinale Muskelatrophie und diabetische Neuropathie

Doctoral thesis for a doctoral degree at the Graduate School of Life Sciences, Julius-Maximilians-Universität Würzburg, Neuroscience Section

submitted by

Christian Marc Simon

from

Hanau, Germany

Würzburg, 2011

Submitted on: ……..……..

Office stamp

Members of the *Promotionskomitee*:

Chairperson: Professor Dr. Wolfgang Rössler

Primary Supervisor: Professor Dr. Michael Sendtner

Supervisor (Second): Professor Dr. Rudolf Martini

Supervisor (Third): Professor Dr. Erich Buchner

Date of Public Defense: ……..……

Date of Receipt of Certificates: ……..

Für Jenny, meine Eltern, Freunde und Roger

Table of contents

Summary

In this study I investigate the role of Schwann cell and axon-derived trophic signals as modifiers of axonal integrity and sprouting in motoneuron disease and diabetic neuropathy (DNP). The first part of this thesis focuses on the role of the Schwann-cell-derived ciliary neurotrophic factor (CNTF) for compensatory sprouting in a mouse model for mild spinal muscular atrophy (SMA). In the second part, the role of the insulin-like growth factor 1 (IGF-1) and its binding protein 5 (IGFBP-5) is examined in the peripheral nerves of patients with DNP and in two corresponding mouse models.

Proximal SMA is caused by homozygous loss or mutation of the *SMN1* gene on human chromosome 5. The different forms of SMA can be divided into four groups, depending on the levels of SMN protein produced from a second *SMN* gene (*SMN2*) and the severity of the disease. Patients with milder forms of the disease, type III and type IV SMA, normally reach adulthood and regularly show enlargement of motor units, signifying the reinnervation of denervated muscle fibers. However, the underlying mechanisms are not understood. $Smn^{+/-}$ mice, a model of type III/IV SMA, are phenotypically normal, but they reveal progressive loss of motor neurons and denervation of motor endplates starting at 4 weeks of age. The progressive loss of spinal motor neurons reaches 50% at 12 months but muscle strength is not reduced. The first evidence for axonal sprouting as a compensatory mechanism in these animals was the more than 2-fold increase in amplitude of single motor unit action potentials (SMUAP) in the gastrocnemius muscle. Confocal analysis confirmed pronounced sprouting of innervating motor axons. As CNTF is highly expressed in Schwann cells and known to be involved in sprouting, its role for this compensatory sprouting response and the maintenance of muscle strength in $Smn^{+/-}$ mice was investigated. Deletion of CNTF in this mouse model results in reduced sprouting and decline of muscle strength in $Smn^{+/-}$ $Cntf^{/-}$ mice. These findings indicate that CNTF is necessary for a sprouting response and thus enhances the size of motor units in skeletal muscles of $Smn^{+/-}$ mice.

DNP afflicting motor and sensory nerve fibers is a major complication in diabetes mellitus. The underlying cellular mechanisms of motor axon degeneration are poorly understood. IGFBP-5, an inhibitory binding protein for IGF-1, is highly upregulated in peripheral nerves in patients with DNP. The study investigates the pathogenic relevance of this finding in transgenic mice overexpressing IGFBP-5 in motor axons. These mice develop motor axonopathy similar to that seen in DNP. Motor axon degeneration is also observed in mice in which the IGF-1 receptor (IGF-1R) was conditionally depleted in motoneurons, indicating that reduced activity of IGF-1 on IGF-1R in motoneurons is responsible for the observed

effect. These data provide evidence that elevated expression of IGFBP-5 in diabetic nerves reduces the availability of IGF-1 for IGF-1R on motor axons leading to progressive neurodegeneration, and thus offers novel treatment strategies.

Zusammenfassung

In dieser Arbeit habe ich die Rolle der neurotrophen Faktoren Ciliary neurotrophic factor (CNTF) und Insulin-like-growth factor 1 (IGF-1), die in Schwannzellen gebildet werden, als Modulatoren der axonalen Integrität bei einer degenerativen Motoneuronenerkrankung und bei diabetischer Neuropathie (DNP) untersucht. Im ersten Teil dieser Arbeit wird gezeigt, dass CNTF für ein kompensatorisches Sprouting von motorischen Axonen in einem Mausmodell für spinale Muskelatrophie (SMA) verantwortlich ist. Im zweiten Teil wird die Rolle von IGF-1 und dessen Bindeprotein, IGFBP-5, in Axonen motorischer Nerven bei Patienten mit DNP und zwei korrespondieren Mausmodellen gezeigt.

Die proximale SMA wird durch einen homozygoten Verlust oder Mutation des *SMN1* Gens auf dem Chromosom 5 verursacht. Bei der spinalen Muskelatrophie unterscheidet man verschiedene Schweregrade, abhängig von der Menge an SMN Protein, das vom zweiten *SMN* Gen (*SMN2*) produziert werden kann. Patienten mit einer milderen Form von SMA (Typ III und IV) erreichen das Erwachsenenalter und zeigen oft vergrößerte motorische Einheiten, im Gegensatz zu Patienten mit den schweren kindlichen Formen der Erkrankung. $Smn^{+/-}$ Mäuse, ein Modell für die leichten SMA Formen Typ II und IV, zeigen denervierte Endplatten bereits 4 Wochen nach der Geburt und einen fortschreitenden Verlust von Motoneuronen, der nach 12 Monaten mehr als 50% beträgt, ohne dass sich die Muskelkraft der Tiere verringert. Die Amplitude der Summenpotenziale von einzelnen motorischen Einheiten (Single motor unit action potential, SMUAP) im Wadenmuskel ist mehr als 2-fach erhöht. Konfokale Aufnahmen bestätigen ausgeprägtes Sprouting der noch innervierenden Axone. $Smn^{+/-}$ Mäuse ohne CNTF, das normalerweise stark in Schwann-Zellen exprimiert ist, zeigen reduziertes Sprouting und verringerte Muskelkraft. Diese Ergebnisse sprechen dafür, dass CNTF für das Sprouting und die vergrößerten motorischen Einheiten in $Smn^{+/-}$ Mäusen verantwortlich ist. Dieser kompensatorische Mechanismus könnte neue Behandlungs-möglichkeiten für Motoneuronerkrankungen eröffnen.

Die Diabetische Neuropathie (DNP), eine der Hauptkomplikationen bei Diabetes Mellitus, betrifft sowohl motorische als auch sensorische Nervenfasern. Die zugrunde liegenden zellulären Mechanismen, die zur Degeneration motorischer Axone in Spätstadien der Erkrankung führen, sind größtenteils noch ungeklärt. IGFBP-5, ein IGF-1 hemmendes Bindeprotein, ist in peripheren Nervbiopsien von DNP Patienten stark überexprimiert. Diese potenzielle pathogene Relevanz wurde bei IGFBP-5 überexprimierenden transgenen Mäusen untersucht. Diese Mäuse entwickeln ähnlich wie die DNP Patienten eine motorische Axonopathie. Diese Axondegeneration zeigen auch Mäuse, bei denen der IGF-1 Rezeptor

(IGF-1R) neuronenspezifisch ausgeschaltet wurde. Das bedeutet, dass reduzierte Wirkung von IGF-1 am IGF-1R auf Axonen von Motoneuronen für die beobachtete Axonopathie verantwortlich ist. Zusammenfassend zeigen diese Daten, dass erhöhtes IGFBP-5 in diabetischen Nerven die Verfügbarkeit von IGF-1 für den IGF-1R reduziert und zu progressiver Neurodegeneration führt. Diese Erkenntnis könnte neue Behandlungsstrategien für Patienten mit DNP eröffnen.

1 Introduction

One of the most important evolutionary steps during the formation of the nervous system was the development of the motor system. This allows interactions with other organisms and the peripheral environment by accomplishing voluntary, involuntary and complex locomotions (e.g. hunting). The current positions of objects as well as environmental changes are recognized by the sensory system. This includes sensory neurons whose cell bodies are located in ganglia outside of the brain and spinal cord and therefore count as part of the peripheral nervous system (PNS). Sensory neurons convey different external sensory inputs (e.g. pain, touch, vision) and recent posture information about the body via axons to the spinal cord or brain, i.e., the central nervous system (CNS). In this way sensory neurons convert external stimuli into internal stimuli. These internal stimuli are processed in the CNS and appropriate locomotion responses are planned and executed by the motor system [1].

1.1 Motor system

The motor system is part of the CNS and consists of the extrapyramidal and pyramidal system. Both systems work synergistically. The extrapyramidal system is responsible for rough locomotions and adaption of body posture. Several regions of the brain are involved, including the premotor cortex, basal ganglia, cerebellum, red nucleus and olivary nuclei.

In contrast, the pyramidal system is responsible for fine motor skills and voluntary locomotion, and is most pronounced in primates. It originates from the somatotopically arranged primary motor cortex (precentral gyrus, Brodmann's area 4). The pyramidal cells (also: upper motoneurons) lie within this primary motor cortex. Their axons descend through the corticospinal tract (pyramidal tracts) to the brain stem and spinal cord. In the spinal cord these axons innervate interneurons or spinal (also: lower) motoneurons to modulate their activity pattern [1]. Spinal motoneurons are located in the grey matter of the ventral horn of the spinal cord. Their axons leave the spinal cord as bundles in the form of ventral roots as part of the PNS and innervate voluntary muscles by synapses. These synapses between motoneuron and muscle fibers are called neuromuscular junctions (NMJs) [1]. Neurodegenerative diseases often lead to denervation of the NMJ which then could lead to atrophy of the denervated muscle fibers. Neurotrophic factors are essential to enable the axon to stay in contact with the postsynaptic part of the NMJ whether in a state of health or disease.

1.2 Neuromuscular junction

The NMJ is a synapse formed between motoneurons and skeletal muscle fibers. NMJs have been investigated since the mid 19th century. The easy accessibility, simple postsynaptic geometry (i.e., lack of dendritic spines) and large size of NMJs has allowed fundamental studies of synaptic properties. With help of the neurotoxin curare and microscopic observations, Claude Bernard (1813-1878), Wilhelm Kühne (1837-1900) and Ramon y Cajal (1852-1934) proved the neuron doctrine and at the same time disproved Gerlach's and Golgi's reticular theory, which described the nervous system as a mesh of fused cells. The term "synapse," established by Charles Sherrington (1857-1952), was based on the finding that a NMJ consists of a pre- (motoneurons) and postsynaptic (muscle fiber) part divided by a synaptic cleft [1]. Otto Loewi (1873-1961) and Henry Dale (1875-1968) demonstrated in the 1920s and 30s that the neurotransmitter acetylcholine (ACh), released from the presynaptic part of the NMJ in the synaptic cleft, is responsible for the transmission between neuron and muscle [2]. In the 1950s Bernhard Katz and colleagues found that up to 10,000 molecules of ACh [3] are packed in vesicles (vesicular hypothesis) which enable a controlled release of ACh in specific quantities or quanta (quantal release hypothesis, 1 quanta = 1 vesicle) [4]. These ACh-packed vesicles are located in a specialized, thickened portion of the presynaptic membrane. These sites are called active zones, the place where vesicles fuse with the membrane (exocytosis) to release the ACh into the synaptic cleft [5]. With the discovery of the enzyme acetylcholinesterase (AChE) in the synaptic cleft and the nicotinic acetylcholine receptor (AChR) located in the postsynaptic membrane of muscle, two further components of the transmission machinery were identified. AChE is an enzyme that rapidly hydrolyzes and inactivates ACh and hence regulates the duration of chemical signaling. AChR is activated by ACh, which is released from motoneurons, and generates contraction in muscle fibers [6,7].

Every NMJ is composed of four different elements: (1) A presynaptic motoneuron nerve terminal, capped by a cluster of (2) terminal Schwann cells, (3) an opposing postsynaptic muscle fiber apparatus and (4) the basal lamina (~50nm) in the synaptic cleft (~100nm) separating neuron from muscle fiber (Fig. 1-1) [7,8].

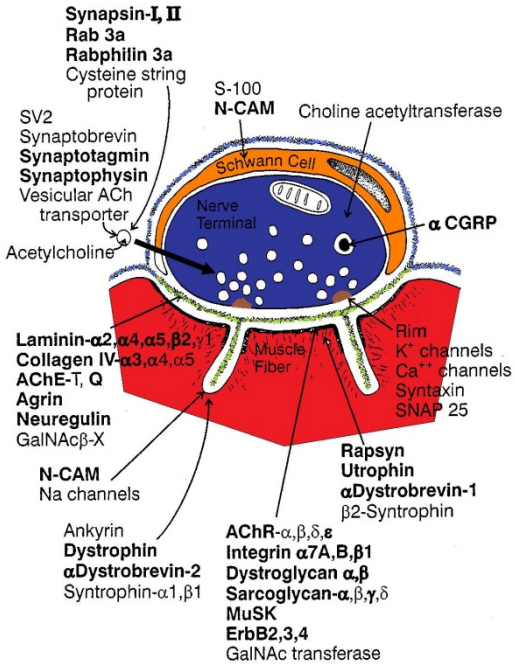

Figure 1-1: Structure and molecular architecture of the neuromuscular junction
Four components of a NMJ: the nerve terminal of the motoneuron (blue), the terminal Schwann cell (orange), postsynaptic part of the muscle fiber (red) and the basal lamina (extrasynaptic = blue; synaptic = green). Active zones (brown), the sites of neurotransmitter release, in the nerve terminal are opposite the junctional folds in the postsynaptic membrane. Some of the important proteins at the NMJ and their subcellular locations are depicted (modified figure from Sanes and Lichtman, 1999 [9]).

1.2.1 Motoneuron

Motoneurons constitute an exceptional class of somatic cells. Their size and lifespan are two special features that distinguish them from other cells. Motoneurons are post-mitotic cells that last a lifetime. The cell bodies of this cell type reside in the central nervous system, i.e., the brain stem or the ventral spinal cord, from where they extend myelinated axons into the periphery to innervate skeletal muscles. The axons of the motoneurons that innervate parts of the foot can reach up to 1 meter in length. Several neurotrophic factors are essential for the proper development, repair mechanisms and maintainance of motoneurons (e.g., IGF-1, CNTF, *1.3 Neurotrophic Factors*, Table 1-1) [10].

In adult muscles, each muscle fiber is innervated by a single motoneuron. However, each motoneuron innervates a group of about 100 to 1,000 muscle fibers. This working connection is known as a *motor unit* [11]. At the distal end of each motor axon branch a nerve terminal is formed—the so-called presynapse or bouton. This contains specialized machinery (active zones) for releasing ACh-packed 50 nm vesicles in response to an action potential (Fig. 1-1) [1]. An action potential is generated by a sodium influx close to the cell body and moves towards the presynapses at 80 m/s. There it opens voltage-dependent calcium channels (P/Q-type) in

the active zones, the sites of neurotransmitter release, allowing the influx of calcium [12,13]. The resulting elevated calcium concentration activates a Ca^{2+}/calmodulin dependent protein kinase II (CaM kinases) which phosphorylates synapsin I, an anchor protein located in the synaptic vesicle membrane. In the resting state of neurons, unphosphorylated synapsin connects vesicles with components of the cytoskeleton which prevents them from migrating to the presynaptic membrane and releasing transmitters [1]. Through phosphorylation of synapsin I, synaptic vesicles disconnect from the actin cytoskeleton. The vesicles can be navigated to the active zones by Rab3A and Rab3C (a member of the Rab GTPases) -binding and GTP hydrolysis [14-17]. The exocytosis occurs when specific integral proteins in the vesicle membrane (vesicle-SNARE or v-SNARE) bind to certain receptor proteins in the target presynaptic membrane (target SNARE or t-SNARE). Syntaxin, a nerve terminal integral membrane protein and SNAP-25, a peripheral membrane protein, have been identified as t-SNAREs. Further, VAMP (synaptobrevin) was discovered as a v-SNARE in the synaptic vesicle membrane [18-20]. In addition to the CaM kinase mediated step there is a second calcium-sensitive step that is involved in vesicle release. The calcium sensor synaptotagmin is located in the vesicle membrane and is involved in early synaptic vesicle docking to the presynaptic membrane. Synaptotagmin interacts with presynaptic membrane proteins β-neurexin [21] and SNAP-25 [22] as well as mediating calcium-evoked synaptic vesicle fusion with the membrane. Synaptotagmin 1 also displaces the inhibitory complexin from the SNARE complex in the presence of calcium and consequently enforces the exocytosis (Fig. 1-1) [23,24].
The amount of ACh quanta that are released by a single nerve impulse can vary from 20 to 200 depending on the size of the NMJ and the number of active zones. The frog NMJ is bigger than the murine one which in turn is greater in size than the human NMJ [7]. The ACh quanta release is about five times higher than the minimal number required to generate a postsynaptic action potential. This excessive vesicle release is called the “safety factor” and ensures that transmission does not fail during repetitive firing [7,25,26]. The released acetylcholine molecules traverse the synaptic cleft (~100 nm in frog NMJ) to bind to their postsynaptic receptors in the skeletal muscle [8,9].

1.2.2 Skeletal muscle

A skeletal muscle is subdivided into bundles of string-like multinucleated cells called muscle fibers. In mammals, muscle fibers reach a length of 2-6 cm and a diameter of 50-100µm [1]. Every muscle fiber contains a cluster of acetylcholine receptors located in a small part of recessed membrane with a subjacent specialized scaffold of proteins in the cytoplasm. This

structure is called the postsynaptic apparatus and lies exactly opposite the presynaptic terminal. The density of the AChR in this region is much greater (10,000/μm^2) [27] than in extrasynaptic areas (10/μm^2) [28]. The recessed membrane of the NMJ contains numerous invaginations, termed postsynaptic folds, which are precisely aligned with the active zones of the motoneuron. The depth of synaptic folds is inversely proportional to the surface area of the NMJ between vertebrate species (i.e., human NMJs contain deeper folds than murine and frog ones) [26]. While the AChR are mainly located in the unfolded, linear membrane and in the border area of the folds close to the presynaptic terminal [29], voltage-gated sodium channels are predominant in the depths of the folds to enhance the efficacy of transmission (Fig. 1-1) [7,26,30,31].

The AChR is also a channel for cations and consists of five subunits ($\alpha_2\beta\gamma\delta$). When two molecules of ACh bind to extracellular portions of the α-subunits, the receptor-channel undergoes a conformational change which results in the opening of an intrinsic pore for sodium and potassium. By following the electrochemical gradient the sodium inflow is higher than the potassium outflow and thus the muscle fiber membrane depolarizes, producing an endplate potential. A single stimulation of a motoneuron produces an endplate potential of about 50 mV (from -90 to -40 mV). As soon as an endplate potential reaches the threshold of -55 mV a sufficient number of sodium channels deep in the synaptic folds open and generate an action potential that propagates relatively slow in both directions along the muscle fiber (3-5 m/s) [1,9,32-35]. This action potential leads to Ca^{2+} release from the cisternae of the sarcoplasmic reticulum into the myofibril. Increased Ca^{2+} concentration allows myosin heads to attach and form cross bridges between actin and myosin filaments. Attached myosin heads rotate and pull the filaments into greater overlaps that result in shortening the muscle fiber. The sum of many muscle fibers shortening leads to a muscle contraction [1,36-38].

1.2.3 Schwann cells

In the mid-nineteenth century the German physiologist Theodor Schwann (1810-1882) discovered that certain cells are wrapped around axons in the peripheral nervous system. These so-called Schwann cells have the capability to divide indefinitely throughout life. They are involved in the conduction of nerve impulses, and the development, maintenance and regeneration of axons.

Schwann cells are originally derived from neural crest cells in an early phase of embryonic development [39]. In mice, the neural crest cells first develop into precursors of Schwann cells at embryonic day 12 (E12). Subsequently, the transformation of precursors into immature

Schwann cells lasts from E15 until birth and is mediated by neuregulin 1-Type III (NRG1-III). This protein is secreted by axons which are essential for the survival of immature, but not for mature Schwann cells [40-42]. Postnatal immature Schwann cells can adopt one of two alternative phenotypes distinguishable by their anatomic relationship to the axon. Postnatal immature Schwann cells can develop into myelinating Schwann cells after birth and sort themselves to larger axons (>1µm) in a 1:1 relationship. Myelination is a spiral sheath of axons with lipid-rich myelin that guarantees faster stimulus conduction. In rodents it starts at postnatal week one and peaks three or four weeks after birth [43]. IGF-1 plays a major role for the induction of myelination (*1.3.4 Insulin-like growth factor*) [44-47]. Demyelination is a hallmark of neurodegenerative diseases and can lead to conduction loss and nerve degeneration [1].

Alternatively to the myelination pathway, immature Schwann cells could enter a non-myelination pathway and ensheath multiple small unmyelinated axons, like the sensory C-fibers, forming a Remak bundle [42,48]. The fate of myelination is determined by the levels of secreted NRG1-III. Larger axons release higher levels of NRG1-III which leads to myelination of axons (e.g., motoneurons). In contrast, low levels of NRG1-III lead to ensheathment of unmyelinated axons (i.e., Remak bundle) [49] (Fig. 1-3).

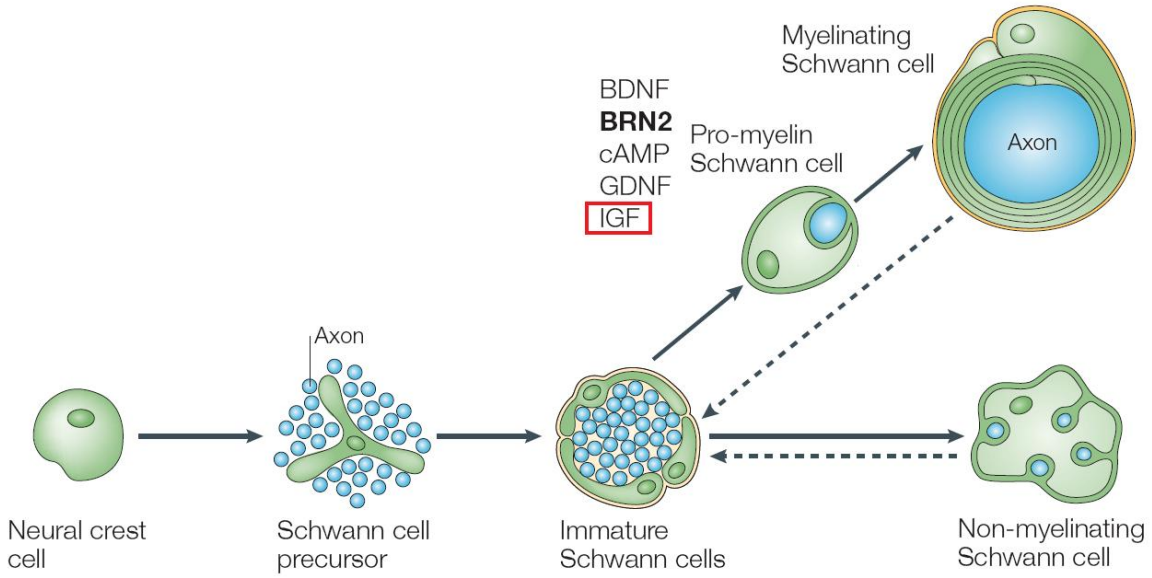

Figure 1-2: Cell lineage of myelinating and non-myelinating Schwann cells
Schematic illustration of Schwann cell development. Immature Schwann cells can differentiate into axon myelinating Schwann cells or into non-myelinating Schwann cells embedding unmyelinated axons. For the myelination process certain factors (i.e. IGF-1) are important (figure modified from Jessen, 2005 [42]).

Axons of motoneurons are normally surrounded by myelinating Schwann cells (see above). However, close to NMJ there are a few non-myelinating Schwann cells, called terminal or perisynaptic Schwann cells, which associate intimately with the non-synaptic portions of motor nerve terminals. Three to five terminal Schwann cells are necessary for maturation and maintenance of the NMJ [50]. These perisynaptic Schwann cells also play an important role for motoneuron survival by secreting trophic factors, e.g. IGF-1 and CNTF, to guide regenerating motor axons, modulation of synaptic function and removal of debris following injury [51-54].
Schwann cells play a key role in wallerian-like degenerative processes. After axon degeneration, Schwann cells proliferate and initiate breakdown of the myelin sheath and clearance of its debris. Additionally, they release a wide variety of chemokines and cytokines, such as leukaemia inhibitory factor (LIF), after injury. Some of these factors recruit macrophages to the degenerating nerve, and these also clear the debris of the myelin. Schwann cells, macrophages, and fibroblasts in the distal stump of the lesioned nerve express a wide range of neurotrophic molecules that allow axon outgrowth and regeneration, including nerve growth factor (NGF), glial-derived neurotrophic factor (GDNF), brain-derived neurotrophic factor (BDNF), CNTF, IGF-1, and LIF [55]. Mature Schwann cells can inhibit their apoptosis by an autocrine release of growth factors including IGF-1, platelet derived growth factor-BB (PDGF-BB), and neurotrophin-3 (NT-3) [42]. NT-3 reduction in Schwann cells leads to impaired nerve regeneration after a crush lesion in the sciatic nerve and increase in the abnormal neurofilament packing in axons [56]. By release of neurotrophic

factors and production of the basal lamina by contact with axons, Schwann cells secure the survival of axons in the peripheral nervous system in healthy as well as in disease conditions [57]. They also play a major role in axonal sprouting (see *1.3.2.1 Sprouting*), a compensatory mechanism to reinnervate denervated targets [58].

1.2.4 Basal lamina

The basal lamina is a specialized extracellular matrix that surrounds muscle fibers, terminal Schwann cells and nerve fibers as they traverse into the synaptic cleft. The size of the synaptic cleft of the NMJ (up to 100 nm) is 5 times bigger than that of synapses from the central nervous system. For interaction between motoneuron and muscle fiber the basal lamina is essential to bridge the distance and forms a cleft for ACh diffusion. The lamina is composed of four kinds of proteins: collagen IV, nidogens, laminins and heparin sulfate proteoglycans (HSPGs) [7,35,59]. The synaptic basal lamina of the synaptic cleft is adapted to its function of forming and maintaining the NMJ and therefore contains different isoforms of the four components (e.g., laminin β2 for clustering of voltage-gated calcium channels at actives zones [60]) compared to the extrasynaptic basal lamina. Collagen IV and laminins form their own networks within the basal lamina that are connected by special glycoproteins called nidogens. Including HSPG, all four components have structural and bioactive functions. All of them, but mainly HSPG (e.g., agrin), can be enriched in the extracellular matrix by binding of many other proteoglycan/glycoproteins, regulatory proteins (e.g. IGFBP-5), matrix molecules, neurotrophic factors (e.g., fibroblast growth factor), activating receptor molecules (neuregulin) and enzymes (AChE, terminates neurotransmission) that are essential for motoneuron muscle interaction. By mediating the communication for pre- and postsynaptic elements, the basal lamina is essential for development (e.g., agrin for AChR clustering), maintenance and modulation of the NMJ [61-65].

Taken together, the motoneurons, Schwann cells, muscle fibers and basal lamina are essential for the proper development, maintenance and regeneration of the NMJ. The communication between these four components of the NMJ is mediated by membrane-bound proteins/receptors or secreted factors that guarantee a functional NMJ. One of the most important secreted factors is the group of neurotrophic factors which have an impact on all four components of the NMJ.

1.3 Neurotrophic factors

Neurotrophic factors are small proteins that exert survival-promoting and trophic actions first identified in embryonic neuronal cells. The long journey of the discovery of neurotrophic factors started in the 1920s with a German neuroembryologist named Viktor Hamburger. Together with Rita Levi-Montalcini, and by using transplantation experiments in chicken and amphibian embryos, over 3 decades they established the *neurotrophic factor hypothesis*. The hypothesis implies that the target cells of developing embryonic neurons produce a limited amount of an essential trophic factor that is taken up by nerve terminals. Hamburger and colleagues isolated the first neurotrophic factor, named NGF, by co-culturing sarcoma cells with sensory neurons [66].

The released amount of neurotrophic factor is not sufficient for all neurons, leading to death of about half of all embryonic motor and sensory neurons during embryonic development. By a 50% surplus of neurons and the specific induction of programmed cell death (apoptosis), the organism is adapted to fit the needs and ensure that every target is innervated [67-71]. In neurons which receive a sufficient dose of neurotrophic factors during development, specific neurotrophic receptors are activated. These mediate an anti-apoptotic downstream program through different pathways including RAS/mitogen-activated protein kinase (MAPK), phosphoinositide 3-kinase (PI-3K)/AKT, and PKA, the latter inhibiting the anti-apoptotic factor BAD by phosphorylation [10,72-77]. Unphosphorylated BAD translocates to the outer membrane of the mitochondria and inhibits pro-aptoptotic proteins Bcl-XL or Bcl-2 by forming heterodimers, and thus leads to apoptosis [78-80].

Nowadays, it is confirmed that neurotrophic factors have a far broader function than only in survival of embryonic neurons. They are involved in development, survival and maintenance of neurons, differentiation of glia cells and regulation of synaptogenesis and synaptic plasticity in mature neurons [81-86]. The neurotrophic factors can be divided into several genetic related families which are still growing [87]. Table 1-1 shows a partial list of the most important neurotrophic factors and their receptor for motoneurons [88].

Besides their in vivo functions, they have a direct impact on motoneuron survival and axon maintenance as shown in pure cultured embryonic motoneurons [89,90]. These neurotrophic survival factors for motoneurons consist of several families including CNTF, IGF-1, CT-1, GDNF and BDNF [89].

	Receptor on motoneurons
1. Neurotrophins	
Brain-derived neurotrophic factor (BDNF)	$p75^{NTR}$, trk-B
Neurotrophin-3 (NT-3)	$p75^{NTR}$, trk-C
Neurotrophin-4/5 (NT-4/5)	$p75^{NTR}$, trk-B
2. CNTF/LIF family	
Ciliary neurotrophic factor (CNTF)	CNTFRα, LIFRβ, gp130
Leukemia inhibitory factor (LIF)	LIFRβ, gp130
Cardiotrophin-1 (CT-1)	?, LIFRβ, gp130
Cardiotrophin-1-like cytokine (CLC)	?, LIFRβ, gp130
3. Hepatocyte growth factor/scatter factor (HGF/SF)	c-met
4. Insulin-like growth factors	
IGF-I	IGFR-1
IGF-II	IGFR-1, mannose-6P receptor
5. Glial-derived neurotrophic factor and related factors	
Glial-derived neurotrophic factor (GDNF)	GFRα1, c-ret
Neurturin (NTR)	GFRα2, c-ret
Persephin	GFRα4, c-ret
Artemin	GFRα3, c-ret

Table 1-1: Neurotrophic factors and their receptors
Overview of important neurotrophic factors and their receptors. These factors affect motoneurons and other cell types (e.g., glia cells). (Table from Sendtner, 2000 [10]).

1.3.1 Brain-derived neurotrophic factor

BDNF belongs to the family of neurotrophins (Table 1-1). It binds to a monomer of tropomyosin-related kinase B (TrkB) receptor that then dimerizes with another monomer of TrkB. This leads to autophosphorylation of the cytoplasmatic domains of the receptor complex. TrkB plays a role in maintenance and formation of the postsynaptic receptor clusters of the NMJ [91,92].

BDNF supports other types of peripheral neurons than does NGF, another neurotrophin. For example, in contrast to NGF, BDNF does not support the survival of sympathetic neurons. Contrary to this BDNF has a supportive effect on the survival of placode-derived sensory neurons, whereas NGF does not [87,93]. BDNF supports also motoneuron survival in culture [94]. BDNF knockout mice show ataxia, loss of myelinated sensory neurons, vestibular neurons and die after a few days [87]. In contrast to CNTF, BDNF mRNA is detectable in skeletal muscle. Muscle-derived BDNF could act as a retrograde signal for survival of innervating motor neurons throughout their lifespan via the TrkB receptor [94]. However the level of skeletal BDNF decreases during maturation.[95]

BDNF is undetectable in healthy rat sciatic nerves. However, BDNF mRNA rises slowly in Schwann cells, starting at 3 days after nerve lesion, and reaches maximal levels after 3-4 weeks exclusively in distal nerve pieces [96]. NGF also increases after lesion. It increases faster and almost reaches a plateau at day 7. However, BDNF concentration increases gradually after lesion, and after 4 weeks it is 10 times higher than NGF, indicating the long-lasting

regeneration potential of BDNF for sensory and motoneurons [96]. Furthermore, BDNF treatment prevents facial motoneurons in new-born rats after lesion [97] .

Taken together, muscle-derived BDNF plays an important role in maintenance of the postsynaptic receptor at the NMJ and also acts on motoneurons in development as seen in BDNF knockout mice. After nerve lesion, BDNF is expressed in Schwann cells in a period of 4 weeks and could be responsible for later postinjury stages [87]. Therefore it is unlikely that BDNF plays a major role in axonal maintenance due to its undetectable expression in Schwann cells under physiological healthy conditions. It is more likely that more abundant factors in Schwann cells, such as GDNF and CNTF, or IGF-1 support axonal regeneration and maintenance in the first place.

1.3.2 Glial-derived neurotrophic factor

GDNF, the first identified member of the GDNF family, is a transforming growth factor-β related survival factor (Table 1-1) [98]. It was originally isolated from the rat glioma cell-line supernatant as trophic factor for dopamine neurons in primary cultures from the embryonic midbrain. Later it was found that GDNF has also supportive effects on other neuronal cells, including motoneurons. GDNF is expressed in Schwann cells and the skeletal muscle of developing and adult mammals [99]. Homodimeric GDNF binds to the cognate GDNFa-receptor which then interacts with the extracellular domain of the RET receptor, a receptor tyrosin kinase. The RET receptor contains four intracellular tyrosine residues. The receptor beomes activated when the residues are phosphorylated [100]. Homozygous GDNF-deficient mice die at birth and already show a 37% loss of lumbar spinal motoneurons on embryonic day 18.5, indicating the importance for motoneuronal development. Muscle-specific overexpression of GDNF starting embryonically leads to increased number of motoneurons compared to neonatal control mice [99]. Another muscle-specific GDNF overexpressing mouse model showed the maintenance of hyperinnervation of NMJs beyond the normal developmental period after 6 weeks [101]. By promoting terminal branching, this extra innervation could counteract synapse elimination, indicating that GDNF is important in the regulation of synaptic plasticity in the developing NMJs. Experiments directly focused on motoneurons revealed that GDNF is very potent in supporting the survival of purified cultured embryonic motoneurons, and after axotomy GDNF rescues and prevents atrophy of facial motoenurons in vivo [98]. Additionally, GDNF slows the loss of motoneurons, but does not prevent axon loss or prolong survival in *pmn* mice, a mouse model for ALS [102]. However, CNTF application via CNTF-secreting stem cells to the same *pmn* model not only slows motoneuron loss, like

GDNF, but even prolongs survival of the mice and leads to improved maintenance of motor axons in this model [103]. This, and the fact that GDNF knockout mice die at birth, strengthens the idea that GDNF is important in motoneuron development and innervation of the NMJ, but CNTF may be more effective in axon maintenance or compensating in degenerative processes.

1.3.3 Ciliary Neurotrophic Factor, Leukaemia inhibitory factor and Cardiotrophin-1

CNTF is a member of a large family of neurotrophic cytokines which also includes LIF and CT-1. CNTF was first identified and partially purified in embryonic chick eye tissues in the 1970s and supports the survival of embryonic chick ciliary neurons in culture [104]. Besides this, CNTF supports the survival of a broad spectrum of neurons including sympathetic, sensory nodose, trigeminal, and particulary motoneurons [105]. Additionally it plays a role in glial precursor cells of the oligodendrocytes lineage [81] and their survival in culture [106], and has a major role in motoneuron sprouting [107,108]. CNTF is a neurocytokine which consists of 200 amino acids (24 kDa). It differs from neurotrophins by lacking the hydrophobic leader sequence [109] which is necessary for the cellular release by the conventional secretory pathway. High amounts of CNTF are localized in the cytoplasm of myelinating Schwann cells as well as in astrocytes [110]. Up to now it is not clear whether CNTF can be actively released by Schwann cells or only passively diffuses from damaged Schwann cells (e.g., due to a lesion) to maintain the survival of lesioned neighboring motor and sensory neurons. However, endogenous CNTF released from lesioned Schwann cells supports the survival of axotomized rapid-degenerating motoneurons [111].

CNTF expression in the rat sciatic nerve becomes apparent by postnatal day 4 and reaches maximum levels in fully differentiated Schwann cells in the third postnatal week [78,112,113]. CNTF knockout mice develop normally until 3 weeks after birth, but develop a progressive loss of 20% spinal motoneurons thereafter [114]. This differs from other GDNF and BDNF knockout mouse that die shortly after birth with major defects of neuronal development. This emphasizes their role in axonal development. In contrast, CNTF knockout mice develop completely normally, which complies with the fact that CNTF is first highly expressed after the third postnatal week. The lack of CNTF leads in adult mice to progressive motoneuron loss. This and the fact that CNTF is not expressed in the muscle (unlike BDNF and GDNF), but is highly expressed in Schwann cells that supply motoneurons in direct contact, strengthen the role of CNTF in axonal integrity in the healthy and disease state.

A specific low-affinity receptor for CNTF was first found in neuronal tissue and skeletal muscle [115]. LIF and CT-1 tranduce their signals through the same receptor components as CNTF. LIF can induce sprouting of postganglionic sympathetic fibers into the dorsal root ganglia in adult rats following peripheral nerve injury [116]. Investigations of CNTF, LIF and CT-1 in double and triple knockout mice revealed that muscle-derived CT-1 is particularly important for developing motoneurons, but does not play a major role in adult axonal maintenance and regeneration [117]. CNTF and LIF are essential for postnatal maintenance of motoneurons, whereas LIF seems to play a specific role in the control of NMJ size which cannot be compensated by CNTF and/or CT-1 [118].

CNTF receptor consists of the CNTF binding protein (CNTFR alpha) as well as the components of LIF receptor, LIFR beta (the LIF binding protein) and gp130 (the signal transducer of interleukin-6 [IL-6]).

In contrast to other known cytokine receptors, CNTFR alpha does not have a cytoplasmic or transmembrane region. However, it is anchored to the cell surface membrane by a glycosyl-phosphatidylinositol (GPI) anchor [119]. Cleavage of this GPI linkage by phospholipase C can release CNTFRα to become a soluble receptor and enables CNTF signaling in cells without CNTFRα, but with gp130 and LIFRβ [120]. CNTF binding to CNTFR alpha (α receptor subunit) in a 1:1 stoichiometry permits the recruitment of gp130, followed by LIFR beta (β receptor subunits) membrane signal transducing units [121] that are associated with Janus kinases (JAKs) in the cytosol. The heterodimerization of β-subunits triggers the activation of JAKs which in turn phosphorylate tyrosine residues of these subunits. This creates docking sites for SH2 domain-containing signaling molecules such as Signal Transducer and Activator of Transcription (STAT-3) [122]. Activated STAT-3 can form both homodimers with another STAT-3 and heterodimers with other STAT proteins. The dimer translocates into the nucleus to promote transcription of pro-apoptotic genes including cyclin D1, c-myc, Bcl-2 and Bcl-XL [123].

Furthermore, JAKs activate the PI3K/AKT and RAS/MAPK pathway, which could also support survival in crosstalk with the JAK-STAT pathway [124,125]. Moreover, cytoplasmic STAT-3 binds to and inhibits stathmin, a destabilising protein of microtubules, and thus supports the stability of the cytoskeleton and outgrowth of neurons [126]. This could be important for the function of CNTF in axonal sprouting. Daily CNTF injection for 1 week directly over the surface of the adult mouse gluteus muscle induces axonal sprouting near the NMJs [107]. Furthermore, CNTF-deficient mice showed no sprouting response after sprouting-inducing stimuli, such as injection of botulinum and transection of a nerve branch. However,

exogenous CNTF administration given in parallel to the stimuli induces sprouting in CNTF knockout mice [108]. This positive effect complies with the finding that CNTF acts as a positive modifier in motoneuron diseases such as amyotrophic lateral sclerosis and prevents axon loss with prolongation of survival in *pmn* mice [103,127]. Thus, CNTF plays a major role in axonal maintenance and motoneuron sprouting as a compensatory mechanism in neurodegenerative diseases.

1.3.3.1 Sprouting

Sprouting is a remarkable ability of neurons in the central and peripheral nervous system to form new neuritic processes (sprouts) to respond to denervated targets [58]. It is part of the mechanisms contributing to synaptic plasticity, when remaining neurons form new sprouts to reinnervate recently denervated neurons or muscle fibers [128]. They can appear from motor nerve terminals (terminal or ultra terminal sprouts) or from nearby nodes of Ranvier (nodal or axonal sprouts) (Fig. 1-4).

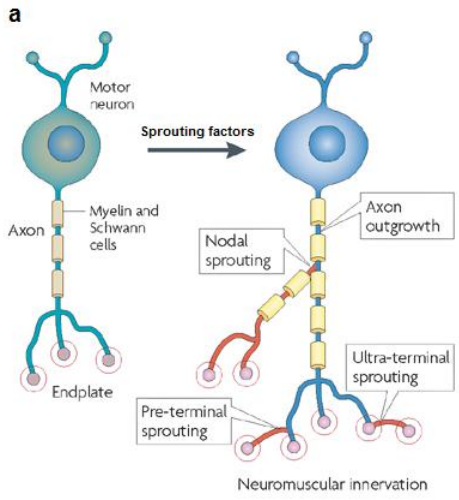

b

Ligand	*Produces sprouting*	*Blocked by antagonist, antibody, knockout*	*Signaling pathway*	*Source*	*Signaling partner*	*Reference*
Neuroleukin	Not studied	Yes	G-Protein	Muscle?	Neuron?	Gurney, 1982
NCAM	Not studied	Yes	PY*	Neuron & Muscle	Neuron	Boothe *et al.*, 1990
IGF	Yes	Yes	PY	Muscle	Neuron	Caroni & Grandes, 1990
NT-4	Yes	Not studied	PY	Muscle	Neuron	Funakoshi *et al.*, 1995
CNTF	Yes	Yes	PY	Schwann cell	Muscle	Gurney *et al.*, 1995; Siegel *et al.*, 2000
FGF-2	**	Not studied	PY	Muscle	Neuron	Gurney *et al.*, 1995
GDNF	***	Not studied	Ret-GNFRα	Neuron	Schwann cell	Nguyen *et al.*, 1998

*via FGF receptor and non-receptor tyrosine kinase; **enhances CNTF-induced sprouting; ***effective in neonatal muscle.
PY = tyrosine phosphorylation.

Figure 1-3: Sprouting events at the NMJ and their inducing factors
(a) A single motoneuron innervates many endplates (NMJ). Due to a neurodenerative event, muscle fibers can be denervated and then reinnervated by sprouting branches of neighbouring motoneurons. (b) Putative sprouting factors with their sources and signaling partners. (Figure adapted from (a) Zacchigna, 2008 [129] and (b) English, 2003 [130])

A number of studies with paralyzed muscles showed that sprouting can be induced by the lack of electrical and contractile activity in denervated muscle fibers [131-133]. This lack of activity of the target cell leads to an upregulation of cell surface and basal lamina proteins that could guide new axon sprouts to the endplate [134]. Furthermore, it has been shown that exogenously administered trophic factors, including CNTF, induce sprouting [107,135]. The sprouted axon is guided by processes of Schwann cells that play a primary role in initiating sprouting and guidance [136,137]. The exact mechanism is not completely known, but it is feasible that inactive

or denervated muscle fibers release sprouting factors (Fig. 1-4b, e.g. IGF-1 in response to an unknown trigger released from the Schwann cells or the inactive fiber itself. This leads to an extension of elaborated branches of terminal Schwann cells on a denervated muscle fiber to form bridges to intact synapses [137,138]. These bridges could guide new sprouts from an intact motoneuron terminal to a denervated target [130,139,140], which could serve as a compensatory mechanism in motoneuron disease to counteract motoneuron loss.

In *Smn*$^{+/-}$ mice, a model for mild SMA, a slow progressive loss starting in adulthood is observed, peaking in 50% loss of lumbar spinal motoneurons after 1 year. Despite this strong motoneuron loss, the mice show no signs of atrophy and remain clinically normal [141]. Therefore there must exist a compensatory mechanism. It will be interesting to investigate whether CNTF-induced sprouting is involved in this compensatory mechanism.

1.3.4 Insulin-like growth factor

The insulin-like growth factor belongs to a complex system referred to as the IGF axis. It consists of two cell-surface receptors (types 1 and 2; IGF1-R and IGF2-R), two ligands (IGF-1 and IGF-2) and at least six insulin-like growth factor binding proteins (IGFBPs) [142,143]. IGF-1 (7.6 kDa) and IGF-2 (7.4 kDa) display a sequence homology of approximately 62% with each other and 47% sequence similarity with insulin. They are generated by cleavage of longer precursor molecules at the amino- and carboxyterminal ends [144,145]. IGFs are synthesized in a variety of tissues, including liver, pituitary and nervous system, and are found in the serum and cerebrospinal fluid (CSF) [87,146]. IGF-1 and 2 bind to three receptors with different affinities. The IGF1-R is a disulfide-linked heterotetrameric transmembrane glycoprotein of 350 kDa. It consists of two extracellular alpha subunits (135kDa) with a high affinity ligand binding site for both IGFs and two transmembrane beta subunits (90 kDa) which possess intracellular tyrosine kinase domains [147,148]. However, the affinity to IGF-1 is 15- to 20-fold higher than to IGF-2 [149]. The second IGF receptor, IGF2-R, binds IGF-2 with high and IGF-1 with low affinity [150,151]. It consists of a single-chain polypeptide and due to the absence of a tyrosine kinase domain it cannot transduce a signal. This receptor seems to be involved in clearance and degradation of IGF-2 [152,153]. The third receptor is the insulin receptor, which shows high similarity to the IGF-1 receptor [154,155]. However, the IGF1 binding affinity is about 100-fold lower than the binding affinity to insulin [156]. Binding of IGF-1 and insulin to their receptors leads to the autophosphorylation of the beta subunit and also to the phosphorylation of insulin receptor substrate (IRS) which in turn activates phosphoinositol 3-kinase (PI 3-kinase). The IGF-1 receptor, activated by IGF-1, and the insulin receptor are

tyrosine kinases that mediate phosphorylation of IRS proteins including IRS-1, IRS-2, IRS-3, and IRS-4 [157-159]. Phosphorylated IRS proteins can activate multiple signaling pathways, including MEK/extracellular signal-regulated kinase (Erk), Ras-Raf-MAPK and PI-3K/AKT cascades [160-163]. Although IGF-1 receptor and the insulin receptor both function via the AKT pathway, they lead to phosphorylation of different amino acids on a subgroup of forkhead proteins known as FKHR proteins. These data provide a potential explanation for the different effects of insulin and IGF-1 on gene expression [164].

There is also evidence for heterotrimeric G-protein associated signaling [165]. IGF-1 promotes neuronal survival and cytoskeleton rearrangement by activation of the IGF-1 receptor through the PI3K/AKT pathway by phospohorylation of BAD [79,80,166-168]. In contrast the MAPK pathway is important for differentiation [169]. IGF-1 promotes oligodendrocyte progenitor cell proliferation and survival in vitro [161,170] and is critical for myelination in vivo [44,45,171,172].

In peripheral nerves, IGF-1 is mainly expressed in Schwann cells of postnatal rodents [173] and acts on motoneurons to support survival [89,174,175], myelination [46,176-179] and regenerative reactions—for example, IGF-1 administration to adult rat or mouse gluteus muscle led to intramuscular nerve sprouting [135]. This complies with the idea that IGF-1 supports motoneuron axon outgrowth during development and in the adult nervous system [180]. In the sciatic nerve, IGF-1 is detected in Schwann cells and axons after nerve crush and accumulates in damaged axons within 2 hours of injury. At the distal stump, IGF-1 expression peaks in Schwann cells at 2 weeks after transection [180].

IGF-1 plays an important regulatory function during myelin membrane formation by stimulating de novo fatty acid biosynthesis through the PI3K/AKT pathway [47]. 2-month-old IGF-1 knockout mice show reduced number of axons and myelination [44]. Reduced or impaired myelination often results in reduced conduction velocity and nerve fiber diameter. Decreased NCV was found in mice with reduced or absent IGF-1. Exogenous IGF-1 restores the conduction velocities. Reduced nerve conduction and demyelination are features of several neuropathies, including DNP which also involves the IGF system. Therefore the role of IGF-1 is very interesting in neuropathies, especially in diabetic neuropathy [180]. IGF-1 mRNA is quickly reduced in Schwann cells upon induction of diabetes in adult rats. IGF-1 replacement prevents neuropathy in these diabetic nerves. Thus, the profound loss of IGF-1 activity could lead to a relatively rapid onset of DNP [181].

The inhibition of IGF-1 could also lead to features of a neuropathy. 90% of circulating IGF-1 in the blood is associated with high affinity 6 insulin-like growth factor binding proteins (1-6

IGFBP), which modulate IGF-1 availability for the receptors and prolong IGF-1 half-life by preventing its proteolysis [182].

1.3.4.1 Insulin-like growth factor binding protein-5 (IGFBP-5)

IGBFBs bind with high affinity and inhibit or promote the action of IGF-1 and IGF-2 [183,184]. IGFBP-5, a 29 kDa glycosylated protein [185] binds IGF-1 and IGF-2 in vitro and reduces autophosphorylation of the IGF-1 receptor [186]. In postnatal peripheral nerves, IGFBP-5 immunoreactivity is detectable in Schwann cells and in close association with or even within myelinated axons, suggestive of anterograde axonal transport and release from axons [178,187]. In contrast to IGFBP-1, -3 and -4, which sequester IGF-1 in extracellular fluid reservoirs to inhibit IGF-1 [188], IGFBP-5 binds with high affinity to the extracellular matrix (ECM) [189,190] (e.g., by binding the extracellular glycoprotein vitronectin) and provides IGF-1 close to its receptor to potentate its effect in healthy conditions [62,189].

Thus IGFBP-5 could regulate local functions of IGF-1 and IGF-2 at the interface between motoneurons and Schwann cells.

1.3.4.2 A possible role of IGBFP-5 in neurodegenerative diseases

Diabetes mellitus is a metabolic disease which results from either reduced insulin production or insulin uptake deficiency (see *1.4.2 Diabetic neuropathy*). One consequence of this disease is an increased expression of inflammatory markers in the heart, which in turn decrease the activity of IGF-1, IRS-2 and AKT. Consequently the level of pro-apoptotic BAD protein increases and thus apoptosis is promoted [191]. Additionally, a significant down-regulation in the expression of IGF-1 and IGF-1R was seen in the small DRG neurons of streptozotocin-induced (STZ) rodents, a model for painful DNP [192]. In addition, an upregulation of IGFBP-5 in the rat eye was observed in this model [193]. A possible reason for this might be that IGFBP-5 is overexpressed and inhibits the IGF-1 pathway and thus could lead to apoptosis in neurons. For this reason, IGFBP-5 levels of patients with diabetes and the consequences of overexpressed IGFBP-5 in a mouse model were investigated.

1.4 Motoneuron diseases

Neurological disorders that selectively affect motoneurons are classified as motoneuron diseases (MND). They can be subdivided into three classes that affect either the upper or the

lower motoneurons or both. Hereditary spastic paraplegia (HSP, incidence of 7.4 per 100,000 in Norway[194]) is an example of an MND affecting only the upper motoneurons (pyramidal cells in the primary motor cortex, see *1.1 Motor system*). This degeneration of the upper motoneurons and their axons in the pyramidal tract leads to the lack of inhibition from the CNS which results in control loss of the lower motoneurons in the spinal cord. This leads to a progressive spasticity in the lower limbs [195].

The amyotrophic lateral sclerosis (ALS, incidence of 5.2 per 100,000 in Western countries [196]) is a progressive neurodegenerative disease which affects both upper and lower motoneurons. Depending on which motoneurons are affected first or more severely, the symptoms can vary. If the upper motoneurons are more affected, spasticity is predominant and there is loss of fine motor skills. On the other hand, muscle denervation, atrophy and paralysis occur when the lower motoneurons degenerate first [197].

A classical MND that affects only lower motoneurons is childhood SMA. In addition, there are several other neurodegenerative diseases that affect many parts of the nervous system, including the sensory, autonomic and motor system, e.g. DNP. Nevertheless, to understand these diseases, it is important to investigate single parts in more detail to obtain further insights into the pathology.

1.4.1 Spinal muscular atrophy

SMAs are a heterogeneous group of neuromuscular disorders that have different genetic causes, but all share the characteristics of the loss of lower motoneurons and a resulting atrophy of muscles [198]. The most frequent form of SMA is the proximal spinal muscular atrophy that is normally referred to as SMA. It is an inherited autosomal neurodegenerative disease where mainly the proximal limbs of the patients are affected. With an incidence of 1 in 10,000 live births and a carrier frequency of 1:35, it is the leading monogenetic cause of infantile mortality [199]. Depending on the age of onset, the severity of disease and the achieved motor abilities, SMA can be subdivided into four forms [200-203] (Table 1-2).

The most severe form of SMA (Type I) is known as the Werding-Hoffmann disease and has its onset during the first 6 months after birth. Diseased children can never sit or walk due to a loss of motoneurons in the entire spinal cord as well as in the motonuclei of the cranial nerves in the brainstem resulting in strong hypotony of the musculature. The degeneration of the phrenic nerve that innervates the diaphragm leads to lethal respiratory paralysis within the first two years [198,203]. The intermediate form of SMA referred as Type II starts after 6 months and affected children are able to sit and can reach adolescence or even adulthood [200].

Type	Age at onset	Motor abilities
0	Prenatal onset	Reduced fetal movements *in utero*; some degree of spontaneous ventilation and movement at birth
I	At birth or <6 months	Never able to sit
II	<18 months	Unable to stand or walk unaided
III	>18 months	Able to walk unassisted
IV	Adult onset	Mild proximal muscle weakness

Table 1-2: Diagnostic features in the classification of spinal muscular atrophy
Table shows different types of spinal muscular atrophy. They are defined by the time point of onset and the severity of the motor abilities. (Modified table from Briese, 2005 [204].)

Patients with the juvenile SMA form (Type III, Kugelberg-Welander disease) have a normal lifespan and are able to sit and walk, but not to run. Their disease pattern is very similar to Duchenne muscular dystrophy (DMD). Type IV SMA patients are comparatively mildly affected, with an onset later than 30 years and a normal lifespan [205]. The SMA forms of Type I-III could be all mapped to a specific region in the genome [204,206].

1.4.1.1 Genetic background of SMA

In 1990 three different forms (I-III) of SMA were mapped to the long arm of the human chromosome 5 (region 5q11.2-q13.3) using linkage analysis [207-209]. In the mid-nineties this 500 kilobase (kb) region was characterized and four genes with their respective inverted copy were found. A telomeric (t) and an inverted centromeric (c) copy of each gene have been found (Fig. 1-5):

1. *survival of motoneuron gene (SMN) 1* (t) or *2* (c) [210]
2. *neuronal apoptosis inhibitory protein* (*NAIP* (t) or *ψNAIP* (c)) [211]
3. *basal transcription factor subunit p44t* (t) *or p44c* (c) [212,213]
4. *H4F5t* (t) or *H4F5c* (c) [214]

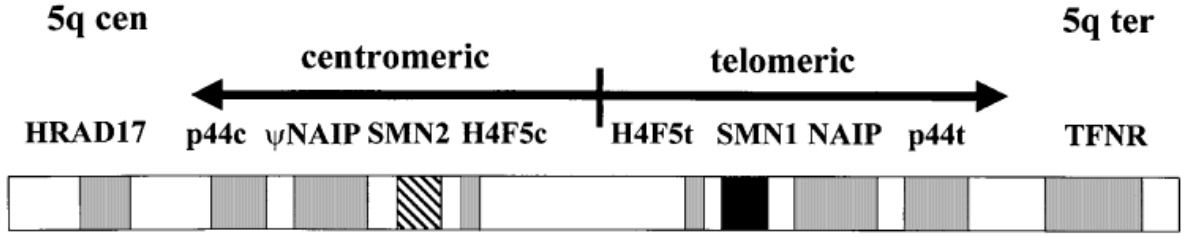

Figure 1-4: Scheme of the 500 kilobase SMA region on chromosome 5
Showing the telomeric SMA region and its inverted and duplicated centromeric region (5q13), including the four genes: SMN, H4F5, NAIP and BTFp44. (Figure from Wirth, 2000 [215].)

In 1995, the telomeric *SMN1*, but not the centromeric *SMN2* copy, was identified in this region as the disease-determining gene [210], although these genes are almost identical. Both encompass 27 kilobases (kb) including nine exons (1, 2a, 2b, 3-8) [216,217]. The 1.7 kb SMN full-length transcript encodes for a protein of 294 amino acids [210]. These two *SMN* copies differ only in 5 base pairs at the 3´ end of the genes, while the cDNA only differs in 2 base pairs in exon 7 and 8 and still encodes for the same protein [210,216]. However, the single point mutation which transforms the *SMN1* copy to the disease-determining gene is a cytosine-thymine (C-T) transition at position + 6 of exon 7 [218]. Although this mutation is localized within the coding region, it does not change the codon and hence does not affect the amino acid sequence of the encoded protein (silent mutation). Nevertheless, due to the presence of thymine in *SMN2* only 10% of the full length (FL) transcripts, but 90% of alternatively spliced transcripts that lack exon 7, are produced and result in a truncated transcript (*SMN2Δ7*). However, since some full-length SMN is produced from the *SMN2* locus, it can be considered as a gene with reduced function, but not a loss of function. The cytosine-containing *SMN1* gene expresses 100% of the FL transcript [210,219].

The truncated transcripts arise from alternative splicing. Exon 7 spans 54 bp with a weak 3´ splice site [220] and needs additional auxiliary cis-regulatory splicing elements for recognition by the splicing machinery. These auxiliary cis-splicing elements are specific sequences of a precursor RNA which regulate correct splicing located on that same molecule of RNA. On the other hand, trans-regulatory elements are DNA or RNA sequences that encode for trans-acting splicing proteins/factors, including SR proteins (serine-argine-rich proteins), SR-like proteins and heterogenous ribonucleoproteins (hnRNP), that regulate splicing through binding to a cis-regulatory element [206,215]. Depending on their localization and function, cis-regulatory splicing elements comprise 1. exonic splicing enhancer (ESE) and 2. intronic splicing enhancer (ISE) that facilitate the inclusion of exon 7 in the FL transcript, as well as 3. exonic splicing silencer (ESS) and 4. intronic splicing silencer (ISS) that have a negative effect on the correct splicing of exon 7 and support a truncated Δ7 transcript [206].

The key cis-regulatory splicing element for the inclusion of exon 7 in the *SMN1*-derived gene transcript is an ESE located within the 5´ end of exon 7 that is recognized by the trans-acting splicing factors SF2/ASF. This ESE is destroyed by the C-T transition in the *SMN2* gene. Therefore SF2/ASF do not recognize this sequence anymore and consequently exon 7 is spliced out together with intron 6 and 7 leading to *SMN2Δ7* [206,221-223] (Fig. 1-6). Now the major question is why the *SMN2* gene can still produce 10% of the FL transcript. There is another ESE in the mid-part of exon 7 that is recognized by a number of splicing factors

including Htra2-β1, which all promote the exon 7 inclusion and are responsible for the 10% FL transcript of the *SMN2* gene [206,215,224-226].

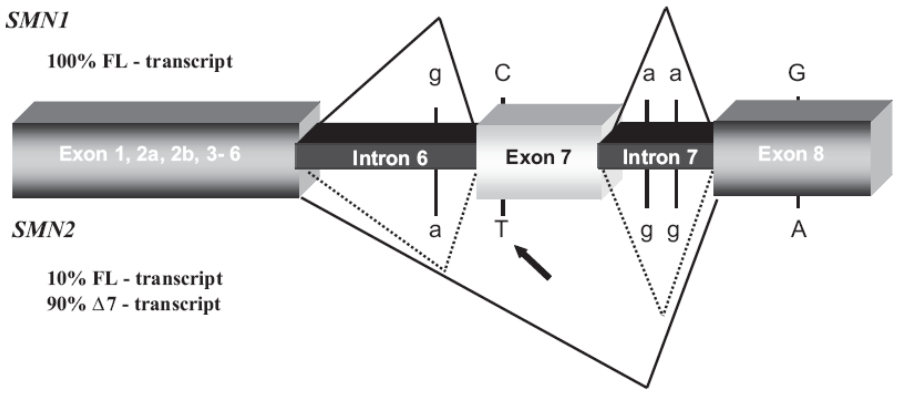

Figure 1-5: Differences between human SMN1 and SMN2 gene
The two copies differ only in 5 base pairs. Only the C-to-T transition in exon 7 (arrow) is responsible for the predominant deletion (90%) of exon 7 in the *SMN2* pre-mRNA. (Figure from Wirth, 2006 [206].)

1.4.1.2 The SMN protein

The protein structure of SMN is highly conserved between species [227-229]. SMN is a housekeeping gene that is essential for splicing. Therefore the SMN protein is expressed in all cell types and is found homogenously distributed in the cytoplasm and as dot-like clusters in the nucleus [230-232]. 100% of the *SMN1* and 10% of the *SMN2* genes encode for the FL transcript with 9 exons, which is translated into SMN protein. The SMN protein is composed of 294 amino acids and has a molecular weight of 38 kiloDalton (kDa).

Exon 2 encodes for a lysine rich (K-rich) protein domain close to the N-terminal end that is important to bind GEMIN2/SIP1 (SMN interacting protein 1) as well as for self-association [233,234]. Exon 5 and part of exon 6 encoded domains contain a proline-rich (P-rich) domain that may influence profilin binding [235]. The conserved YG box is in the C-terminal domain encoded by exon 6 and is important for SMN self-association [234,236]. Exon 7 encoded domains are essential for the oligomerization of SMN protein (Fig. 1-7). The amino acids that are normally encoded by exon 7 are lost in the truncated SMN2Δ7 protein and this results in instability of the SMN protein and leads to degradation of the monomers [237,238]. The SMN1 protein forms stable oligomers in vitro [239]. 90% of the SMA patients with homozygous deletion of SMN1 reveal absence of both exons 7 and 8, whereas about 10% show only homozygous deletion of exon 7 but not of exon 8 [206].

Exon 3 codes for a Tudor domain, a conserved motif of 50 amino acids that is found in several RNA associated proteins (Fig. 1-7). This domain binds to seven human Sm core proteins (B, D_{1-3}, E, F and G) which are essential for the assembly of spliceosomal uridine-rich small nuclear ribonucleoproteins (U snRNP) complexes [233,240-242] (Figure 1-8). Six

different U snRNPs are crucial for splicing by accomplishing the recognition of splice sites and removal of introns from preRNA in the nucleus. Each particle is composed of one of 6 different uridine-rich small nuclear RNAs (snRNA) (U1, U2, U4, U5, U11 and U12) and a heptameric ring of Sm proteins [243,244].

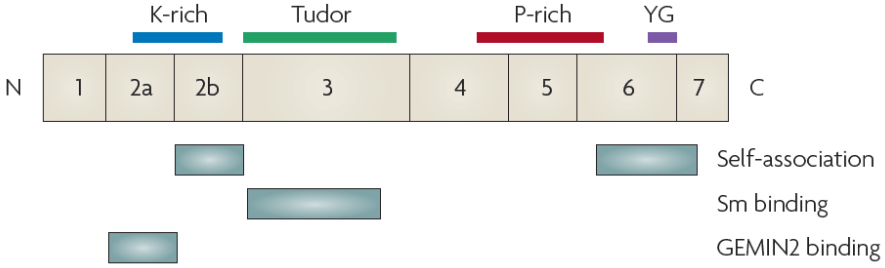

Figure 1-6 Exons and domains of SMN
Exon 2B encodes a domain that is important in GEMIN2 binding and for self-association [161]. The K domain is rich in lysine (K-rich), and exon 3 encodes for a Tudor domain that binds Sm proteins. Exon 5 and part of exon 6 contain a proline-rich (P-rich) domain that may influence profilin binding. The domain of exon 6 contains the conserved YG box and is important for self-association. Exon 8 is not displayed. (Figure from Burghes, 2009 [231].)

During snRNP assembly, Sm proteins are first bound and methylated in the cytoplasma by a complex consisting of the chloride conductance regulatory protein and the protein arginine methyltransferase 5 (pICln–PRMT5 complex) [245]. This complex transfers the Sm proteins to the SMN complex that consists of multiple SMN molecules (oligomer), Gemin 2-8 and UNR-interacting protein (UNRIP). Then the SMN complex facilitates the assembly of the Sm proteins onto the snRNA via its Tudor domain and 5´ cap hypermethylation of the snRNAs. Newly formed snRNPs which are still bound to the SMN complex are imported into the nucleus via snurportin and importin. In the nucleus snRNPs and the SMN complex localize to the Cajal body (CB) and the snRNPs undergo further maturation [206,215,231]. CBs are dynamic structures in the nucleus that consists of p80 coilin, SMN, snRNPs and play a role in splicing, histone mRNA 3´ maturation and pre-rRNA processing [246-248]. Other structures found in the nucleus that relate to the function of SMN and SMN complexes are the Gemini of coiled bodies (gems). They are indistinguishable in comparison to CB in size and shape, but they do not contain snRNPs and a high amount of SMN [230]. The number of gems and the amount of SMN is significantly reduced in SMA patients [249]. The loss of SMN protein correlates with the severity of the SMA disease. The most severe form of SMA (Type I) expresses less protein than the milder forms (Type II and III) in patients and mouse models [249-251].

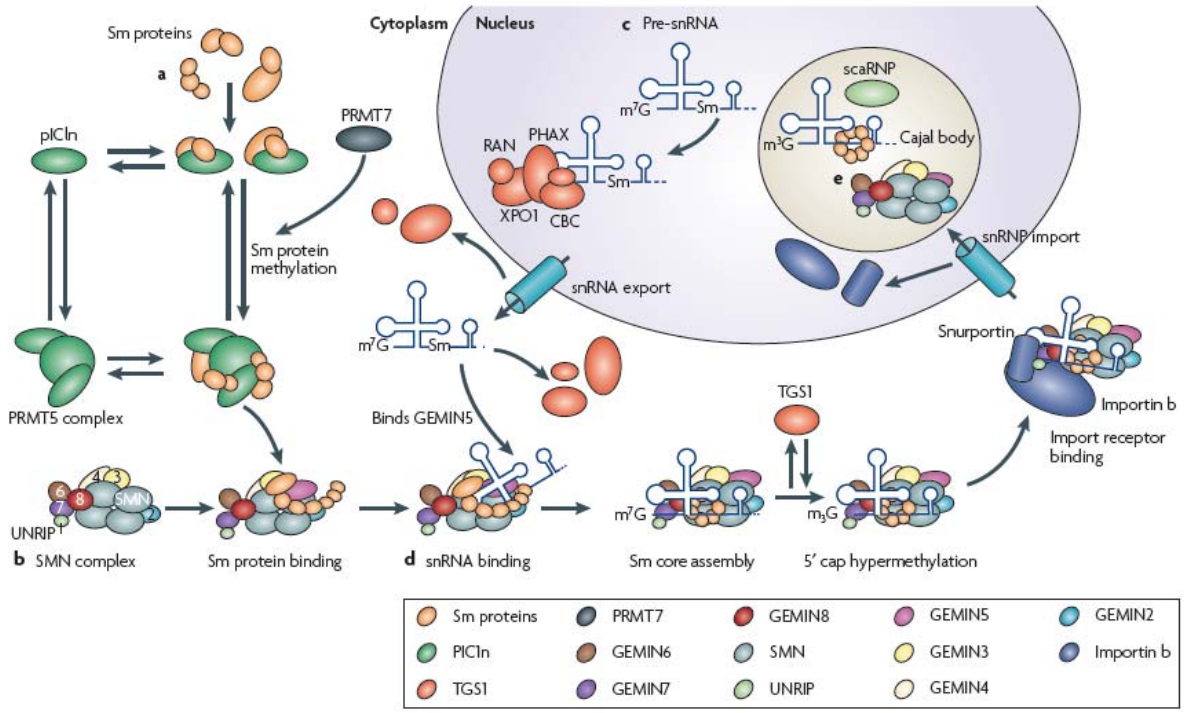

Figure 1-7: snRNP assembly is mediated by the SMN complex
(a) The Sm proteins are bound and methylated by pICln–PRMT5 complex. (b) This complex transfers the Sm proteins to the SMN complex. (c) The SMN complex facilitates the assembly of the Sm proteins onto the snRNA via its Tudor domain and 5′ cap hypermethylation of the snRNAs. (d) Newly formed snRNPs are transported to the nucleus, still bound to the SMN complex. Both localize to the Cajal body in the nucleus and snRNPs undergo further maturation (Figures from Burghes, 2009 [231].)

As mentioned above, SMN protein is needed for correct splicing in every cell. Surprisingly, only neurons are affected in SMA patients with lowered SMN protein levels. One hypothesis is that the decreased SMN level is still sufficient to assemble enough spliceosomes for correct splicing in non-neuronal cells. However, this level might not be sufficient in motoneurons because they belong to the largest cells in the body and have a higher rate of mRNA expression, processing and translation than other cell types. Therefore more spliceosomes may be needed [252]. Another hypothesis that could go along with the first one is that the SMN protein has an additional function. SMN can form a complex with heterogenous nuclear ribonucleoprotein R (hnRNP R), that can bind to the 3′ untranslated region (UTR) of the β-actin mRNA and supports its transport into the axons and growth cones [253,254]. A reduced number of β-actin mRNA and protein molecules was found in distal parts of the axon and in the growth cone in Smn-deficient motoneurons [253]. The reduced level of β-actin could lead to shortened axon outgrowth, reduced movement of the growth cone and impairment of synaptic vesicle release [255-257]. Reduced vesicle release results in distal-starting axonopathy including denervation of the NMJ that propagates proximally to the soma of the motoneurons in the spinal cord. Thus SMA is referred to as a dying-back motoneuron disease [258].

1.4.1.3 SMA mouse models

There exist several mouse models for SMA. The major difference between the human and murine genome in regard to SMA is the number of the *SMN* genes. Due to an evolutionarily late duplication of the *SMN* gene, only primates including humans possess two copies of *SMN* gene, *SMN1* and *SMN2* [259]. In contrast, the mouse genome contains only one copy (*Smn*), that is 81% identical to the human *SMN* gene [227,260]. A homozygous knockout of both murine *Smn* alleles ($Smn^{-/-}$) leads to embryonic lethality in the blastocyst stage, due to the lack of function in splicing [227]. In 2000, the human *SMN2* gene was introduced into mice lacking the murine *Smn* to mimic the genetics of the human SMA in mice [261,262]. These $Smn^{-/-}$ *SMN2* mice resemble the human severe form of SMA (Type I). Two copies of *SMN2* rescue the embryonic lethality, but they already show a 20% loss of motoneurons at postnatal day 1 (P1), that reaches a peak of 35% loss at P3-5 in the spinal cord and brainstem compared to controls, and death occurs within 5 days after birth [262]. An increment to eight copies of the *SMN2* in the *Smn* null background leads to complete amelioration of SMA disease symptoms [262]. Overexpression of SMN only in neurons rescues the loss of motoneurons and extends the survival of SMA mice, suggesting that the SMN produced by *SMN2* is sufficient for normal function in most tissues, but that motoneurons require higher levels [263]. It was also shown that an introduction of *SMNA2G* (an Ala-Gly mutation at position 2) into the Type I $Smn^{-/-}$ *SMN2* mice prolongs the survival from 5 to 227 days [264]. This mutation was found in SMA patients [265] and its protein is unable to efficiently self-associate, which is required for forming a functional SMN complex. Anyway, *SMN A2G* could associate with full-length SMN protein that serves as a scaffold and so could increase the number of functional complexes in this mouse model [264]. A similar mechanism might be possible in a mouse model that carries the SMN protein lacking exon 7 (SMNΔ7) also in a Type I $Smn^{-/-}$ *SMN2* background. SMNΔ7 is unstable and lacks the ability of self-association, but it can be stabilized by remaining a full-length protein and so increases the level of functional SMN complex and prolongs the survival from 5 to 14 days [266,267]. Another mouse model for the mild form of SMA Type III, $Smn^{+/-}$, was investigated in this thesis. While $Smn^{-/-}$ mice are embryonic lethal [227] and $Smn^{-/-}$ *SMN2* mice already show a 20% motoneuron loss at birth compared to controls [262], $Smn^{+/-}$ mice develop a progressive motoneuron loss starting after birth [141]. This resembles the disease progression of a mild form of human SMA. During development the Smn level clearly drops between P5 and P15 in wild type spinal cord and decreases even more during life span. Compared to control mice, the Smn level in $Smn^{+/-}$ mice is reduced by about 45% at embryonic stages and in adulthood. At birth, $Smn^{+/-}$ mice show no motoneuron loss in the

spinal cord. However, 40% of motoneurons degenerate during the first 6 months, and after 1 year as much as 54% have been lost. Furthermore, these mice develop a 23% loss of facial motoneurons between the fifth month and 1 year. Surprisingly, the mice show no clinical phenotype [141]. Therefore compensatory mechanisms must exist that prevent the muscle atrophy. Sprouting by neighbouring intact axons could be preventing the denervation of the NMJs.

1.4.2 Peripheral neuropathy

Neuropathy is a genus of peripheral nerve diseases. Neuropathies can be subdivided into several groups, whereas a certain disease can fit in more than one group. Peripheral neuropathies are classified according to the number of affected nerves or the affecting process (e.g., inflammation) or which types of nerve cell are affected (autonomic, sensory or motor nerves).

First of all, neuropathies can be distinguished into mononeuropathy, where only a single nerve is affected, or polyneuropathy, where many different nerves are involved. An inflammation of a single nerve would be a mononeuropathy, albeit that it also counts as part of another group, the inflammatory neuropathies. If the inflammation is caused by the patient's own immunsystem, the disease is termed autoimmune neuropathy (e.g., Chronic inflammatory demyelinating polyradiculoneuropathy (CIDP) or Guillain-Barré-Syndrome (GBS). If the primary cause is not identifiable, it is called idiopathic neuropathy. Depending which type of nerve cells are affected, the neuropathy can be classified as autonomic, motor or sensory [268].

A subtype of sensory neuropathy is the small-fiber neuropathy. Small somatic or autonomic fibers, or both, may be involved. Small somatic fibers include unmyelinated C fibers (diameter of about 1-1.6 µm) and thin myelinated A-delta fibers (1-5 µm in diameter). The slower conductive C fibers (2 m/s) mediate warmth perception, pain fibers respond to pressure and some chemical stimuli. The faster conductive A-delta (20 m/s) fibers carry touch, fast pain, cold, pressure, and cutaneous nociception [269]. Large fibers are myelinated and can include motor axons and the sensory axons responsible for vibration sense, proprioception and light touch [270]. Diabetes patients with predominantly small-fiber involvement show sharp burning, or shooting pain sensations whereas those with large-fiber peripheral neuropathy tend to experience numbness and tingling in the feet [271]. The most frequent neuropathy is the DNP caused by diabetes mellitus [272,273].

1.4.2.1 Diabetic neuropathy

DNP is a class of neurodegenerative disorders caused by diabetes mellitus. It is a group of diseases with different causes leading to high blood glucose. Two main forms of diabetes are: Type I diabetes, which mainly affects children and is characterized by the loss of insulin-producing beta cells in the pancreas. This leads to the lack of insulin which is normally essential for the uptake of glucose from the blood into the cells of liver, fat tissue and muscle where it is usually stored as glycogen. Type 2 diabetes, which results in an insulin resistance that could involve the insulin receptor, combined with relatively reduced insulin secretions. In 2000 at least 171 million (2.8%) people suffered from diabetes mellitus, whereas about 90% of the affected patients in the US and German population suffered from the Type 2 form [274-276]. Several metabolic changes in diabetes mellitus, such as chronic high blood sugar levels, abnormal blood fat, and neurovascular factors, lead to damage of blood vessels that supply neurons with oxygen and nutrients. This lack of essential supplies predisposes neurons to other disease factors and causes neuronal death, named DNPs. 60-70% of patients with diabetes show different forms of neuropathies. The symptoms can vary and affect autonomous, sensory and motor nerve fibers. In the peripheral nervous system the loss of sensory neurons first becomes apparent by pain sensitation and numbness. Motor failures often remain undiscovered in the beginning, but occur and get more severe over time. The nerve defects are revealed by electromyography (EMG) and nerve conduction studies [272]. Little is know about the cause of motor fiber degeneration in DNP. Because neurotrophic factors play a major role in regeneration and maintenance of motoneurons, it is feasible that their downregulation or inhibition could be a cause of large fiber degeneration in diabetic patients.

Patients with DNP show altered levels of IGF-1. IGF-1 is downregulated and can participate in the process of nerve degeneration (see *1.3.4 Insulin-like Growth Factor*) [181,277,278]. In STZ rodent model for diabetes a downregulation of IGF-1 and an upregulation of its binding protein IGFBP-5 was observed [192,193,279]. IGF-1 treatment improves peripheral nerve function in this diabetic animal model [181]. It is important to determine whether IGFBP-5 is elevated in patients with DNP and whether increased IGFBP-5 could inhibit the motoneuron survival-promoting effect of endogenous IGF-1.

1.5 Goals of the thesis

1.5.1 Sprouting as a potential compensatory mechanism in a mouse model for SMA

In a mouse model (*Smn*$^{-/-}$ *SMN2*) for the severe form of SMA (Type I), about 20% of motoneurons in the spinal cord are lost, which results in a strong muscular atrophy and death within 5 days of birth [262]. In contrast, the mouse model *Smn*$^{+/-}$ for a mild form of SMA (Type III) is characterized by a slow progressive loss of motoneurons starting after birth, culminating in 54% loss in one-year-old mice [141]. It is astonishing that this model shows no phenotype despite having a higher loss of motoneurons than the severe SMA model.

This indicates that motor function does not correlate with the loss of spinal motoneurons, and that compensatory mechanisms are active in milder forms of SMA but not in the severe forms. It might be that the slower progression of spinal motoneuron degeneration provides sufficient time for compensatory mechanisms to be effective. To get insight into possible compensatory mechanisms, the morphological architecture of the neuromuscular junction (NMJ) and the axonal branches in the gastrocnemius muscle of *Smn*$^{+/-}$ and *Smn*$^{+/+}$ mice were investigated. The gastrocnemius muscle, one of the biggest muscles in the body, is strongly affected in SMA and therefore a strong compensatory mechanism is needed. In patients with milder forms of the disease that normally reach adulthood, an enlargement of motor units is frequently observed.

For this reason, *Smn*$^{+/-}$ mice were analyzed electrophysiologically and histopathologically to characterize single motor units, NMJ architecture, and the route of the axonal branches.

A known compensatory mechanism is sprouting, a strategy to restore nerve–muscle connectivity, which can be induced by CNTF [107]. In order to characterize the role of this neurotrophic factor in this context, *Smn*$^{+/-}$ mice were crossbred with *Cntf*-deficient (*Cntf*$^{-/-}$) mice and the resulting double mutants were investigated to verify whether sprouting induced by CNTF could be a compensatory mechanism in a mouse model for mild SMA.

1.5.2 The role of IGF-1 and IGFBP-5 in the pathogenesis of diabetic neuropathy

Little is known about whether IGF-1 is necessary for motoneuron maintenance in adulthood, in particular under conditions when reduced IGF-1 signaling could play a role in the pathophysiology of motoneuron diseases and motor neuropathies. IGF-1 is a pluripotent growth and survival factor for a variety of cell types, including glial and neuronal cells. It supports the survival of motoneurons *in vitro* and *in vivo* [89,174,175]. It is known that the IGF-1 level and its receptor is downregulated in STZ rodents, a model for painful DNP [192,279]. In the

same model, an upregulation of IGFBP-5 in the rat eye was observed [193]. Our group found that IGFBP-5 levels are highly increased in nerve biopsies of patients with DNP. To confirm this result, more biopsies of patient were investigated by microarray and western blot analysis. To study the role of the IGF-1/IGFBP-5/IGF-1R system for maintenance of motor axons in adulthood our group established two transgenic mouse lines. In one of these models, IGFBP-5 is overexpressed in motoneurons under control of the neurofilament-light chain (NF-L) promoter. Furthermore, to test whether reduced availability of IGF-1 is responsible for the degeneration of motoneurons, mice were generated which feature an IGF-1R inactivation exclusively in motoneurons. These two models were investigated in terms of motoneuron degeneration to get a clearer insight of the role of IGF-1. In addition to that, cultured motoneurons were used to determine whether IGF-1 promotes survival that could be blocked by application of IGFBP-5. These investigations might give a better insight into the role of IGFBP-5 in the pathogenesis of motor axonopathy in DNP.

2 Material and Methods

2.1 Material

2.2.1 Devices

Device	Manufacturer
SDS polyacrylamide gel electrophoresis	Mini Protean Tetra Cell BioRad, Munich, Germany
Semi-dry western blot chamber	Trans-blot SD, Semi-dry transfer cell BioRad, Munich, Germany
Power supplies	Standard Power Pack P25 Powerpac HC 250V 3A 300W BioRad, Munich, Germany
Centrifuges	Centrifuge 5417R Centrifuge 5804R Centrifuge 5810R Eppendorf, Hamburg, Germany
Heat block	Thermomixer 5437 Thermomixer comfort Eppendorf, Hamburg, Germany
Thermocycler	Thermocycler personal Thermocycler gradient Eppendorf, Hamburg, Germany
Horizontal agarose gel electrophoresis chamber	PEQLAB Biotech. GMBH Erlangen, Germany
Cryostat	Modell CM 1950, Leica, Wetzlar, Germany
Confocal microscope	FluoView FV1000, Olympus, Hamburg TCS SP2, Leica, Wetzlar, Germany
X-ray developer	X-Omat 2000, Stuttgart, Germany
Tissue homogenizer for RNA	POLYTRON PT2100 Kinematica, Luzern, Switzerland
Photometer	BioPhotometer Eppendorf, Hamburg, Germany
Grip strength measurement	Digital Force Gauge DFL 2 Chatillon, Largo, Florida, USA
Tissue sonication for protein lysates	UP50H - Compact Lab Homogenizer Hielscher Ultrasound Technology Teltow, Germany
Nanodrop-Spektrophotometer	PEQLAB Biotech. GMBH Erlangen, Germany

Table 2-1: List of devices

2.2.2 Material for immunohistochemistry methods

Item	Manufacturer
Heparin	Heparin-Natrium 25000/5 ml Ratiopharm
Blocking buffer	10% BSA, 0.3% TritonX-100 in PBS
Phosphate buffer for PFA	Solution A: 0.2 M Na_2HPO_4 *2H_2O Solution B: 0.2 M NaH_2PO_4 *2H_2O
Fixative solution PFA	410 ml Solution A: 0.2 M Na_2HPO_4 * 2 H_2O 90 ml Solution B: 0.2 M NaH_2PO_4 * 2 H_2O 40 g PFA (Abcam) in 500 ml H_2O pH 7.4
Dehydration solution	30% Sucrose PBS 1x
PBS 1x	Dulbecco's PBS PAA Laboratories, A-Pasching pH 7.4
Postsynaptic marker	α-bungarotoxin Alexa Fluor 488,594 Molecular Probes, Eugene OR
Nucleus dye	4,6-diamidino-2-phenylindole dihydrochloride (DAPI) Stock 1 mg/ml

Table 2-2: Solutions and dyes for immunohistochemistry

Item	Manufacturer
Tissue mount DABCO	25 ml PBS, 0.625 ml DABCO 225 ml Glycerin
Tissue mount Mowiol	10% w/v Mowiol 40-88 25% v/v Glycerin 100 mM Tris(hydroxymethyl)aminomethane HCl pH 8
Tissue mount Aqua	Aqua Poly/Mount 18606 Polysciences, Warrington, PA, USA
Tissue mount frozen sections	O.C.T Mount medium Tissue Tek Sakura
Object slides 76 x 26 mm	R. Langenbrinck Emmendingen
Coverslips No. 1, 10 mm	Marienfeld GmbH & Co.KG Lauda-Königshofen
Wax pencil Liquid Blocker	Super Pap-Pen-Mini SCI Science Services, München

Table 2-3: Tissue mounting items

2.2.3 Antibodies

Antigen	Species	Dilution	Application	Reference
anti-neurofilament	rabbit	1:500	IF (muscle, nerve)	150 kD AB1981, Millipore
anti-neurofilament	mouse	1:500	IF (muscle, nerve)	SMI31R, Covance
anti-neurofilament	chicken	1:500	IF (muscle, nerve)	AB5539, Millipore
anti-CNTF (K10)	rabbit	1:250	IF (muscle, nerve)	made by Prof. Sendtner [114]
anti-S100B	mouse	1:350	IF (nerve)	S2532 beta-subunit, Sigma
anti-actin	mouse	1:5000	WB	MAB1501R Clone C4, Millipore
anti-IGFBP-5	rabbit	1:1000	WB	H100 sc-13093, Santa Cruz
anti-IGFBP-5	goat	1:5000	WB, IF (culture)	GT15183, Neuromics
anti-IGFBP-5	rabbit	1:200	IF	ab4255, Abcam
anti-tau	rabbit	1:1000	IF (cell culture)	T6402, Sigma
anti-laminin	rat	1:500	IF (nerves)	MAB1928, Millipore
anti-p75	mouse	1:2000	Panning	MLR2, monoclonal, Abcam

Table 2-4: Overview of primary antibodies

Antigen	Species	Dilution	Application	Reference
anti-rabbit-HRP	goat	1:10000	WB	JacksonImmunoresearch #111-035-003
anti-mouse-HRP	goat	1:10000	WB	JacksonImmunoresearch #115-035-003
anti-goat-HRP	donkey	1:10000	WB	JacksonImmunoresearch #705-035-147
anti-rabbit-FITC	swine	1:40	IF	F0205, Dako, Denmark
anti-rabbit-Cy2	goat	1:400	IF	JacksonImmunoresearch #111-225-003
anti-rabbit-Cy3	goat	1:400	IF	JacksonImmunoresearch #111-165-003
anti-rabbit-Cy5	goat	1:400	IF	JacksonImmunoresearch #111-175-003
anti-rabbit-Cy3	donkey	1:400	IF	JacksonImmunoresearch #711-165-152
anti-goat-Cy2	donkey	1:400	IF	JacksonImmunoresearch #705-225-003
anti-goat-Cy3	donkey	1:400	IF	JacksonImmunoresearch #705-165-003
anti-goat-Cy5	donkey	1:400	IF	JacksonImmunoresearch #705-175-003
anti-mouse-Alexa633 IgG1	goat	1:500	IF	A21126, Invitrogen
anti-mouse-Cy2	goat	1:400	IF	JacksonImmunoresearch #115-225-003
anti-mouse-Cy3	goat	1:400	IF	JacksonImmunoresearch #115-165-003
anti-mouse-Cy5	goat	1:400	IF	JacksonImmunoresearch #115-175-003
anti-chicken-Cy5	goat	1:400	IF	ab6569-100, Abcam
anti-chicken IgG DyLight 649	donkey	1:500	IF	JacksonImmunoresearch #703-495-155

Table 2-5: Overview of secondary antibodies

2.2.4 Histology

Item	Solution
Haemalum solution (Mayer's haematoxylin)	1 g Haematoxylin 0.2 g Sodium iodide 50 g Potassium alum 50 g Chloral hydrate 1 g Citric acid ad 1 l H_20
ATPase solution A	19.4 g Sodium acetate 29.4 g Sodium barbital ad 1 l H_2O
Acidic preincubation solution	200 ml Solution A 400 ml 0.1 M Hydrochloric acid 80 ml 8.5% NaCl pH 4.3
Main incubation solution	200 ml 0.1 M Sodium barbital solution 100 ml 0.18 M Calciumchloride ad 1 l H_20 pH 9.4
Main incubation solution with ATP	250 mg ATP in 100 ml Main incub. Solution
Cresyl violet	10 g Cresyl violet 100 ml Ethanol absolut ad 1 l aqua dest.
Vitro-Clud	Langenbrinck

Table 2-6: Histological solutions

2.2.5 Chemicals

Chemicals were supplied by Applichem (Darmstadt), Calbiochem (Darmstadt), Roth (Karlsruhe), Merck (Darmstadt), Serva (Heidelberg) and Sigma (München).

2.2.6 Material for proteinbiochemistry methods

Item	Composition
Lysis buffer	150 mM NaCl 1% Triton 2 mM EDTA 50 mM Tris pH 7,4 H_2O
Electrophoresis buffer 10x	30.3 g Trisbase 144 g Glycin 10 g SDS
Electrophoresis buffer 1x	100 ml Electrophoresis buffer 10x 900 ml H_2O
Transfer buffer 1x	700 ml H_2O 100 ml Electrophoresis buffer 10x 200 ml Methanol
Laemmli-SDS-PAGE-Loading buffer	100 mM Tris(hydroxymethyl)aminomethane HCl (pH6.8) 10% 2-β-Mercapto-Ethanol 4% SDS 20% Glycerin 0.2% Bromophenol blue
TBS buffer 10x	100 mM Tris(hydroxymethyl)aminomethane HCl(12.1g/l) 1.5 M NaCl (87.6 g/l) pH 8
TBST buffer 1x	900ml H_2O 100 ml TBS buffer 10x 10 ml 20% TWEEN20
Blocking buffer	5% milk powder in TBST

Table 2-7: List of buffers for proteinbiochemistry

Item	Manufacturer
Acrylamide	Rotiphorese Gel 30 (37.5:1) Roth, Karlsruhe
Protein Assay	BioRad Protein Assay BioRad, Munich
Tris-glycine SDS-Polyacrylamide Stacking gel 5%	30% Polyacrylamide 0.850 ml 1 M Tris(hydroxymethyl)aminomethane HCl (pH 6.8) 0.625 ml 10% Ammonium persulfate 0.05 ml 10% SDS 0.05 ml TEMED 0.005 ml H_2O 3.4 ml
Tris-glycine SDS-Polyacrylamide Separating gel 12%	30% Polyacrylamide 4 ml 1.5 M Tris(hydroxymethyl)aminomethane HCl (pH 8.8) 2.5 ml 10% Ammonium persulfate 0.1 ml 10% SDS 0.1 ml TEMED 0.004 ml H_2O 3.3 ml
Molecular protein ladder	PageRulerTM #SM0671 Prestained Protein Ladder Fermentas
Protease inhibitor	Complete Mini Roche Diagnostics, Mannheim
Phosphatase inhibitors	Phosphatase Inhibitor Cocktail 1 Sigma
Nitrocellulose transfer membrane	Protran Schleicher&Schüll
PVDF transfer membrane	Immun-Blot PVDF Membrane (0.2 µm) 26 cm x 3.3 m BioRad Hercules CA 94547
Blot paper	Extra Thick Blot Paper Criterion size (8.6 x 13.5 cm) BioRad Hercules CA 94547
Detection kit	ECL (normal and Plus) Western blotting detection reagents GE Healthcare UK Limited
X-ray cassette	Suprema 13 x 18 cm Dr. Goos
X-ray films	Super RX 13 x 18 cm Fuji Film

Table 2-8: Items for proteinbiochemistry methods

2.2.7 Material for molecular methods

Item	Manufacturer
Lysispuffer	10 ml 5 M NaCl 25 ml 10% Sarcosyl solution 25 g Chelex ad 500 ml Aqua bidest
dNTPs	dNTP Set 100 mM Gene Craft Germany
Enhancer	5 x TaqMaster PCR Enhancer 5′ Prime, Hamburg
Taq polymerase	5′ Prime, Hamburg
50 x TAE	2 M Tris(hydroxymethyl)aminomethane 25 mM Sodium acetate 50 mM Ethylenediaminetetraacetate
6 x Loading buffer	30% Glycerin 0.15% Bromophenol blue 0.15% Xylene cyanol 1x TAE
Ethidium bromide solution	10 µg/ml Merck, Darmstadt, Germany
Tail lysis buffer	2 M Tris(hydroxymethyl)aminomethane HCl pH 7.5 100 mM Ethylenediaminetetraacetate 150 mM Sodium chloride 0.5% SDS 10 mg/ml Proteinase K
TE buffer	10 mM Tris(hydroxymethyl)aminomethane HCl pH 7.5 1mM Ethylenediaminetetraacetate
Reverse Transcriptase Kit	SuperScript III First-Strand Synthesis Invitrogen, Carslbad, CA 92008 USA
RNA purification solution	TRIzol Reagent Invitrogen, Carslbad, CA 92008 USA
Betaine 5 M	Betaine solution 5 M, PCR reagent Sigma-Aldrich, Munich, Germany
Bromophenol blue	B0126 Sigma-Aldrich, Munich, Germany
Aqua bidest, steril/ad iniectabilia	DeltaSelect, Pfullingen, Germany
DNA size standards	GeneRulerTM 100 bp DNA Ladder GeneRulerTM 100 bp plus DNA Ladder GeneRulerTM 1 kb DNA Ladder MBI-Fermentas, St.Leon-Roth
DEPC water	0.1 ml Diethylpyrocarbonate in 100 ml H_2O

Table 2-9: Items for molecular methods

PCR	Line	Primer name	Primer sequence
Smn genotyping	26	SMN GMS 11	GGC CTG GAA TTC AAT ATG CTA GAC TGG CC
		SMN MSMN 11	GTT TCA AGG GAG TTG TGG CAT TCT TC
		SMN GNA 3ab	CAA GGC GAT TAA GTT GGG TAA CG
Cntf genotyping	33	CNTF E1S	GAG CAA TCA CCT CTG ACC CTT
		CNTF/1A	CAG GCT GGA TGA AGA CAG TAA G
		5′NEO	AGC CGA TTG TCT GTT GTG CCC
IGFBP-5 genotyping	61	NFL-SEQ	TCG CAG GCT GCG TCA GGA G
		BP5PCR	CTT GCA GGT AGA GCA GGT GCT CTC
Floxed IGF-1-R genotyping	64	Rec Seq	CTA CTA GTT CAT GCC CAG AGC CCA
		X3 Seq	CAG GAG TGT CCC TCA GGC TCC ATC
NF-L-Cre genotyping	64	NFL-SEQ	TCG CAG GCT GCG TCA GGA G
		pMC-Cre	GGT ATG CTC AGA AAA CGC C
RT-PCR IGF-R	64	Forwardpr4	GGATGCGGTGTCCAATAACT
		Reversepr4	CTCCGTTGTTCCTGGTGTTT
Real-time PCR IGFBP-5	61	ForwardIGFBP	CAAGAGAAAGCAGTGTAAGCC
		ReverseIGFBP	CACTCAACGTT ACTGCTGTC
β-actin		ForwardprAktin	GCCAACCGTGAAAAGATGAC
		ReverseprAktin	GGCGTGAGGGAGAGCATAG

Table 2-10: Primer sequences

2.2.8 Material for motoneuron culture

Item	Manufacturer
Hank's balanced salt solution (HBSS)	Invitrogen
Trypsin	Worthington
Trypsin inhibitor	Sigma
Neurobasal	Invitrogen
Falcon	Greiner
B27 Serum-Supplement	Invitrogen
Boric acid	AppliChem
Coverslips	Ø 10 mm, Ø 22mm, Saur
Falcon tubes	15 ml, 50 ml, Greiner
Horse Serum	Linaris
Laminin-221	Invitrogen
L-Alanyl-L-Glutamin (Glutamax)	Invitrogen
poly-D, L-Ornithin	Sigma-Aldrich
Dishes	24-well dish, 6-well dish, Nunclon

Table 2-11: Items for motoneuron culture

Solutions	Composition
Depolarization solution	30 mM KCl
	0.8% NaCl
	Aqua bidest
Panning solution	Anti-p75 antibody (1:2000)
	10 mM TRIS buffer (pH 9.5)
Boratpuffer (pH 8.3)	0.15 M Borsäure
	Aqua bidest
Laminin solution	Laminin-221 2.5 µg/ml
	HBSS
Motoneuron medium	Neurobasal
	10% Horse serum
	500 µM Glutamax
	2% B27 Supplement
Neurobasal medium (NB-Medium)	500 µM Glutamax
	Neurobasal
100x PORN	500 mg poly-D, L-Ornithin
	10 ml 0.15M Boratpuffer (pH 8.3)
1x PORN	500 µl 100x PORN
	50 ml 0.15 M Boratpuffer (pH 8.3)
1% Trypsin solution	1 g Trypsin in 100 ml HBSS: HEPES (40:1)
	HEPES: 1M, pH 7.3; sterile filtration
0.1% Trypsin inhibitor solution	500 mg TI in 49 ml HBSS + 1 ml HEPES (1M) Sterile filtration

Table 2-12: Solutions for motoneuron culture

Neurotrophic factors / Inhibitors	Concentration	Reference
BDNF	5 ng/ml	Professor Sendtner, Würzburg
IGF-1	1/5 ng/ml	human IGF-1, PeProTech
CNTF	1 ng/ml	Professor Sendtner, Würzburg
Recombinant mouse IGFBP-5	5 ng/ml	FAC-BP5DU020, GroPep, Adelaide, Australia

Table 2-13: Neurotrophic factors and IGFBP-5 in motoneuron culture

2.2 Methods

2.2.1 Animal husbandry

The mice used in this study had been backcrossed at least 5 times to C57Bl/6 mice, and subsequently every third generation in order to maintain them on a clean C57Bl/6 background. They were housed in the central animal facilities of the University of Wuerzburg. The animal care and ethic committees of our institutions approved all described procedures and experiments. All laboratory animals were kept in an artificial 12 h / 12 h day-night-rhythm with free access to forage and water at a temperature at 21 ± 1 °C and 50-60% humidity.

2.2.2 Immunohistochemistry and microscopy

2.2.2.1 Preparation of the gastrocnemius muscle for immunohistochemistry

Mice were anesthetized by CO_2 and killed by cervical dislocation. The skin of the hindlimbs and the connective tissue around the calf (gastrocnemius muscle) were removed. The native gastrocnemius muscle was dissected by cutting the tendon and detaching it from the bone. For wholemount stainings the native dissected gastrocnemius muscle was placed on a cover slip. It was immediately covered with 4% paraformaldehyde (PFA) in phosphate-buffered saline (Dulbecco's PBS 1x from PAA) and mechanically squeezed by a second cover slip for 5 minutes.

2.2.2.2 Wholemount staining of the gastrocnemius muscle in thy1-YFP-H^{tg} mice

The flattened gastrocnemius muscles from adult *Smn*$^{+/+}$ *thy*1-*YFP-H*^{tg} and *Smn*$^{+/-}$ *thy*1-*YFP-H*^{tg} mice were fixed with 4% PFA for 2 hours. After fixation of the gastrocnemius muscles, they were washed in 1x PBS and 0.5% Triton X-100 (Sigma) two times for 30 minutes. YFP is expressed in less than 10% of the motoneurons and their axonal processes in *thy*1-*YFP-H*^{tg} mice [280]. The postsynaptic part of neuromuscular endplates was stained with α-bungarotoxin Alexa Fluor 594 (1:500, Molecular Probes) for 30 minutes. The tissue was then washed in 1x PBS for 2 hours. Finally the tissue was mounted with a DABCO-solution (9.97% PBS, 89.77% Glycerin and 0.26% DABCO). Pictures were taken with the SP2 confocal microscope from Leica, and an Olympus FluoView™ FV1000 confocal microscope with 3 channel detectors. For quantification of the enhanced arborization in the upper medial branch of the

tibial nerve, we traced individual axons back from neuromuscular endplates to the trunk of the nerve and counted the number of branching points.

2.2.2.3 Wholemount staining of the gastrocnemius muscle with neurofilament

The flattened gastrocnemius muscles of *Smn*$^{+/+}$, *Smn*$^{+/-}$, *Cntf* $^{-/-}$, and *Smn*$^{+/-}$ *Cntf*$^{-/-}$ mice were fixed in 4% PFA for 2 hours. After washing with 1x PBS and 1% Triton X-100 two times for 30 minutes, the postsynaptic part of neuromuscular endplates was stained with α-bungarotoxin Alexa Fluor 594 (1:500) in 1x PBS and 1% Triton X-100 for 30 minutes. Subsequently, the tissue was washed in 1x PBS and 1% Triton X-100 for 2 hours, and a blocking solution containing 3% bovine serum albumin (BSA, Sigma) and 5% Triton X-100 to penetrate into the thick muscles was applied for 4 hours. Rabbit anti-neurofilament antibodies (150 kDa AB1981, Chemicon) were diluted 1:350 in the blocking solution and applied overnight at 4°C. Thereafter the muscles were washed three times for 30 minutes in 1x PBS and 1% Triton X-100. As second antibody, swine anti-rabbit FITC (1:40, Dako) was diluted in the blocking solution and applied for 4 hours at room temperature. Finally, the tissue was washed three times in 1x PBS and 1% Triton X-100 for 30 minutes and mounted with DABCO. The pictures were taken with an Olympus FluoView™ FV1000 microscope. For 3D reconstruction, 2D confocal stacks were saved in an Olympus.oib format and opened in Bitplane Imaris 5.7.0 Software supplied by Olympus. An isosurface was generated with a Gaussian filter width of 0.3 µm. Sprouting events were defined as one axon innervating two neighboring endplates.

2.2.2.4 Staining and teasing of single muscle fibers

The native gastrocnemius muscles of *Smn*$^{+/+}$, *Smn*$^{+/-}$, *Cntf* $^{-/-}$, and *Smn*$^{+/-}$ *Cntf*$^{-/-}$ mice were fixed in 4% PFA for 20 min. Subsequently the muscle was teased into single muscle fibers using forceps and washed for 30 min with PBS with 0.1 M glycine to block reactive aldehyde groups. α-bungarotoxin Alexa Fluor 594 (1:500) in 1x PBS for 20 minutes was applied to stain the postsynaptic part of neuromuscular endplates. After washing 20 min with PBS, the fibers were permeablized with icecold methanol for 2 min at –20 °C. The fibers were washed with PBS for 20 minutes and blocked for 1 hour with 10% BSA and 0.3% Triton-X100 in PBS. Rabbit anti-neurofilament antibodies (150 kDa AB1981, Chemicon) were diluted 1:350 in the blocking solution and applied overnight at 4°C. Thereafter the muscle fibers were washed three times for 10 minutes in 1x PBS and the second antibody, swine anti-rabbit FITC

(1:40, Dako), was diluted in the blocking solution and applied for 1 hour at room temperature. Finally, the tissue was washed three times in 1x PBS for 10 minutes and mounted with DABCO/Aqua Poly/Mount and the pictures were taken with an Olympus FluoView™ FV1000 microscope. The area of the postsynaptic part of a NMJ was measured by surrounding α-bungarotoxin signal by using ImageJ.

2.2.2.5 Preparation and staining of cryostat slices of muscle and nerve

Mice were anesthetized with CO_2 and the thoracic cavity was opened to expose the heart. The perfusions needle was inserted into the left ventricle and the right atrium was cut to allow the efflux of the perfusate. First the blood was washed out with 0.4% heparine in 1x PBS solution and then the mice were perfused with a 4% PFA solution. After perfusion the gastrocnemius muscles and sciatic nerves were prepared. The murine tissues and the human sural nerves were postfixed for 24 h in 4% PFA at 4°C. The nerves were then transferred into buffer with increasing (10%-30%) sucrose content. After the tissue was submerged in the 30% sucrose solution, it was embedded in Tissue Tek (Sakura) and frozen within 2-methylbutane cooled with liquid N_2. Subsequently, the gastrocnemius muscles were cut in 100 µm-thick longitudinal sections and the nerves in 10 µm thick cross-sections with the cryostat and placed on gelatinized cover slides. For immunostaining, the sections were blocked with 10% BSA and 0.3% Triton X-100 in 1x PBS for 1 hour. The first and second antibodies were diluted in blocking solution. The gastrocnemius muscles were stained with α-bungarotoxin Alexa Fluor 594 (1:500), mouse anti-neurofilament (1:350, SMI31R, Covance) and rabbit anti-CNTF (K10, 1:1000) [114] solution, whereas the sciatic nerves were stained with mouse anti-S100 (1:350, beta-subunit, Sigma), rabbit anti-CNTF, rabbit anti-IGFBP-5 (ab4255, 1:200, Abcam) and rat anti-laminin B1 (MAB1928, 1:500, Millipore). The human nerves were stained with mouse anti-neurofilament (1:500, SMI31R, Covance) and rabbit anti-IGFBP-5 (ab4255, 1:200, Abcam). After washing three times per 10 minutes, secondary antibodies were applied in blocking solution for 1 hour. Cy5 goat anti-mouse (1:200, Jackson Immuno) or Alexa Fluor 633 goat anti-mouse IgG1 (A21126, 1:500, Invitrogen) and swine anti-rabbit FITC (1:350, Dako) were used for the muscles. Cy3 goat anti-mouse (1:200, Jackson Immuno), Alexa Fluor 633 goat anti-mouse IgG1 (A21126, 1:500, Invitrogen), donkey Cy3 anti-rat (712-165-150, 1:600, Jackson ImmunoResearch Laboratories, Inc) and swine anti-rabbit FITC were used for the nerves. Finally, the tissue was washed three times for 10 minutes and mounted in DABCO or Aqua Poly/Mount, and investigated with the Olympus FluoView™ FV1000 microscope. For a 3D reconstruction, 2D confocal stacks were saved in an Olympus.oib format and opened

in Bitplane Imaris 5.7.0 Software supplied by Olympus. An isosurface was generated with a Gaussian filter width of 0.3 µm.

2.2.3 Muscle strength tests in mice

Grip strength measurement on forelimbs was performed with a Digital Force Gauge DFL 2 from Chatillon with every mouse tested at least 10 times, and the mean was taken [114]. All tests were done blindly. In detail, the animals were placed on a platform and allowed to grasp a triangular formed wire with their forelimbs. Then they were pulled away by their tails until the grip was broken, while the hindlimbs were not in contact with the ground. The grip strength was measured in newtons with a computerized electronic pull strain gauge which was directly fitted to the grasping ring.

2.2.4 Histology

2.2.4.1 Myosin ATPase reaction and muscle fiber typing

The gastrocnemius muscle was freshly prepared from mice after cervical dislocation and frozen immediately in nitrogen-cooled 2-methylbutane. ATPase staining was performed on 10 µm-thick cryosections on a slide under acidic pH 4.3 conditions. First, slides were incubated in the preincubation solution pH 4.3 at room temperature for 5 minutes. Then they were washed with the main incubation solution 9.4 (without ATP) to balance the pH. After adding the main incubation solution 9.4 with ATP, the slides were placed in the incubator at 37 °C for 45 minutes. Afterwards the samples were consecutively incubated with 1% calcium chloride solution for 10 minutes (changing the solution twice in the meantime), 2% cobalt chloride solution for 3 miuntes and 0.01 M sodium barbital solution for 10 minutes (changing the solution twice in the meantime) at room temperature. The slides were washed once with faucet water and treated with 1% ammonium sulphide in aqua dest for 45 seconds under the laboratory hood. Then they were rinsed with faucet water and dehydrated in an isopropyl alcohol series starting with 70%. Finally the slides were incubated with xylol twice for 5 minutes and mounted with Vitro-Clud. Data presented in this study are from reactions at pH 4.3. Type I (slow twitch) muscle fibers are resistant to acidic conditions and show ATPase activity and therefore stain dark. Type 2 (A and B) fibers are not resistant and do not stain. Type 2C fibers show intermediate (grey color) staining.

2.2.4.2 HE staining and quantification of muscle fiber size

The muscle was prepared from mice immediately after cervical dislocation and freshly frozen in nitrogen-cooled 2-methylbutane. 10 µm-thick cryosections were prepared and stained with a standard HE protocol. To do so, the sections were dried for 30 minutes and stained with haemalum (Mayer's haematoxylin) solution for 10 minutes. Afterwards the samples were rinsed under flaucet water, and 1% eosin with 3 drops of 100% acetic acid was added for 25 seconds. Increasing ethanol series (70%, 96%, 100%) were added 3 times for 2 minutes each and xylol was applied twice for 10 minutes each. Finally the sections were mounted with Vitro-Clud. The caliber of 150 muscle fibers per muscle biopsy and animal were analyzed. The muscle fibers with a caliber higher than 150% of the mean were determined as hypertrophic fibers, whereas hypotrophic fibers have a caliber less than 50% of the mean caliber [281].

2.2.4.3 Nissl staining and quantification of spinal cord sections

Mice were deeply anaesthetized and transcardially perfused with 4% PFA. 12.5 µm paraffin serial sections of the spinal cord were prepared for Nissl staining as followed [282]. First the sections were postfixed overnight, washed 3 times for 10 minutes with PBS afterwards and placed into molds. These were washed in water for 10 minutes and put into an embedding machine which first dehydrates the section with an increasing ethanol series and then coats them with paraffin (program C, 660 minutes). The next day, the sections were covered with hot paraffin in new molds. As soon as the paraffin blocks had cooled off, they were trimmed and cut by the microtome. Then the sections were dried at 37 °C overnight and incubated in xylol twice for 10 minutes. Subsequently the sections were treated with the following steps for 2 minutes each: 100% isopropyl alcohol, 100% ethanol, 100% ethanol, 96% ethanol, 96% ethanol, 90% ethanol, 80% ethanol, 70% ethanol, 70% ethanol. Cresyl violet (Nissl staining) was added to the sections for 10 minutes following another alcohol series (short: 96% ethanol with acetic acid (3.5 ml/200 ml ethanol), 96% ethanol, 100% ethanol, 100% isopropyl alcohol). Finally the sections were placed in xylol and mounted with Tissue Mount. Cresyl violet stains acidic structures within cells intensively, and thus makes the nucleolus and the rough endoplasmatic reticulum visible. Motoneurons differ from other types of neurons in the spinal cord in having a distinct nucleolus and a prominent rough endoplasmatic reticulum, particularly the interneurons. Even atrophy motoneurons can be clearly distinguished by this technique, as previously shown in *Cntf/Lif/Ct-1* triple deficient mice [118], *bcl-2* deficient mice [283] and *Smn*$^{-/-}$*SMN2tg* mice, a mouse model of type I SMA[262]. Only motoneurons with a

clearly distinguishable nucleolus and a Nissl-stained rough endoplasmatic reticulum-like structure in the cell body were counted in every 10th section of the lumbar spinal cord (L1–L7). Raw counts were corrected for double-counting of split nucleoli as described [114].

2.2.4.4 *Quantitative morphometry on cross-sections of the sciatic nerve*

The perfusion and sectioning was performed by Dr. Bettina Holtmann and Dr. Massimiliano Braga. Briefly, 0.1 M cacodylate buffers containing 4% PFA and 2% glutaraldehyde were used for perfusion. The proximal part of the sciatic was then dissected and postfixed in the same fixative overnight. After osmification and dehydration, all samples were embedded in Spurr's medium. Semithin (1 µm) cross-sections for light microscopic examination were cut with a diamond knife on an ultramicrotome. Sections were stained with azur-methylenblue for histomorphological analysis and subsequent morphometric evaluation. Myelin thickness was divided by axon diameter for M-ratio calculations [284]. At least 150 M-ratios and circumferences per nerve were measured in at least 3 individuals per group.

2.2.5 Human sural biopsies

Sural nerve biopsies were obtained by collaboration with Prof. Dr. Claudia Sommer. The biopsies were taken from the neuropathology archive of the Neuromuscular pathology labs at the Department of Neurology, Wuerzburg. All patients had sural nerve biopsies for diagnostic reasons and had given informed consent for their biopsy material to be included in upcoming research projects with their names kept anonymously. This procedure and the consent form had been approved by the Medical School Ethics Committee.

A total of 27 biopsies were included in this study: 22 patients and 5 controls (see Table 3-2-1 for demographic and clinical data). Diabetic neuropathy (DNP, n = 6, 1 type I, 5 type II) was diagnosed when diabetes mellitus was present according to established criteria [285]. Chronic inflammatory demyelinating polyradiculoneuropathy (CIDP, n = 9) was diagnosed by INCAT criteria [286] for CIDP. As disease controls, samples from three patients with a non-diabetic neuropathy were included (vitamin B12 deficiency, SMA and ALS with mild axonal neuropathy). Normal controls were obtained from the Pathology and Forensic Medicine departments (n = 3) and from two patients in whom chronic motor neuropathy had been suspected, but sensory nerve involvement was deemed unlikely due to the completely normal appearance of sural nerve biopsy (n = 2).

2.2.6 Protein biochemistry

2.2.6.1 Preparation of tissue lysates

The mice were anesthetized by CO_2. After perfusion with 0.4% heparin in PBS solution, the tissues were dissected and transferred in a reaction tube into liquid nitrogen. Afterwards the frozen tissues were dispersed in a lysis buffer by sonication (intensity = 100%, 5 sec., 5 min. on ice, 3 times). 2 µl of the lysates were used for protein concentration measurement and the rest of the lysates were stored at –20 °C.

2.2.6.2 Measurement of protein concentration

The BioRad protein assay was performed to measure the protein concentration of the tissue lysates. This assay is based on the Bradford method, where Coomassie® Brilliant Blue G-250 binds to proteins under acidic conditions [287]. This leads to a color change from brown to blue in lysates and the optical density of blue color was measured by photometer (600 nm).

Protein samples

Tissue lysate [µl]	2
H_2O [µl]	98
1x Bio-Rad Protein assay [µl]	900

Table 2.14: Composition of protein samples for Bradford protein measurement

A calibration curve was generated by measuring the optical density from known protein concentrations to determine the protein amount of the samples.

Calculation curve

Protein amount [µg]	**0**	**2**	**4**	**6**	**8**	**10**	**12**
BSA (100ng/µl) [µl]	0	20	40	60	80	100	120
Lysis buffer [µl]	2	2	2	2	2	2	2
H_2O [µl]	98	78	58	38	18	0	0
1x Bio-Rad Protein assay [µl]	900	900	900	900	900	900	900

Table 2.15: Calculation curve for Bradford protein measurement

2.2.6.3 Sodium dodecyl sulfate polyacrylamide gel electrophoresis (SDS-PAGE)

The proteins of each lysate were separated on a sodium dodecyl sulfate polyacrylamide gel electro-phoresis (SDS-PAGE) under denaturating conditions. First, a laemmli buffer was added to the lysates containing 30µg proteins and heated to 99 °C for 5 minutes. The laemmli buffer contains SDS and β-mercaptoethanol to denature, negatively charge the proteins and

reduce disulfide bonds. These samples were loaded on a 1 mm-thick SDS-PAGE gel which consists of a 5% stacking and a 12% separating gel. The negatively charged proteins move towards the positive pole and get separated by their molecular weight which determines the migration velocity in the gel of each protein. The SDS PAGE ran at 18 mA per gel for 2 hours.

2.2.6.4 Western Blot

The transfer of the proteins from the gel to a PVDF transfer membrane was done by the semi-dry blotting technique. First the PVDF transfer membrane was activated by a methanol bath and then transferred into TBST. A blot paper was placed on the anode of a semi-dry western blot chamber, followed by the activated PVDF transfer membrane and covered with another blot paper. After the cathode plate was connected, the semi-dry western blot chamber ran at 0.32 A and 20 V for 40 min per gel.

2.2.6.5 Protein immunodetection and quantification

After blotting, the membrane was transferred into a blocking buffer consisting of Tris-buffered saline (10 mM Tris, 0.15 M NaCl, pH 8) with 0.02% Tween20 and 5% skimmed milk. Overnight at 4 °C, the membrane was probed in a blocking buffer with a rabbit anti-IGFBP-5 (H-100, 1:5000, Santa Cruz biotechnology, Inc.) for human lysates, goat anti-IGFBP-5 antibody (GT15183, 1:5,000, Neuromics) for mouse lysates and mouse anti-actin antibody (Clone C4, 1:7,000, Millipore) as loading control. The blots were subsequently washed three times for 10 min in TBST buffer and incubated with a horseradish peroxidase (HRP)-coupled goat anti-rabbit, goat anti-mouse or donkey anti-goat antibody (1:10,000, Jackson ImmunoResearch Laboratories, Inc.) for 1 h. The blots were again washed three times and detection was performed with the ECL Plus Western Blotting Detection System (RPN2132, GE Healthcare, Lifesciences) according to the manufacturer's protocol (5 min incubation). The chemiluminescent detection reagents are based on the oxidation of the luminal (1, 2) catalyzed by peroxide and horseradish peroxidase. After incubation the ECL Plus was removed and the blots were exposed to X-ray films for periods ranging from 10sec to 10min. The X-ray films were developed by X-Omat 2000. Film images were scanned and the intensity of the IGFBP-5 was measured with Raytest AIDA Software and standardized to mouse anti-actin. A minimum of n = 3 per group were tested in 3 independent experiments

and the mean of each group was normalized to the control group (if not stated differently) which was assigned as 1.

2.2.7 Molecular biology

2.2.7.1 Extraction of genomic DNA

Mouse tail biopsies of three-week-old mice were dispersed in a 200µl lysis buffer plus 15 µl proteinase K at 55° C for 2 hours. Afterwards the samples were heated to 100° C for 8 minutes and centrifuged for 5 minutes at 14,000 rpm. 100 µl of the supernatant was transferred to a new reaction tube.

2.2.7.2 Polymerase chain reaction (PCR)

The polymerase chain reaction (PCR) is a technique invented by Kary Mullis to multiply a particular DNA sequence into millions of copies. This technique is the basis of several applications in medicine and biology, such as diagnosis of hereditary diseases, DNA cloning, identification of genetic fingerprints and mice genotyping. The PCR consists of several steps. An initial denturation step separates the double-stranded DNA (~10-500 µg) into single-stranded templates at a high temperature (94 °C) to allow the annealing of primers. Primers are specific short nucleotide sequences (18-30 nucleotides, final concentration = 200 nM), which bind complementarily to the 3′ ends of the target DNA fragment to be amplified. The optimal annealing temperature is adjusted to the melting temperature of the primers and depends mainly on the guanidine-cytosin content of the primer sequence ranging from 50 to 65 °C. The elongation step at 72 °C follows next. Here a temperature-resistant DNA Tag polymerase (final concentration = 0.05-0.1 units) synthesizes a new DNA strand by adding a complementary deoxyribonucleotide (dNTP, final concentration = 200 µM) to the template strand in the 5′-3′ direction. DNA polymerase requires a magnesium chloride concentration of 1.5 mM to work properly. Other substances can be added to optimize the PCR reation, such as an enhancer which impoves processivity and thermo stability of the Tag polymerase, or betaine which equalizes the contribution of GC- and AT-base pairing. These three steps are repeated for 20-40 cycles. During each cycle the amount of amplified sequence doubles and therefore shows exponential amplification [288,289].

2.2.7.3 Gel electrophoresis

Gel electrophoresis uses an electric field to separate DNA fragments by their molecular weight within a gel consisting of 1%-2% agarose in 1x TAE. The negatively charged DNA fragments move towards the anode according to their size. The smallest fragments run the fastest, whereas the highest bands display the largest fragments in the gel. The DNA intercalating dye ethidium bromide (0.4 mg/ml) was added to the gels to detect the fragments under an ultraviolet light.

2.2.7.4 Mice genotyping

Genotyping is a procedure based on PCR and follows gel electrophoresis. It is used to determine the genotype of an individual mouse. By using specific primer pairs the genotype of a certain gene can be investigated. All gel electrophoreses were run with a 1.5% agarose gel in 1X TAE buffer at 120 V for 45 minutes.

2.2.7.4.1 Smn genotyping

A wild-type (primers: SMN GMS 11 and SMN MSMN 11) and a knockout PCR approach (primers: SMN GMS 11 and SMN GNA 3ab) were performed separately for *Smn* genotyping. The expected size of the wild-type product is 800 base pairs and the knockout band has 600 base pairs.

Components	Volume in [µl]	Final concentration
DNA template	1	~ 10-500 µg
10X PCR-Puffer (15 mM $MgCl_2$)	5	1.5 mM $MgCl_2$
dNTP-Mix [10 mM]	1	200 µM
Taq DNA-Polymerase [5 U/µl]	0.4	0.04 units
Forward-Primer [10 µM]	1	200 nM
Reverse-Primer [10 µM]	1	200 nM
ddH_2O	40.6	
Total volume	50	

Table 2-16: PCR protocol for *Smn* genotpying

Steps	Temperature [°C]	Duration [minutes]
Initial denaturation	94	3
Denaturation	94	0.5
Annealing	55	0.5
Elongation	72	1.5
Terminal elongation	72	5
Hold	15	∞

Table 2-17: PCR program for *Smn* genotyping.
The double bars show the beginning and end of a cycle (34 cycles).

2.2.7.4.2 Cntf genotyping

A wild-type (primers: CNTF E1S and CNTF/1A) and a knockout PCR approach (primers: CNTF E1S and 5′NEO) were performed separately for *Cntf* genotyping. Expected size of the wild-type product is 321 base pairs and the knockout band has 450 base pairs.

Components	Volume in [µl]	Final concentration
DNA template	1	~ 10-500 µg
10X PCR-Puffer (15 mM $MgCl_2$)	3	1.5 mM $MgCl_2$
dNTP-Mix [10 mM]	0.6	200 µM
Taq DNA-Polymerase [5 U/µl]	0.3	0.05 units
Forward-Primer [10 µM]	0.6	200 nM
Reverse-Primer [10 µM]	0.6	200 nM
Betaine [5 M]	6	1 M
ddH_2O	17.9	
Total volume	30	

Table 2-18: PCR protocol for *Cntf* genotpying

Steps	Temperature [°C]	Duration [minutes]
Initial denaturation	94	5
Denaturation	94	0.5
Annealing	64	0.5
Elongation	72	1
Terminal elongation	72	7
Hold	15	∞

Table 2-19: PCR program for *Cntf* genotyping

The double bars show the beginning and end of a cycle (34 cycles).

2.2.7.4.3 NF-L-IGFBP-5 genotyping

One PCR approach (primers: NFL-SEQ and BP5PCR) was performed for *NF-L-IGFBP-5* genotyping. Expected size for the product of a part of transgenic cDNA sequence of *IGFBP-5* under a *NF-L*-promoter is 400 base pairs.

Components	Volume in [µl]	Final concentration
DNA template	1	~ 10-500 µg
10X PCR-Puffer (15 mM $MgCl_2$)	3	1.5 mM $MgCl_2$
dNTP-Mix [10 mM]	1	333 µM
Taq DNA-Polymerase [5 U/µl]	0.3	0.05 units
Forward-Primer [10 µM]	0.6	200 nM
Reverse-Primer [10 µM]	0.6	200 nM
Enhancer	6	0.5 M
ddH_2O	17.5	
Total volume	30	

Table 2-20: PCR protocol for *NF-L-IGFBP-5* genotpying

Steps	Temperature [°C]	Duration [minutes]
Initial denaturation	94	5
Denaturation	95	0.75
Annealing	59	0.75
Elongation	72	0.5
Terminal elongation	72	7
Hold	15	∞

Table 2-21: PCR program for *NF-L-IGFBP-5* genotyping
The double bars show the beginning and end of a cycle (45 cycles).

2.2.7.4.4 Floxed IGF-1 receptor (IGF-$R^{lox\ P}$) genotyping

One PCR approach (primers: Rec Seq and X3 Seq) was performed for *IGF-*R^{loxP} genotyping. Expected size for the wild-type product of *IGF-*R^{wt} is 500 base pairs and the *IGF-*R^{loxP} is 600 base pairs.

Components	Volume in [µl]	Final concentration
DNA template	1	~ 10-500 µg
10X PCR-Puffer (15 mM $MgCl_2$)	5	1.5 mM $MgCl_2$
dNTP-Mix [10 mM]	1	200 µM
Taq DNA-Polymerase [5 U/µl]	0.4	0.04 units
Forward-Primer [10 µM]	1	200 nM
Reverse-Primer [10 µM]	1	200 nM
Betaine [5 M]	10	1 M
ddH_2O	30.6	
Total volume	50	

Table 2-22: PCR protocol for *IGF-R*^{loxP} genotpying

Steps	Temperature [°C]	Duration [minutes]
Initial denaturation	94	5
Denaturation	94	0.75
Annealing	65	0.5
Elongation	72	0.75
Terminal elongation	72	10
Hold	22	∞

Table 2-23: PCR program for *IGF-R*^{loxP} genotyping
The double bars show the beginning and end of a cycle (35 cycles).

2.2.7.4.5 NF-L-Cre recombinase

This PCR reaction detects the unique combination of the human neurofilament-light chain promoter (NF-L) with the Cre recombinase cDNA. Expected size of the product is 250 base pairs.

Components	Volume in [µl]	Final concentration
DNA template	1	~ 10-500 µg
10X PCR-Puffer (15 mM $MgCl_2$)	3	1.5 mM $MgCl_2$
dNTP-Mix [10 mM]	0.6	200 µM
Taq DNA-Polymerase [5 U/µl]	0.3	0.05 units
Forward-Primer [10 µM]	0.6	200 nM
Reverse-Primer [10 µM]	0.6	200 nM

Enhancer	3	
ddH_2O	20.9	
Total volume	30	

Table 2-24: PCR protocol for *NF-L-Cre* genotpying

Steps	Temperature [°C]	Duration [minutes]
Initial denaturation	94	5
Denaturation	94	1
Annealing	59	0.5
Elongation	72	1
Terminal elongation	72	7
Hold	15	∞

Table 2-25: PCR program for *NF-L-Cre* genotyping
The double bars show the beginning and end of a cycle (34 cycles).

2.2.7.5 RNA purification and quantification

RNA for microarray, real-time PCR and reverse transcriptase PCR was extracted by the standard TRIzol reagent protocol (Cat. No. 15595-026, Invitrogen, Life Technologies). First, the tissue was homogenized in 1 ml TRIzol with a tissue homogenizer (POLYTRON PT2100) and incubated for 5 minutes at room temperature. After the addition of 200 µl chloroform, the samples were shaken by hand two times for 15 seconds. Following this was a further 3 minutes incubation at room temperature and shaking by hand for 15 seconds. To separate the solution in different phases, the samples were centrifuged at 12,000 g at 4 °C for 15 minutes. The water phase of each sample, containing the RNA, was transferred into a new reaction tube and 500 µl isopropyl alcohol was added. That was incubated for 10 minutes at room temperature and centrifuged at 12,000 g at 4 °C for 10 minutes. Subsequently the supernatant was discarded and the pellet was washed with 1 ml 75% ethanol. Again the samples were centrifuged at 7,500 g at 4 °C for 5 minutes. The supernatant was again discarded and the pellet was resuspended in 10 µl DEPC water. After incubation at 60 °C for 10 minutes, the RNA amount and purity was quantified by the NanoDrop. The purity of RNA is determined by two ratios of the optical densities of 260 nm / 280 nm and 260 nm / 230 nm. Nucleic acids have their maximum absorbance at 260 nm. Carbohydrates, peptides and aromatic compounds have their maximum absorbance at 230 nm, whereas proteins show their maximum at 280 nm. The ratio of OD_{260}/OD_{280} should be 2 and OD_{260}/OD_{230} should be 2.2 for good RNA purity.

2.2.7.6 Reverse transcriptase polymerase chain reaction (RT-PCR)

Reverse transcriptase polymerase chain reaction (RT-PCR) is a variant of the PCR. Instead of a DNA strand template, an RNA strand is reverse-transcribed into its DNA complement (cDNA) using the enzyme reverse transcriptase. The RNA was transcribed into cDNA with the Superscript III First-Strand Kit (Cat no. 18080-05, Invitrogen). 1 µg of the purified RNA was inserted for the RT-PCR and 1 µl of 50µM oligo$(dT)_{20}$ primer, 1µl of 10 mM dNTP mix and ad 10 µl DEPC-treated water. This RNA/primer mixture was incubated at 65 °C for 5 minutes and then placed on ice for at least 1 minute. Meanwhile the cDNA Synthesis Mix was prepared as follows: 2 µl of 10X RT buffer, 4 µl of 25 mM $MgCl_2$, 2µl of 0.1 M DTT, 1 µl of RNaseOUT (40 U / µl) and 1 µl of SuperScript III RT (200 U / µl). Afterwards the cDNA Synthesis Mix was added to the RNA/primer mixture and incubated for 50 minutes at 50 °C. Subsequently the reaction was terminated at 85 °C for 5 minutes and then chilled on ice. A brief centrifugation followed and 1 µl of RNase H was added and incubated for 20 minutes at 37 °C. This cDNA synthesis reaction can be stored at -20 °C or used for PCR immediately.

2.2.7.7 PCR for Igfr exon 3 deletion

A PCR was performed to ascertain the level of deletion of exon 3 in NF-L-Cre, *Igfr*$^{loxP/loxP}$ mice in exclusively neuronal tissue, and the cDNA levels in brain, spinal cord and heart were determined accordingly. Heart was used as a non-neuronal negative control. PCRs with following exon 3 spanning primer set were performed, where the forward primer binds to exon 2 and the reverse primer binds to exon 6. The expected full-length product size with exon 3 is 971 base pairs and the product with exon 3 deletion is 658 base pairs. β-actin primers were used as a standard and the expected product size is 183 base pairs. Both PCR reactions have the same protocol (Table 2-25).

Components	Volume in [µl]	Final concentration
cDNA template	1	~ 1 µg
10X PCR-Puffer (15 mM $MgCl_2$)	3	1.5 mM $MgCl_2$
dNTP-Mix [10 mM]	1	333 µM
Taq DNA-Polymerase [5 U/µl]	0.3	0.03 units
Forward-Primer [10 µM]	0.6	200 nM
Reverse-Primer [10 µM]	0.6	200 nM
Betaine [5 M]	3	0.5 M

ddH_2O	20.5	
Total volume	30	

Table 2-26: PCR protocol for *Igfr* exon 3 deletion and β-actin in NF-L-Cre, $Igfr^{loxP/loxP}$ tissue.

Steps	Temperature [°C]	Duration [minutes]
Initial denaturation	95	5
Denaturation	95	0.5
Annealing	56	0.5
Elongation	72	1
Terminal elongation	72	5
Hold	4	

Table 2-27: PCR program for *Igfr* exon 3 deletion and β-actin in NF-L-Cre, $Igfr^{loxP/loxP}$ tissue
The double bars show the beginning and end of a cycle (β-actin PCR = 35 cycles, *Igfr* exon 3 deletion = 25 cycles).

DNA-gel electrophoresis was run on a 2% agarose gel in 1x TAE buffer at 80 V for 1 hour.

2.2.7.8 Quantitative real-time polymerase chain reaction of NF-L-IGFBP-5 mice

Quantitative real-time polymerase chain reaction (qRT-PCR) is another variety of the PCR which is used to amplify and simultaneously quantify a targeted DNA molecule. A fluorescence dye specifically intercalates into the double strand of the amplified PCR products during each PCR cycle. After each cycle the ongoing amplification is monitored by measuring the fluorescence increase. To measure the cDNA IGFBP-5 and β-actin levels of the spinal cord of *NF-L-IGFBP-5* and control mice the LightCycler Fast start DNA Master SYBR Green I kit (Roche) was used.

Components	Volume in [µl]	Final concentration
cDNA template	1	~ 1 µg
10X PCR-Puffer (3 mM $MgCl_2$)	1.6	0.24 mM $MgCl_2$
Forward-Primer [10 µM]	0.2	100 nM
Reverse-Primer [10 µM]	0.2	100 nM
Fast stat	2	
ddH_2O	15	
Total volume	20	

Table 2-28: Real-time PCR protocol for *NF-L-IGFBP-5* mice with primers for IGFBP-5 and β-actin.

Samples were centrifuged at 700 g for 5 seconds and quantification was made by LightCycler 1.5 (Roche) using the comparative C_T method (also known as the $\Delta\Delta C_T$ method), which is similar to the Relative Standard Curve Method with the difference that it uses arithmetic formulas to achieve the result for relative quantitation.

Steps	Temperature [°C]	Duration
Initial denaturation	95	10 min
Denaturation	95	10 sec
Annealing	55	10 sec
Elongation	72	5 sec

Table 2-29: Real-time PCR program for *NF-L-IGFBP-5* mice with primers for IGFBP-5 and β-actin. The double bars show the beginning and end of a cycle (45 cycles).

2.2.7.9 Microarray

The RNA was purified as stated above (*2.2.7.5 RNA purification and quantification*) and then the microarray was performed by Dr. Susanne Kneitz (Laboratory for Microarray Applications, Interdisciplinary Centre for Clinical Research (IZKF), University of Würzburg, Versbacher-Str. 7, 97078 Würzburg, Germany). Insulin-related genes were selected between a patient with diabetic mellitus and a healthy control.

2.2.8 Cell culture

2.2.8.1 Isolation of embryonic motoneurons

After pregnant mice were killed at embryonic day 13.5 (E13.5), the abdominal wall was opened, the uterus was dissected and the embryos were abstracted. The embryonic heads were removed and placed into 200 µl lysis buffer for genotyping. Then the dorsal skin was removed and the lumbar spinal cord was dissected. The spinal cord was transferred into a dish containing Hank's balanced salt solution (HBSS) buffer and the membrane of the spinal cord with the attached dorsal root ganglia was removed. The cleaned lumbar spinal cord was transferred into 180 µl HBSS with 20 µl 1% trypsin and incubated for 15 minutes at 37 °C. Afterwards the tissue was transferred in 20 µl into 180 µl Neurobasal medium (Invitrogen) with 20 µl 0.1% trypsin inhibitor and triturated until the tissue was separated into single cells. 800 µl Neurobasal medium was added. The panning plates had been previously prepared as follows: Delta surface Nunclon plates (Nunc) were precoated with anti-p75 NGF receptor

antibody (1:2,000, MLR2, monoclonal, Abcam) in 5 ml TRIS-Puffer (10 mM, pH 9.5) for at least 20 minutes. After the panning plates were washed three times with 500 µl Neurobasal, the cells suspension was transferred to them and incubated for 30 minutes at room temperature. This panning step enriches motoneurons that uniquely express p75 NGF receptors, whereas other cell types do not express this receptor and were not bound by the panning antibody. These unbound cells were removed by three washing steps of 37 °C Neurobasal. By adding depolarization solution and smooth trituration, the bound motoneurons were detached from the dish and transferred into 1 ml warm motoneuron full medium (2% horse serum, 1x B27 in Neurobasal medium with 1x Glutamax) in 15 ml falcons. The cells were counted by a Neubauer counting chamber and were diluted to a concentration of 20 cells/µl.

2.2.8.2 Culturing and fixation of motoneurons

Before plating the cells, the coverslips were placed into dishes and coated with 200 µl poly-D,L-ornithine (0.5 mg/ml in 0.15 M Boratpuffer pH 8.35) and incubated overnight at 4° C. After washing the coverslips three times with aqua bidest, they were coated with laminin-211/221 for 30 minutes. Laminin-211/221 is an extracellular matrix protein and mediates motoneuron cell growth and differentiation of the growth cone.

Subsequently, 4000 cells in 200µl full medium per dish were plated on special coated coverslips for culturing and incubated for one hour at 37 °C. After the cells were attached to the laminin-coated coverslips, the dish was flooded with full medium supplemented with the neurotrophic factors CNTF and BDNF.

The motoneurons were cultured for 7 days at 37 °C and 5% CO_2 in an incubator and full medium with CNTF and BDNF was exchanged every 48 hours. After fixation for 30 minutes with 4% PFA, cells were prepared for immunofluorescence.

2.2.8.3 Staining of fixed motoneurons

The PFA-fixed motoneurons were washed three times with 1x TBST. Then 200 µl of blocking solution containing 10% BSA in 1x TBST was applied for one hour at room temperature, before first antibody staining was performed with anti-Tau (1:1000, Sigma) and anti-IGFBP-5 (1:500, Neuromics) in blocking solution overnight at 4 °C. The next day the cells were washed three times with 1x TBST and subsequently incubated with second antibodies (donkey anti-goat Cy5 1:400 and swine anti-rabbit FITC 1:40) in blocking solution

for one hour. After the samples were washed again three times with 1x TBST, the coverslips were mounted upside-down on object slides with Mowiol.

2.2.9 Software

Following computer programs were used during the work for this thesis: Adobe Photoshop, Adobe Illustrator, Bitplane Imaris 5.7.0 Software, Graph PadPrism, ImageJ, Microsoft PowerPoint, Microsoft Word, Microsoft Excel, Olympus Confocal Software, Primer3Plus and Raytest AIDA.

2.2.10 Statistical analysis

All data are expressed as mean ± SD. The data were subjected to a statistical analysis with the two-tailed Student's t-test when comparing two groups and one-way ANOVA with the Tukey post-hoc test for comparison of more than two groups. The frequency distribution of axon circumferences in sciatic nerves and the branching level in the gastrocnemius muscle were analyzed by two-way ANOVA with the Bonferroni post-hoc test. Significance level was set as $P < 0.05$. Statistical analysis was performed with Graph Pad Prism Software (San Diego, USA).

3 Results

3.1 Ciliary neurotrophic factor-induced sprouting preserves motor function in a mouse model of mild spinal muscular atrophy

[Most of these results have been published in the manuscript "Simon et al., Ciliary neurotrophic factor-induced sprouting preserves motor function in a mouse model of mild spinal muscular atrophy, Hum. Mol. Genet., 19 (2010) 973-986", referred to as [276] in the following sections.]

3.1.1 Smn$^{+/-}$ mice show motoneuron loss, but no changes in NMJ architecture and muscle strength

Despite a loss of at least 40% of spinal motoneurons (L1-L7) at an age of 12 months, Smn$^{+/-}$ mice show no clinical phenotype (all spinal motoneuron counts were performed by Dr. Sibylle Jablonka) [141]. To further characterize the muscle strength of *Smn*$^{+/-}$ mice, grip strength measurements of the forelimbs were performed. Indeed, while a 40% loss of spinal motoneurons occurred (Fig. 3-1-1b) (P = 0.0003, two-tailed Student's t-test), no loss of grip strength could be observed compared to control animals (Fig. 3-1-1a) (P = 0.6530, two-tailed Student's t-test) [290]. First of all the size of the neuromuscular junction (NMJ) of the calf (gastrocnemius muscle) was investigated (Fig. 3-1-1c) to get an insight into the underlying compensatory mechanisms. However, there were no differences in the NMJ size between Smn$^{+/-}$ and control mice (P = 0.4648, two-tailed Student's t-test) (Fig. 3-1-1d, diploma thesis by Christian Simon, "Charakterisierung von präsynaptischen Veränderungen an neuromuskulären Endplatten bei einem Mausmodell für spinale Muskelatrophie").

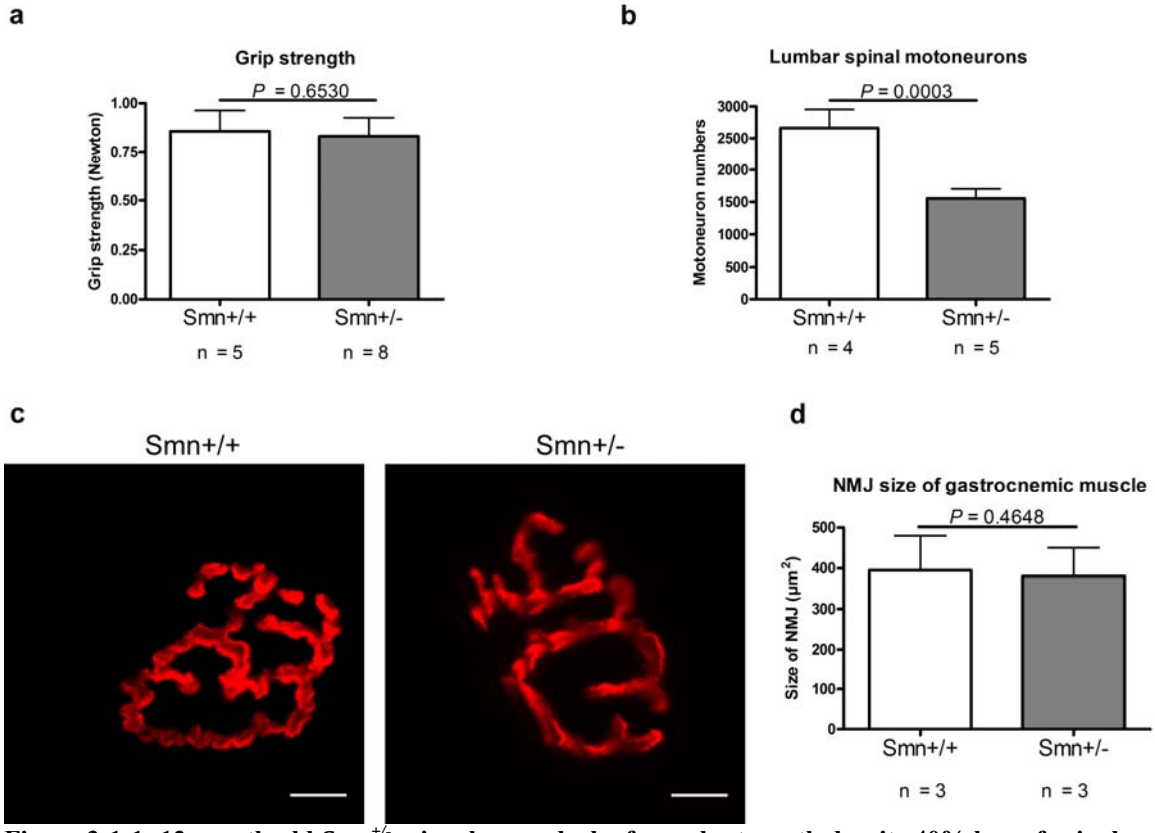

Figure 3-1-1: 12-month-old *Smn*$^{+/-}$ mice show no lack of muscle strength despite 40% loss of spinal motoneurons

(a) No alteration in grip strength of 12-month-old *Smn*$^{+/-}$ mice (control = 0.86 ± 0.11 N, n = 5; *Smn*$^{+/-}$ = 0.83 ± 0.10 N, n = 8; *P* = 0.6530, two-tailed Student's t-test). (b) Counts of motoneuron cell body in the lumbar spinal cord reveal a 40% loss in *Smn*$^{+/-}$ mice (control = 2660 ± 289 motoneurons, n = 5; *Smn*$^{+/-}$ = 1553 ± 151 motoneurons, n = 4; *P* = 0.0003, two-tailed Student's t-test). (c, d) Morphology and size of the postsynaptic part of the NMJ appeared unchanged. Acetylcholine receptors are visualized by α-bungarotoxin (BTX) in single teased muscle fibers. 60 NMJs in 3 individuals per genotype were investigated (control = 394 ± 84 µm^2, n = 3; *Smn*$^{+/-}$ = 381±69µm^2, n = 3; *P* = 0.4648, two-tailed Student's t-test). Scale bar = 5µm.

3.1.2 Increased mean motor unit size in the gastrocnemius muscle of Smn$^{+/-}$ mice

In collaboration with Prof. Dr. Lucia Tabares and Dr. Rocio Ruiz (Department of Medical Physiology and Biophysics, School of Medicine, University of Seville, 41009 Seville, Spain), the motor function of the gastrocnemius muscle in 12-month-old Smn$^{+/-}$ and Smn$^{+/+}$ littermate controls were investigated by EMG measurements [291]. The gastrocnemius muscle was utilized because of its advantages compared to other muscles. It was convenient for our experiments that this muscle is one of the largest muscles and contains large motor units. Furthermore, the gastrocnemius muscle is more affected in SMA patients than small muscle groups, e.g. finger muscles. Moreover, the innervation pattern of this muscle has been studied in great detail and it is easily accessible for electrophysiological and immunohistochemical investigations of alterations of motor units such as sprouting [107]. To define the size and total number of muscle fibers, the maximum compound motor action potential (CMAP) was recorded. For this reason

the sciatic nerve was stimulated by a single current pulse of supramaximal amplitude. Despite the loss of lumbar motoneurons in Smn$^{+/-}$ mice at this age (Fig. 3-1-1b), the mean amplitude of the maximum CMAP in the Smn$^{+/-}$ mice did not alter. This finding corresponds to the lack of weakness and normal gross morphology of the gastrocnemius muscle (Fig. 3-1-1a, Fig. 3-1-2a) in 12-month-old Smn$^{+/-}$ mice [290]. Although the mean fiber caliber is similiar in Smn$^{+/-}$ mice and controls (Fig. 3-1-2b) (P = 0.7876, two-tailed Student's t-test), the Smn-deficient mice show higher quantities of both atrophic (P = 0.0099, two-tailed Student's t-test) and hypertrophic fibers (P = 0.0011, two-tailed Student's t-test) (Fig. 3-1-2c, d), indicating denervation and subsequent reinnervation by sprouting of remaining motoneurons, respectively [290].

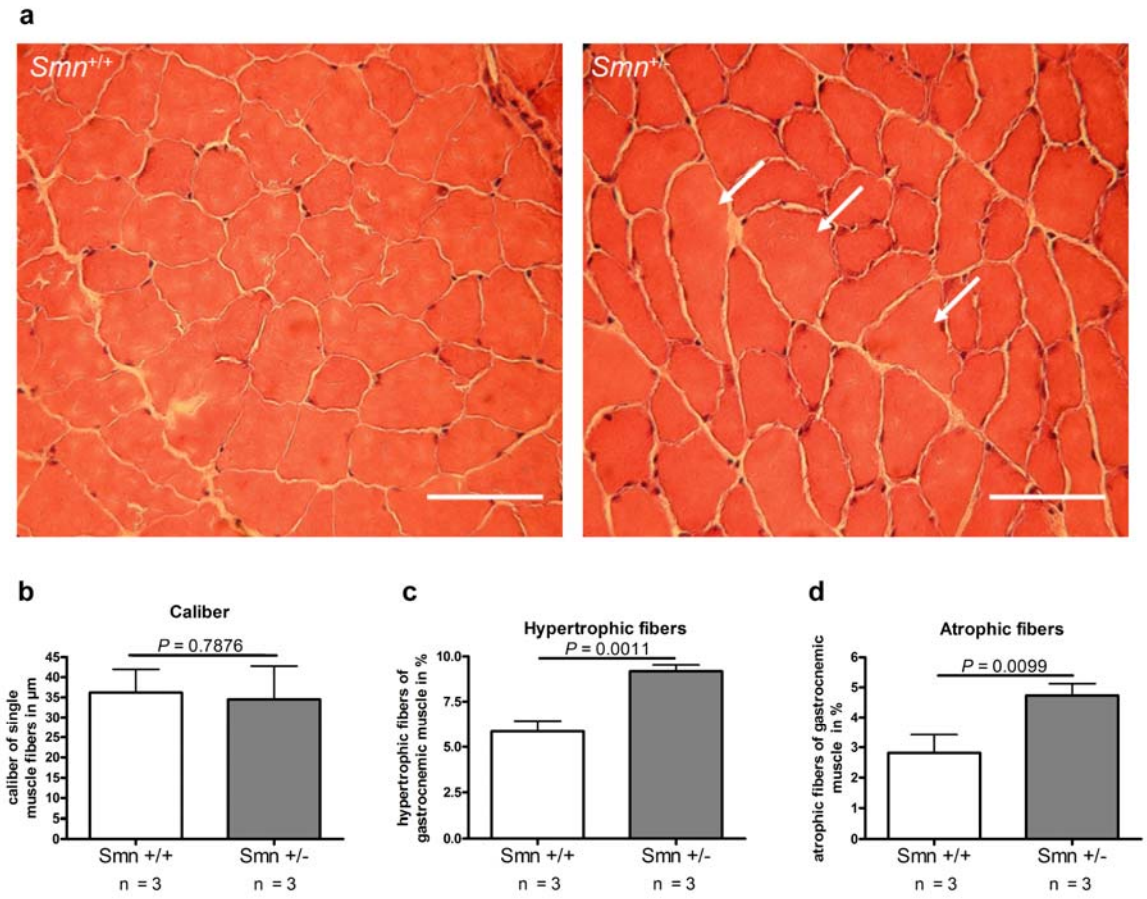

Figure 3-1-2: Fiber caliber in gastrocnemius muscles of control and *Smn*$^{+/-}$ mice
(a) Gross morphology of the muscle appears normal in 12-month-old *Smn*$^{+/-}$ mice, but some of the muscle fibers showed increased caliber (white arrows in the right panel). At least 150 fibers per muscle per animal were investigated. (b) The average caliber of muscle fibers did not differ significantly between both groups (control = 34 ± 8µm, n = 3; *Smn*$^{+/-}$ = 36 ± 6µm, n = 3; P = 0.7876, two-tailed Student's t-test). (c) Number of fibers with a caliber higher than 150% of the mean increased in *Smn*$^{+/-}$ muscle (control = 2.8 ± 0.6%, n = 3; Smn$^{+/-}$ = 4.7 ± 0.4%, n = 3; P = 0.0099, two-tailed Student's t-test). (d) The same was true for fibers with a caliber less than 50% of the mean caliber, indicating that both the number of hypertrophic and of atrophy muscle fibers increased in *Smn*$^{+/-}$ muscle (control = 5.9 ± 0.6%, n = 3; Smn$^{+/-}$ = 9.2 ± 0.4%, n = 3; P = 0.0011, two-tailed Student's t-test).

To investigate whether remaining motoneurons have formed new sprouts to reinnervate neighboring denervated muscle fibers and hence rescue them from functional loss and atrophy, the sizes of the motor units were measured. A motor unit consists of an α-motoneuron and all associated muscle fibers which are innervated by this motorneuron. All muscle fibers which are innervated by a specific motorneuron belong to the same type (slow or fast twitch fibers) [1]. When a motoneuron reinnervates denervated neighboring muscle fibers, the motor unit grows bigger, because the newly innervated muscle fibers are included in this motor unit. This can be quantified by measuring the single motor unit action potential (SMUAP) of each unit.

To test this hypothesis, successive incremental stimuli were applied, starting from a subthreshold level until recruiting twelve individual responses. The size of the amplitude increments was larger in *Smn*$^{+/-}$ than in *Smn*$^{+/+}$ control mice. The average amplitude of the responses, measured as the mean single motor unit action potential (SMUAP), was more than three times higher in *Smn*$^{+/-}$ mice compared to controls, indicating that this massive enlargement of the mean motor unit size is responsible for maintenance of muscle strength in *Smn*$^{+/-}$ mice (for data see [290]). This suggests that despite the loss of motoneurons in the spinal cord, compensatory mechanisms allow muscle fibers to remain active in this mouse model of SMA type III (Fig. 3-1-1a, b) [141,290]. One potential mechanism to compensate for the motoneuron loss is axonal sprouting.

3.1.3 Enhanced arborization of nerve endings in 12-month-old Smn$^{+/-}$ *mice*

12-month-old *Smn*$^{+/-}$ mice exhibit a reduced number of lumbar spinal motoneurons and at the same time increased amplitudes of SMUAPs in the gastrocnemius muscle. In order to study the underlying structural alterations in motor axons innervating the skeletal muscle and in neuromuscular junctions, we crossed *Smn*$^{+/-}$ mice with mice expressing the yellow fluorescent protein (YFP) gene under the *Thy1* promoter (line YFP-H) in individual motoneurons [280]. The *Thy1* gene encodes for a 111 amino acid glycoprotein which belongs to the immunoglobulin superfamily. It is expressed in several neurons in the nervous system and in nonneuronal cell types (e.g. thymocytes). The Thy-1 protein is anchored to the surface of the cell membrane by a phospholipid tail and is likely to be involved in mediating cell–cell interaction [292-294]. In *Thy1-YFP* (line YFP-H) mice the fluorescent tracer is expressed in less than 10% of the motoneurons [280]. This allows for tracking all terminals of individual motoneurons within the gastrocnemius muscle. We isolated muscles from *Smn*$^{+/-}$ *Thy1-YFP-H*^{tg} and *Smn*$^{+/+}$ *Thy1-YFP-H*^{tg} mice. After counterstaining with Alexa594-conjugated α-bungarotoxin, a snake

venom that binds highly specifically to nicotinic acteylcholine receptors (nAChR) at the postsynaptic part of the NMJ, nerve fibers were visualized in wholemount gastrocnemius muscles by confocal microscopy. The gastrocnemius muscle is innervated by at least three major branches from the tibial nerve [295]. The number of branching points of individual axons in the upper medial branch of the tibial nerve was quantified (Fig. 3-1-3) due to the fact that it could be reproducibly identified and analyzed in the isolated gastrocnemius muscles. This branch comes from the main trunk and enters into the medial gastrocnemius muscle (white arrow in Fig. 3-1-3a). Individual axons were traced back from neuromuscular endplates to the trunk of the nerve and the number of branching points was determined (Fig. 3-1-3b) (as established in the diploma thesis by Christian Simon, "Charakterisierung von präsynaptischen Veränderungen an neuromuskulären Endplatten bei einem Mausmodell für spinale Muskelatrophie"). The quantification of branching points is shown in Fig. 3-1-2c. In the gastrocnemius muscle of *Smn*$^{+/-}$ mice, enhanced branching and sprouting of nerve terminals could be observed (Fig. 3-1-2c, d). The number of axons with 4, 5, and 6 branches is increased in *Smn* heterozygous-deficient mice, whereas the number of axons with 1 to 3 branches is decreased ($P < 0.0001$, two-way ANOVA), indicating that enhanced axonal sprouting of terminal motor fibers could be responsible for reinnervation of denervated muscle fibers, due to the loss of spinal motoneurons in the corresponding region of the lumbar spinal cord [290].

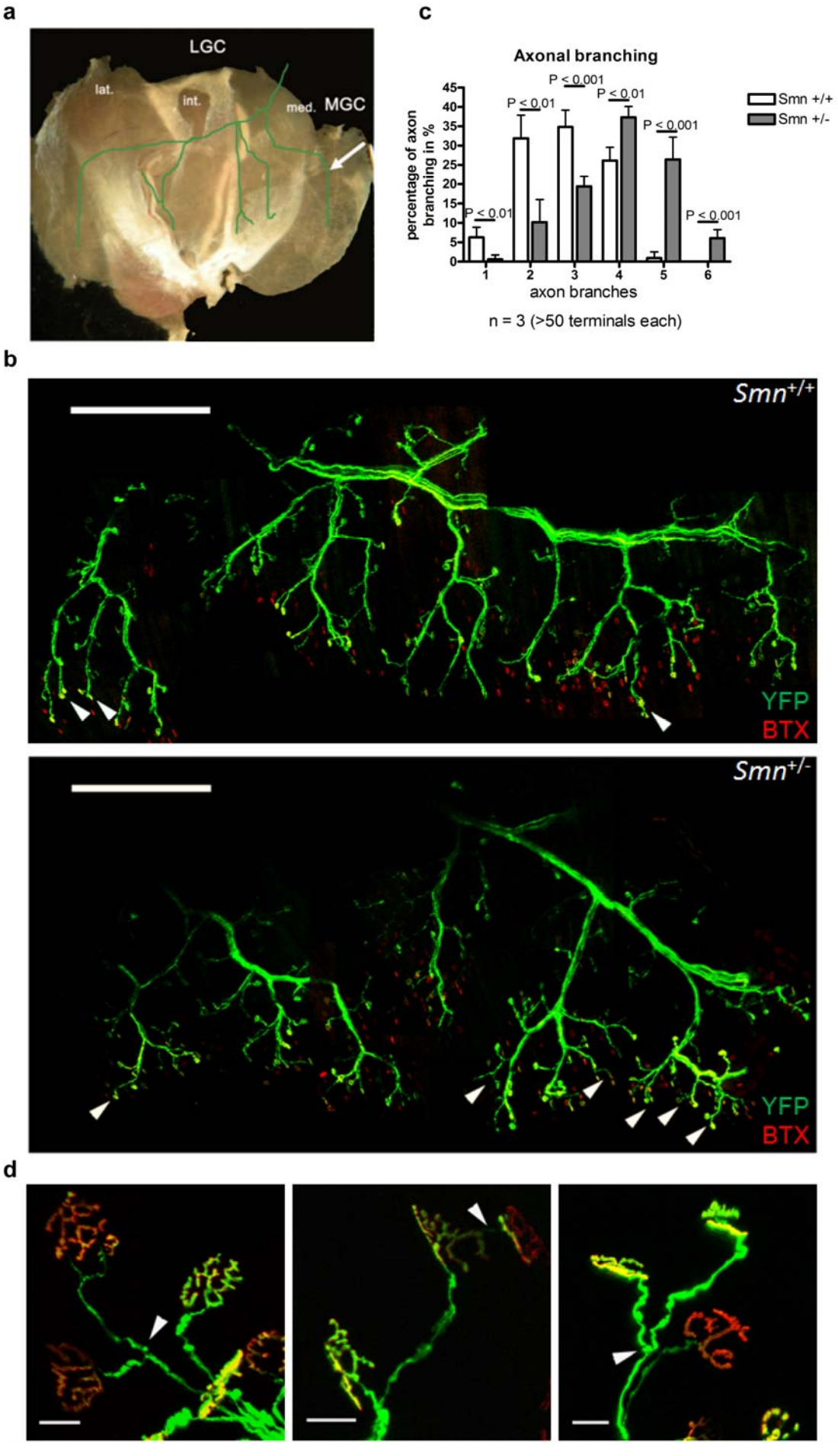
a
LGC
lat.
int.
med.
MGC
c
Axonal branching
P < 0.001
P < 0.01
P < 0.01
P < 0.001
P < 0.01
P < 0.001
Smn +/+
Smn +/-
percentage of axon branching in %
45
40
35
30
25
20
15
10
5
0
1
2
3
4
5
6
axon branches
n = 3 (>50 terminals each)
b
Smn+/+
YFP
BTX
Smn+/-
YFP
BTX
d

Figure 3-1-3: Enhanced arborization and terminal sprouting of motor fibers innervating the gastrocnemius muscle in *Smn*$^{+/-}$ mice

(a) Overview of a mechanically squeezed gastrocnemius muscle and the arborization pattern of the innervating tibial nerve in muscle wholemount preparation. The arrow points to the investigated area. MGC = medial gastrocnemius muscle, LGC = lateral gastrocnemius muscle. (b) The upper medial branch of the tibial nerve in *Smn*$^{+/+}$ *thy*1-*YFP-H*^{tg} and *Smn*$^{+/-}$ *Thy*1-*YFP-H*^{tg} mice. Scale bar = 250 µm, arrowheads point to sprouting events. (c) Quantification of the arborization level (white bars represent data from *Smn*$^{+/+}$ *Thy*1-*YFP-H*^{tg} mice and grey bars from *Smn*$^{+/-}$ *Thy1-YFP-H* ^{tg} mice). Individual axon terminals (at least n = 50) were traced back to the main medial branch innervating the MGC muscle as outlined in Fig 3-1-3a, and the number of branching points were counted. Levels of axon arborization reflect formation of additional branches distal from the main trunk. In *Smn*$^{+/-}$ gastrocnemius muscle, axons with additional branching points, in particular in the distal segments, are significantly more abundant compared to *Smn*$^{+/+}$ muscle, indicative of enhanced axonal sprouting. In addition, in *Smn*$^{+/-}$ gastrocnemius muscle, more axons are present that show additional sprouts close to neuromuscular endplates (arrowheads). (n = 3 independent animals for each group, muscles from both sides were investigated from each animal), (1 branch: Smn$^{+/-}$ = 0.6 ± 1.1%, controls = 6.3 ± 2.6%; 2 branches: Smn$^{+/-}$ = 10.2 ± 5.9%, controls = 31.9 ± 6.0%; 3 branches: Smn$^{+/-}$ = 19.4 ± 2.6%, controls = 34.8 ± 4.4%; 4 branches: Smn$^{+/-}$ = 37.3 ± 2.8%; controls = 26.1 ± 3.4%; 5 branches: Smn$^{+/-}$ = 26.4 ± 5.8%, controls = 0.9 ± 1.6%; 6 branches: Smn$^{+/-}$ = 6.1 ± 2.2%, controls = 0.0 ± 0.0%); $P < 0.0001$, two-way ANOVA). (d) High-power micrographs of sprouting axons. Arrowheads point to sprouting events. The panel in the middle shows terminal sprouting. Scale bar = 20 µm.

3.1.4 ATPase staining revealed fiber grouping in 12-month-old Smn$^{+/-}$ *mice*

To prove the axonal sprouting seen in immunohistochemical analyses and to investigate the fiber types involved in this mechanism, the fiber composition in the gastrocnemius muscle was determined. The isoforms of the MHC define the contraction velocity of a fiber by their rate of hydrolyzing ATP. The myofibrillar ATPase activity is different in each isoform of MHC (e.g., MHC Type I slowly hydrolyzes ATP and determine the characteristics of a slow twitch fiber) [296,297]. The isoforms of MHC have different ionic, fixation and pH sensitivities. These properties enable the determination of fiber composition of a muscle through histochemical staining. Slow Type I fibers are resistant to acidic conditions (pH 4.3) and show dark staining due to ATPase activity. In contrast, type 2 (A and B) fibers are susceptible to acidic conditions which leads to an inhibition of the ATPase activity and consequently the fibers do not stain. The fiber composition of each muscle is adapted to its main function. The muscle fibers of the diaphragm (which are innervated by the phrenic nerve and are responsible for respiratory paralysis, being the main cause of death in SMA patients [198,203,262]) contain exclusively slow Type I fibers. In contrast, the gastrocnemius muscle contains mostly fast Type II fibers and only a small percentage of Type I fibers [298]. The type of each individual fiber is determined by the innervating motoneuron. A tonic firing (slow) motoneuron causes a moderate but constant calcium influx into the innervating muscle fiber and differentiates it into a slow Type I fiber. In turn, phasic firing (fast fatiguable) motoneurons cause a short but high calcium influx and differentiate the innervated fibers into

fast Type II fibers [1,299,300]. The actino-myosin ATPase activity of the heavy myosin chain resembles the fiber type. ATPase staining reveals the fiber composition of a muscle and the types of innervating motoneurons, showing physiological changes (e.g. sprouting).

Enhanced fiber grouping of slow twitch fibers in 12-month-old *Smn*$^{+/-}$ mice was found (Fig. 3-1-4), as visualized by ATPase staining of frozen gastrocnemius muscle sections at pH 4.3.

This suggests that fast motoneurons are more affected in Smn$^{+/-}$ mice which leads to denervation of fast twitch fibers. These in turn can be reinnervated by sprouting of neighbouring slow motoneurons. After reinnervation the tonic firing (slow) motoneurons lead to calcineurin-dependent NFAT and MEF2 mediated expression of a slow MHC isoform that reprograms these fibers into slow twitch fibers [1,299,300]. This corresponds to findings in a mouse model for familiar amyotrophic lateral sclerosis (FALS), where fast fatiguable motoneurons denervate first, followed by fast fatigue-resistant motoneuron axons which are affected at symptom-onset. Axons of slow motoneurons are resistant and compensate through sprouting and reinnervation [295].

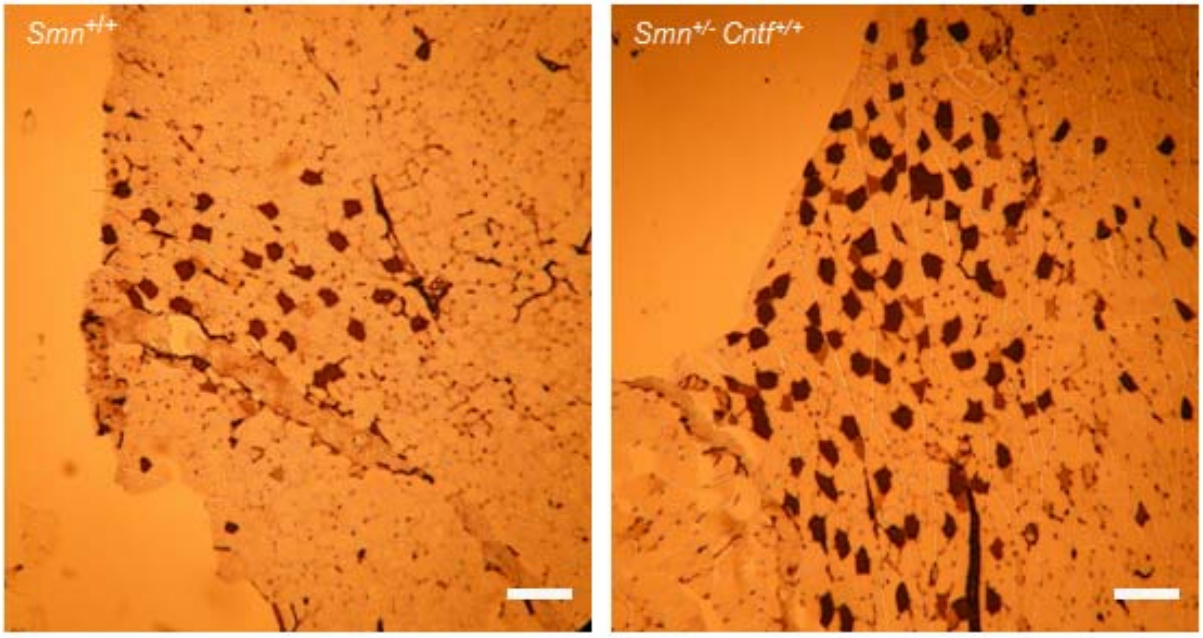

Figure 3-1-4: Fiber grouping in gastrocnemius muscle of 12-month-old *Smn*$^{+/-}$ mice
The murine gastrocnemius muscle consists mostly of fast twitch fibers that are destained by the ATPase staining at pH 4.3. In contrast, slow twitch fibers stain dark, and the number of these fibers appears increased in *Smn*$^{+/-}$ muscle. Scale bar = 150 µm.

3.1.5 Development of motoneuron loss, denervation of neuromuscular endplates and compensation by sprouting in Smn$^{+/-}$ mice

In order to investigate the time point when denervation and sprouting begins, *Smn*$^{+/+}$ and *Smn*$^{+/-}$ mice were analyzed at an age of 4 weeks, and 6 and 12 months. First signs of denervation of neuromuscular endplates were already observed in 4-week-old *Smn*$^{+/-}$ mice

(Fig. 3-1-5a). In those the postsynaptic staining with fluorescence-coupled BTX was not covered by immunofluorescence against the NF-L chain, a presynaptic marker of innervating motor axons (Fig. 3-1-6a). NF-L antibodies were applied in this experiment in order to avoid potential bias caused by the selective expression of YFP. In contrast to NF-L antibodies that label all neuromuscular endplates, YFP is expressed in less than 10% of the motoneurons in Thy1-YFP-H mice, a subgroup that is potentially not representative of all lumbar motoneurons. We counted denervated neuromuscular junctions and found 8 out of 334 (2.4%, in comparison to 1.7% (6/344) in *Smn*$^{+/+}$ mice) in the gastrocnemius muscle of 4-week-old *Smn*$^{+/-}$ animals. Three or more animals were investigated, with at least 80 neuromuscular junctions screened per animal. Denervation of neuromuscular endplates was more prominent (15/293, corresponding to 5.1%) in 6-month-old *Smn*$^{+/-}$ mice (Fig. 3-1-5b), in comparison to age-matched Smn$^{+/+}$ mice (7/280, corresponding to 2.5%).

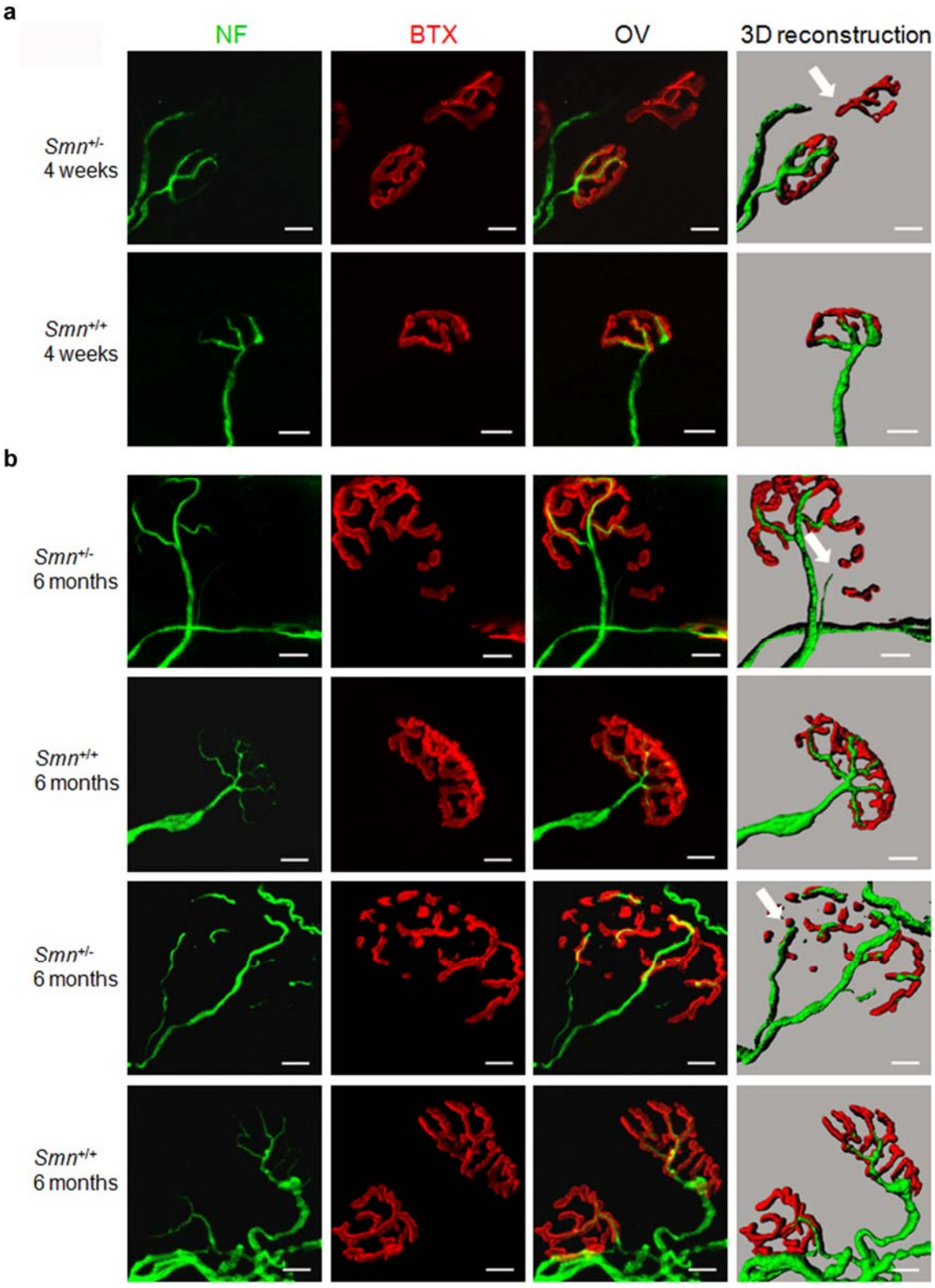

Figure 3-1-5: Denervated neuromuscular endplates in *Smn*$^{+/-}$ mice

The figure shows examples of denervated neuromuscular endplates in 4-week-old (a) (upper 2 panels) and 6-month-old (b) (lower 4 panels) *Smn*$^{+/-}$ mice (wholemount preparation). Morphology of neuromuscular endplates in corresponding control animals (*Smn*$^{+/+}$ mice from the same litters) is also shown. Denervation is shown by lack of covering of the postsynaptic side of neuromuscular endplates, stained with BTX by innervating axonal branches that are stained with antibodies against the neurofilament light chain. The corresponding 3D reconstructions generated from the original confocal stacks with Imaris software are shown on the right hand side. Individual denervated neuromuscular endplates are marked by arrows. Scale bar = 10 µm.

In order to find out when motoneuron cell bodies die and when reinnervation of individual neuromuscular endplates first occurs in *Smn*$^{+/-}$ mice, we counted motoneuron numbers in the lumbar spinal cord (L1-L7) in 4 week-, and 6- and 12-month-old *Smn*$^{+/-}$ and control mice (Fig. 3-1-6a). In 4-week-old mice, motoneuron numbers were not reduced (P = 0.2959, two-tailed Student's t-test), whereas a 23% loss of motoneurons was observed in 6-month- (P = 0.0063, two-tailed Student's t-test) and 42% in 12-month-old *Smn*$^{+/-}$ mice P = 0.0003, two-tailed Student's t-test), thus confirming previously published data [141]. However, despite the loss of motoneurons, no loss of muscle strength was observed in 4-week- (P = 0.2162, two-tailed Student's t-test), 6-month- (P = 0.8673, two-tailed Student's t-test) and 12-month-old mice (P = 0.6530, two-tailed Student's t-test) (Fig. 3-1-6b).

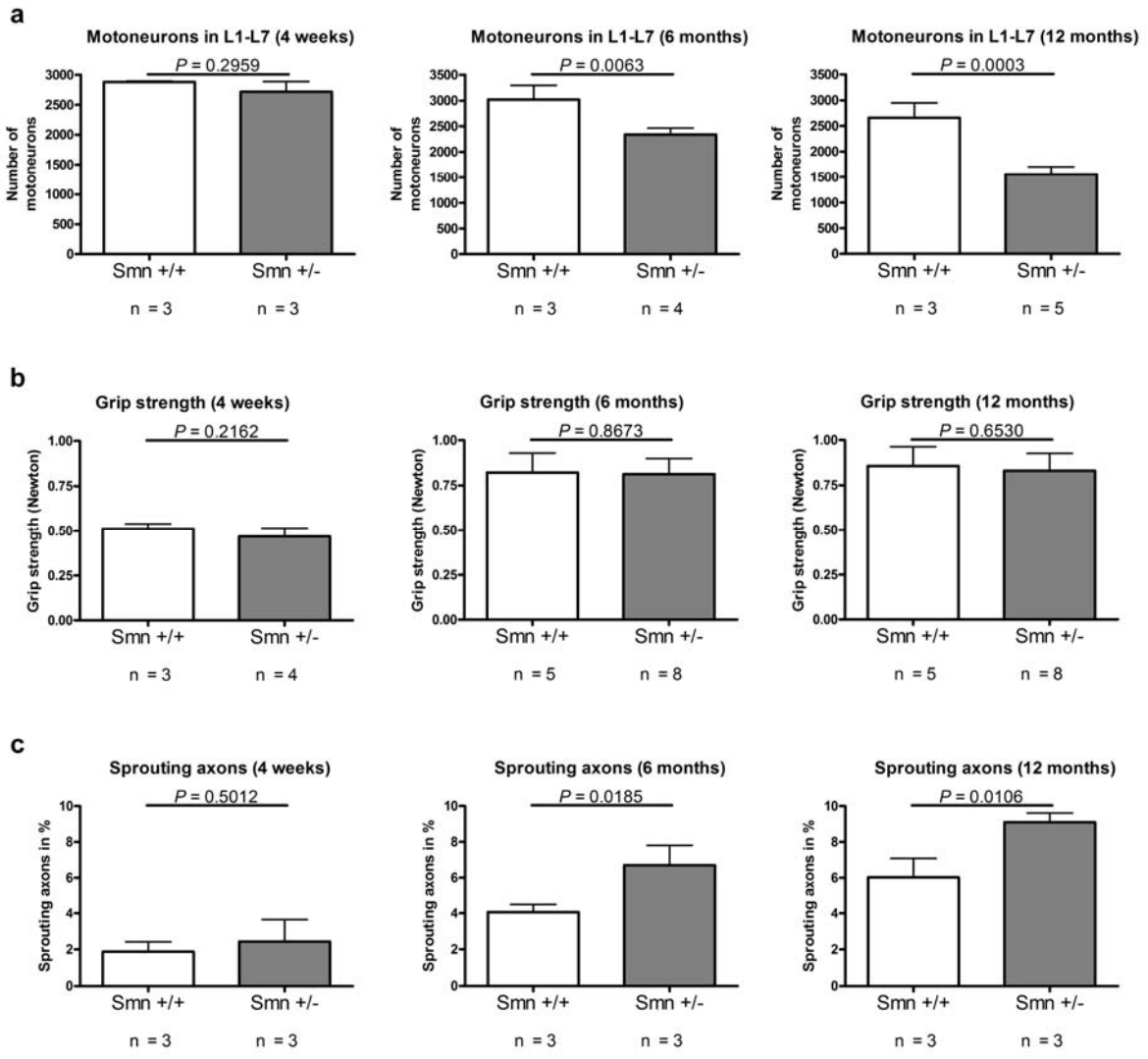

Figure 3-1-6: Development of motoneuron loss is compensated by axonal sprouting to maintain muscle strength in *Smn*$^{+/-}$ mice

(a) Motoneurons were counted in the lumbar spinal cord (L1-L7) of 4-week-, 6-month- and 12-month-old *Smn*$^{+/-}$ and *Smn*$^{+/+}$ mice (n = at least 3 for each group). Whereas motoneuron numbers appeared unaffected in 4-week-old *Smn*$^{+/-}$ mice, a significant loss was observed in 6- and 12-month-old *Smn*$^{+/-}$ mice. (4-week-old mice: control = 2880 ± 17, n = 3; *Smn*$^{+/-}$ = 2718 ± 172, n = 3; P = 0.2959, two-tailed Student's t-test; 6-month-old mice: control = 3021 ± 272, n = 3; *Smn*$^{+/-}$ = 2342 ± 124, n = 4; P = 0.0063, two-tailed Student's t-test; 12-month-old

mice: control = 2660 ± 289, n = 3; *Smn*$^{+/-}$ = 1553 ± 151, n = 5, *P* = 0.0003, two-tailed Student's t-test). (b) Grip strength was unaffected in *Smn*$^{+/-}$ mice at any stage between 4 weeks and 12 months, indicating that the loss of motoneurons was functionally compensated in *Smn*$^{+/-}$ mice. (4-week-old mice: control = 0.51 ± 0.03 N, n = 3; *Smn*$^{+/-}$ = 0.47 ± 0.05 N, n = 4; *P* = 0.2162, two-tailed Student's t-test; 6-month-old mice: control = 0.82 ± 0.11 N, n = 5; *Smn*$^{+/-}$ = 0.81 ± 0.09 N, n = 8; *P* = 0.8673, two-tailed Student's t-test; 12-month-old mice: control = 0.86 ± 0.11 N, n = 5; *Smn*$^{+/-}$ = 0.83 ± 0.10 N, n = 8; *P* = 0.6530, two-tailed Student's t-test). (c) A significant increase in the frequency of axon terminals innervating 2 neuromuscular endplates was observed in 6- and 12-month-old *Smn*$^{+/-}$ mice. A first tendency of enhanced sprouting, although not significant, was also observed in 4-week-old *Smn*$^{+/-}$ mice. At least 150 axon terminals were investigated per animal in the gastrocnemius muscles from both sides (n = at least 3 animals per group). (Sprouting events; 4-week-old mice: control = 1.9 ± 0.6%, n = 3; *Smn*$^{+/-}$ = 2.4 ± 1.2%, n = 3; *P* = 0.5012, two-tailed Student's t-test; 6-month-old mice: control = 4.1 ± 0.42%, n = 3; *Smn*$^{+/-}$ = 6.7 ± 1.1%; n = 3; *P* = 0.0185, two-tailed Student's t-test; 12-month-old mice: control = 6.0 ± 1.0%, n = 3; *Smn*$^{+/-}$ = 9.1 ± 0.5%, n = 3; *P* =0.0106, two-tailed Student's t-test).

For the analysis of sprouting, more than 150 endplates in different areas of the gastrocnemius muscle were investigated in order to quantify synapses innervated by axon terminals that had developed terminal branches by sprouting, thus innervating two or more nearby endplates (Fig. 3-1-7). Compensatory mechanisms by enhanced terminal arborization and sprouting already occurred in 4-week-old *Smn*$^{+/-}$ mice. In these mice, a tendency towards enhanced sprouting was observed (Fig. 3-1-6c) (*P* = 0.5012, two-tailed Student's t-test), and the difference became significant in 6-month-old (*P* = 0.0185, two-tailed Student's t-test) and even more pronounced in 12-month-old *Smn*$^{+/-}$ mice (*P* = 0.0106, two-tailed Student's t-test). This is consistent with previously published data that the disease process in mouse models for SMA reflects a dying-back process [258]. Our data indicate that denervation of neuromuscular endplates occurs early, starting in 4-week-old *Smn*$^{+/-}$ mice before loss of motoneuron cell bodies becomes apparent in the lumbar spinal cord (Fig 3-1-5a, Fig. 3-1-6a). No loss of muscle strength was observed in 4-week-, 6-month- or 12-month-old mice (Fig. 3-1-6b), indicating that the mechanism of sprouting compensation for denervation of individual neuromuscular endplates and motoneuron loss is robust in these mice (Fig. 3-1-6c)[290].

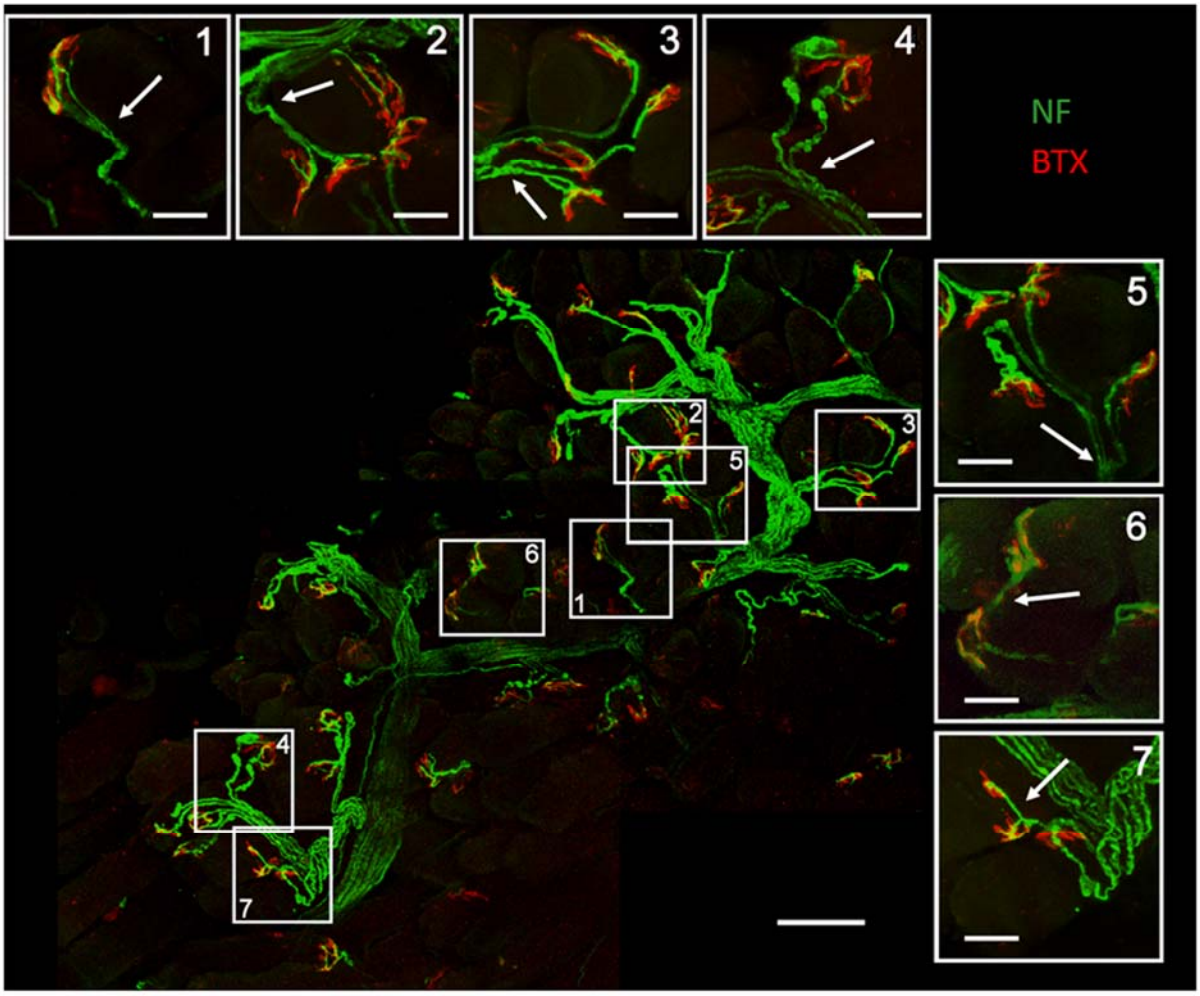

Figure 3-1-7: Overview of the innervation pattern in the gastrocnemius muscle of a 12-month-old wild-type mouse

Staining of a wholemount gastrocnemius muscle of 12-month-old wild-type mouse with α-bungarotoxin and antibodies against neurofilament in order to trace all motor axons. Seven areas with neuromuscular synapses were magnified to demonstrate terminal sprouting. The upper panel shows examples of neuromuscular endplates with axon terminals innervating only one endplate (no sprouting, indicated by arrows). The right column shows rare examples of axon terminals innervating more than one endplate (sprouting, indicated by arrows). Scale bar overview = 100µm, scale bar magnified area = 30µm. In total, more than 150 endplates were investigated for each genotype to quantify the frequency of terminal sprouting.

3.1.6 Ciliary neurotrophic factor is located in Schwann cells of innervating motor axons in the gastrocnemius muscle of Smn$^{+/-}$ mice

In adult mammals, myelinating Schwann cells express high levels of the neurotrophic factor CNTF. CNTF has also been shown to protect against axonal destruction in *pmn* mice, a mouse model for ALS [103,301,302]. Furthermore, CNTF application protects the maintenance of innervation of motor endplates in SOD G93A mice, a mouse model of familial ALS [295]. Therefore we tested expression of CNTF in Schwann cells surrounding motor axons in the gastrocnemius muscle of *Smn*$^{+/-}$ mice. CNTF immunoreactivity is prominent in both myelinating Schwann cells and Schwann cells close to neuromuscular junctions (Fig. 3-1-8a).

To confirm the specificity of the CNTF staining and its localization in the Schwann cells, we stained frozen cross-sections of the sciatic nerve of *Smn*$^{+/-}$ and *Cntf* knockout mice. CNTF expression was also detected in the cytoplasm of myelinating Schwann cells in the sciatic nerve of *Smn*$^{+/-}$ mice, confirmed by S100 costaining, a Schwann cell marker (Fig. 3-1-8b), as previously observed in other models of motoneuron diseases such as *pmn* [111] and SOD1 G93A mutant mice [127]. In the *Cntf*$^{-/-}$ sciatic nerve no CNTF staining was detectable, proving the specificity of the staining (Fig. 3-1-8b) [290].

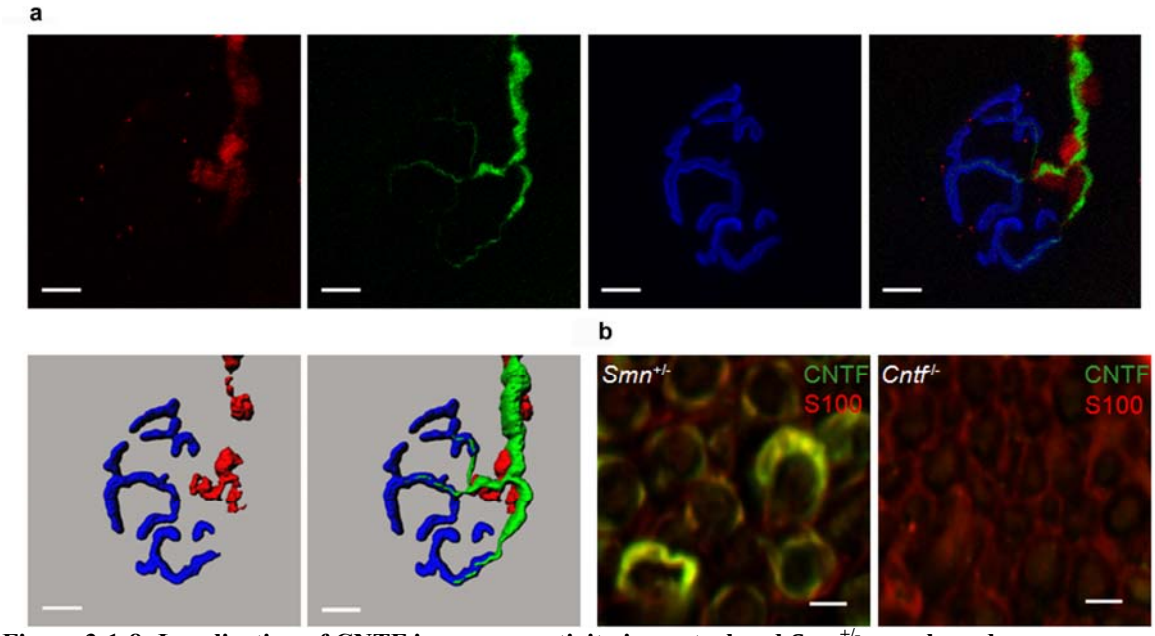

Figure 3-1-8: Localization of CNTF immunoreactivity in control and *Smn*$^{+/-}$ muscle and nerves
(a) High magnification of an *Smn*$^{+/-}$ neuromuscular endplate in frozen sections to demonstrate CNTF expression in Schwann cells. Scale bar = 10 µm. A 3D reconstruction of the triple staining, generated by Imaris software from the complete confocal stack, is shown in the lower panel. CNTF immunoreactivity is detectable at high levels around the axons before they enter and branch into the pretzel-like structure of the neuromuscular endplate. (b) Double staining for CNTF and S100 in frozen sections of the sciatic nerve from *Smn*$^{+/-}$ and *Cntf*$^{-/-}$ mice. A S100 antibody was used as a Schwann cell marker in combination with the CNTF antibodies to confirm the localization of CNTF in the Schwann cells. CNTF colocalizes with S100 in the cytoplasm of Schwann cells and in *Smn*$^{+/-}$ nerves. No CNTF signal was detected in *Cntf*$^{-/-}$ nerve. Scale bar = 5µm.

3.1.7 Reduced axonal sprouting in Smn$^{+/-}$ *Cntf*$^{-/-}$ *skeletal muscle*

To investigate whether the loss of CNTF reduces compensatory sprouting which is detectable in *Smn*$^{+/-}$ muscle via morphological and electrophysiological techniques (Fig. 3-1-3c, and for electrophysiological data see [290]), we crossbred *Smn*$^{+/-}$ with *Cntf*$^{-/-}$ mice in order to obtain *Smn*$^{+/-}$ *Cntf*$^{-/-}$ and corresponding *Smn*$^{+/-}$ and *Cntf*$^{+/+}$ control mice. At first, the CNTF distribution in these mice was tested by analysis of neuromuscular endplates from *Smn*$^{+/+}$, *Smn*$^{+/-}$, *Cntf*$^{-/-}$ and *Smn*$^{+/+}$ *Cntf*$^{-/-}$ mice (Fig. 3-1-9). In *Smn*$^{+/-}$ and *Smn*$^{+/+}$ mice with the CNTF deletion the lack of CNTF was confirmed by no immunoreactivity in surrounding Schwann cells (Fig. 3-1-9, 3rd and 4th panel from top).

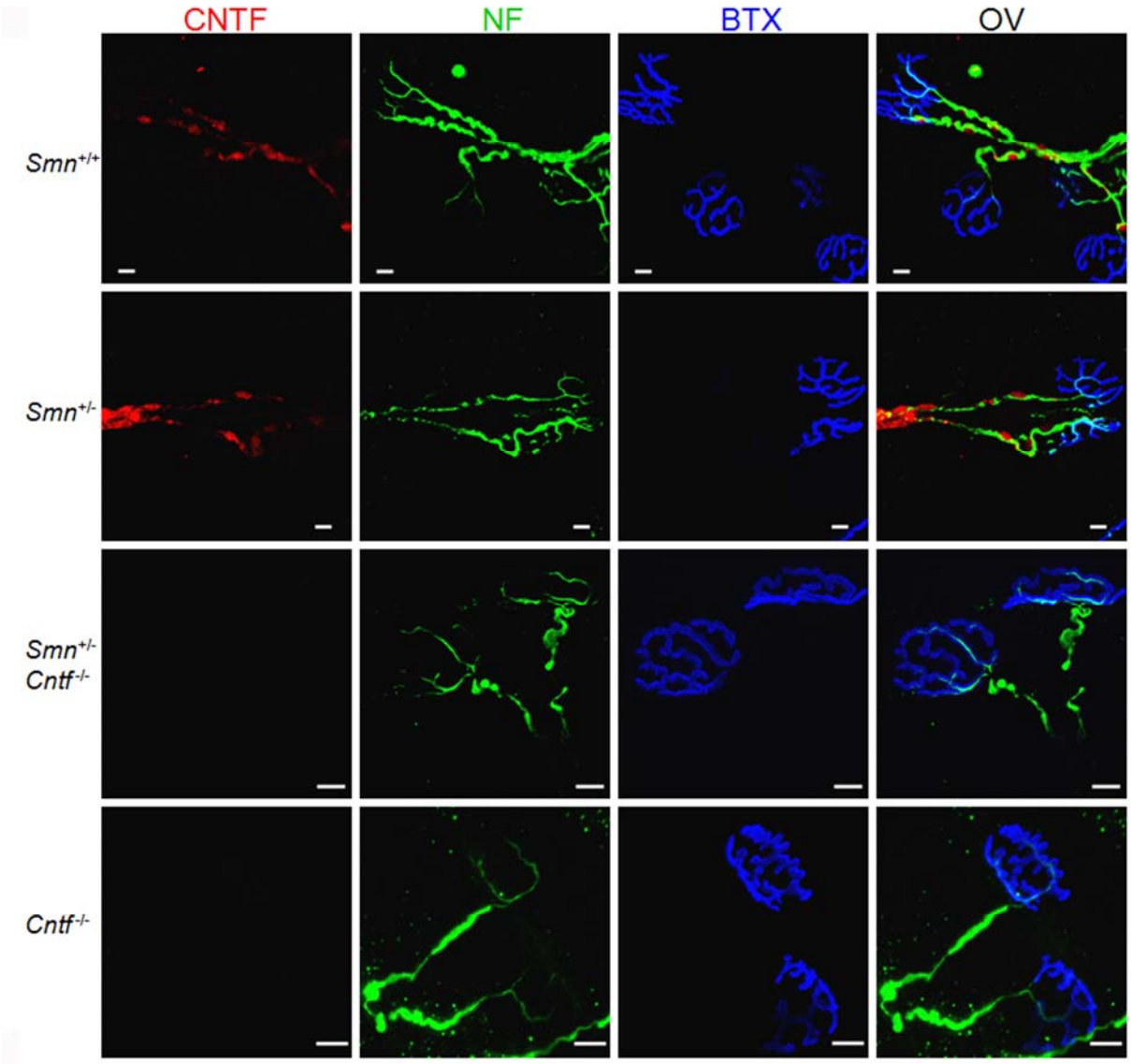

Figure 3-1-9: Localization of CNTF immunoreactivity in control and *Smn*$^{+/-}$ and CNTF-deficient neuromuscular junctions

Localization of CNTF in 100 µm-thick longitudinal frozen sections of the gastrocnemius muscle from *Smn*$^{+/+}$, *Smn*$^{+/-}$, *Smn*$^{+/-}$ *Cntf*$^{-/-}$ double mutant and *Cntf*$^{-/-}$ mice. Triple staining against α-bungarotoxin (BTX, blue), neurofilament (NF, green) and CNTF (CNTF, red) was performed. Individual channels for CNTF, NF and BTX staining are shown, as well as an overlay (OV) on the right hand side. In *Smn*$^{+/+}$ and *Smn*$^{+/-}$ muscle, CNTF is located in Schwann cells surrounding the axons. As a negative control, the CNTF signal was undetectable in *Smn*$^{+/-}$ *Cntf*$^{-/-}$ double mutant and *Cntf*$^{-/-}$ single mutant muscle tissues. Scale bar = 10 µm.

Subsequently, we counted the numbers of motoneuron cell bodies in the spinal cord (L1-L7). Previous studies [114,118,303] have shown that *Cntf*$^{-/-}$ mice exhibit loss of motoneurons between 4 weeks and 6 months. Similar results were observed for the *Cntf*$^{-/-}$ mice used in this study (Fig. 3-1-10a). 4-week-old mice of all genotypes did not show motoneuron loss (Fig. 3-1-10a, Fig. 11) ($P > 0.05$, one-way ANOVA), or an impact on grip strength (Fig. 3-1-10b) ($P > 0.05$, one-way ANOVA).

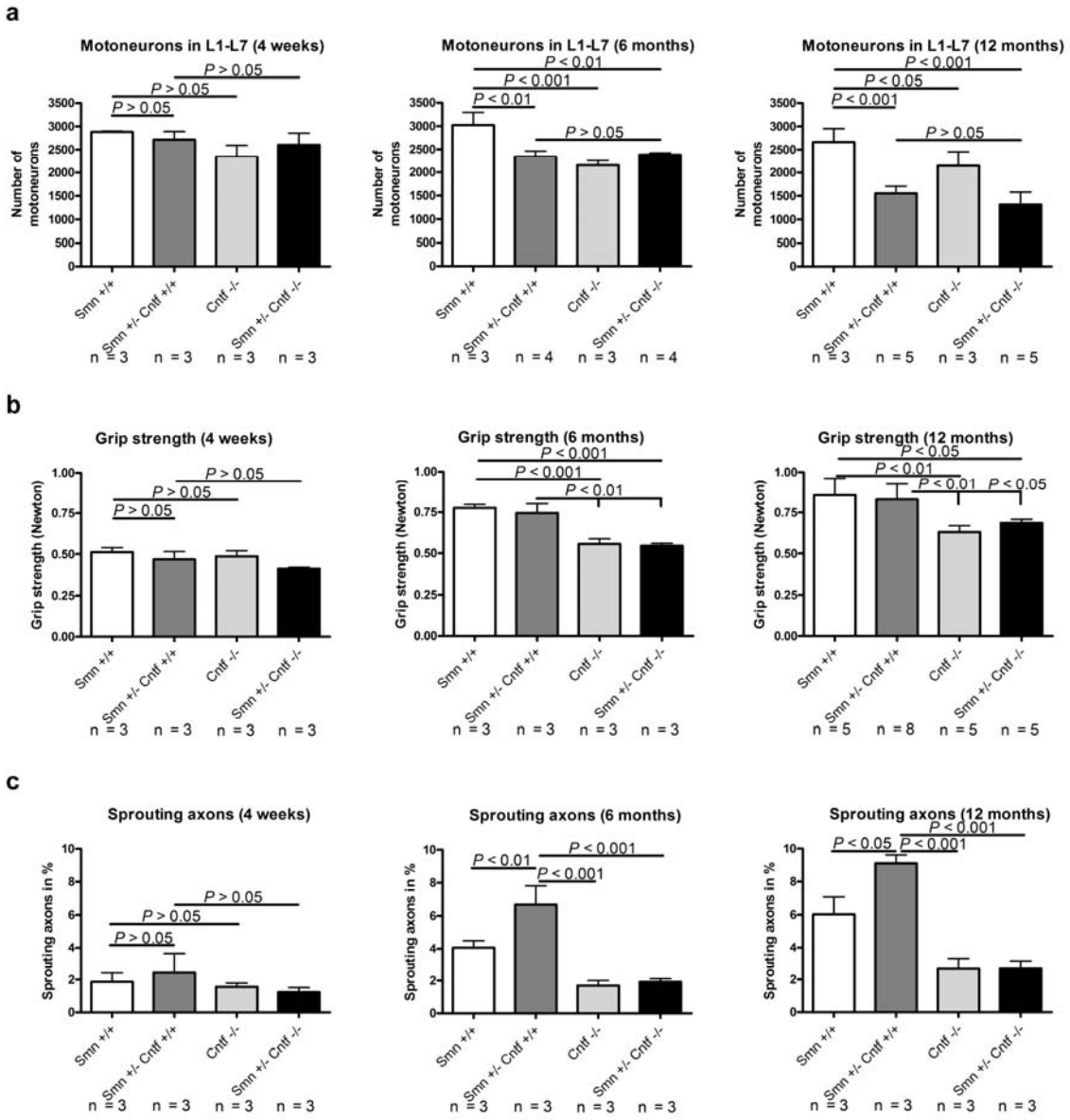

Figure 3-1-10: Lack of CNTF abolishes the sprouting of motor nerves in the gastrocnemius muscle of *Smn*$^{+/-}$ mice

(a) Counts of motoneuron cell bodies in the lumbar spinal cord (L1-L7) of 4-week-, 6-month- and 12-month-old *Smn*$^{+/+}$, *Smn*$^{+/-}$ *Cntf*$^{+/+}$, *Cntf*$^{-/-}$ and *Smn*$^{+/-}$ *Cntf*$^{-/-}$ double mutant mice. (Spinal motoneurons, 4 weeks: *Smn*$^{+/+}$ mice = 2880 ± 17; *Smn*$^{+/-}$ *Cntf*$^{+/+}$ mice = 2718 ± 172; *Cntf*$^{-/-}$ mice = 2346 ± 246; *Smn*$^{+/-}$ *Cntf*$^{-/-}$ mice = 2606 ± 250; $P > 0.05$, one-way ANOVA; 6 months: *Smn*$^{+/+}$ mice = 3021 ± 272; *Smn*$^{+/-}$ *Cntf*$^{+/+}$ mice = 2342 ± 124; *Cntf*$^{-/-}$ mice = 2151 ± 106; *Smn*$^{+/-}$ *Cntf*$^{-/-}$ mice = 2381 ± 41; $P < 0.001$, one-way ANOVA; 12 months: *Smn*$^{+/+}$ mice = 2660 ± 289; *Smn*$^{+/-}$ *Cntf*$^{+/+}$ mice = 1553 ± 151, *Cntf*$^{-/-}$ mice = 2148 ± 306; *Smn*$^{+/-}$ *Cntf*$^{-/-}$ mice = 1315 ± 266; at least n = 3 for each genotype; $P < 0.001$, one-way ANOVA). (b) Grip strength in 4-week-, 6-month- and 12 month-old *Smn*$^{+/+}$, *Smn*$^{+/-}$ *Cntf*$^{+/+}$, *Cntf*$^{-/-}$ and *Smn*$^{+/-}$ *Cntf*$^{-/-}$ mice. (Grip strength, 4 weeks: *Smn*$^{+/+}$ mice = 0.51 ± 0.03; *Smn*$^{+/-}$ *Cntf*$^{+/+}$ mice = 0.47 ± 0.05, *Cntf*$^{-/-}$ mice = 0.49 ± 0.06; *Smn*$^{+/-}$ *Cntf*$^{-/-}$ mice = 0.42 ± 0.01; $P > 0.05$, one-way ANOVA; 6 months: *Smn*$^{+/+}$ mice = 0.78 ± 0.02; *Smn*$^{+/-}$ *Cntf*$^{+/+}$ mice = 0.75 ± 0.06; *Cntf*$^{-/-}$ mice = 0.56 ± 0.05; *Smn*$^{+/-}$ *Cntf*$^{-/-}$ mice = 0.55 ± 0.02; $P < 0.001$, one-way ANOVA; 12 months: *Smn*$^{+/+}$ mice = 0.86 ± 0.11; *Smn*$^{+/-}$ *Cntf*$^{+/+}$ mice: 0.83 ± 0.10; *Cntf*$^{-/-}$ mice = 0.63 ± 0.08; *Smn*$^{+/-}$ *Cntf*$^{-/-}$ mice = 0.69 ± 0.05; at least n = 3 for each genotype; $P < 0.001$, one-way ANOVA). (c) Quantification of axonal sprouting, using the same technique as in Fig. 2C. In *Smn*$^{+/-}$ *Cntf*$^{+/+}$ muscles, a significantly increased number of synapses innervated by collateral or terminal sprouts was observed in comparison to *Smn*$^{+/+}$ muscle at 6 and 12 months. Increased sprouting in *Smn*$^{+/-}$ *Cntf*$^{+/+}$ mice was abolished when CNTF was depleted in *Smn*$^{+/-}$ *Cntf*$^{-/-}$ double deficient mice. At least 150 neuromuscular endplates were investigated per animal (n = at least 3 in each group). (Sprouting events, 4 weeks:

Smn$^{+/+}$ mice = 1.9 ± 0.6, *Smn*$^{+/-}$ *Cntf*$^{+/+}$ mice = 2.4 ± 1.2, *Cntf*$^{-/-}$ mice = 1.6 ± 0.4; *Smn*$^{+/-}$ *Cntf*$^{-/-}$ mice = 1.2 ± 0.5; at least n = 3 for each genotype; $P > 0.05$, one-way ANOVA; 6 months: *Smn*$^{+/+}$ mice = 4.1 ± 0.4, *Smn*$^{+/-}$ *Cntf*$^{+/+}$ mice = 6.7 ± 1.1, *Cntf*$^{-/-}$ mice = 1.7 ± 0.4, *Smn*$^{+/-}$ *Cntf*$^{-/-}$ mice = 1.9 ± 0.3; at least n = 3 for each genotype; $P < 0.001$, one-way ANOVA; 12 months: *Smn*$^{+/+}$ mice = 6.0 ± 1.0, *Smn*$^{+/-}$ *Cntf*$^{+/+}$ mice = 9.1 ± 0.5, *Cntf*$^{-/-}$ mice = 2.7 ± 1.1, *Smn*$^{+/-}$ *Cntf*$^{-/-}$ mice = 2.7 ± 0.5; at least n = 3 for each genotype; $P < 0.001$, one-way ANOVA).

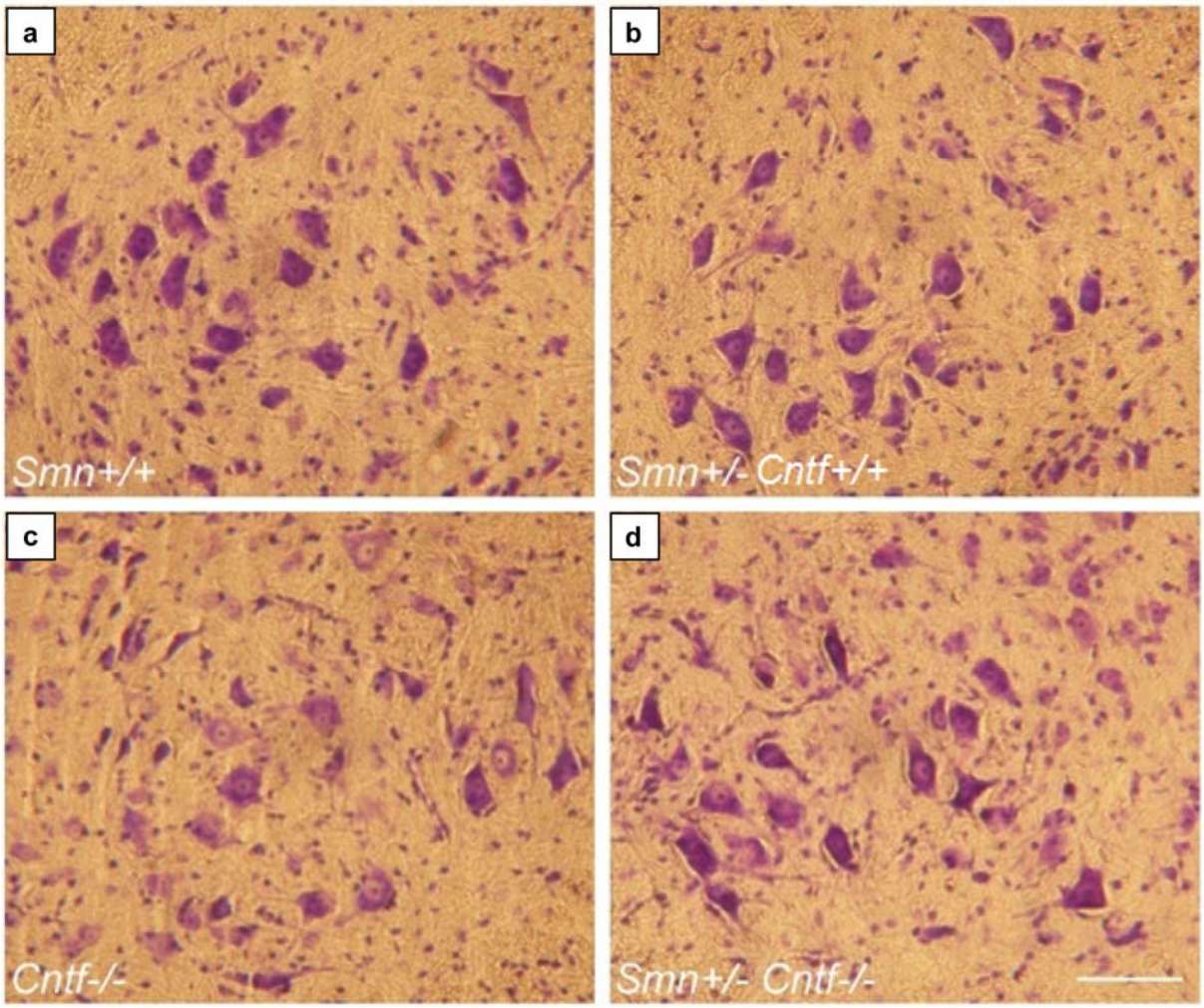

Figure 3-1-11: Morphology of lumbar spinal motoneurons in 4-week-old-*Smn*$^{+/+}$, *Smn*$^{+/-}$ *Cntf*$^{+/+}$, *Cntf*$^{-/-}$ and *Smn*$^{+/-}$ *Cntf*$^{-/-}$ mice

(a-d) Examples of lumbar spinal cord sections showing Nissl-stained lumbar spinal motoneurons from 4-week-old *Smn*$^{+/+}$, *Smn*$^{+/-}$ *Cntf*$^{+/+}$, *Cntf*$^{-/-}$ and *Smn*$^{+/-}$ *Cntf*$^{-/-}$ mice. Scale bar = 100 µm.

A tendency for enhanced sprouting in *Smn*$^{+/-}$ was detectable (Fig. 3-1-10c) ($P > 0.05$, one-way ANOVA). *Smn*$^{+/-}$, *Smn*$^{+/-}$ *Cntf*$^{+/+}$ and *Smn*$^{+/-}$ *Cntf*$^{-/-}$ show a significant loss of motoneurons at 6 and 12 months in comparison to controls (Fig. 3-1-10a, Fig. 3-1-12). However, there were no additive effects of CNTF and Smn deficiency. The difference between *Smn*$^{+/-}$ *Cntf*$^{+/+}$ and *Smn*$^{+/-}$ *Cntf*$^{-/-}$ was not significant at any age studied (Fig. 3-1-10a) (6 months: $P < 0.001$, one-way ANOVA; 12 months: $P < 0.001$, one-way ANOVA). Functional analysis by grip strength measurements [118] revealed a reduction in muscle strength of about 15% in *Cntf*$^{-/-}$ and *Smn*$^{+/-}$ *Cntf*$^{-/-}$ mice. However, although *Smn*$^{+/-}$ *Cntf*$^{+/+}$ mice exhibit even higher losses of spinal motoneurons than *Cntf*$^{-/-}$ mice, there was no reduction in muscle strength at 6 and 12 months.

In contrast, 6- and 12-month-old *Smn*$^{+/-}$ mice that were CNTF-deficient showed reduced muscle strength (Fig. 3-1-10b) (6 months: $P < 0.001$, one-way ANOVA; 12 months: $P < 0.001$, one-way ANOVA).

To address the question of whether CNTF-induced sprouting provides a functional compensation for motoneuron loss in *Smn*$^{+/-}$ *Cntf*$^{+/+}$ mice, we investigated the innervation pattern of endplates in the gastrocnemius muscle. Terminal axons were therefore stained with antibodies against neurofilament. Additionally, more than 150 endplates in different areas of the gastrocnemius muscle were investigated and quantified as in Fig. 3-1-7 (sprouting events = synapses innervated by axon terminals that had developed terminal branches by sprouting, thus innervating two or more nearby endplates). Figure 13 shows examples of axons innervating at least two endplates of *Smn*$^{+/+}$, *Smn*$^{+/-}$ *Cntf*$^{+/+}$, *Cntf*$^{-/-}$ and *Smn*$^{+/-}$ *Cntf*$^{-/-}$ mice (sprouting). Applying these criteria, we investigated endplates with the nearby axon innervating more than one synapse in all four genotypes. In 6- and 12-month-old *Smn*$^{+/-}$ *Cntf*$^{+/+}$ gastrocnemius muscles, the number of axon terminals innervating 2 endplates is significantly enhanced, about 2-fold (Fig. 3-1-10c) compared to control *Smn*$^{+/+}$ mice. In CNTF-deficient mice, only few terminal sprouts were observed, both in *Cntf*$^{-/-}$ and *Smn*$^{+/-}$ *Cntf*$^{-/-}$ mice (Fig. 3-1-10c) (6 months: $P < 0.001$, one-way ANOVA; 12 months: $P < 0.001$, one-way ANOVA).

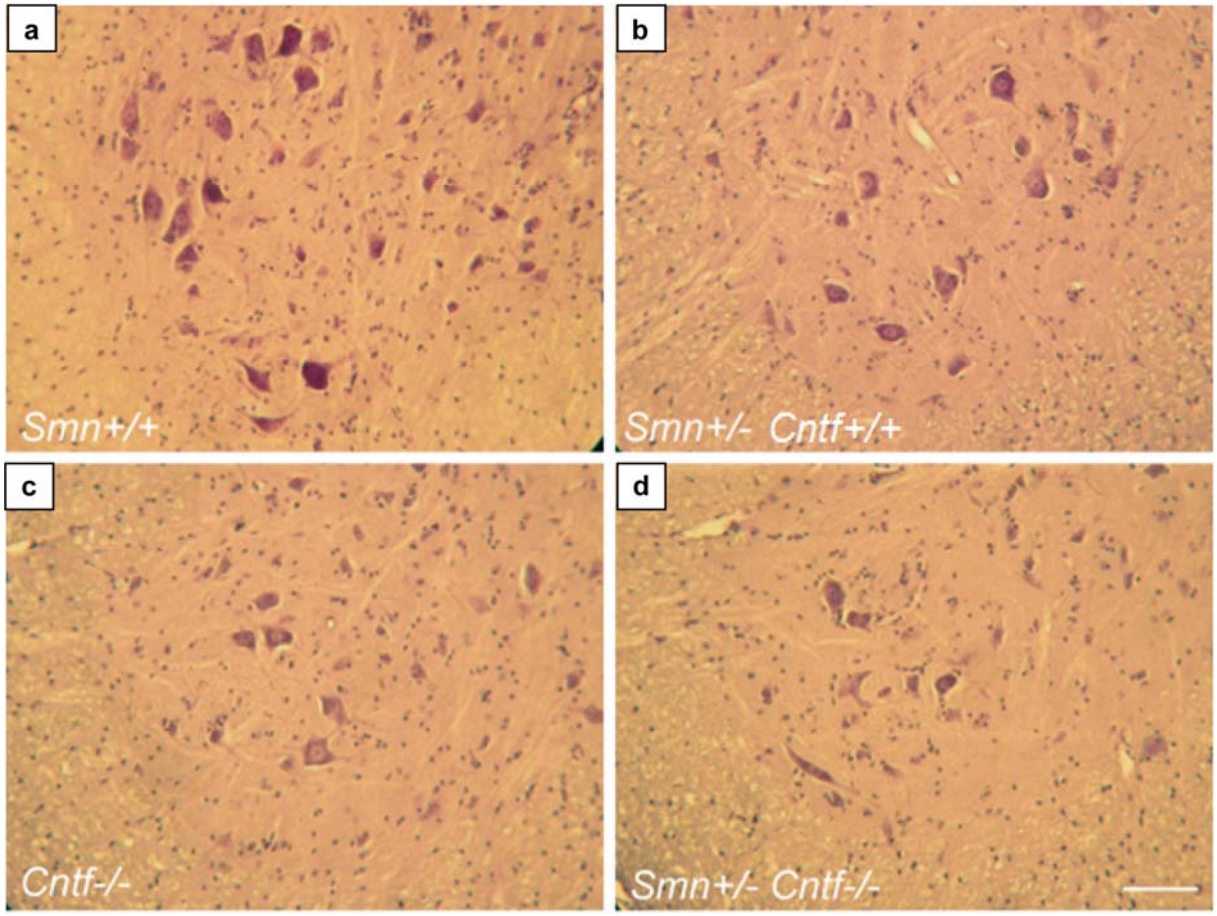

Figure 3-1-12: Morphology of lumbar spinal motoneurons of 12-month-old *Smn*$^{+/+}$, *Smn*$^{+/-}$ *Cntf*$^{+/+}$, *Cntf*$^{-/-}$ and *Smn*$^{+/-}$ *Cntf*$^{-/-}$ mice

(a-d) Examples of lumbar spinal cord sections showing Nissl-stained lumbar spinal motoneurons from 12-month-old Smn$^{+/+}$, *Smn*$^{+/-}$ *Cntf*$^{+/+}$, *Cntf*$^{-/-}$ and *Smn*$^{+/-}$ *Cntf*$^{-/-}$ mice. Note the loss of motoneurons in *Smn*$^{+/-}$ (b), *Cntf*$^{-/-}$ (c) and *Smn*$^{+/-}$ *Cntf*$^{-/-}$ (d) mice. Scale bar = 100 µm.

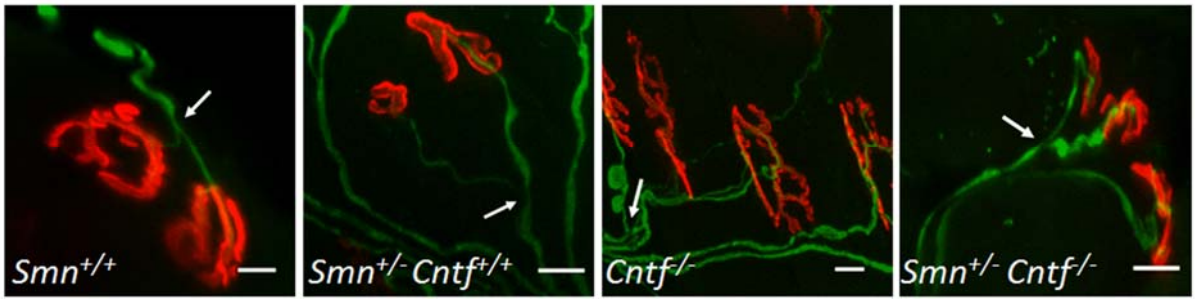

Figure 3-1-13: Sprouting events in the gastrocnemius muscle

Examples of neuromuscular endplates in gastrocnemius muscle of 12-month-old Smn$^{+/+}$, *Smn*$^{+/-}$ *Cntf*$^{+/+}$, *Cntf*$^{-/-}$ and *Smn*$^{+/-}$ *Cntf*$^{-/-}$ mice. Arrows point to the position of terminal sprouts. Scale bar = 10 µm.

To provide additional confirmation of the lack of sprouting in *Cntf*-deficient *Smn*$^{+/-}$ mice, the soma size of lumbar motoneurons in the spinal cord (L4-L5) of 4-week- and 12-month-old mice were measured (Fig. 3-1-14). When a motor unit increases by sprouting, the soma of the motoneuron becomes hypertrophic, because it grows bigger to maintain the proper connections to the muscle fibers. The soma size of motoneurons is related to the number of axonal sprouts each cell produces [304]. A slightly increased number of motoneurons with a size over 1000 µm^2 in 12-month-old *Smn*$^{+/-}$ *Cntf*$^{+/+}$ mice was found compared to *Smn*$^{+/-}$ mice without *Cntf* (percentage of motoneuron soma > 1000 µm^2: *Smn*$^{+/+}$ mice = 12.3%, *Smn*$^{+/-}$ *Cntf*$^{+/+}$ mice = 22.4%, *Cntf*$^{-/-}$ mice = 16.7%, *Smn*$^{+/-}$ *Cntf*$^{-/-}$ mice = 10.9%, at least n = 3 for each genotype). All these data indicate that CNTF induces sprouting and compensates for the loss of muscle strength in *Smn*$^{+/-}$ *Cntf*$^{+/+}$ mice.

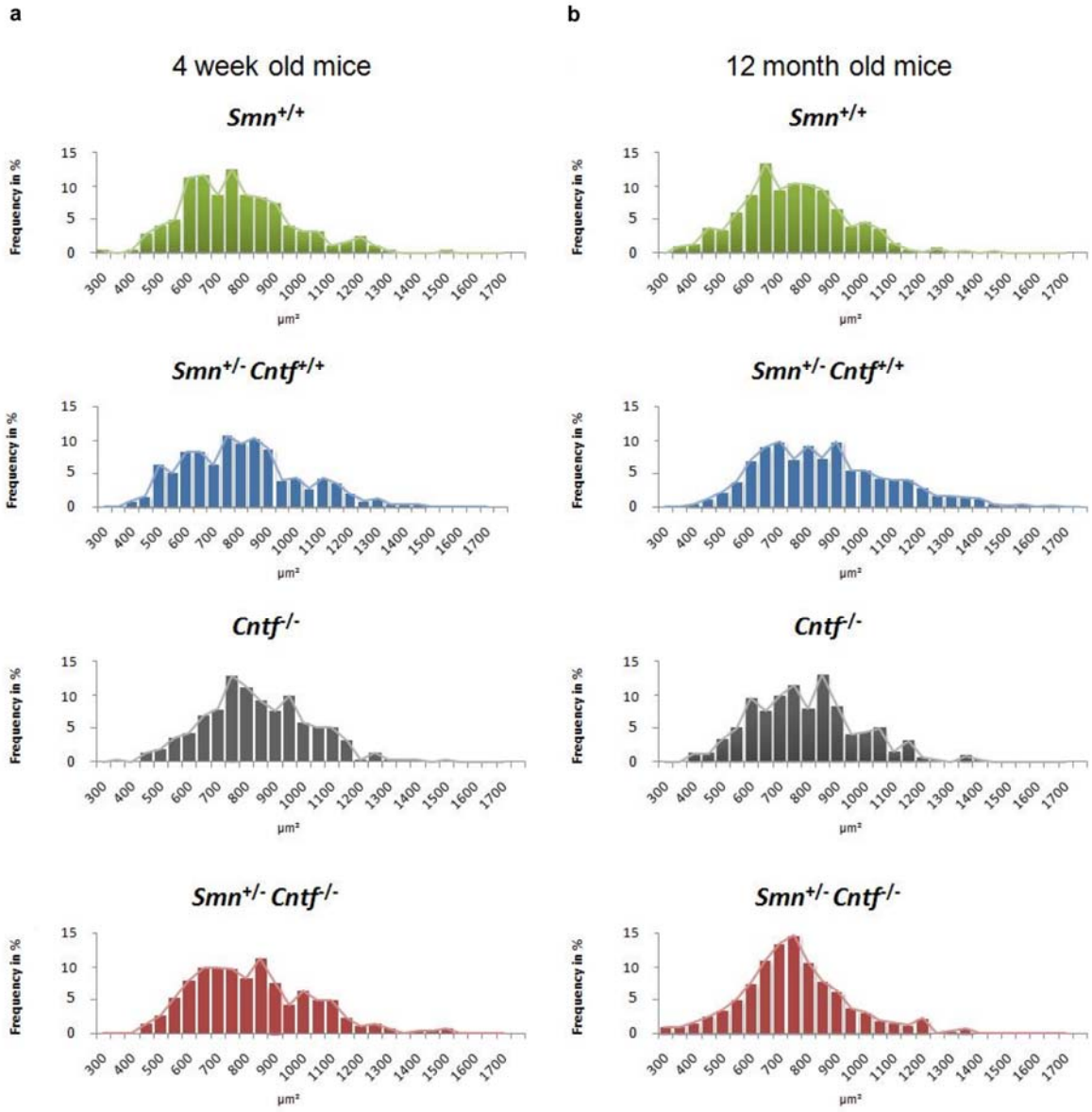

Figure 3-1-14: Frequency of motoneuron size in the ventral L4-L5 spinal cord region of 4-week and 12-month-old *Smn*$^{+/+}$, *Smn*$^{+/-}$ *Cntf*$^{+/+}$, *Cntf*$^{-/-}$ and *Smn*$^{+/-}$ *Cntf*$^{-/-}$ mice

(a) Motoneuron size in 4-week-old *Smn*$^{+/+}$, *Smn*$^{+/-}$ *Cntf*$^{+/+}$, *Cntf*$^{-/-}$ and *Smn*$^{+/-}$ *Cntf*$^{-/-}$ mice. (b) Motoneuron size in 12-month-old *Smn*$^{+/+}$, *Smn*$^{+/-}$ *Cntf*$^{+/+}$, *Cntf*$^{-/-}$ and *Smn*$^{+/-}$ *Cntf*$^{-/-}$ mice. Note the small proportion of enlarged motoneurons in 12-month-old *Smn*$^{+/-}$ *Cntf*$^{+/+}$ spinal cord (n = 500 motoneurons measured from 5 different animals for *Smn*$^{+/+}$, *Smn*$^{+/-}$ *Cntf*$^{+/+}$, and n = 350 from 3 different animals for *Cntf*$^{-/-}$ and *Smn*$^{+/-}$ *Cntf*$^{-/-}$).

3.1.8 Reduction of the mean single motor unit action potential size in Smn$^{+/-}$ *Cntf*$^{-/-}$ *muscle to wild-type levels correlates with reduced muscle strength*

Reduced sprouting after deletion of the *Cntf* gene in *Smn*$^{+/-}$ mice results in reduction of muscle strength (Fig. 3-1-10b). To get insight into whether the size of individual motor units is also affected in these mice, electrophysiological analyses were performed in collaboration with Dr. Rocio Ruiz and Dr. Lucia Tabares (Department of Medical Physiology and Biophysics, School of Medicine, University of Seville, 41009 Seville, Spain). Using a ring electrode placed at mid-thigh, the mean single motor unit action potential (SMUAPs) sizes in

Smn$^{+/+}$, *Smn*$^{+/-}$ *Cntf*$^{+/+}$, *Cntf*$^{-/-}$ and *Smn*$^{+/-}$ *Cntf*$^{-/-}$ were estimated by applying successive incremental stimuli starting from a subthreshold level until recruiting ten individual responses (Fig. 3-1-15a). As shown previously by results obtained with the needle electrode placed into the gastrocnemius muscle, *Smn*$^{+/-}$ *Cntf*$^{+/+}$ mice show about 2 times larger SMUAPs than *Smn*$^{+/+}$ mice (for data see [290]). *Cntf*$^{-/-}$ mice exhibit lower SMUAPs than *Smn*$^{+/-}$ mice. *Smn*$^{+/-}$ *Cntf*$^{-/-}$ exhibit almost 4-fold lower SMUAPs than *Smn*$^{+/-}$ mice (Fig. 3-1-15b) ($P < 0.001$, one-way ANOVA). This result indicates that motor units are smaller in *Smn*$^{+/-}$ *Cntf*$^{-/-}$ double mutant mice. These data confirm the functional relevance of the morphological alterations shown in Fig. 3-1-10.

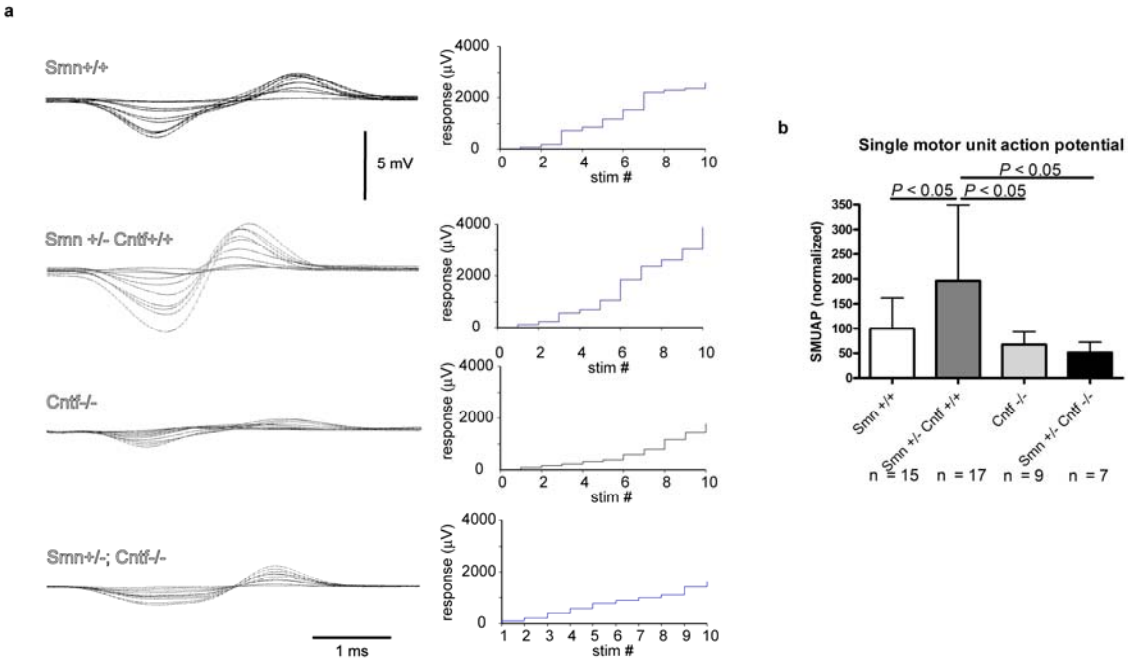

Figure 3-1-15: Lack of CNTF abolishes the compensatory increase of motor unit size in *Smn*$^{+/-}$ mice
(a) Representative examples of SMUAP amplitude increments recorded from 12-month-old *Smn*$^{+/+}$, *Smn*$^{+/-}$ *Cntf*$^{+/+}$, *Cntf*$^{-/-}$ and *Smn*$^{+/-}$ *Cntf*$^{-/-}$ mice in response to ten nerve stimuli of increasing amplitude. A circumferential surface electrode was placed around the flexor and extensor compartments of the distal hind-limb. (b) Quantification of normalized SMUAP in *Smn*$^{+/+}$, *Smn*$^{+/-}$ *Cntf*$^{+/+}$, *Cntf*$^{-/-}$ and *Smn*$^{+/-}$ *Cntf*$^{-/-}$ mice. The amplitude of SMUAPs was increased in *Smn*$^{+/-}$ mice, pointing to increased size of motor units due to increased sprouting. In *Smn*$^{+/-}$ *Cntf*$^{-/-}$ mice, SMUAP amplitudes were not increased (normalized SMUAPs: *Smn*$^{+/+}$ mice = 100 ± 61.8, *Smn*$^{+/-}$ *Cntf*$^{+/+}$ mice = 196.3 ± 152.6, *Cntf*$^{-/-}$ = 67.3 ± 26.2; *Smn*$^{+/-}$ *Cntf*$^{-/-}$ = 51.4 ± 20.8; at least n = 7 for each genotype $P < 0.001$, one-way ANOVA). (Electrophysiology was performed by Dr. Rocio Ruiz.)

A summary of the progressive loss of motoneurons in *Smn*$^{+/-}$ *Cntf*$^{+/+}$ mice from 4 weeks to 12 months in Fig. 3-1-16 is shown. In 6-month-old mice the loss is about 20%, and reaches over 40% in 12-month-old mice. To maintain the same grip strength, axonal sprouting and size of motor units increase correspondingly. Thus CNTF appears necessary for the compensatory sprouting response that maintains muscle strength in *Smn*$^{+/-}$ *Cntf*$^{+/+}$ mice.

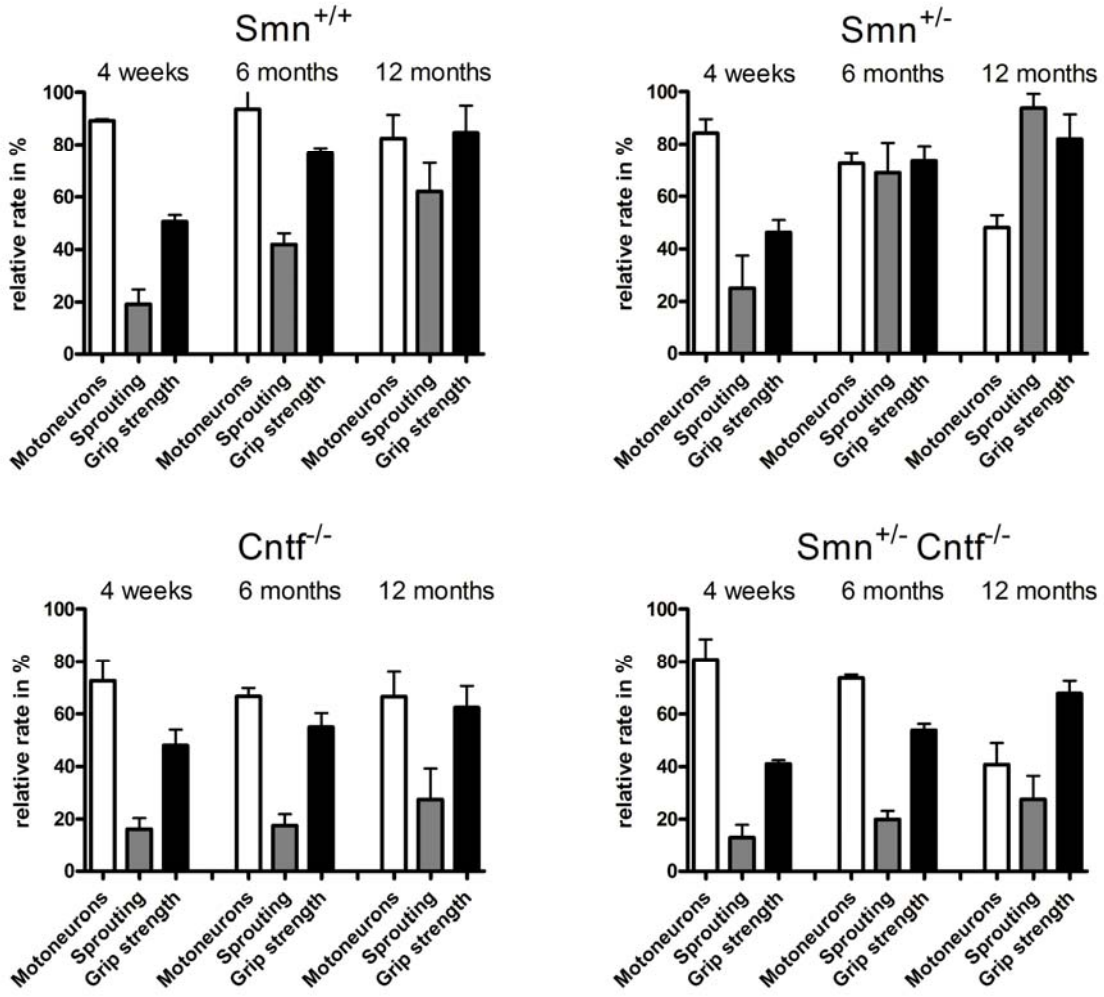

Figure 3-1-16: Overview of normalized motoneuron numbers, grip strength and sprouting events in all four genotypes

Summary of motoneuron numbers (Motoneurons), muscle strength (Grip strength) and number of axons innervating at least 2 neighboring neuromuscular endplates (Sprouting) in 4-week, 6-month and 12-month-old mice of all four genotypes. Values are given as percentages relative to the highest value in each investigation.

3.2 Dysregulated IGFBP-5 expression causes axonal degeneration and motoneuron cell death in diabetic neuropathy

The majority of the results shown here are part of the manuscript: "Simon et al., Dysregulated IGFBP-5 Expression Causes Axonal Degeneration and Motoneuron Cell Death in Diabetic Neuropathy, Nature Neuroscience, under review). Suralis biopsies from all patients investigated in this study were provided by Prof. Dr. Claudia Sommer. Microarray analysis was performed by Dr. Susanne Kneitz. Survival assays of cultured motoneurons were performed by Dr. Carsten Drepper. Motoneuron cell body and axon counts of the mice were performed by Dr. Bettina Holtmann (*IGF-R knockout*) and Dr. Massimiliano Braga (*NF-L-IGFBP-5*).

3.2.1 IGFBP-5 protein levels are elevated in nerve biopsies in DNP

Previous studies have shown that IGF-1 levels are downregulated in peripheral nerves in diabetic [279] and non-diabetic [305] types of neuropathy. We therefore investigated expression of members of the IGF family, their receptors and IGFBPs by microarray analysis of a sural nerve biopsy from a patient with DNP and compared these data with a sural nerve from an age-matched control individual (Fig. 3-2-1). These results confirmed decreased IGF-1 level in DNP [279] and also showed a more than 7-fold upregulation of IGFBP-5 expression.

Upregulated	GENE SYMBOL	NP-Control Fold change
insulin-like growth factor binding protein 5	IGFBP5	7.48
insulin-like growth factor 1 receptor	IGF1R	5.28
insulin-like growth factor binding protein 7	IGFBP7	4.59
insulin-like growth factor 2 receptor	IGF2R	2.87
insulin-like growth factor 2 mRNA binding protein 3	IGF2BP3	1.53
insulin-like growth factor binding protein-like 1	IGFBPL1	1.35
insulin-like growth factor binding protein 2, 36kDa	IGFBP2	1.27
IGF-like family member 2	IGFL2	1.26

Downregulated	GENE SYMBOL	NP-Control Fold change
insulin-like growth factor 1 (somatomedin C)	IGF1	4.65
insulin-like growth factor 2 mRNA binding protein 1	IGF2BP1	2.26
insulin-like growth factor 2 mRNA binding protein 2	IGF2BP2	2.19
insulin-like growth factor binding protein 4	IGFBP4	2.07
insulin-like growth factor binding protein, acid labile subunit	IGFALS	1.98
IGF-like family member 1	IGFL1	1.74
insulin-like growth factor binding protein 3	IGFBP3	1.37
insulin-like growth factor binding protein 6	IGFBP6	1.27
insulin-like growth factor binding protein 1	IGFBP1	1.10

Figure 3-2-1: Microarray expression analysis of sural nerves biopsies of control and DNP patients
Among IGF related genes, IGFBP-5 mRNA levels are increased more than 7-fold in DNP. (Analysis of the amount of purified RNA was performed by microarray in collaboration with Dr. Susanne Kneitz.)

In order to confirm this result, protein extracts from 21 patients and 5 control (Table 3-2-1) individuals were investigated by western blot analysis (Fig. 3-2-2). IGFBP-5 expression was low in healthy individuals and more than 60-fold upregulated in 6 patients with DNP (Fig. 2a, b) ($P < 0.001$, one-way ANOVA). More than 60-fold upregulation was also observed in 3 patients with combined diabetic neuropathy and chronic inflammatory demyelinating polyradiculoneuropathy (DNP+CIDP) ($P < 0.001$, one-way ANOVA) (Fig. 3-2-2a, b). Upregulation in patients with pure CIDP was only observed in 2 out of 9 patients, and did not reach statistical significance when compared to controls ($P > 0.05$, one-way ANOVA). This

suggests an association of IGFBP-5 overexpression with the DNP rather than with the superimposed CIDP in this mixed group. IGFBP-5 expression was also low in patients with amyotrophic lateral sclerosis (ALS), spinal muscular atrophy (SMA) and neuropathy due to vitamin B12 deficiency (Fig. 3-2-2a, b). This reveals that the strong upregulation of IGFBP-5 is specifically observed in patients with DNP.

Demographic data of patients

	DNP	DNP and CIDP	CIDP	Disease controls	Normal controls
N	6	4	9	3	5
Median age (range) [years]	60.5 (47-88)	68 (57-73)	69 (49-74)	64 (54-67)	33 (31-65)
Gender M; F	2; 4	1; 3	5; 4	1; 2	4; 1
Diabetes Type I;II	1;5	0;4	n.a.	n.a.	n.a.
Median disease duration until biopsy (range) [years]	1.4 (0.01-9)	1 (1-2)	2 (0.1-9)	2 (0.5-5)	n.a.
Type of neuropathy	SM: 6 A:6	SM: 4 A: 2; D: 2	SM: 7; M 9 D: 9	SM: 3 A: 3	n.a.

Table 3-2-1: Demographic data for all patients investigated in this study
DNP: Diabetic neuropathy. CIDP: Chronic inflammatory demyelinating polyradiculoneuropathy. Others: One case of amyotrophic lateral sclerosis, spinal muscular atrophy, and vitamin B12 deficiency each. n.a.: not applicable. Type of neuropathy: M = pure or predominantly motor; SM = sensorimotor; A: predominantly axonal; D: predominantly demyelinating. (This overview of patients was generated by Prof. Dr. Claudia Sommer)

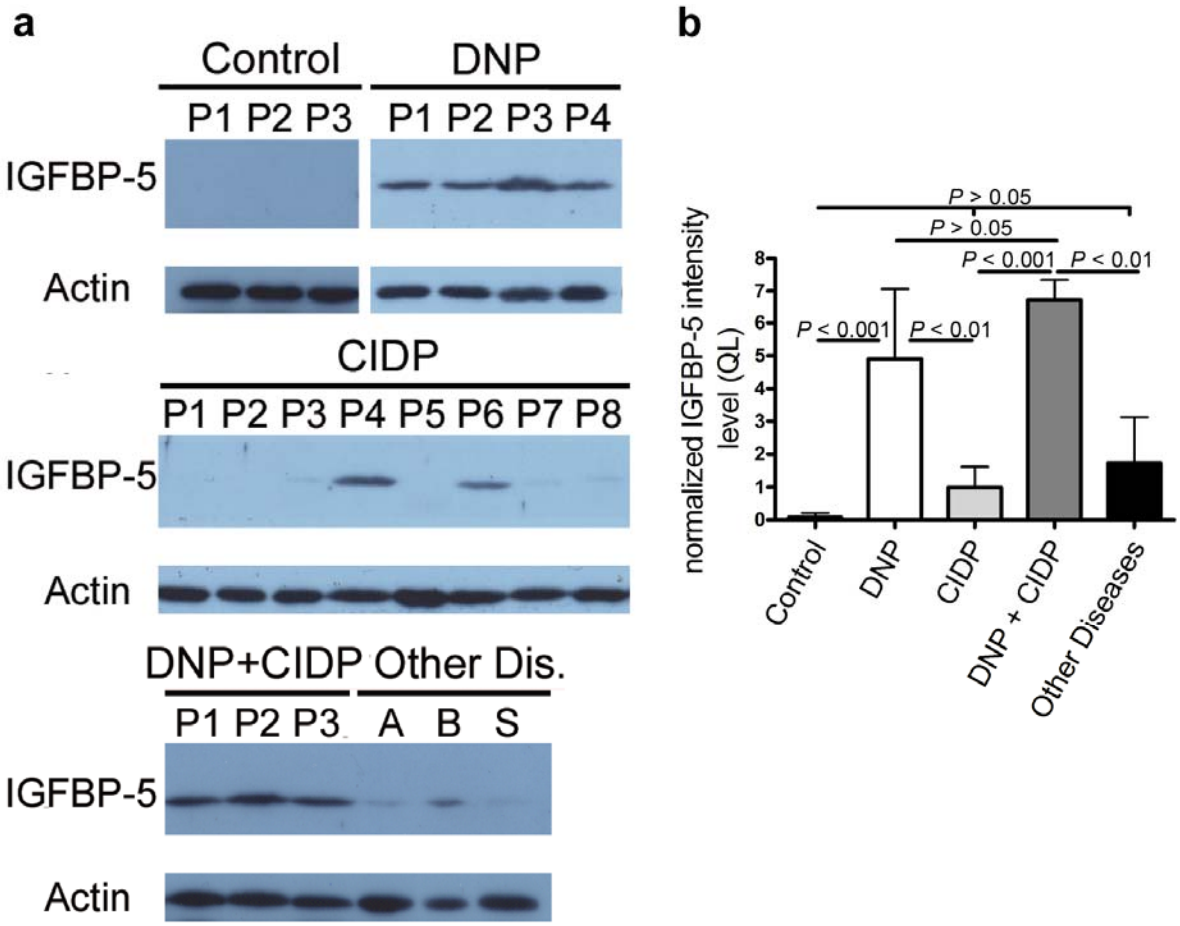

Figure 3-2-2: Western blot of IGFBP-5 protein levels in human sural nerve in control individuals and patients

(a) Western blot of IGFBP-5 protein levels in human sural nerve from control individuals, patients (P) with DNP, CIDP, DNP+CIDP and other diseases (Other Dis.): amyotrophic lateral sclerosis (A), vitamin B12 deficiency (B) and spinal muscular atrophy (S). (b) IGFBP-5 protein levels are specifically upregulated in patients with DNP. Biopsies of patients with DNP show a 64-fold upregulation compared to control individuals (DNP = 4.9 ± 2.2, n = 6; control = 0.1 ± 0.1, n = 5; $P < 0.001$, one-way ANOVA). Upregulation in DNP patients with additional CIDP is not significantly higher than patients with DNP alone (DNP+CIDP = 6.7 ± 0.6, n = 3; DNP = 4.9 ± 2.2, n = 6; $P > 0.05$, one-way ANOVA). Other disease controls with neuropathies and patients with CIDP show no significant upregulation to controls (control = 0.1 ± 0.1, n = 5; CIDP = 1 ± 1.8, n = 9; other disease control = 1.7 ± 1.4, n = 3; $P > 0.05$, one-way ANOVA). All values are normalized to CIDP biopsies.

Enhanced levels of IGFBP-5 could also be detected by immunohistochemistry of peripheral nerve sections (Fig. 3-2-3), particularly in axons, as displayed by co-localization with neurofilament H immunoreactivity. Faint IGFBP-5 immunoreactivity was also observed in the extracellular matrix surrounding the axons (arrows in Fig. 3-2-3).

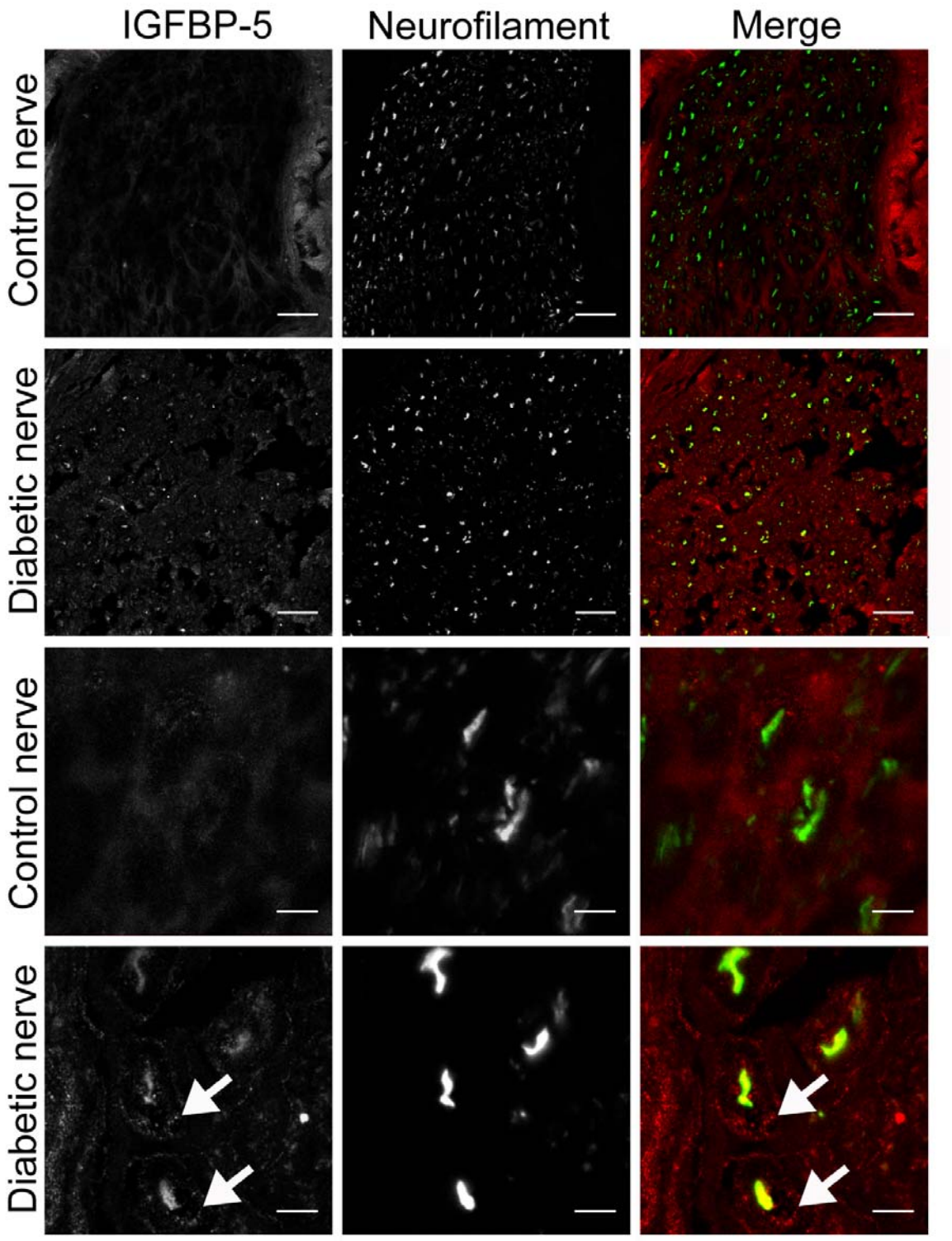

Figure 3-2-3: IGFBP-5 localization in control and diabetic suralis nerves
IGFBP-5 (red) localization with neurofilament (green) costaining in human sural nerves from a control individual and a patient with DNP is shown. Note that IGFBP-5 levels are increased in large axons and in the extracellular matrix (ECM) (arrows) in DNP. Scale bar = 5 µm.

3.2.2 IGFBP-5 inhibits motoneuron survival and axon growth

Based on the dramatic upregulation of IGFBP-5 expression in nerves of diabetic patients, and to study this effect in vivo, transgenic mice with neuron-specific overexpression of IGFBP-5 under a neurofilament promoter were generated by Dr. Jennifer Gunnersen. Briefly summarized, an 8 kb fragment including the human NF-L promoter, mouse Igfbp5 cDNA, the polyA signal from pMC-Cre and exons 2-4 of the NF-L gene was injected into fertilized mouse eggs.

First, the localization of wild-typic and overexpressed IGFBP-5 was investigated on isolated and cultured motoneurons from IGFBP-5 transgenic embryos and control litter mates (embryonic day (E) 13.5). The IGFBP-5-overexpressing motoneurons showed increased IGFBP-5 immunoreactivity in cell bodies and axons after 7 days in vitro (Fig. 3-2-4a). IGFBP-5 was predominantly localized on the surface of these neurons. This correlates with previous data showing that IGFBP-5 binds to the surface of producing cells and the surrounding extracellular matrix [306].

From previous studies in our lab, it was known that at a concentration of 5ng / ml IGF-1 has a positive effect on survival of cultured motoneurons. Therefore with the help of Dr. Carsten Drepper, a possible negative effect of recombinant and endogenously overexpressed IGFBP-5 on the survival of IGF-1 cultured motoneurons was investigated. Motoneurons were cultured 7 days in a medium supplemented with brain-derived neurotrophic factor (BDNF) as positive control (and without any factor as negative control). BDNF supports 55% survival, whereas only 12% of initially plated motoneurons survive without neurotrophic factors after 7 days in culture.

As expected, at a concentration of 5 ng / ml IGF-1 is a potent motoneuron survival factor and supports 46% (Fig. 3-2-4b). Addition of a 4-fold molar excess of IGFBP-5 (80 ng / ml) reduced survival to 20% ($P < 0.001$, one-way ANOVA) (Fig. 3-2-4b). When IGFBP-5 was added at a 20-fold molar excess, the survival effect of IGF-1 was completely blocked to the low control levels without survival factors (data not shown). IGFBP-5 has no effect on BDNF mediated survival ($P > 0.05$, one-way ANOVA) (Fig. 4b).

IGFBP-5 transgenic motoneurons showed a different survival response to IGF-1 than wild-type motoneurons (Fig. 3-2-4b) ($P < 0.001$, one-way ANOVA). While survival of IGFBP-5-overexpressing motoneurons was unchanged in the presence of BDNF, survival in the presence of 5 ng / ml of IGF-1 was reduced in comparison to wild-type motoneurons derived from non-transgenic controls ($P < 0.001$, one-way ANOVA). Furthermore, a very low level of

IGF-1 (1 ng / ml), which supported 32% survival in wild-type motoneurons, was not able to support IGFBP-5 transgenic motoneurons (data not shown) ($P < 0.001$, one-way ANOVA).

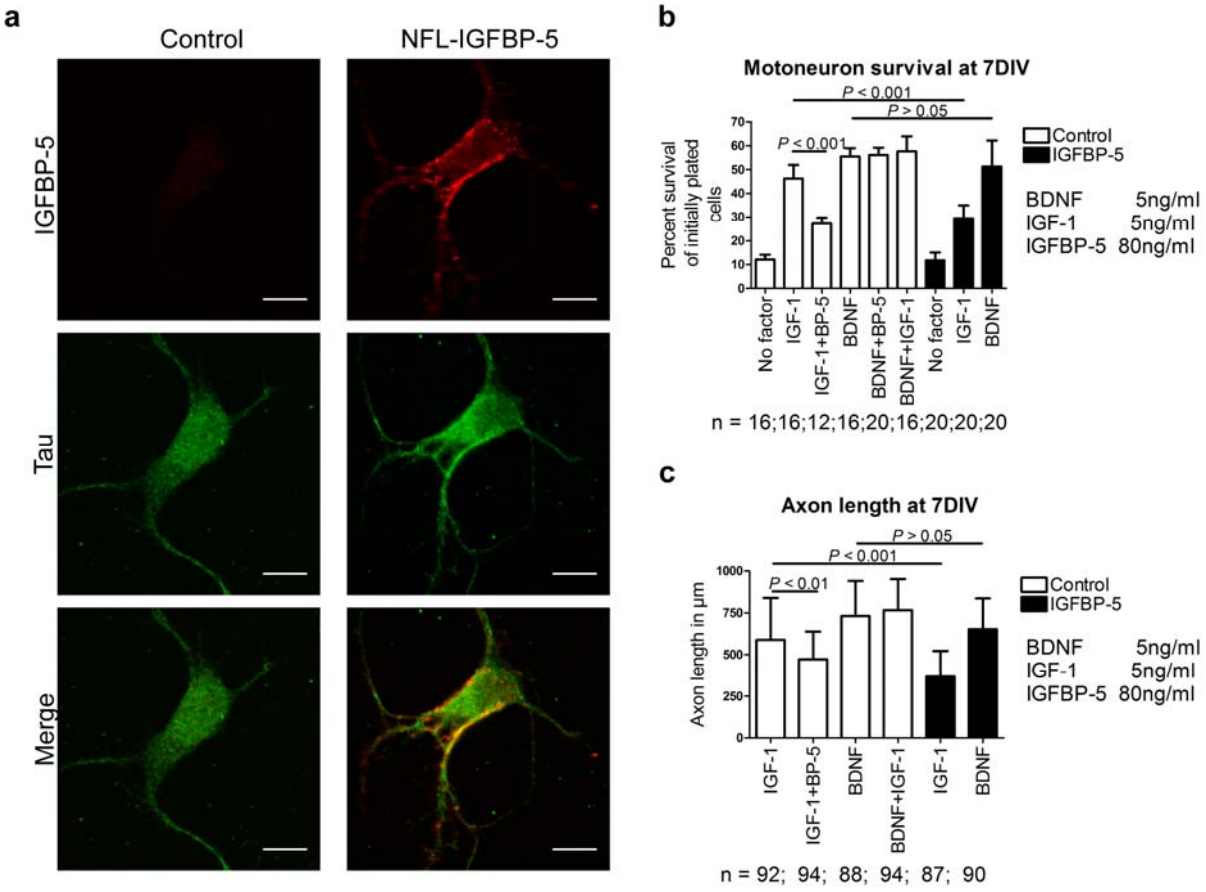

Figure 3-2-4: IGFBP-5 overexpression in cultured motoneurons reduces survival rate and axon length
(a) IGFBP-5 expression in cultured motoneurons (7 DIV), stained by using antibodies to tau and IGFBP-5. IGFBP-5 is increased in the soma and neurites of *NF-L-IGFBP-5*-overexpressing motoneurons. IGFBP-5 appears associated with the cell membrane. Scale bar = 5 µm. (b) The positive effect of IGF-1 on survival is reduced by 17% in IGFBP-5-overexpressing motoneurons (tg = 29.5 ±5.4%, n = 20 wells; control = 46.3 ± 5.7%, n = 16 wells; $P < 0.001$, one-way ANOVA). Motoneuron survival was unchanged in the presence of BDNF (tg motoneurons = 51.3 ± 10.8%, n = 16; wild-type motoneurons = 55.5 ± 3.5%, n = 20; $P > 0.05$, one-way ANOVA) (performed by Dr. Carsten Drepper). (c) IGFBP-5 (BP-5) inhibits IGF-1 induced axon outgrowth in wild-type motoneurons at a 4-fold molar excess (mean axon length with IGF-1 = 588.9 ± 249.6 µm; IGF-1 + BP-5 = 472.3 ± 166.3 µm; n = 4 embryos, n > 90 axons; $P < 0.01$, one-way ANOVA). IGFBP-5-overexpressing motoneurons show shorter axons than wild-type axons while they were cultured with IGF-1 (tg = 367.6 ± 154.5 µm; controls = 588.9 ± 249.6 µm; n = 4 embryos each, n > 85 axons; $P < 0.01$, one-way ANOVA). Axon growth stimulated by BDNF (5 ng / ml) was not affected in IGFBP-5-overexpressing motoneurons (tg = 652 ± 184.2 µm; controls = 731 ± 210.2 µm, n = 4 embryos each, n > 85 axons, $P > 0.05$, one-way ANOVA). Data sets are expressed as mean ± SD (performed by Dr. Carsten Drepper).

Motoneurons overexpressing IGFBP-5 also exhibited reduced axon growth (Fig. 3-2-4c) when cultured with IGF-1 at a concentration of 5 ng / ml ($P < 0.001$, one-way ANOVA). Axon growth was normal when these motoneurons were cultured with 5 ng / ml BDNF ($P > 0.05$, one-way ANOVA), indicating that IGFBP-5 not only reduces survival but also specifically inhibits the effects of IGF-1 on axon growth.

3.2.3 Transgenic IGFBP-5 overexpression in motoneurons leads to impaired motor function, degeneration and loss of motor axons and cell bodies

In order to quantify expression of IGFBP-5 in these transgenic (tg) mouse lines, Igfbp-5 mRNA levels were determined by real-time PCR of spinal cord and found to be 1.8-fold upregulated (P = 0.0002, two-tailed Student's t-test) (Fig 3-2-5a). Western blots were prepared with extracts from spinal cord, sciatic nerve and brain. Enhanced IGFBP-5 protein levels were detected in the sciatic nerves of 6-month-old transgenic mice (Fig. 5b). In IGFBP-5-overexpressing mice, elevated IGFBP-5 immunoreactivity was observed in axons and the extracellular matrix surrounding the axons in the sciatic nerve (Fig. 3-2-5c), closely resembling the distribution of IGFBP-5 in peripheral nerves from sural biopsies of patients with DNP (Fig. 3-2-3).

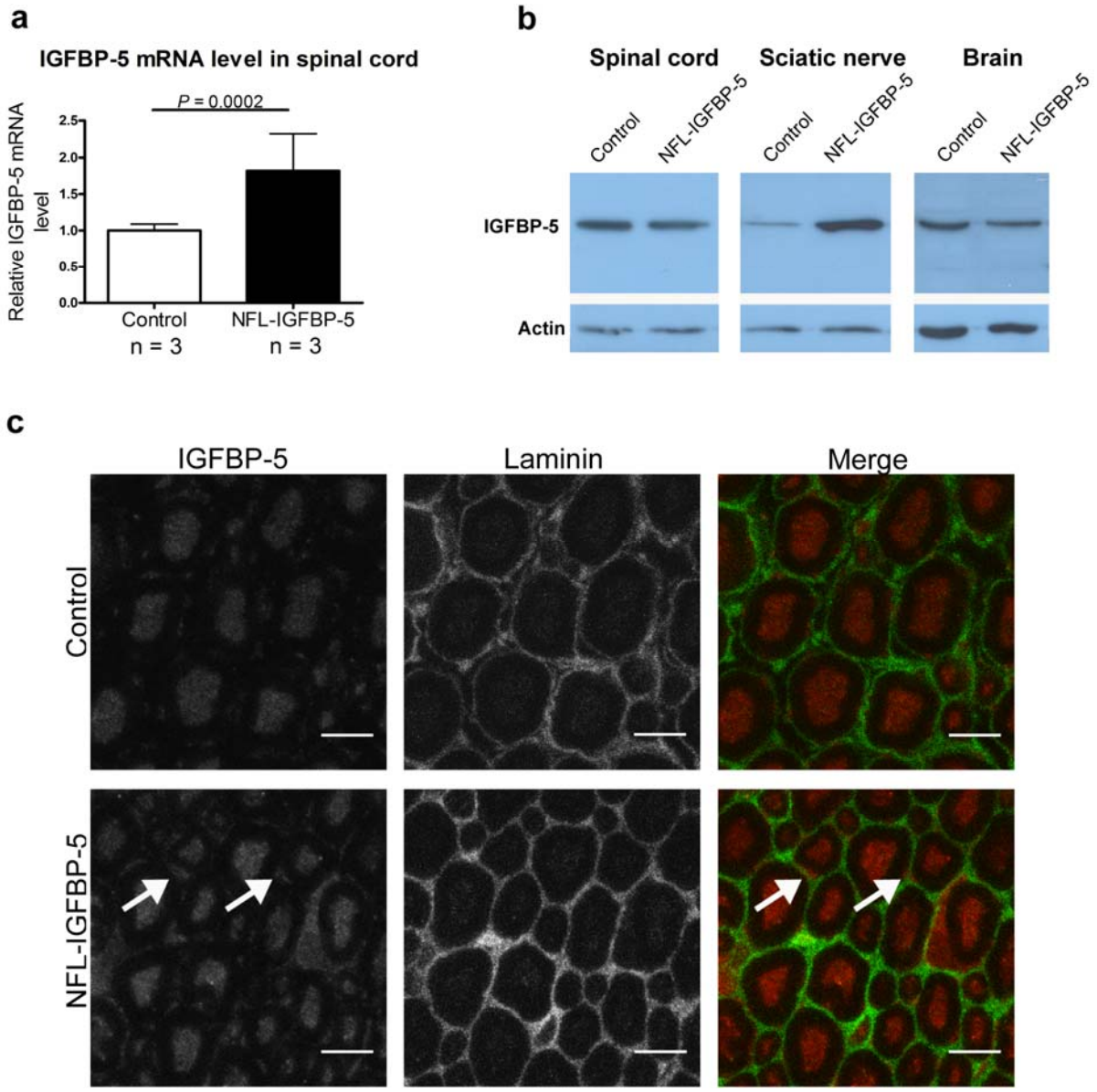

Figure 3-2-5: IGFBP-5 overexpression in adult mouse tissues
(a) Real-time PCR revealed a 1.8 fold increase of the IGFBP-5 mRNA level in transgenic IGFBP-5 animals (tg). Scored values were obtained by normalizing to β-actin mRNA levels (normalized control = 1.0 ± 0.1, n = 3; tg = 1.8 ± 0.5, n = 3; *P* = 0.0002, two-tailed Student's t-test). (b) IGFBP-5 protein elevation was detected in sciatic nerve but not in spinal cord and brain compared to controls. Actin was used as loading control. (c) Localization of IGFBP-5 in frozen cross-section. IGFBP-5 is increased in axons and extracellular matrix in transgenic animals. Arrows depict extracellular matrix staining. Scale bar = 5µm.

To investigate whether IGFBP-5 overexpression in vivo leads to impaired motor function, degeneration and loss of motor axons and cell bodies, Dr. Massimiliano Braga counted fibers of different nerves and motoneuron numbers in spinal cord of IGFBP-5 transgenic and control litter mates. If IGFBP-5 overexpression would inhibit IGF-1 in vivo, this could result in reduced motoneuron survival and myelination [44,174].

6-month-old IGFBP-5 transgenic mice showed no overt phenotype variation however a significant reduction of forelimb grip strength was observed. The numbers of myelinated

nerve fibers of the sciatic and phrenic nerve were reduced by about 15% (Table 3-2-2). A progressive loss of facial and spinal motoneuron cell bodies was also detected in IGFBP-5 transgenic animals and became apparent after 6 months (Table 3-2-2).

Morphometric analysis of NFL-IGFBP-5 transgenic and control mice

Tissue	Age	Control mean ± SD	(n)	NFL-IGFBP-5 mean ± SD	(n)	Ratio IGFBP-5-Control	P-value
Facial motoneuron number	P1	3312 ± 53	3	3258 ± 231	3	0.984	0.7167
	P21	3404 ± 212	4	3015 ± 264	4	0.886	0.2438
	5-6 months	3260 ± 182	6	2696 ± 266	6	0.827	0.0016
Lumbar spinal motoneurons	5-6 months	2951 ± 100	4	2373 ± 140	6	0.804	0.0001
Phrenic nerve fiber number	P21	298 ± 27	4	252 ± 14	6	0.846	0.0075
	5-6 months	274 ± 13	5	247 ± 12	6	0.901	0.0490
Sciatic nerve fiber number	5-6 months	4628 ± 172	4	3969 ± 180	6	0.858	0.0233

Table 3-2-2: Morphometric analysis of *NF-L-IGFBP-5* transgenic and control mice
Overview of degeneration of axons and motoneurons in neuron-specific IGFBP-5-overexpressing mice. (Quantification was performed by Dr. Massimiliano Braga.)

3.2.4 IGFBP-5 overexpression leads to reduction of myelination and a motor axonopathy

In addition, myelin thinning was observed in sciatic nerve sections from 6-month-old IGFBP-5 transgenic mice (Fig. 3-2-6a), as also observed in IGF-1 knockout mice [44]. The M-ratio (myelin thickness/axon diameter) was significantly reduced by 20% in the transgenic animals (Fig. 3-2-6b) ($P = 0.02$, two-tailed Student's t-test). In addition, a change in fiber size distribution in the sciatic nerve became apparent, with a significant reduction in larger fibers with a circumference between 20 µm and 25 µm in IGFBP-5-overexpressing mice (Fig. 3-2-6c) ($P < 0.01$, two-way ANOVA). This suggests that local inhibition of IGF-1 not only affects larger axons but also the degree of myelination in Schwann cells.

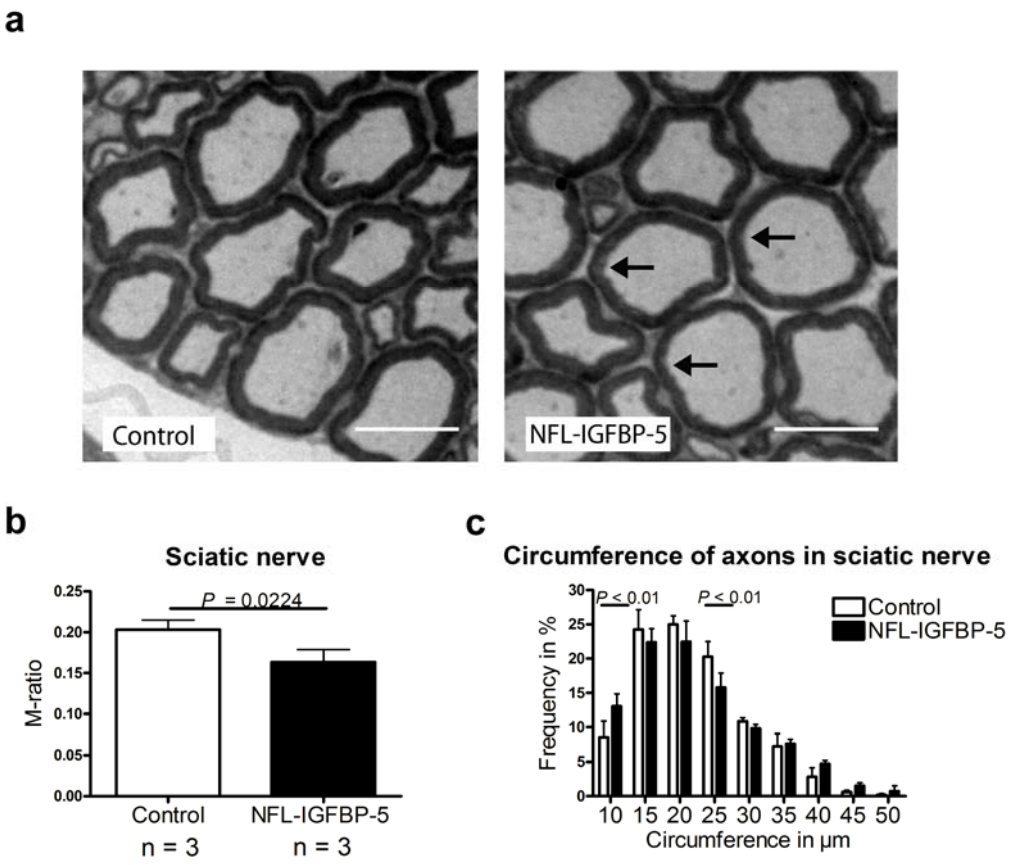

Figure 3-2-6: Myelination of sciatic nerve is impaired in IGFBP-5-overexpressing mice
(a) Examples of sciatic nerve sections showing representative myelinated axons. (b) Quantification of M-ratio for myelin thickness in sciatic nerve from IGFBP-5-overexpressing and control mice (control = 0.20 ± 0.01, n = 3; tg = 0.16 ± 0.02, n = 3, n > 150 axons; $P = 0.02$, two-tailed Student's t-test). Scale bar =10 µm. (c) Change in fiber size distribution in 6-month-old sciatic nerve by a 4.5% reduction of larger fibers with a circumference between 20 µm and 25 µm in IGFBP-5-overexpressing mice (tg = 15.8 ± 2.1%, n = 5, more than 2500 axons; control = 20.3 ± 2.0%, n = 3, more than 1400 axons; $P < 0.01$, two-way ANOVA).

In order to functionally characterize whether elevated IGFBP-5 leads to a large-fiber neuropathy similar to that observed in patients with DNP, and to detect a potential functional contribution of reduced myelin thickness, the distal and proximal CMAP amplitudes and nerve conduction velocities (NCV) were measured by Dr. Jürgen Zielasek and Professor Dr. Klaus Toyka using electrophysiological techniques [307,308]. The first pair of stimulating electrodes was placed in the left sciatic notch and 2 cm laterally (proximal stimulation for proximal CMAP). A second pair of stimulating electrodes was inserted subcutaneously along the tibia1 nerve just above the ankle (distal stimulation for distal CMAP). Recording electrodes were placed in the skin close to the hallux, and between digits 2 and 3 of the left foot of 5- to 6-month-old IGFBP-5-overexpressing mice [308]. The electrophysiological signal travels a shorter distance when stimulated at the distal stimulation to the recording electrodes and therefore the distal CMAP is higher (Fig. 3-2-7a, b). The proximal CMAP is smaller, because it loses strength over distance. In control animals the loss of the signal between

promixal to distal CMAP is in the range of approximately 5 to 25% [308]. Due to myelination defects this range can be increased in mutant mice.

As expected, in control mice the mean of the proximally elicited CMAP was smaller than the distally elicited CMAP, but the difference was not statistically significant. In transgenic animals, the proximal CMAP showed a significant reduction of 32% compared to the distal CMAP, indicating a partial lack of signal transmission due to myelination abnormalities (Fig. 3-2-7c, d). In addition, a significant 18% reduction in motor conduction velocity was observed in the sciatic nerve of IGFBP-5 transgenic animals compared to the wild-type controls, which could be explained by reduced myelination (Fig. 3-2-7e).

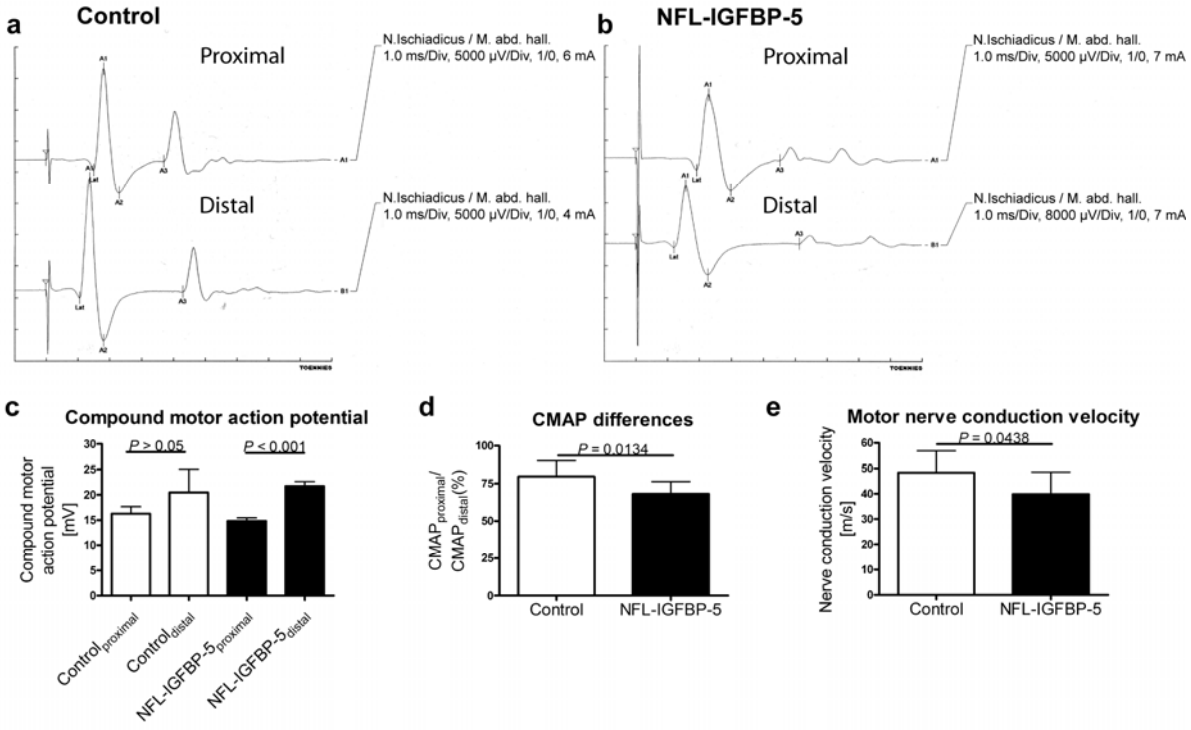

Figure 3-2-7: IGFBP-5-overexpressing mice show reduced CMAP and nerve conduction velocity

(a) NCV studies in the sciatic nerve of control animals and (b) 5- to 6-month-old IGFBP-5 transgenic mice. Note that for the distal CMAP of the IGFBP-5 tg animals a higher gain of 8 mV/division instead of 5 mV/division was used for better display. Control mice show only a slightly reduced proximal CMAP compared to the distal one. In *NF-L-IGFBP-5* animals, the proximal and distal CMAPs are reduced.

(c, d) Quantification of the proximal and distal CMAPs in control and IGFBP-5 transgenic animals. The proximal CMAP was 21% smaller than the distal CMAP in control mice (proximal CMAP: 16.3 ± 3.9 mV, n = 8; distal CMAP: 20.5 ± 4.6 mV, n = 8; $P > 0.05$, one-way ANOVA). In IGFBP-5 transgenic animals, the proximal CMAP showed a significant reduction by 32% as compared to the distal CMAP (proximal CMAP: 14.8 ± 2.2 mV, n = 12; distal CMAP: 21.7 ± 3.0 mV, n = 12; $P < 0.001$, one-way ANOVA).

(e) Motor NCV is reduced by 18% in sciatic nerve of *NF-L-IGFBP-5* transgenic mice (controls: 48.4 ± 8.4 m/s, n = 8; tg: 39.8 ± 8.8 m/s, n = 12; $P = 0.04$, two-tailed Student's t-test). Data sets are expressed as mean ± SD. (Electrophysiology was performed by Dr. Zielasek and Professor Dr. Toyka.)

3.2.5 Conditional depletion of IGF-1 receptor (Igfr) in motoneurons results in axonopathy and motoneuron loss similar to that seen with IGFBP-5 overexpression

In order to investigate whether the axon and motoneuron loss occurring with IGFBP-5 overexpression is due to reduced availability of IGF-1 for axons, we analyzed mice with neuron-specific inactivation of the type 1 IGF receptor (NF-L-Cre, *Igfr*$^{loxP/loxP}$) and corresponding littermate controls (*Igfr*$^{loxP/loxP}$). These mice were generated by Dr. Jennifer Gunnersen. For this purpose, mice carrying loxP sites flanking exon III of the mouse *Igfr* gene were generated. Exon III encodes most of the cysteine-rich ligand-binding domain of the α-subunit of the receptor, and disruption of this exon generates an inactive receptor [309]. The Cre recombinase is under the control of the NF-L gene promoter [310]. A reverse transcription-PCR was used for detection of the neuron-specific disruption of exon 3 (Fig. 3-2-8).

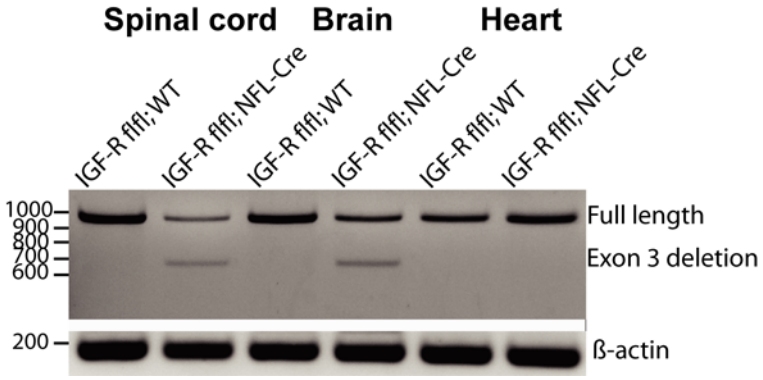

Figure 3-2-8: Deletion of the IGF-1 binding domain (exon 3) in *Igfr* neuron specific knockout mouse
Reverse transcriptase PCR reveals exon 3 deletion in neuronal tissue of NF-L-Cre, *Igfr*$^{loxP/loxP}$ mice.

Exon 3 spanning primers were used for this reverse trancription (forward primer exon 2, reverse primer exon 6, transcript size: PCR: 313bp). A partial deletion in neuronal tissue was found and can be explained by the composition of the brain and spinal cord which contain more glial cells than neurons, in which no neurofilament promoter is active and hence no deletion occurs. This result confirms a specific inactivation of the *Igfr* in neurons of these mice. Heart tissue as a non-neuronal tissue showed no deletion of exon 3.

NF-L-Cre, *Igfr*$^{loxP/loxP}$ mice also did not show any overt phenotype. Histological analysis of the phrenic nerve of 6-month-old NF-L-Cre, *Igfr*$^{loxP/loxP}$ mice revealed a significant reduction in nerve fibers similar to that seen in *NF-L-IGFBP-5* mice (Table 3-2-3, performed by Dr. Bettina Holtmann). Interestingly, the number of myelinated axons was significantly reduced in the sciatic nerve of the NF-L-Cre, *Igfr*$^{loxP/loxP}$, as in IGFBP-5-overexpressing mice (Table 3-2-3), but the M-ratio of myelin thickness to axon diameter was normal (Fig. 3-2-9a, b) (P = 0.7859, two-tailed Student's t-test), indicating no myelination defect in these mice. Furthermore, NF-L-Cre, *Igfr*$^{loxP/loxP}$ mice, like the IGFBP-5-overexpressing mice, also showed

a decrease of 6% in large fibers with a circumference between 20 and 25 µm ($P < 0.05$, two-way ANOVA) (Fig. 3-2-9c).

Morphometric analysis of IGF1 receptor knockout and control mice

Tissue	Age	Control mean ± SD	(n)	IGF-1 R ko mean ± SD	(n)	Ratio IGFR-1ko-Control	P-value
Facial motoneuron number	P1	3337 ± 115	4	3262 ± 242	3	0.978	0.5973
	9 months	2558 ± 186	4	2147 ± 267	4	0.839	0.045
Lumbar spinal motoneurons	P1	2866 ± 451	4	2710 ± 325	3	0.946	0.6341
	9 months	2890 ± 96	4	2281 ± 300	4	0.789	0.0083
Phrenic nerve fiber number	6 months	246 ± 19	4	219 ± 4	4	0.890	0.0335
Sciatic nerve fiber number	6-7 months	4527 ± 328	7	3956 ± 445	7	0.874	0.0182

Table 3-2-3: Morphometric analysis of IGF-1 receptor knockout and control mice
Overview of degeneration of axons and motoneurons in control and *Igfr* knockout mice. (Quantification was performed by Dr. Bettina Holtmann.)

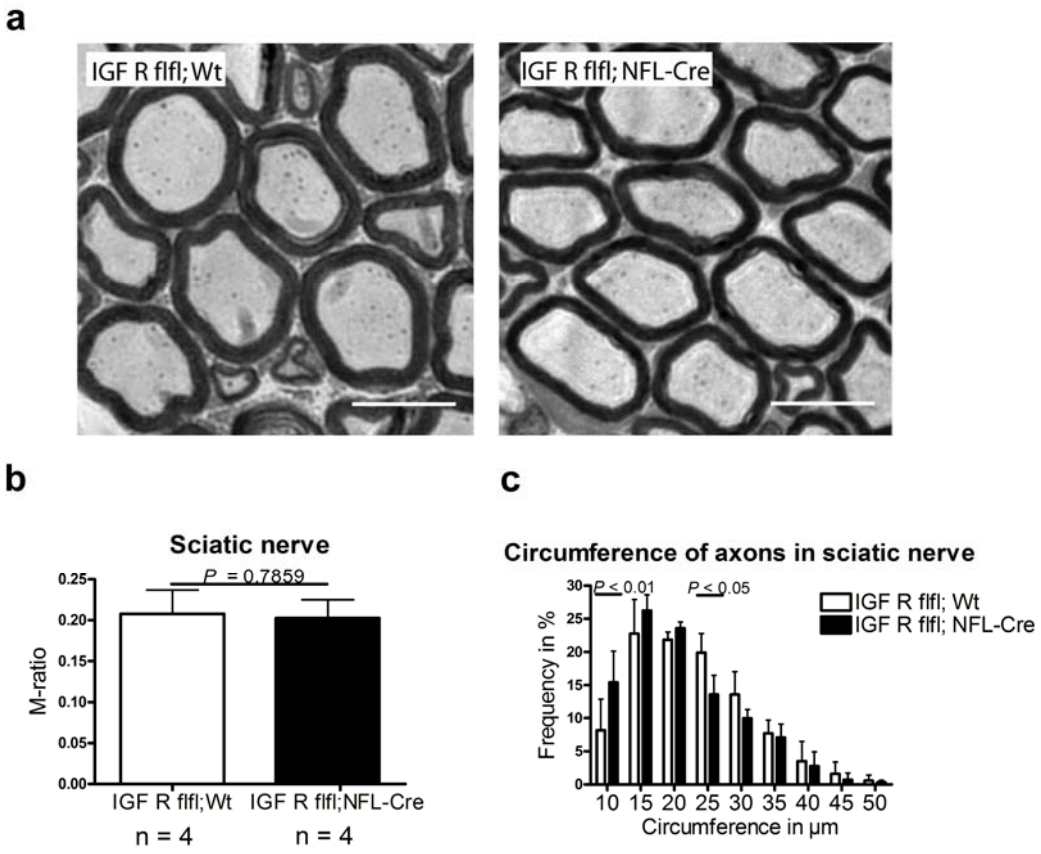

Figure 3-2-9: *Igfr* knockout mice show no abnormalities in myelination of the sciatic nerve
Sciatic nerve sections (a) showing that the M-ratio of myelin thickness and axon diameter was normal (b) (control = 0.20 ± 0.03, n = 4; *Igfr* knockout: 0.20 ± 0.02, n = 4, n > 200 axons; $P = 0.7859$, two-tailed Student's t-test). Scale bar = 10µm. (c) NF-L-Cre, $Igfr^{loxP/loxP}$ mice showed a decrease of 6% of larger fibers with a circumference between 20 µm and 25 µm (*Igfr* knockout = 13.6 ±2.9%, n = 4, more than 2200 axons; control: 19.9 ± 2.9%, n=4, more than 1800 axons; $P < 0.05$ two-way ANOVA).

Determination of the number of facial and lumbar spinal motoneurons showed a progressive loss of cell bodies in NF-L-Cre, *Igfr*$^{loxP/loxP}$ compared to Cre-negative littermates. No reduction in cell number was apparent in newborn NF-L-Cre, *Igfr*$^{loxP/loxP}$ facial and lumbar spinal motoneurons (Table 3-2-3, performed by Dr. Bettina Holtmann). On the other hand, a significant reduction became apparent in 9-month-old *Igfr* conditional knockout mice in the facial nucleus (16%) as well as in the lumbar spinal cord (21%), resembling the IGFBP-5-overexpressing phenotype (compare Table 3-2-3 with Table 3-2-2). Taken together, these results suggest that the loss of motoneurons and axons result from the lack of transduction of the IGF-1 pathway over its receptor.

4 Discussion

Neurotrophic factors have a wide range of functions which include development, survival and maintenance of neurons, differentiation of glia cells and regulation of synaptogenesis and synaptic plasticity in mature neurons [81-86]. Several neurotrophic factors have a direct impact on motoneuron survival and maintenance, as shown in pure cultured embryonic motoneurons or in vivo [89,311]. These survival factors for motoneurons include CNTF, LIF, CT-1, IGF-1, GDNF and BDNF [89] (for details see Table 1-1). In this thesis I investigated the role of the neurotrophic factor CNTF as a compensatory sprouting mechanism in a mouse model for mild spinal muscular atrophy and the effects of IGF-1 on axon maintenance in a mouse model for DNP.

CNTF is expressed as a soluble protein in Schwann cells in peripheral neurons, and in the central nervous system mostly in astrocytes [110]. CNTF expression is very low during embryonic development, but becomes apparent in the rat sciatic nerve by day 4, reaching its maximum level in fully differentiated Schwann cells in the third postnatal week [78,112,113]. This, and the fact that *CNTF* knockout mice develop completely normally, leads to the conclusion that CNTF has no central role in the development of the nervous system. After sciatic nerve lesion, CNTF is rapidly upregulated in Schwann cells for 1 week and increased in the extracellular matrix at the distal nerve segment to support the regeneration of the axon [113]. *CNTF* knockout mice show a progressive motoneuron loss of 20% that correlates with a mild loss of muscle strength within the first 6 months (Fig. 3-1-10) [114,118]. This indicates the importance of CNTF in motoneuron and axon maintenance in adulthood.

Further studies reveal CNTF to be an inducer of axonal sprouting near the NMJ when injected over the surface of the adult mouse gluteus muscle [107]. Furthermore, mice lacking CNTF showed no sprouting response after sprouting-inducing stimuli, such as injection of botulinum and transection of a nerve branch. However, exogenous CNTF administration given in parallel to the stimuli induces sprouting in CNTF knockout mice [127]. The important role of the compensatory mechanism of CNTF in other diseases could also be shown. 2% of the Japanese and German populations have a G to A transition at position –6 in the first intron of the human *CNTF* gene. This transition creates a new splice acceptor site that leads to aberrant splicing of the mRNA and to a truncated, inactive CNTF protein. Patients with motoneuron diseases show a similar CNTF deletion frequency of 2%, indicating that CNTF deficiency is not directly related to neurological diseases [312,313]. However, a study identified *CNTF* as a modifier gene in familial and sporadic amyotrophic lateral sclerosis ALS (FALS, SALS).

These ALS patients exhibit an earlier onset and a more severe progression of the disease when they also carried the homozygous CNTF gene defect. These findings were confirmed by a FALS mouse model *(hSOD-1G93A)* that was crossbred with *CNTF* null mutations. *hSOD-1G93A* mice without CNTF show a significantly earlier onset of motor defects and shorter survival compared to the *hSOD-1G93A* mice with a functional CNTF gene [314]. Other mouse models confirmed the finding of CNTF as a positive modifier gene in motoneuron diseases. Addition of CNTF by application via CNTF-secreting stem cells [103] or by local injection into skeletal muscle [302] leads to improved maintenance of motor axons in *pmn* mutant mice or neuromuscular endplates in *hSOD-1 G93A* mice [295].

GDNF also supports motoneuron survival in vitro and in vivo (Table 1-1) [98]. GDNF is very potent in supporting the survival of purified cultured embryonic motoneurons, and after axotomy GDNF rescues and prevents atrophy of facial motoenurons in vivo [98]. Additionally, GDNF slows the loss of motoneurons in *pmn* mice. However, it does not prevent axon loss or prolong survival in *pmn* mice in the way that CNTF does [102]. Furthermore, GDNF knockout mice that die at birth show the importance of GDNF for motoneuronal development as opposed to the compensatory mechanism in adult stages. Additionally, muscle-specific GDNF has a more important role in the maintenance of hyperinnervation of NMJs, rather than inducing axonal sprouting in adult animals. This strengthens the proposal that GDNF is important in motoneuron development and innervation of the NMJ, but that CNTF is more effective in axon maintenance or inducing sprouting in degenerative processes.

Besides CNTF, Schwann cells are also the source of BDNF, another important neurotrophic factor. BDNF belongs to the family of neurotrophins (Table 1-1). BDNF knockout mice show ataxia, loss of myelinated sensory neurons and vestibular neurons, and die after a few days [87]. In contrast to CNTF, BDNF mRNA is undetectable in healthy rat sciatic nerves. However, BDNF mRNA rises slowly, starting at 3 days after nerve lesion in Schwann cells, and reaches maximal levels after 3-4 weeks exclusively in distal nerve pieces [96], indicating the long-lasting regeneration potential of BDNF for sensory- and motoneurons [96]. Thus CNTF could support degenerating or lesioned axons within the first few days and BDNF could be responsible for later postinjury recovery stages [87]. However, the high endogenous concentration of CNTF in the Schwann cells of adult healthy animals could lead to the conclusion that CNTF plays a more prominent role than BDNF in axon maintenance, and could trigger a possible mechanism, such as axonal sprouting, to compensate for neurodegenerative processes. All this is evidence that CNTF is the most promising

neurotrophic factor that can play a role as a positive modifier able to counteract motoneuron degeneration, among other mechanisms by sprouting.

IGF-1 is a pluripotent hormone with several functions in the body: for example, growth during development and anabolic effects [315]. IGF-1 also promotes neuronal survival and myelination by acting on neurons and Schwann cells respectively [89,44,45,171,172]. It is also involved in regenerative reactions like nerve sprouting in denervated muscles, indicating its important role for axon maintenance [135]. The impact of IGF-1 is modulated by 6 binding proteins. In this study it was shown that IGFBP-5 can inhibit the survival-promoting effect of IGF-1 on motoneuron maintenance, leading to murine axon and motoneuronal degeneration in vitro and in vivo.

4.1 Ciliary neurotrophic factor-induced sprouting preserves motor function in a mouse model of mild spinal muscular atrophy

Patients with severe forms of SMA (Type I) have its onset during the first 6 months after birth. The fast progression of axonal and motoneuron loss in the entire spinal cord results in strong hypotony of the musculature and leads to death within the first two years [198,203]. These patients show no signs of axon regeneration during the course of their motoneuron disease, and experience a rapid decline of musculature because the axon degeneration and skeletal muscle denervation occurs too fast [198,203]. Patients with the mild SMA form Type III develop an atrophy in juvenile age and have a normal lifespan [205]. They can walk and sit and are diagnozed later. Their muscle strength then declines; however, this decline decelerates and muscle strength stabilizes at a low level. In parallel, signs of compensation by increased motor units are observed. This was also seen in some ALS patients with slow progression of the disease. In ALS patients with fast progression of neuronal loss and atrophy, no compensation was found [203]. Taken together, this indicates that diseases with slow progressive denervation allow time for compensatory mechanisms, such as sprouting, at least in some degree to reinnervate newly denervated muscle fibers and prevent them from atrophy. In this study, I was able to show that *Smn*$^{+/-}$ mice, a mouse model of mild forms of SMA, can maintain muscle strength through the increase in amplitude of single motor action potentials in skeletal muscles. The loss of motoneurons is thus compensated by sprouting from remaining motor axon terminals so that neuromuscular endplates remain innervated. Electrophysiological analyses and muscle strength measurements indicated that a lack of CNTF reduces this sprouting response on both morphological and functional levels.

The most severe form of spinal muscular atrophy, SMA type I, or Werdnig-Hoffmann's disease, differs from the milder forms SMA type II, type III and type IV by its fast progression and high mortality in early childhood [198,203]. In accordance with this, *Smn*$^{-/-}$ *SMN2*^{tg} mice expressing two copies of the human *SMN2* gene on a mouse *Smn* null background die within few days after birth and do not survive beyond postnatal day 6 [198,262]. In these SMA type I mice a 20% motoneuron loss at postnatal day 1 (P1) could be observed, which reaches a peak of 35% loss at P3-P5 in the spinal cord and brainstem at the final stage of the disease [262]. The fast progression of the disease suggests an absence of compensatory mechanisms in comparison to mouse models with a more moderate phenotype and a slower disease progression, as has been found in a model for SMA type III (*Smn*$^{+/-}$ mice) [141]. This corresponds to observations that survival of isolated *Smn*$^{-/-}$ *SMN2*^{tg} motoneurons in cell culture is not impaired, but that axon growth and presynaptic differentiation are disturbed due to the reduced amount of β-actin mRNA and protein in the distal axon and growth cone [253]. Defective axon growth in motoneuron development has also been observed in Smn-deficient zebrafish, suggesting that these early defects lead to subsequent motoneuron loss [316]. Also, the dysfunction of neuromuscular transmission plays a major role in these mouse models for severe SMA. Thus, most of the NMJs are innervated 1 day before death, but show reduced vesicle content, and this contributes to failed post-natal maturation of motor units and muscle weakness [249]. Severe SMA mice show no defects in motor axon formation. However, denervation of the NMJ already occurs in embryogenesis [313]. Similar defects were found in an SMA fly larvae, which shows disorganized motoneuron bouton clusters and reduced neurotransmitter receptor subunits in the muscle [317].

Insufficient SMN protein arrests the postnatal development of the NMJ. Postsysnaptically, the mature clustering of ACh receptors is impaired. Presynaptically, poor terminal arborization and intermediate filament aggregates, resulting in disturbed neurotransmission [314].

Taken together, axon finding and innervation occurs normally in mice models of severe SMA during embryonic development. However, a reduction in Smn protein of about 90% leads to the developmental stop of the axon growth cone and a functional NMJ cannot maturate. This means that despite the loss of motoneurons, almost all NMJs are innvervated; however, they lack proper function, and this leads to muscle atrophy. This declares SMA to be a growth-cone maturation defect and NMJ synaptopathy that is at least partially caused by reduced β-actin. The major task in mice models of severe SMA is maintaining function at the NMJ.

In contrast, *Smn*$^{+/-}$ mice, which lack only 50% of functional Smn protein, survive and do not show any overt signs of motoneuron disease, despite progressive and significant loss of

motoneuron cell bodies at a level even higher than the SMA type I mice. *Smn*$^{+/-}$ mice have no motoneuron loss at birth, but then develop a progressive motoneuron loss that reaches 50% after 1 year [141]. Apparently, these motoneurons could develop normally, and are more functional than the ones in the severe models. Obviously, 50% of Smn protein is not sufficient to maintain all motoneurons. However, the remaining motoneurons are able to sprout and reinnervate denervated motor endplates to maintain muscle strength (Fig. 3-1-1a, b).

Most of endplates in the *Smn*$^{+/-}$ mice appear fully innervated and do not differ in size and shape to wild-type NMJs (Fig. 3-1-1c, d). However, first signs of increased denervation and fragmented endplates become apparent in 4-week-old mice (2.4%, in comparison to 1.7% in controls) and become more frequent after 6 months (5.1% *Smn*$^{+/-}$ mice to 2.5% in controls) (Fig. 3-1-5). Nevertheless, the number of denervated endplates remains small at any given time compared to what would be expected from a 50% motoneuron loss. This could be explained by slow progressive denervation that can be compensated by sprouting events of axons at neighbouring intact NMJs. This study was able to demonstrate this through electrophysiological investigations of motor units of the gastrocnemius muscle. The SMUAPs show a more than two-fold increase in *Smn*$^{+/-}$ mice. Similar electrophysiological findings, such as the lack of abnormal spontaneous activity and enlarged motor units, were reported for patients with milder forms of SMA [198]. These increased motor units are abolished in *Smn*$^{+/-}$ mice lacking *CNTF*, which is normally expressed in Schwann cells (Fig. 3-1-15). Confocal analysis confirmed the hypothesis of CNTF-dependent sprouting in *Smn*$^{+/-}$ mice. In 6 month-old *Smn*$^{+/-}$ mice, increased axonal sprouting close to the NMJs was detected, which was also CNTF-dependent (Fig. 3-1-10, 3-1-13). Histological investigations of muscle fibers reinforce the idea that sprouting is a compensatory mechanism. *Smn*$^{+/-}$ mice show more atrophic and hypertrophic muscle fibers (Fig. 3-1-2). Additionally, enhanced fiber grouping of slow twitch fibers in 12-month-old *Smn*$^{+/-}$ mice was found (Fig. 3-1-4), indicating denervation and subsequent reinnervation by sprouting of remaining motoneurons. This corresponds to findings in a FALS mouse model where slow motoneurons are more resistant to denervation events than fast fatiguable motoneurons. In this study axonal vulnerability was alleviated by peripheral application of CNTF [295]. Slow motoneurons compensate through sprouting and reinnervation of denervated muscle fibers.

These data indicate that CNTF is responsible for the sprouting response that leads to this enlargement of motor units and thus compensates for loss of motoneurons in the milder forms of the disease.

4.1.1 The physiological consequences of SMN deficiency in motoneurons

For a better understanding of how CNTF-induced sprouting could rescue the *Smn*$^{+/-}$ mice, the consequences of SMN deficiency will be described in the following paragraph. Although the disease-determining gene *SMN* as well as one of its major functions have been identified, the pathomechanism of SMA is not fully understood. There are two hypotheses about the mechanism that leads to motoneuron degeneration in SMA; these hypotheses are not contradictory and could also be linked. It is very important to understand previous findings concerning the SMA pathomechanisms in motoneurons to get a better insight into how CNTF can counteract the muscle atrophy by sprouting.

The first hypothesis suggests that reduced levels of SMN protein lead to lower assembly activity of certain UsnRNPs and affect splicing of pre-mRNAs in all cells [231]. Consequently, this could lead to lower splicing rates, resulting in alternatively mRNAs [318]. Obviously, the reduced amount of SMN protein in SMA patients is sufficient for development, survival and function of all cell types, with the exception of motoneurons. The specific vulnerability of motoneurons could be explained by their large cell size (with axons of the sciatic nerve, for example, reaching a length of up to 1 meter) and their higher need for proper mRNA processing and translation into proteins (e.g., axon growth and maintenance) [252]. Furthermore, reduced snRNP assembly could negatively influence the splicing of mRNAs that are only essential for motoneurons. This might be a reason why motoneurons are more vulnerable than other cell types in SMA [231].

The second hypothesis suggests that the SMN protein has an additional neuron-specific function besides UsnRNP assembly. It has been shown that the expression of neuronal Smn protein corrected SMA in mice while muscle-specific SMN protein failed to provoke such an effect [263]. This finding suggests that deficiency of Smn in neurons rather than in muscle is relevant for this disease. This idea is also supported by observations made with isolated motoneurons from SMN-deficient mice [253,319] that show specific defects in axon growth when grown under conditions in which they do not have any contact with other types of cells. Similarly, morpholino-mediated knockdown of Smn in motoneurons results in reduced and misguided axon growth in zebrafish embryos [316,320-322].

These data show that axons of motoneurons are the most vulnerable part in the SMA pathology. Endogenous or pharmacological factors for axon maintenance could have a positive effect on SMA motoneurons and could alleviate the atrophy. In this mild SMA mouse model under investigation, CNTF maintains muscle strength by supporting unaffected motoneurons to take over the function of degenerating axons.

The SMN protein is present in axons and growth cones of motoneurons in culture and as part of a multiprotein complex containing gemins and profilin but lacking Smn proteins [296,323]. Furthermore, in axons Smn interacts with HuD and hnRNP-R proteins, which are involved in RNA transport [254,324]. The finding of shorter axons and reduced β-actin protein and mRNA transport along axons to the growth cone in severe SMA cultured motoneurons led to the commonly accepted hypothesis that hnRNP-R interacts with the 3′-UTR of actin mRNA and translocates it with its binding partner Smn towards growth cones of motoneurons [253]. Lentiviral knockdown of hnRNP-R in motoneurons reduces β-actin mRNA translocation to the axonal growth cone and axon elongation [325]. These observations resemble the phenotype of Smn-deficient motoneurons. The interaction between hnRNP-R and Smn in motoneuron axons indicates that reduced Smn protein cannot bind sufficient hnRNP-R with β-actin mRNA. Therefore, the transport and supply of β-actin mRNA to the growth cone is disturbed and results in reduced β-actin protein levels and corresponding deficiencies in the actin cytoskeleton [254]. The actin cytoskeleton is involved in axonal growth and sprouting (for details see 4.1.2**)**. Therefore, CNTF could induce endogenous actin polymerisation in more resistant motoneurons of *Smn*$^{+/-}$ mice and counteract the actin cytoskeleton pathomechanism in SMA.

In the vertebrate retina, it was demonstrated that the actin cytoskeleton regulates ion channel clustering, for example $Ca_v2.2$ calcium channels [326,327]. Indeed, it was observed that cultured motoneurons derived from mice with severe SMA [319] were incapable of accumulating $Ca_v2.2$ in axon growth cones. This reduction of $Ca_v2.2$ has two consequences. First, the local influx of calcium and the linked vesicle release is impaired in axon terminals [257,319]. Second, the interaction of presynaptic located $Ca_v2.2$ with motor endplate-specific laminin-221 is reduced. Laminin-221 mediates the development of active zones and presynaptic differentiation [328,329]. Consequently, NMJs of SMA mice appear immature with abnormal development, accumulation of neurofilament, altered intracellular Ca^{2+} homeostasis, reduced vesicle release and terminal arborisation [257,258,330-332].

All these data suggest a second function of Smn protein in axonal transport. Smn interacts with mRNA binding proteins such as hnRNP-R and HuD, which facilitate the localization of associated poly(A) mRNAs in axons [324]. Actin mRNA is one of the important targets and its reduced transport into the growth cone leads to disturbed axon growth and development. Another proof is that the overexpression of plastin 3 rescues axon length and outgrowth in Smn-deficient motoneurons of SMA mice [333]. Plastin 3 is a filamentous actin-stabilizing protein, which is important for axonogenesis through increasing the F-actin level [334].

These results indicate that reduced actin protein levels are related to motoneuronal death and the SMA phenotype. The CNTF-induced sprouting mechanism also requires actin. Growth cones of newly sprouted axons contain a highly dynamic actin cytoskeleton to reinnervate denervated muscle fibers. Possible pathways for CNTF to induce sprouting and act on the actin cytoskeleton will be discussed in the following sections.

4.1.2 How could CNTF or other neurotrophic factors act on maintenance of motor endplates and induction of sprouting in Smn$^{+/-}$ mice?

Sprouting is the ability of neurons in the central and peripheral nervous system to form new neuritic processes (sprouts) to respond to denervated targets [58]. As a response, remaining neurons form new sprouts to reinnervate recently denervated neurons or muscle fibers [128]. Sprouting can be subdivided into terminal or ultra-terminal sprouts from motor nerve terminals, and nodal or axonal sprouts from nearby nodes of Ranvier (Fig. 1-4). Lack of activity in paralyzed muscles leads to an upregulation of cell surface and basal lamina proteins that could guide new axon sprouts to the endplate [131-134]. Furthermore, it was shown that exogenously administered trophic factors, including CNTF, induce sprouting [107,135]. The sprouted axon is guided by processes of Schwann cells that play a primary role in initiating sprouting and guidance [136,137]. Furthermore, Schwann cells or denervated muscle fibers might be involved in releasing sprouting factors in response to an unknown trigger. These sprouting factors, which could include CNTF, IGF-1, BDNF or LIF-1, lead to extension of elaborated branches of terminal Schwann cells on a denervated muscle fiber to form bridges to intact synapses [137,138]. These bridges could guide new sprouts from an intact motoneuron terminal to a denervated target [130,139,140].

Injection of CNTF into rat muscles induced nodal and terminal sprouting, whereas *Cntf* knockout mice showed decreased sprouting [107,108]. Our investigations of *Smn*$^{+/-}$ *Cntf*$^{/-}$ and *Cntf*$^{/-}$ animals confirmed these data and also showed reduced numbers of sprouts when compared to *Smn*$^{+/-}$ and control mice (Fig. 3-1-10c). However, it is still unknown how CNTF induces sprouting. Although CNTF is clearly detectable in myelinating Schwann cells, it is absent or only weakly expressed in non-myelinating terminal Schwann cells [130]. In this study, this expression pattern was also observed at NMJs (Fig. 3-1-8a). It still remains uncertain whether CNTF is actively secreted or only released by damaged Schwann cells. However, it is generally thought that only CNTF-negative terminal Schwann cells are involved in sprouting. They do so by forming extensions of their elaborated branches on a denervated muscle fiber to form bridges with intact synapses [137,138]. This contradiction could be explained by looking

at the CNTF binding receptor component CNTFRα. CNTFRα is found in Schwann cells, motoneurons and muscle fibers. Therefore, CNTF could induce sprouting directly by binding to CNTFRα in motoneurons or Schwann cells. Thus, CNTF released by myelinating Schwann cells could indirectly induce sprouting by activating CNTF receptors in muscle fibers. In response, muscle fibers could release muscle-derived sprouting factors such as IGF-1, which induces sprouting processes in motoneurons and Schwann cells [130]. Alternatively, CNTF could be released by myelinating Schwann cells located near the NMJ, which directly induces sprouting in the intact axon, which in turn sprouts out to neighboring denervated postsynapses by nodal sprouting. In this thesis most of the sprouts were nodal, while terminal sprouts were rarely observed (Fig. 3-1-3d, 3-1-13).

Among CNTF, other factors could play a role in the observed sprouting events. LIF also could play a role in *Smn*$^{+/-}$ mice. LIF transduces its signal through the same receptor components as CNTF and can induce sprouting of postganglionic sympathetic fibers into the dorsal root ganglia in adult rats following peripheral nerve injury [116]. Furthermore, it is essential for postnatal maintenance of motoneurons and plays a specific role in the control of motor endplate size [118].

Neurotrophins, especially BDNF, could also be involved in the CNTF-induced sprouting mechanism. TrkB, the receptor for BDNF, plays a role in the maintenance and formation of the NMJ [91,92]. The BDNF level is increased in denervated muscle fibers both in lesioned mice and ALS patients [335,336]. Additionally, it is also upregulated in axotomized motoneurons and plays an important role in their survival [337,113]. In axotomized motoneurons, low doses of BDNF treatment enhance motor axon regeneration [338].

BDNF could therefore be involved in anterograde signaling for sprouting, released by axons or Schwann cells and acting on muscle fibers, which in turn releases sprouting factors. Another possibility would be that BNDF is released as a sprouting factor by muscle fibers to act in a retrograde manner on motoneurons. Although there is no direct evidence that BDNF is involved in motoneuron sprouting, it could play a role in the CNTF-induced sprouting mechanism.

4.1.3 Possible downstream targets of CNTF receptor complex and IGF-1 receptor that induce sprouting

When the ligand binds the CNTF receptor complex, classical signaling pathways such as B-Raf [77] and the phosphatidylinositol 3 kinase (PI-3K) pathways are activated, which not only maintain survival but also mediate effects on the cytoskeleton [339]. In addition, activation of

the CNTF receptor complex leads to activation of Stat-3. Interestingly, activated Stat-3, phosphorylated at Ser 727, has been shown to affect mitochondrial potential in non-neuronal cells. One possibility is that a local effect of activated Stat-3 on mitochondria is responsible for the effects of CNTF on synapse maintenance and sprouting [340]. In accordance with that, in a mouse model with conditional inactivation of the *Stat3* gene in motoneurons, these cells are more vulnerable in adult stages after nerve lesion [310].

For axon outgrowth, elongation and sprouting, a change of the axonal cytoskeleton – particularly microfilaments and microtubules – is necessary to form new sprouts [341]. Stat3 can interact with the microtubule-destabilizing protein stathmin. Stathmin has the ability to bind α/β-tubulin heterodimers to facilitate the depolymerization of microtubules [342]. By CNTF release from the Schwann cells, Stat-3 could be activated downstream through the CNTF receptor complex in motoneurons. Stat-3 then binds stathmin in the cytoplasm, which leads to more accessible α/β-tubulin heterodimers. Free α/β-tubulin heterodimers can be polymerized to prolong existing microtubules and form a cytoskeleton base for new sprouts. Furthermore, it was shown that Smn deficiency leads to severe structural and functional alterations in the organization of the cytoskeleton of motor nerve terminals within the first week of a mouse model of severe SMA, including limitation of microtubule maturation [343]. CNTF is not expressed in the first week and so cannot be counteracted by inhibition of stathmin in this severe model. However, CNTF expression starts at the end of the first postnatal week and reaches a high concentraton in the third week [112,344], and so could counteract in the *Smn*$^{+/-}$ mice model.

Cytoskeletal rearrangement needs axonal translation of anterograde transported mRNAs. It is also possible that CNTF mediates sprouting via local translation in motoneurons. The CNTF-Stat3 pathway includes the activation of the mammalian target of rapamycin (mTOR) [345]. Recently, it was shown that depletion of Phosphatase and tensin homolog (PTEN), a negative regulator of mTOR, leads to increased growth cone size, promotion of axonal elongation and increased survival of SMA motoneurons, meaning that activation of mTOR leads to downstream signaling pathways for local synthesis to restore β-actin protein levels in growth cones of SMN-deficient motoneurons [346]. This local translation of β-actin RNA could lead to more actin polymerization and trigger sprouting.

RhoA, a small GTPase, can be also locally translated [347]. RhoA activates over RhoA kinase (ROCK) profilin which promotes actin polymerization. At the same time, ROCK activates LIM kinase that inhibits cofilin's ability to bind and depolymerizes actin by phosphorylation [348].

Thus, CNTF could support the actin cytoskeleton for sprouting either by local translation of β-actin mRNA or by modulating targets for actin.

Neurofilament might play a minor role in the sprouting mechanism. The absence of Neurofilament light (NF-L) protein in mice resulted in a 20-fold decline of neurofilament medium and heavy protein levels in the sciatic nerve, while increases of other cytoskeletal proteins such as tubulin and growth associated protein 43 (GAP-43) were detected. Besides slightly hypotrophic axons, these NF-L knockout mice appear totally normal. In crush injury experiments it was shown that NF-L deficient axons of the sciatic nerves maintain the capacity to regrow and remyelinate, albeit at a slower rate. This indicates that neurofilament as a major axonal cytoskeleton component is not involved in axonal sprouting [349].

CNTF could also act on muscles which respond with the release of sprouting factors such as IGF-1. It has been shown that IGF-1 is a muscle-derived factor and its injection into adult rat and mouse gluteus muscle resulted in terminal sprouting and elevated levels of nerve-specific GAP-43, which is associated with axon growth. High levels of GAP-43 are usually found only during development, where axon growth cones find their target, and in nerve lesions. Thus, after a denervation event, IGF-1 could be released by muscle or Schwann cells and bind to neuronal IGF-1 receptors. Through tyrosine phosphorylation the expression of GAP-43 is increased. GAP-43 is associated with F-actin and is linked to nerve-terminal sprouting [130,135,350].

Injection of a recombinant adeno-associated virus (AAV) vector, encoding human IGF-1 (AAV2/1-hIGF-1), into the deep cerebellar nucleus (DCN) of a type III SMA mouse model, cannot rescue the phenotype. After 8 months the spinal motoneuron showed changes in endogenous Bax and Bcl-xl levels that were consistent with IGF-1-mediated anti-apoptotic effects. Although the loss of motoneurons was reduced, the rescued motoneurons lacked functionality due to the loss of innervating axons [351].

Thus IGF-1 has a positive effect on motoneuron survival, but obviously cannot rescue the “dying back” phenomenon of axons. One explanation could be that the induction of IGF-1 also increases the IGFBP-5 expression in a negative feedback loop manner [352,353]. IGFBP-5 in the extracellular matrix could prevent IGF-1 action. On the other hand, IGF-1 could be more important for the survival of the motoneuron soma than of the axon. Experiments on motoneurons in culture confirmed that axons of motoneurons grow shorter when cultured with IGF-1 compared to BDNF-cultured ones (Fig. 3-2-4c).

4.1.4 Why does CNTF not compensate in the severe forms of SMA in Smn$^{-/-}$ SMN2^{tg} mice?

CNTF expression is low during embryonic development [110,112]. In the peripheral nervous system, high levels of expression are only reached when myelinating Schwann cells are fully mature. CNTF expression only becomes upregulated in Schwann cells starting at the end of the first postnatal week [112,344]. In rodents, CNTF expression reaches the high levels found in the adult nervous system in the third postnatal week, which correlates with the myelination process of Schwann cells [43]. Therefore CNTF is not present during the first days after birth, when these mice become severely paralyzed [262] and show pathologies such as depletion of synaptic vesicles at active zones and reduced synaptic transmission [257].

Addition of CNTF by application via CNTF-secreting stem cells [103] or by local injection into skeletal muscle [302] leads to improved maintenance of motor axons in peripheral nerves of *pmn* mutant mice or neuromuscular endplates in SOD G93A mice [295]. Interestingly, this effect appears to be relatively specific for CNTF, since other neurotrophic factors for motoneurons such as GDNF were without any effect in the same disease models [295,302].

Schwann cells close to neuromuscular endplates play a major role in triggering terminal sprouting [137,354]. As shown here, these cells express CNTF, and a lack of CNTF expression strongly reduces terminal sprouting and augmentation of motor unit size. Terminal Schwann cells have been found to express Semaphorin-3, and it has been suggested that the upregulation of Semaphorin-3 in terminal Schwann cells could suppress sprouting and contribute to loss of neuromuscular synapses in motoneuron disease [354].

Other studies demonstrated that depletion of synaptic vesicles precedes the loss of synapses in a mouse model of ALS, and that CNTF could prevent the depletion of synaptic vesicles and thus maintain function of these synapses. This effect of CNTF correlates with reduced accumulation of neurofilaments [295], a hallmark of motoneuron disease in Smn deficient mice [257,258] and in SOD G93A mice, and reduced expression of stress-related genes such as Bcl-2a1-a that are normally upregulated in SOD G93A mice at a stage when synapse loss occurs.

4.1.5 Why is the progression of the disease in CNTF-deficient Smn$^{+/-}$ mice not accelerated?

CNTF is a member of a large family of neurotrophic cytokines that bind to receptor complexes involving gp130 and LIF-Rβ receptor subunits as signal-transducing subunits. This family further includes LIF, which is also expressed in Schwann cells, and cardiotrophin-1. Analysis of double and triple mutant mice for these factors revealed that atrophy of neuromuscular endplates and loss of muscle strength increases, if more than one of these ligands is missing [118]. When LIF-Rβ is ablated, these mice die at birth, because they are

unable to breathe and feed [355]. Despite these severe signs of paralysis, they exhibit a loss of only 40% of motoneurons, indicating that the loss of neuromuscular transmission rather than the loss of motoneuron cell bodies is responsible for the severe phenotype. Taken together, these data suggest that in this mouse model for mild forms of SMA, CNTF is not the only ligand responsible for maintenance of neuromuscular endplates, but plays a predominant role for the induction of sprouting.

4.1.6 General therapeutic treatments and the possible role of CNTF in SMA patients

Due to the fact that reduced SMN protein levels lead to development of SMA, the most reasonable therapeutic approaches deal with increasing the level of full-length SMN to oppose the cause of motoneuron loss. Sprouting as a compensatory mechanism induced by application of CNTF or other factors could counteract the muscle atrophy due to motoneuron loss, as muscle fibers remain innervated. As expected, then, the major strands of research focus on restoration of the SMN protein.

4.1.6.1 Increasing endogenous SMN protein level

Extra copies of the *SMN2* gene fully rescued the phenotype in SMA mice due to an increase the SMN full-length level protein [262]. Patients with homozygous absence of the *SMN1* gene also appeared completely healthy, due to having more than two copies of the *SMN2* gene [356].

To detect factors which increase full-length *SMN2* expression in SMA patients endogenously, drug screens were performed. Three members of the group of histone deacetylase (HDAC) inhibitors were identified to promote *SMN* transcription. Sodium butyrate, trichostatin A and valproic acid increase the transcription of 2% of all genes, including SMN. Unfortunately, all three drugs show very little beneficial effects in SMA mice and patients, and have several side effects due to their lack of specificity [357].

Another strategy to increase the endogenous level of full-length SMN protein in humans is based on antisense oligonucleotide (AON) technology. Short DNA fragments can be used to bind and knockdown RNAs based on sequence specificity. AON can also be used to modulate pre-RNA splicing, for instance in *SMN2* preRNA. It does so presumably by binding to regions of exon 7 that form RNA structures, or masking regions with a splicing silencer for exon 7 and therefore promoting exon 7 inclusion [358]. The disadvantage of AONs is that the application is restricted to the injection site, which makes the delivery to the target tissue, e.g.

motoneurons, more difficult [357]. To overcome this delivery problem, viral vectors can be used to ensure a specific targeting and long-term expression.

4.1.6.2 Viral gene therapy

Lentiviruses or adeno-associated viruses (AAV) are two vector types used to deliver genetic material into organisms or cells. Lentivirus is a retrovirus and its genome is RNA coded. As soon as it infects a cell, the RNA will be reverse-transcribed into DNA and integrated into the genome of the host cell. In contrast to other retroviruses that can only integrate into dividing cells, the lentivirus can also integrate into non-dividing cells. The integration into the genome involves the danger of mutation of genes or activation of oncogenes in the host system. In comparison with lentiviruses, AAVs have higher gene-delivery efficiency in most cell types including dividing and non-dividing cells and do not integrate into the genome.

In one study, a regular single-stranded AAV and a self-complementary AAV (scAAV) vector, characterized by a double-stranded DNA genome encoding hSMN, were injected into the CNS of a mouse SMA model. This self-complementary variant of AAV features earlier gene expression compared to the single-stranded one. It was shown that a subset of transduced cells were motoneurons in the spinal cord after CNS injection. The injection of a regular AAV increases the lifespan from 15 days to 50, whereas the self-complementary AAV caused a rescue of even up to 157 days [359]. However, the immunological response might be a bigger issue in humans [357,360]. To minimize the risk of viral vectors or drug injections, human induced pluripotent stem (hiPS) cells could be used in the near future.

4.1.6.3 Human induced pluripotent stem (hiPS) cells

Human induced pluripotent stem (hiPS) cells derive from reprogrammed patient fibroblasts. The generation of iPS cells is crucially dependent on the genes c-Myc, Oct3/4, Klf4 and SOX2 used for induction. These genes can be inducted into the cell by viral infection, or recombinant cell-penetrating reprogramming proteins can be induced to avoid using genetic material [361-363]. The resulting iPS cells derived from SMA patients already exist and could be further differentiated into motoneurons [364 365].

Once functional motoneurons derived from SMA patients and healthy persons exist in culture, all findings which have been made in cultured motoneurons over the years could be investigated in human motoneurons. Specific drug or virus application can be tested in a model system very close to human. With the help of electrophysiological methods these iPS

cell-derived motoneurons can be tested for whether they also show the similar pathologies of incapability of accumulating $Ca_v2.2$ in axon growth cones, abnormal development and reduced vesicle release as found in murine motoneurons [257,258,330-332]. Even co-cultures of motoneurons and muscle cells derived from iPS cells could give rise to new therapeutic approaches.

4.1.6.4 CNTF-induced sprouting as a compensatory mechanism in humans?

CNTF induces sprouting in the mouse model for mild forms of SMA. Sprouting compensates the loss of motoneurons and maintains muscle strength. Unfortunately, when CNTF is given systemically to human patients with motoneuron disease, it elicits severe side-effects such as fever and cachexia [366], most probably due to effects on liver cells [367] and the cells of the immune system. These side-effects preclude its use for therapy in SMA patients. Recently, techniques have been developed for local application of growth factors such as VEGF to motoneurons and neuromuscular endplates [368]. It is possible that such new strategies for growth factor delivery could reduce side-effects associated with systemic delivery. Local expression of CNTF appears attractive under circumstances when endogenous CNTF expression is low, at developmental stages when myelination of peripheral nerves is still incomplete. In summary, our observation that sprouting in milder forms of SMA prevents the decline of muscle strength despite massive loss of spinal motoneurons could guide the way for development of therapies for severe forms of SMA in which such sprouting reactions do not occur. In dying-back diseases such as ALS and SMA, synapses and axons collapse before the motoneuron cell bodies die. Patients only become clinically apparent once a large proportion of motor units are lost. Consequently, by that stage many motoneurons have already degenerated and a proper treatment for restoration of muscle strength is no longer possible. For that reason, one should focus on the maintenance of motor neuron terminals in order to prevent the progressive degradation. Besides all efforts to restore the decreased SMN level in patients and mice, an approach focusing on terminal/nodal sprouting to maintain the muscle strength could be of interest. It is clearly worthwhile to identify either the sprouting mechanism or a pathway that leads to endogenous upregulation of CNTF to induce sprouting first in SMA animals, then in patients. Once the sprouting mechanism is entirely revealed and inducible by drugs, it could delay or even prevent neuronal degeneration in several diseases.

4.2 Dysregulated IGFBP-5 expression causes axonal degeneration and motoneuron cell death in diabetic neuropathy

In the second part of the thesis, the potential role in adult axon maintenance of IGF-1 and its binding protein IGFBP-5 was investigated with respect to DNP.

Reduced IGF-1 leads to hypomyelination and reduced NCV which can be restored by IGF-1 application. Demyelination is a feature of several neuropathies, including DNP which also involves the IGF system. The role of IGF-1 is therefore very interesting in diabetic neuropathy. 60-70% of patients with diabetes show some form of neuropathy [274-276]. In 2000 at least 171 million (2.8%) people suffered from diabetes mellitus [264], thus making DNP one of the most frequent axonal degenerative diseases in the world.

Abnormal blood fat and neurovascular factors lead to damage of the blood vessels that supply neurons with oxygen and nutrients. This lack of essential supplies predisposes neurons to other factors and diseases, and causes neuronal death. The symptoms can vary, and affect autonomous, sensory and motor nerve fibers, starting by predominantly distal axon loss [264]. Up to now, it remains unclear what causes the axon collapse. A shift in expression of neurotrophic factors or their modulating binding partner might play a role in the axon loss in DNP.

Previous studies have reported reduced levels of circulating IGF-1 as a common feature in diabetes, with the magnitude of the reduction increasing with age and duration of disease [278]. Similarly, reduced IGF-1 expression in peripheral nerves is observed at early stages of disease in the streptozotocin-induced rat model [279].

To detect alterations in expression of insulin-related genes, a microarray analysis of patients with diabetic neuropathy and healthy persons was performed. IGFBP-5 showed the most prominent upregulation, being 7-fold compared to controls (Fig. 3-2-2). Western blot analysis revealed a more than 60-fold upregulation of IGFBP-5 on protein levels in DNP patients (Fig. 3-2-2). Our results indicate that elevated IGFBP-5 protein levels and reduced IGF-1 signaling, found in peripheral nerves of patients with DNP, may be the crucial factors leading to progressive loss of motor fibers and subsequently to loss of motoneurons in corresponding mouse models.

To address the question whether increased levels of IGFBP-5 could be responsible for motoneuron degeneration in these patients, we investigated a possible inhibitory effect of IGFBP-5 on the survival-supporting neurotrophic factor IGF-1. Neuronspecific IGFBP-5-overexpressing mice also exhibit motoneuron and axonal degeneration in different nerves. Another generated mouse model, which lacks a functional IGF-1 receptor in neuronal tissue,

evinces similar levels of motoneuron degeneration and confirmed the negative effect of upregulated IGFBP-5 based on its inhibitory interaction with IGF-1. Collectively, our data indicate that additional components of IGF-1 signaling are dysregulated in the peripheral nervous system.

4.2.1 DNP patients with motor fiber impairment show IGFBP-5 upregulation

50% of patients who suffer from diabetes for 20 years show a neuropathy. DNP is often associated with loss of small caliber sensory nerve fibers. The general opinion that patients with diabetes only show sensory defects is based on medical examinations. Patients on suspicion of DNP are generally investigated by sensory non-invasive tests, because it is cost-efficient and more pleasant. If a biopsy is required, a pure sensory nerve, like the sural nerve, is taken, thus ensuring that motor functions remain unaffected and only a small patch of the skin in the foot is numb after biopsy. However, large motor fibers are also affected and can be detected by needle EMG or the toe-spread test. If patients with DNP cannot spread their toes voluntarily, a motor component is involved. Another reason for overlooking motor involvement is muscular dystrophy: DNP patients who suffer from sensory ache in the limbs reduce their movement in order to reduce the pain. As a result they develop a muscular dystrophy which veils the degeneration of motor fiber. Two studies including over 300 patients with diabetes show, besides sensory fiber loss, also a parallel or slightly delayed motor fiber impairment resulting in a reduced CMAP [369,370].

In this study it was shown that IGF-1R, which mediates the trophic effects of IGF-1 on Schwann cells and neurons, is upregulated in nerve biopsies from DNP patients. The same is true for IGFBP-5, an IGF-1-binding protein that inhibits IGF-1-mediated survival and axon growth in motoneurons. On mRNA level IGFBP-5 is upregulated more than 7-fold and at protein level at least 60-fold in diabetic nerves compared to controls (Fig. 3-2-2, 3-2-1).

4.2.2 NF-L-IGFBP-5 overexpressing and neurospecific IGF-1 receptor knockout mice: Two complementary mouse models

The elevated IGFBP-5 protein level found in DNP patients leads to the question whether upregulated IGFBP-5 could cause neuronal degeneration (Fig. 3-2-1, 3-2-2). In this study two different mouse models were generated to investigate the role of IGFBP-5 in inhibiting the IGF-1-mediated survival effect. In diabetic human nerves, IGFBP-5 is significantly upregulated in axons and the surrounding extracellular matrix (Fig. 3-2-3). In peripheral

nerves, IGF-1 is mainly expressed in Schwann cells in postnatal rodents [173] and acts on motoneurons and Schwann cells to support survival, myelination and regenerative reactions [46,89,178]. IGF-1 promotes neuronal survival by activation of the IGF-1 receptor and cytoskeleton rearrangement over the PI3K/AKT pathway by phosphorylation of BAD in neurons [44-47,166,167]. The reduction of IGF-1 can be also connected to neuronal degeneration in other diseases. For instance, it was shown that IGF-1 is reduced by 50% in early symptomatic age sciatic nerves of an ALS mouse model with reduced Schwann cell-expressed mutant SOD1 [371].

Therefore an increase of IGFBP-5 in the extracellular matrix could reduce these effects by binding IGF-1. To test this hypothesis we generated two mouse models. The first overexpresses IGFBP-5 under a neuronal promoter, the other is a conditional neuronspecific IGF-1 receptor knockout.

The *NF-L-IGFBP-5* transgenic mice show a progressive partial degeneration (about 20%) of several peripheral nerves and loss of motoneurons in the spinal cord over 6 months (Table 3-2-2). Furthermore, a decrease of myelination of Schwann cells was apparent (Fig. 3-2-6) which affects nerve velocity conductance in these mice (Fig. 3-2-7). The loss of motoneurons and velocity conductance correlates with EMG observations made in diabetic patients with motor impairment. These defects progress slowly over time in these mice, as well as in DNP patients.

To confirm that the phenotype of the IGFBP-5 transgenic mouse is based on the binding of IGF-1, a second mouse model was generated which lacks the IGF-1 binding site of IGF-1 receptor in neuronal tissue. Interestingly, the axon and motoneuron loss of the *IGF-R* conditional knockout mice resembles the loss of IGFBP-5 transgenic mice (Table 3-2-3). In contrast to the IGFBP-5-overexpressing mouse model, the myelination was not affected in neuronspecific IGF-1R knockout mice (Fig. 3-2-9).

4.2.3 Why do neuronspecific IGF-1R knockout mice show no loss of myelination?

Interestingly, loss of myelination was not observed in mice lacking the ligand binding domain of the IGF-1R after Cre mediated recombination specifically in motoneurons, indicating that the observed defect in peripheral nerve myelination in IGFBP-5-overexpressing mice may be due to reduced IGF-1 function in Schwann cells. For the induction of myelination, insulin-like growth factor 1 (IGF-1) plays a major role [44]. *Igf1* knockout in mice leads to a broad range of defects in the brain, with hypomyelination as a major phenotype and loss of some neuronal populations in the CNS [44]. These mice die by about 2 months. Postnatally, they do not exhibit

any significant loss of motoneuron cell bodies at early stages, indicating that motoneuron development during embryogenesis does not depend on IGF-1. Similarly, mice overexpressing IGFBP-5 appear normal at birth and at early stages thereafter. By 6 months, prominent loss of myelin occurs. The loss of motor fibers and motoneuron cell bodies was not detectable until 6 months of age, a stage that IGF-1-deficient mice do not reach [372].

Overexpressed IGFBP-5 binds IGF-1 at the extracellular matrix, so that it cannot bind to IGF-1 receptors both on the axon and the Schwann cells. Therefore the trophic support at the axon and the signal for proper myelination at the Schwann cells are missing. This explains the degenerating motoneurons and the reduced myelination in *NF-L-IGFBP-5* transgenic mice. The NF-L-Cre IGF-1R conditional knockout mice also show this phenotype of degenerating motoneurons. However, the myelination appears normal. One explanation could be that the IGF-1R is specifically deleted in neurons due to the neurospecific promoter. This leads to reduced trophic support and neuronal degeneration. The Schwann cell IGF-1R is still intact and IGF-1 can induce proper myelination. To confirm this hypothesis the *Igfr* $^{loxP/loxP}$ mice should be crossbred with a NF-L-Cre under a Schwann-cell-specific promoter, e.g. S100. These mice should also show signs of reduced myelination.

These mutant mice also revealed that axon maintenance is directly dependent on IGF-1R activation, since loss of large motor fibers in the phrenic, facial, and the mixed sciatic nerve was seen in the conditional *Igfr* knockout animals. Thus, the reduced availability of IGF-1 coupled with elevated expression of IGFBP-5 in diabetic nerves would be predicted to have a major effect on myelination and to exert trophic support on axons.

4.2.4 What could cause diabetic neuropathy and IGFBP-5 upregulation?

In diabetes mellitus several metabolic changes – such as chronic high blood sugar levels, abnormal blood fat, and neurovascular factors – lead to damage of the blood vessels that supply neurons with oxygen and nutrients. This weakens neurons and predisposes them to other damaging factors and diseases, and could cause neuronal degeneration, called DNP. It is still unclear why high levels of glucose causes neuronal death. A combination of neuronal and microvascular deficits may cause DNP. Long-lasting hyperglycemia causes free radicals that damage lipids, proteins and nucleic acids. This in turn negatively influences signaling pathways and decreases cellular function, which ends in apoptosis or necrosis [181,277,278].

Patients with DNP show an alteration of the IGF-1 axis; the soluble neurotrophic factor IGF-1 is downregulated and could play a major role in this degenerative process [192,279]. This was confirmed in STZ rodents, a model for painful DNP [353]. The action of IGF-1 is regulated by

IGFBP-5. In our study, IGFBP-5 is at least 60-fold increased at the protein level in diabetic nerves when compared to nerves from healthy non-diabetic control individuals.

What could cause the upregulation of IGFBP-5 in the DNP patients? It is feasible that IGF-1 regulates the IGFBP-5 expression that in turn controls the IGF-1 action in a negative feedback loop. In mammary fibroblasts, IGF-1 treatment increases levels of IGFBP-5 mRNA [352]. IGF-1 leads to autophosphorylation of the IGF-1R which activates downstream the MAPK and PI3K pathways. Both pathways are required for an IGF-1-dependent increase of IGFBP-5 in mammary fibroblasts. Furthermore, in smooth vascular muscle cells the PI3K/AKT pathway but not the MAPK pathway is important for the IGF-1-mediated expression of IGFBP-5 [373]. However, the MAPK pathway inhibits IGFBP-5 expression in mammary epithelial cells after IGF-1 [169]. MAPK pathways are often activated during cell growth and differentiation is mediated by IGF-1 [374]. This IGF-1-mediated effect would be inhibited by high IGFBP-5 levels. Therefore MAPK pathways could mediate cell growth and simultaneously ensure sufficient free IGF-1 by inhibiting IGFBP-5 expression.

Taken together, IGF-1-mediated upregulation of IGFBP-5 expression is controlled differently by MAPK and PI3K/AKT pathways depending on the cell type. It is necessary to identify IGFBP-5-controlling pathways in motoneurons to get a closer insight into the pathology of DNP. It could be possible that MAPK pathways also have an inhibitory effect on IGFBP-5 expression, as in mammary epithelial cells. Maybe this inhibitory effect is disturbed in DNP and this is what leads to the increase of IGFBP-5 observed in this study (Fig. 3-2-1, 3-2-2). It still remains unclear whether long-lasting hyperglycemia causes the upregulation of IGFBP-5, perhaps by oxidative stress that influences inhibitory elements – for example, MAPK or IGFBP-5 upregulation is a parallel event to hyperglycemia.

4.2.5 Further steps to therapeutic approaches

A study on IGF-1 treatment of patients with idiopathic small-fiber neuropathy, which is also a feature of diabetic neuropthy, showed no positive effect [375]. One explanation for the diminished effect could be elevated IGFBP-5, which inhibits IGF-1 function. The observation that upregulated IGFBP-5 can cause progressive neuronal and myelination defects offers options for novel therapeutic strategies. Our data from mouse models suggest that inhibiting the upregulation of IGFBP-5 expression in peripheral nerves might prevent progression of the disease. Similarly, inhibitors of IGFBP-5 that block binding to IGF-1 could be of therapeutic benefit. As shown by X-ray crystallography, the domains of IGF-1 that bind to IGFBP-5 are different from those that bind to the receptor. Thus it should be feasible to discover inhibitors

that prevent the interaction of IGF-1 with IGFBP-5 but not with the IGF-1 receptor. A monoclonal antibody against IGFBP-5 or another inhibiting molecule could be injected in overexpressing IGFBP-5 mice to rescue the phenotype. Such molecules could not only prevent loss of motor axons and motor function but also loss of myelinated sensory axons and thus would open new therapeutic strategies that could be studied in prospective clinical trials for DNP.

The neuronspecific IGFBP-5-overexpressing and IGF-1R knockout mice could be also valuable in obtaining a better insight into the CNTF-induced sprouting mechanism. One hypothesis regarding the sprouting mechanism could be further investigated. CNTF binds to its receptor in the muscle, which releases IGF-1 as a response. IGF-1 then binds to neuronal IGF-1 receptors. Through tyrosine phosphorylation the expression of GAP-43 is increased, which is associated with F-actin and is linked to nerve-terminal sprouting [130,135,350]. The crossbreeding of *Smn*$^{+/-}$ with either the *NF-L-IGFBP-5* or neuronspecific IGF-1R knockout mice could show whether muscle-released IGF-1 is downstream of the CNTF-induced sprouting mechanism. If that is true, the released IGF-1 would be either be bound by overexpressed IGFBP-5 at the extracellular matrix or would not be able to activate the deleted IGF-1R in motoneurons, and the sprouting should be decreased.

5 References

Reference List

1. Kandel, E. R., Schwartz, J. H. & Jessel, T. M. *Principles of Neural Science, 4th ed. McGraw-Hill, New York.* (2000).

2. Valenstein, E. S. The discovery of chemical neurotransmitters. *Brain Cogn* **49**, 73-95 (2002).

3. Kuffler, S. W. & Yoshikami, D. The number of transmitter molecules in a quantum: an estimate from iontophoretic application of acetylcholine at the neuromuscular synapse. *J. Physiol* **251**, 465-482 (1975).

4. DEL, C. J. & KATZ, B. Localization of active spots within the neuromuscular junction of the frog. *J. Physiol* **132**, 630-649 (1956).

5. Couteaux, R. & Pecot-Dechavassine, M. [Synaptic vesicles and pouches at the level of "active zones" of the neuromuscular junction]. *C. R. Acad. Sci. Hebd. Seances Acad. Sci. D.* **271**, 2346-2349 (1970).

6. Duclert, A. & Changeux, J. P. Acetylcholine receptor gene expression at the developing neuromuscular junction. *Physiol Rev.* **75**, 339-368 (1995).

7. Hortsch M & Hisashi H *The Sticky Synapse, Book Chapter 3: Development of the Vertebrate Neuromuscular Junction (Michael A. Fox)*. Springer, (2009).

8. Tatsuoka, H., Kadota, T. & Kono, K. Postsynaptic arch in the frog neuromuscular junction: paramembranous protuberances coating the inner surface of the postjunctional membrane. *J. Neurocytol.* **17**, 87-94 (1988).

9. Sanes, J. R. & Lichtman, J. W. Development of the vertebrate neuromuscular junction. *Annu. Rev. Neurosci.* **22**, 389-442 (1999).

10. Sendtner, M., Pei, G., Beck, M., Schweizer, U. & Wiese, S. Developmental motoneuron cell death and neurotrophic factors. *Cell Tissue Res.* **301**, 71-84 (2000).

11. Freund, H. J. Motor unit and muscle activity in voluntary motor control. *Physiol Rev.* **63**, 387-436 (1983).

12. Robitaille, R., Garcia, M. L., Kaczorowski, G. J. & Charlton, M. P. Functional colocalization of calcium and calcium-gated potassium channels in control of transmitter release. *Neuron* **11**, 645-655 (1993).

13. Robitaille, R., Adler, E. M. & Charlton, M. P. Strategic location of calcium channels at transmitter release sites of frog neuromuscular synapses. *Neuron* **5**, 773-779 (1990).

14. Bahler, M. & Greengard, P. Synapsin I bundles F-actin in a phosphorylation-dependent manner. *Nature* **326**, 704-707 (1987).

15. Evergren, E., Benfenati, F. & Shupliakov, O. The synapsin cycle: a view from the synaptic endocytic zone. *J. Neurosci. Res.* **85**, 2648-2656 (2007).

16. Sons, M. S. & Plomp, J. J. Rab3A deletion selectively reduces spontaneous neurotransmitter release at the mouse neuromuscular synapse. *Brain Res.* **1089**, 126-134 (2006).

17. Leenders, A. G., Lopes da Silva, F. H., Ghijsen, W. E. & Verhage, M. Rab3a is involved in transport of synaptic vesicles to the active zone in mouse brain nerve terminals. *Mol. Biol. Cell* **12**, 3095-3102 (2001).

18. Hanson, P. I., Heuser, J. E. & Jahn, R. Neurotransmitter release - four years of SNARE complexes. *Curr. Opin. Neurobiol.* **7**, 310-315 (1997).

19. Sutton, R. B., Fasshauer, D., Jahn, R. & Brunger, A. T. Crystal structure of a SNARE complex involved in synaptic exocytosis at 2.4 A resolution. *Nature* **395**, 347-353 (1998).

20. Weber, T. *et al.* SNAREpins: minimal machinery for membrane fusion. *Cell* **92**, 759-772 (1998).

21. Fukuda, M. *et al.* Role of the conserved WHXL motif in the C terminus of synaptotagmin in synaptic vesicle docking. *Proc. Natl. Acad. Sci. U. S. A* **97**, 14715-14719 (2000).

22. Schiavo, G., Stenbeck, G., Rothman, J. E. & Sollner, T. H. Binding of the synaptic vesicle v-SNARE, synaptotagmin, to the plasma membrane t-SNARE, SNAP-25, can explain docked vesicles at neurotoxin-treated synapses. *Proc. Natl. Acad. Sci. U. S. A* **94**, 997-1001 (1997).

23. Maximov, A. & Sudhof, T. C. Autonomous function of synaptotagmin 1 in triggering synchronous release independent of asynchronous release. *Neuron* **48**, 547-554 (2005).

24. Pang, Z. P. *et al.* Synaptotagmin-2 is essential for survival and contributes to Ca2+ triggering of neurotransmitter release in central and neuromuscular synapses. *J. Neurosci.* **26**, 13493-13504 (2006).

25. Wood, S. J. & Slater, C. R. Safety factor at the neuromuscular junction. *Prog. Neurobiol.* **64**, 393-429 (2001).

26. Slater, C. R. Structural determinants of the reliability of synaptic transmission at the vertebrate neuromuscular junction. *J. Neurocytol.* **32**, 505-522 (2003).

27. Salpeter, M. M. & Loring, R. H. Nicotinic acetylcholine receptors in vertebrate muscle: properties, distribution and neural control. *Prog. Neurobiol.* **25**, 297-325 (1985).

28. Salpeter, M. M., Marchaterre, M. & Harris, R. Distribution of extrajunctional acetylcholine receptors on a vertebrate muscle: evaluated by using a scanning electron microscope autoradiographic procedure. *J. Cell Biol.* **106**, 2087-2093 (1988).

29. Fertuck, H. C. & Salpeter, M. M. Quantitation of junctional and extrajunctional acetylcholine receptors by electron microscope autoradiography after 125I-alpha-bungarotoxin binding at mouse neuromuscular junctions. *J. Cell Biol.* **69**, 144-158 (1976).

30. Flucher, B. E. & Daniels, M. P. Distribution of Na+ channels and ankyrin in neuromuscular junctions is complementary to that of acetylcholine receptors and the 43 kd protein. *Neuron* **3**, 163-175 (1989).

31. Sanes, J. R. & Lichtman, J. W. Induction, assembly, maturation and maintenance of a postsynaptic apparatus. *Nat. Rev. Neurosci.* **2**, 791-805 (2001).

32. FATT, P. & KATZ, B. An analysis of the end-plate potential recorded with an intracellular electrode. *J. Physiol* **115**, 320-370 (1951).

33. Neher, E. & Sakmann, B. Single-channel currents recorded from membrane of denervated frog muscle fibres. *Nature* **260**, 799-802 (1976).

34. Unwin, N. Neurotransmitter action: opening of ligand-gated ion channels. *Cell* **72 Suppl**, 31-41 (1993).

35. Patton, B. L. Basal lamina and the organization of neuromuscular synapses. *J. Neurocytol.* **32**, 883-903 (2003).

36. Fabiato, A. Calcium-induced release of calcium from the cardiac sarcoplasmic reticulum. *Am. J. Physiol* **245**, C1-14 (1983).

37. Proenza, C. *et al.* Identification of a region of RyR1 that participates in allosteric coupling with the alpha(1S) (Ca(V)1.1) II-III loop. *J. Biol. Chem.* **277**, 6530-6535 (2002).

38. Dulhunty, A. F. Excitation-contraction coupling from the 1950s into the new millennium. *Clin. Exp. Pharmacol. Physiol* **33**, 763-772 (2006).

39. Le Douarin, N. M. Cell line segregation during peripheral nervous system ontogeny. *Science* **231**, 1515-1522 (1986).

40. Jessen, K. R. *et al.* The Schwann cell precursor and its fate: a study of cell death and differentiation during gliogenesis in rat embryonic nerves. *Neuron* **12**, 509-527 (1994).

41. Jessen, K. R. & Mirsky, R. Control of Schwann cell myelination. *F1000. Biol. Rep.* **2**, (2010).

42. Jessen, K. R. & Mirsky, R. The origin and development of glial cells in peripheral nerves. *Nat. Rev. Neurosci.* **6**, 671-682 (2005).

43. Benjamins, J. A. & Morell, P. Proteins of myelin and their metabolism. *Neurochem. Res.* **3**, 137-174 (1978).

44. Beck, K. D., Powell Braxton, L., Widmer, H. R., Valverde, J. & Hefti, F. Igf1 gene disruption results in reduced brain size, CNS hypomyelination, and loss of hippocampal granule and striatal parvalbumin-containing neurons. *Neuron* **14**, 717-730 (1995).

45. Carson, M. J., Behringer, R. R., Brinster, R. L. & McMorris, F. A. Insulin-like growth factor I increases brain growth and central nervous system myelination in transgenic mice 1. *Neuron* **10**, 729-740 (1993).

46. Cheng, H. L., Russell, J. W. & Feldman, E. L. IGF-I promotes peripheral nervous system myelination. *Ann. N. Y. Acad. Sci.* **883**, 124-130 (1999).

47. Liang, G., Cline, G. W. & Macica, C. M. IGF-1 stimulates de novo fatty acid biosynthesis by Schwann cells during myelination. *Glia* **55**, 632-641 (2007).

48. Bhatheja, K. & Field, J. Schwann cells: origins and role in axonal maintenance and regeneration. *Int. J. Biochem. Cell Biol.* **38**, 1995-1999 (2006).

49. Taveggia, C. *et al.* Neuregulin-1 type III determines the ensheathment fate of axons. *Neuron* **47**, 681-694 (2005).

50. Reddy, L. V., Koirala, S., Sugiura, Y., Herrera, A. A. & Ko, C. P. Glial cells maintain synaptic structure and function and promote development of the neuromuscular junction in vivo. *Neuron* **40**, 563-580 (2003).

51. Kang, H., Tian, L. & Thompson, W. Terminal Schwann cells guide the reinnervation of muscle after nerve injury. *J. Neurocytol.* **32**, 975-985 (2003).

52. Auld, D. S. *et al.* Modulation of neurotransmission by reciprocal synapse-glial interactions at the neuromuscular junction. *J. Neurocytol.* **32**, 1003-1015 (2003).

53. Colomar, A. & Robitaille, R. Glial modulation of synaptic transmission at the neuromuscular junction. *Glia* **47**, 284-289 (2004).

54. Feng, Z., Koirala, S. & Ko, C. P. Synapse-glia interactions at the vertebrate neuromuscular junction. *Neuroscientist.* **11**, 503-513 (2005).

55. Vargas, M. E. & Barres, B. A. Why is Wallerian degeneration in the CNS so slow? 2. *Annu. Rev. Neurosci.* **30**, 153-179 (2007).

56. Sahenk, Z., Oblinger, J. & Edwards, C. Neurotrophin-3 deficient Schwann cells impair nerve regeneration. *Exp. Neurol.* **212**, 552-556 (2008).

57. Cornbrooks, C. J., Carey, D. J., McDonald, J. A., Timpl, R. & Bunge, R. P. In vivo and in vitro observations on laminin production by Schwann cells. *Proc. Natl. Acad. Sci. U. S. A* **80**, 3850-3854 (1983).

58. Tsukahara, N. Synaptic plasticity in the mammalian central nervous system. *Annu. Rev. Neurosci.* **4**, 351-379 (1981).

59. Sanes, J. R. The basement membrane/basal lamina of skeletal muscle. *J. Biol. Chem.* **278**, 12601-12604 (2003).

60. Nishimune, H., Sanes, J. R. & Carlson, S. S. A synaptic laminin-calcium channel interaction organizes active zones in motor nerve terminals. *Nature* **432**, 580-587 (2004).

61. Brandan, E. & Inestrosa, N. C. The synaptic form of acetylcholinesterase binds to cell-surface heparan sulfate proteoglycans. *J. Neurosci. Res.* **15**, 185-196 (1986).

62. Nam, T., Moralez, A. & Clemmons, D. Vitronectin binding to IGF binding protein-5 (IGFBP-5) alters IGFBP-5 modulation of IGF-I actions. *Endocrinology* **143**, 30-36 (2002).

63. Li, Q. & Loeb, J. A. Neuregulin-heparan-sulfate proteoglycan interactions produce sustained erbB receptor activation required for the induction of acetylcholine receptors in muscle. *J. Biol. Chem.* **276**, 38068-38075 (2001).

64. Adams, J. C. Molecular organisation of cell-matrix contacts: essential multiprotein assemblies in cell and tissue function. *Expert. Rev. Mol. Med.* **4**, 1-24 (2002).

65. Berrier, A. L. & Yamada, K. M. Cell-matrix adhesion. *J. Cell Physiol* **213**, 565-573 (2007).

66. Cohen, S., Levi-Montalcini, R. & Hamburger, V. A NERVE GROWTH-STIMULATING FACTOR ISOLATED FROM SARCOM AS 37 AND 180. *Proc. Natl. Acad. Sci. U. S. A* **40**, 1014-1018 (1954).

67. Hamburger, V. & Levi-Montalcini, R. Proliferation, differentiation and degeneration in the spinal ganglia of the chick embryo under normal and experimental conditions. *J. Exp. Zool.* **111**, 457-501 (1949).

68. Hamburger, V. Cell death in the development of the lateral motor column of the chick embryo. *J. Comp Neurol.* **160**, 535-546 (1975).

69. Hamburger, V. The journey of a neuroembryologist. *Annu. Rev. Neurosci.* **12**, 1-12 (1989).

70. Thoenen, H. & Barde, Y. A. Physiology of nerve growth factor. *Physiol Rev.* **60**, 1284-1335 (1980).

71. Barde, Y. A. Trophic factors and neuronal survival. *Neuron* **2**, 1525-1534 (1989).

72. Wang, H. G., Rapp, U. R. & Reed, J. C. Bcl-2 targets the protein kinase Raf-1 to mitochondria. *Cell* **87**, 629-638 (1996).

73. Wang, H. G. *et al.* Apoptosis regulation by interaction of Bcl-2 protein and Raf-1 kinase. *Oncogene* **9**, 2751-2756 (1994).

74. Borasio, G. D., Markus, A., Wittinghofer, A., Barde, Y. A. & Heumann, R. Involvement of ras p21 in neurotrophin-induced response of sensory, but not sympathetic neurons. *J. Cell Biol.* **121**, 665-672 (1993).

75. Wang, H. G., Takayama, S., Rapp, U. R. & Reed, J. C. Bcl-2 interacting protein, BAG-1, binds to and activates the kinase Raf-1. *Proc. Natl. Acad. Sci. U. S. A* **93**, 7063-7068 (1996).

76. Dudek, H. *et al.* Regulation of neuronal survival by the serine-threonine protein kinase Akt. *Science* **275**, 661-665 (1997).

77. Wiese, S. *et al.* Specific function of B-Raf in mediating survival of embryonic motoneurons and sensory neurons. *Nat. Neurosci.* **4**, 137-142 (2001).

78. Yang, E. *et al.* Bad, a heterodimeric partner for Bcl-XL and Bcl-2, displaces Bax and promotes cell death. *Cell* **80**, 285-291 (1995).

79. Brunet, A. *et al.* Akt promotes cell survival by phosphorylating and inhibiting a Forkhead transcription factor. *Cell* **96**, 857-868 (1999).

80. Bonni, A. *et al.* Cell survival promoted by the Ras-MAPK signaling pathway by transcription-dependent and -independent mechanisms. *Science* **286**, 1358-1362 (1999).

81. Lillien, L. E. & Raff, M. C. Differentiation signals in the CNS: type-2 astrocyte development in vitro as a model system. *Neuron* **5**, 111-119 (1990).

82. Huang, E. J. & Reichardt, L. F. Trk receptors: roles in neuronal signal transduction. *Annu. Rev. Biochem.* **72**, 609-642 (2003).

83. Dechant, G. & Barde, Y. A. The neurotrophin receptor p75(NTR): novel functions and implications for diseases of the nervous system. *Nat. Neurosci.* **5**, 1131-1136 (2002).

84. Huang, E. J. & Reichardt, L. F. Neurotrophins: roles in neuronal development and function. *Annu. Rev. Neurosci.* **24**, 677-736 (2001).

85. Kaplan, D. R. & Miller, F. D. Neurotrophin signal transduction in the nervous system. *Curr. Opin. Neurobiol.* **10**, 381-391 (2000).

86. Chao, M. V. Neurotrophins and their receptors: a convergence point for many signalling pathways. *Nat. Rev. Neurosci.* **4**, 299-309 (2003).

87. Sendtner, M. Molecular biology of neurotrophic factors. *Baillieres Clin. Neurol.* **4**, 575-591 (1995).

88. Beck, M., Karch, C., Wiese, S. & Sendtner, M. Motoneuron cell death and neurotrophic factors: basic models for development of new therapeutic strategies in ALS. *Amyotroph. Lateral. Scler. Other Motor Neuron Disord.* **2 Suppl 1**, S55-S68 (2001).

89. Hughes, R. A., Sendtner, M. & Thoenen, H. Members of several gene families influence survival of rat motoneurons in vitro and in vivo. *J. Neurosci. Res.* **36(6)**, 663-671 (1993).

90. Henderson, C. E. *et al.* GDNF: a potent survival factor for motoneurons present in peripheral nerve and muscle. *Science* **266**, 1062-1064 (1994).

91. Gonzalez, M. *et al.* Disruption of Trkb-mediated signaling induces disassembly of postsynaptic receptor clusters at neuromuscular junctions
1. *Neuron* **24**, 567-583 (1999).

92. Wells, D. G., McKechnie, B. A., Kelkar, S. & Fallon, J. R. Neurotrophins regulate agrin-induced postsynaptic differentiation
1. *Proc. Natl. Acad. Sci. U. S. A* **96**, 1112-1117 (1999).

93. Barde, Y. A., Edgar, D. & Thoenen, H. Purification of a new neurotrophic factor from mammalian brain. *EMBO J.* **1**, 549-553 (1982).

94. Mousavi, K. & Jasmin, B. J. BDNF is expressed in skeletal muscle satellite cells and inhibits myogenic differentiation. *J. Neurosci.* **26**, 5739-5749 (2006).

95. Griesbeck, O., Parsadanian, A. S., Sendtner, M. & Thoenen, H. Expression of neurotrophins in skeletal muscle: quantitative comparison and significance for motoneuron survival and maintenance of function. *J. Neurosci. Res.* **42**, 21-33 (1995).

96. Meyer, M., Matsuoka, I., Wetmore, C., Olson, L. & Thoenen, H. Enhanced synthesis of brain-derived neurotrophic factor in the lesioned peripheral nerve: different mechanisms are responsible for the regulation of BDNF and NGF mRNA. *J. Cell Biol.* **119**, 45-54 (1992).

97. Sendtner, M., Holtmann, B., Kolbeck, R., Thoenen, H. & Barde, Y. A. Brain-derived neurotrophic factor prevents the death of motoneurons in newborn rats after nerve section. *Nature* **360**, 757-759 (1992).

98. Henderson, C. E. *et al.* GDNF: a potent survival factor for motoneurons present in peripheral nerve and muscle. *Science* **266**, 1062-1064 (1994).

99. Oppenheim, R. W. *et al.* Glial cell line-derived neurotrophic factor and developing mammalian motoneurons: regulation of programmed cell death among motoneuron subtypes. *J. Neurosci.* **20**, 5001-5011 (2000).

100. Airaksinen, M. S. & Saarma, M. The GDNF family: signalling, biological functions and therapeutic value. *Nat. Rev. Neurosci.* **3**, 383-394 (2002).

101. Zwick, M., Teng, L., Mu, X., Springer, J. E. & Davis, B. M. Overexpression of GDNF induces and maintains hyperinnervation of muscle fibers and multiple end-plate formation. *Exp. Neurol.* **171**, 342-350 (2001).

102. Sagot, Y., Tan, S. A., Hammang, J. P., Aebischer, P. & Kato, A. C. GDNF slows loss of motoneurons but not axonal degeneration or premature death of pmn/pmn mice. *J. Neurosci.* **16**, 2335-2341 (1996).

103. Sendtner, M. *et al.* Ciliary neurotrophic factor prevents degeneration of motor neurons in mouse mutant progressive motor neuronopathy
1. *Nature* **358**, 502-504 (1992).

104. Helfand, S. L., Smith, G. A. & Wessells, N. K. Survival and development in culture of dissociated parasympathetic neurons from ciliary ganglia. *Dev. Biol.* **50**, 541-547 (1976).

105. Sendtner, M., Carroll, P., Holtmann, B., Hughes, R. A. & Thoenen, H. Ciliary neurotrophic factor. *J. Neurobiol.* **25**, 1436-1453 (1994).

106. Louis, J. C., Magal, E., Takayama, S. & Varon, S. CNTF protection of oligodendrocytes against natural and tumor necrosis factor-induced death. *Science* **259**, 689-692 (1993).

107. Gurney, M. E., Yamamoto, H. & Kwon, Y. Induction of motor neuron sprouting in vivo by ciliary neurotrophic factor and basic fibroblast growth factor. *J. Neurosci.* **12**, 3241-3247 (1992).

108. Siegel, S. G., Patton, B. & English, A. W. Ciliary neurotrophic factor is required for motoneuron sprouting. *Exp. Neurol.* **166**, 205-212 (2000).

109. Lin, L. F. *et al.* Purification, cloning, and expression of ciliary neurotrophic factor (CNTF). *Science* **246**, 1023-1025 (1989).

110. Stockli, K. A. *et al.* Regional distribution, developmental changes, and cellular localization of CNTF-mRNA and protein in the rat brain. *J. Cell Biol.* **115**, 447-459 (1991).

111. Sendtner, M., Gotz, R., Holtmann, B. & Thoenen, H. Endogenous ciliary neurotrophic factor is a lesion factor for axotomized motoneurons in adult mice. *J. Neurosci.* **17**, 6999-7006 (1997).

112. Stockli, K. A. *et al.* Molecular cloning, expression and regional distribution of rat ciliary neurotrophic factor. *Nature* **342**, 920-923 (1989).

113. Sendtner, M., Stockli, K. A. & Thoenen, H. Synthesis and localization of ciliary neurotrophic factor in the sciatic nerve of the adult rat after lesion and during regeneration. *J. Cell Biol.* **118**, 139-148 (1992).

114. Masu, Y. *et al.* Disruption of the CNTF gene results in motor neuron degeneration. *Nature* **365**, 27-32 (1993).

115. Davis, S. *et al.* The receptor for ciliary neurotrophic factor. *Science* **253**, 59-63 (1991).

116. Thompson, S. W. & Majithia, A. A. Leukemia inhibitory factor induces sympathetic sprouting in intact dorsal root ganglia in the adult rat in vivo
1. *J. Physiol* **506 (Pt 3)**, 809-816 (1998).

117. Oppenheim, R. W. *et al.* Cardiotrophin-1, a muscle-derived cytokine, is required for the survival of subpopulations of developing motoneurons. *J. Neurosci.* **21**, 1283-1291 (2001).

118. Holtmann, B. *et al.* Triple knock-out of CNTF, LIF, and CT-1 defines cooperative and distinct roles of these neurotrophic factors for motoneuron maintenance and function. *J. Neurosci.* **25**, 1778-1787 (2005).

119. Davis, S. *et al.* LIFR beta and gp130 as heterodimerizing signal transducers of the tripartite CNTF receptor. *Science* **260**, 1805-1808 (1993).

120. Sleeman, M. W., Anderson, K. D., Lambert, P. D., Yancopoulos, G. D. & Wiegand, S. J. The ciliary neurotrophic factor and its receptor, CNTFR alpha. *Pharm. Acta Helv.* **74**, 265-272 (2000).

121. Stahl, N. & Yancopoulos, G. D. The tripartite CNTF receptor complex: activation and signaling involves components shared with other cytokines. *J. Neurobiol.* **25**, 1454-1466 (1994).

122. Stahl, N. *et al.* Choice of STATs and other substrates specified by modular tyrosine-based motifs in cytokine receptors. *Science* **267**, 1349-1353 (1995).

123. Turkson, J. & Jove, R. STAT proteins: novel molecular targets for cancer drug discovery. *Oncogene* **19**, 6613-6626 (2000).

124. Peterson, W. M., Wang, Q., Tzekova, R. & Wiegand, S. J. Ciliary neurotrophic factor and stress stimuli activate the Jak-STAT pathway in retinal neurons and glia. *J. Neurosci.* **20**, 4081-4090 (2000).

125. Hirano, T., Nakajima, K. & Hibi, M. Signaling mechanisms through gp130: a model of the cytokine system. *Cytokine Growth Factor Rev.* **8**, 241-252 (1997).

126. Ng, D. C. *et al.* Stat3 regulates microtubules by antagonizing the depolymerization activity of stathmin. *J. Cell Biol.* **172**, 245-257 (2006).

127. Giess, R. *et al.* Early onset of severe familial amyotrophic lateral sclerosis with a SOD-1 mutation: potential impact of CNTF as a candidate modifier gene
1. *Am. J. Hum. Genet.* **70**, 1277-1286 (2002).

128. Thompson, W. & Jansen, J. K. The extent of sprouting of remaining motor units in partly denervated immature and adult rat soleus muscle. *Neuroscience* **2**, 523-535 (1977).

129. Zacchigna, S., Lambrechts, D. & Carmeliet, P. Neurovascular signalling defects in neurodegeneration. *Nat. Rev. Neurosci.* **9**, 169-181 (2008).

130. English, A. W. Cytokines, growth factors and sprouting at the neuromuscular junction. *J. Neurocytol.* **32**, 943-960 (2003).

131. Brown, M. C., Holland, R. L. & Hopkins, W. G. Motor nerve sprouting. *Annu. Rev. Neurosci.* **4**, 17-42 (1981).

132. Brown, M. C., Holland, R. L. & Ironton, R. Nodal and terminal sprouting from motor nerves in fast and slow muscles of the mouse. *J. Physiol* **306**, 493-510 (1980).

133. Duchen, L. W. & Strich, S. J. The effects of botulinum toxin on the pattern of innervation of skeletal muscle in the mouse. *Q. J. Exp. Physiol Cogn Med. Sci.* **53**, 84-89 (1968).

134. Sanes, J. R., Schachner, M. & Covault, J. Expression of several adhesive macromolecules (N-CAM, L1, J1, NILE, uvomorulin, laminin, fibronectin, and a heparan sulfate proteoglycan) in embryonic, adult, and denervated adult skeletal muscle. *J. Cell Biol.* **102**, 420-431 (1986).

135. Caroni, P. & Grandes, P. Nerve sprouting in innervated adult skeletal muscle induced by exposure to elevated levels of insulin-like growth factors. *J. Cell Biol.* **110**, 1307-1317 (1990).

136. Son, Y. J. & Thompson, W. J. Schwann cell processes guide regeneration of peripheral axons. *Neuron* **14**, 125-132 (1995).

137. Son, Y. J. & Thompson, W. J. Nerve sprouting in muscle is induced and guided by processes extended by Schwann cells. *Neuron* **14**, 133-141 (1995).

138. Reynolds, M. L. & Woolf, C. J. Terminal Schwann cells elaborate extensive processes following denervation of the motor endplate. *J. Neurocytol.* **21**, 50-66 (1992).

139. Love, F. M. & Thompson, W. J. Glial cells promote muscle reinnervation by responding to activity-dependent postsynaptic signals. *J. Neurosci.* **19**, 10390-10396 (1999).

140. de, P. A., Meunier, F. A., Molgo, J., Aoki, K. R. & Dolly, J. O. Functional repair of motor endplates after botulinum neurotoxin type A poisoning: biphasic switch of synaptic activity between nerve sprouts and their parent terminals. *Proc. Natl. Acad. Sci. U. S. A* **96**, 3200-3205 (1999).

141. Jablonka, S., Schrank, B., Kralewski, M., Rossoll, W. & Sendtner, M. Reduced survival motor neuron (Smn) gene dose in mice leads to motor neuron degeneration: an animal model for spinal muscular atrophy type III. *Hum. Mol. Genet.* **9**, 341-346 (2000).

142. LeRoith, D. *et al.* The insulin-like growth factor family of peptides, binding proteins and receptors: their potential role in tissue regeneration. *Adv. Exp. Med. Biol.* **321**, 21-28 (1992).

143. Schofield, P. N. Molecular biology of the insulin-like growth factors: gene structure and expression. *Acta Paediatr. Scand. Suppl* **372**, 83-90 (1991).

144. Rinderknecht, E. & Humbel, R. E. Primary structure of human insulin-like growth factor II. *FEBS Lett.* **89**, 283-286 (1978).

145. Rinderknecht, E. & Humbel, R. E. The amino acid sequence of human insulin-like growth factor I and its structural homology with proinsulin. *J. Biol. Chem.* **253**, 2769-2776 (1978).

146. Recio-Pinto, E., Rechler, M. M. & Ishii, D. N. Effects of insulin, insulin-like growth factor-II, and nerve growth factor on neurite formation and survival in cultured sympathetic and sensory neurons. *J. Neurosci.* **6**, 1211-1219 (1986).

147. Ullrich, A. *et al.* Insulin-like growth factor I receptor primary structure: comparison with insulin receptor suggests structural determinants that define functional specificity. *EMBO J.* **5**, 2503-2512 (1986).

148. Czech, M. P. Signal transmission by the insulin-like growth factors. *Cell* **59**, 235-238 (1989).

149. Germain-Lee, E. L., Janicot, M., Lammers, R., Ullrich, A. & Casella, S. J. Expression of a type I insulin-like growth factor receptor with low affinity for insulin-like growth factor II. *Biochem. J.* **281 (Pt 2)**, 413-417 (1992).

150. Nissley, P., Kiess, W. & Sklar, M. Developmental expression of the IGF-II/mannose 6-phosphate receptor. *Mol. Reprod. Dev.* **35**, 408-413 (1993).

151. Kornfeld, S. Structure and function of the mannose 6-phosphate/insulinlike growth factor II receptors. *Annu. Rev. Biochem.* **61**, 307-330 (1992).

152. Nolan, C. M., Kyle, J. W., Watanabe, H. & Sly, W. S. Binding of insulin-like growth factor II (IGF-II) by human cation-independent mannose 6-phosphate receptor/IGF-II receptor expressed in receptor-deficient mouse L cells. *Cell Regul.* **1**, 197-213 (1990).

153. Kiess, W. *et al.* An antibody that blocks insulin-like growth factor (IGF) binding to the type II IGF receptor is neither an agonist nor an inhibitor of IGF-stimulated biologic responses in L6 myoblasts. *J. Biol. Chem.* **262**, 12745-12751 (1987).

154. Adams, T. E., Epa, V. C., Garrett, T. P. & Ward, C. W. Structure and function of the type 1 insulin-like growth factor receptor. *Cell Mol. Life Sci.* **57**, 1050-1093 (2000).

155. De, M. P. & Whittaker, J. Structural biology of insulin and IGF1 receptors: implications for drug design. *Nat. Rev. Drug Discov.* **1**, 769-783 (2002).

156. Adhami, V. M., Afaq, F. & Mukhtar, H. Insulin-like growth factor-I axis as a pathway for cancer chemoprevention. *Clin. Cancer Res.* **12**, 5611-5614 (2006).

157. Yenush, L. & White, M. F. The IRS-signalling system during insulin and cytokine action. *Bioessays* **19**, 491-500 (1997).

158. White, M. F. Insulin signaling in health and disease. *Science* **302**, 1710-1711 (2003).

159. Yamada, M. *et al.* Insulin receptor substrate (IRS)-1 and IRS-2 are tyrosine-phosphorylated and associated with phosphatidylinositol 3-kinase in response to brain-derived neurotrophic factor in cultured cerebral cortical neurons. *J. Biol. Chem.* **272**, 30334-30339 (1997).

160. Saltiel, A. R. New perspectives into the molecular pathogenesis and treatment of type 2 diabetes. *Cell* **104**, 517-529 (2001).

161. Cui, Q. L. & Almazan, G. IGF-I-induced oligodendrocyte progenitor proliferation requires PI3K/Akt, MEK/ERK, and Src-like tyrosine kinases. *J. Neurochem.* **100**, 1480-1493 (2007).

162. Barbacid, M. ras genes. *Annu. Rev. Biochem.* **56**, 779-827 (1987).

163. Myers, M. G., Jr. *et al.* Insulin receptor substrate-1 mediates phosphatidylinositol 3'-kinase and p70S6k signaling during insulin, insulin-like growth factor-1, and interleukin-4 stimulation. *J. Biol. Chem.* **269**, 28783-28789 (1994).

164. Nakae, J., Barr, V. & Accili, D. Differential regulation of gene expression by insulin and IGF-1 receptors correlates with phosphorylation of a single amino acid residue in the forkhead transcription factor FKHR. *EMBO J.* **19**, 989-996 (2000).

165. Hallak, H., Seiler, A. E., Green, J. S., Ross, B. N. & Rubin, R. Association of heterotrimeric G(i) with the insulin-like growth factor-I receptor. Release of G(betagamma) subunits upon receptor activation. *J. Biol. Chem.* **275**, 2255-2258 (2000).

166. Cui, Q. L., Zheng, W. H., Quirion, R. & Almazan, G. Inhibition of Src-like kinases reveals Akt-dependent and -independent pathways in insulin-like growth factor I-mediated oligodendrocyte progenitor survival. *J. Biol. Chem.* **280**, 8918-8928 (2005).

167. Kim, B. & Feldman, E. L. Differential regulation of focal adhesion kinase and mitogen-activated protein kinase tyrosine phosphorylation during insulin-like growth factor-I-mediated cytoskeletal reorganization. *J. Neurochem.* **71**, 1333-1336 (1998).

168. Leventhal, P. S. & Feldman, E. L. Insulin-like Growth Factors as Regulators of Cell Motility Signaling Mechanisms. *Trends Endocrinol. Metab* **8**, 1-6 (1997).

169. Feldman, E. L., Sullivan, K. A., Kim, B. & Russell, J. W. Insulin-like growth factors regulate neuronal differentiation and survival. *Neurobiol. Dis.* **4**, 201-214 (1997).

170. Zaka, M., Rafi, M. A., Rao, H. Z., Luzi, P. & Wenger, D. A. Insulin-like growth factor-1 provides protection against psychosine-induced apoptosis in cultured mouse oligodendrocyte progenitor cells using primarily the PI3K/Akt pathway. *Mol. Cell Neurosci.* **30**, 398-407 (2005).

171. Freude, S. *et al.* IRS-2 branch of IGF-1 receptor signaling is essential for appropriate timing of myelination. *J. Neurochem.* **107**, 907-917 (2008).

172. Ye, P., Carson, J. & D'Ercole, A. J. In vivo actions of insulin-like growth factor-I (IGF-I) on brain myelination: studies of IGF-I and IGF binding protein-1 (IGFBP-1) transgenic mice. *J. Neurosci.* **15**, 7344-7356 (1995).

173. Cheng, H. L. *et al.* Characterization of insulin-like growth factor-I and its receptor and binding proteins in transected nerves and cultured Schwann cells. *J. Neurochem.* **66**, 525-536 (1996).

174. Neff, N. T. *et al.* Insulin-like growth factors: Putative muscle-derived trophic agents that promote motoneuron survival. *J. Neurobiol.* **24**, 1578-1588 (1993).

175. Thoenen, H., Hughes, R. A. & Sendtner, M. Trophic support of motoneurons: Physiological, pathophysiological, and therapeutic implications. *Exp. Neurol.* **124**, 47-55 (1993).

176. Jessen, K. R. *et al.* The Schwann cell precursor and its fate: a study of cell death and differentiation during gliogenesis in rat embryonic nerves. *Neuron* **12**, 509-527 (1994).

177. Gavrilovic, J., Brennan, A., Mirsky, R. & Jessen, K. R. Fibroblast growth factors and insulin growth factors combine to promote survival of rat Schwann cell precursors without induction of DNA synthesis. *Eur. J. Neurosci.* **7**, 77-85 (1995).

178. Syroid, D. E. *et al.* A role for insulin-like growth factor-I in the regulation of Schwann cell survival. *J. Neurosci.* **19**, 2059-2068 (1999).

179. Russell, J. W., Cheng, H. L. & Golovoy, D. Insulin-like growth factor-I promotes myelination of peripheral sensory axons. *J. Neuropathol. Exp. Neurol.* **59**, 575-584 (2000).

180. Sullivan, K. A., Kim, B. & Feldman, E. L. Insulin-like growth factors in the peripheral nervous system 7. *Endocrinology* **149**, 5963-5971 (2008).

181. Ishii, D. N. Implication of insulin-like growth factors in the pathogenesis of diabetic neuropathy 20. *Brain Res. Brain Res. Rev.* **20**, 47-67 (1995).

182. Duan, C. Specifying the cellular responses to IGF signals: roles of IGF-binding proteins 4. *J. Endocrinol.* **175**, 41-54 (2002).

183. Sara, V. R. & Hall, K. Insulin-like growth factors and their binding proteins. *Physiol Rev.* **70**, 591-614 (1990).

184. Clemmons, D. R. *et al.* Role of insulin-like growth factor binding proteins in the control of IGF actions. *Prog. Growth Factor Res.* **6**, 357-366 (1995).

185. Drop, S. L. *et al.* Structural aspects of the IGFBP family. *Growth Regul.* **2**, 69-79 (1992).

186. Kalus, W. *et al.* Structure of the IGF-binding domain of the insulin-like growth factor-binding protein-5 (IGFBP-5): implications for IGF and IGF-I receptor interactions. *EMBO J.* **17**, 6558-6572 (1998).

187. Cheng, H. L., Sullivan, K. A. & Feldman, E. L. Immunohistochemical localization of insulin-like growth factor binding protein-5 in the developing rat nervous system. *Brain Res. Dev. Brain Res.* **92**, 211-218 (1996).

188. Jones, J. I. & Clemmons, D. R. Insulin-like growth factors and their binding proteins: biological actions. *Endocr. Rev.* **16**, 3-34 (1995).

189. Jones, J. I., Gockerman, A., Busby, W. H., Jr., Camacho-Hubner, C. & Clemmons, D. R. Extracellular matrix contains insulin-like growth factor binding protein-5: potentiation of the effects of IGF-I. *J. Cell Biol.* **121**, 679-687 (1993).

190. Clemmons, D. R., Jones, J. I., Busby, W. H. & Wright, G. Role of insulin-like growth factor binding proteins in modifying IGF actions. *Ann. N. Y. Acad. Sci.* **692**, 10-21 (1993).

191. Jiang, Y. & Steinle, J. J. Regulation of IRS-2 signaling by IGF-1 receptor in the diabetic rat heart. *Can. J. Physiol Pharmacol.* **88**, 553-561 (2010).

192. Craner, M. J., Klein, J. P., Black, J. A. & Waxman, S. G. Preferential expression of IGF-I in small DRG neurons and down-regulation following injury. *Neuroreport* **13**, 1649-1652 (2002).

193. Bergman, P. B. *et al.* Expression of the IGF system in normal and diabetic transgenic (mRen-2)27 rat eye. *Invest Ophthalmol. Vis. Sci.* **46**, 2708-2715 (2005).

194. Erichsen, A. K., Koht, J., Stray-Pedersen, A., Abdelnoor, M. & Tallaksen, C. M. Prevalence of hereditary ataxia and spastic paraplegia in southeast Norway: a population-based study 1. *Brain* **132**, 1577-1588 (2009).

195. Fink, J. K. *et al.* Hereditary spastic paraplegia: advances in genetic research. Hereditary Spastic Paraplegia Working group 1. *Neurology* **46**, 1507-1514 (1996).

196. Worms, P. M. The epidemiology of motor neuron diseases: a review of recent studies 1. *J. Neurol. Sci.* **191**, 3-9 (2001).

197. Rowland, L. P. Amyotrophic lateral sclerosis: theories and therapies. *Ann. Neurol.* **35**, 129-130 (1994).

198. Crawford, T. O. & Pardo, C. A. The neurobiology of childhood spinal muscular atrophy. *Neurobiol. Dis.* **3**, 97-110 (1996).

199. Feldkotter, M., Schwarzer, V., Wirth, R., Wienker, T. F. & Wirth, B. Quantitative analyses of SMN1 and SMN2 based on real-time lightCycler PCR: fast and highly reliable carrier testing and prediction of severity of spinal muscular atrophy. *Am. J. Hum. Genet.* **70**, 358-368 (2002).

200. Fried, K. & Emery, A. E. Spinal muscular atrophy type II. A separate genetic and clinical entity from type I (Werdnig-Hoffmann disease) and type 3 (Kugelberg-Welander disease). *Clin. Genet.* **2**, 203-209 (1971).

201. Munsat, T. L. & Davies, K. E. International SMA consortium meeting. (26-28 June 1992, Bonn, Germany). *Neuromuscul. Disord.* **2**, 423-428 (1992).

202. Zerres, K. & Rudnik-Schoneborn, S. Natural history in proximal spinal muscular atrophy. Clinical analysis of 445 patients and suggestions for a modification of existing classifications. *Arch. Neurol.* **52**, 518-523 (1995).

203. Dubowitz, V. *Muscle Disorders*. Saunders, London (1995).

204. Briese, M., Esmaeili, B. & Sattelle, D. B. Is spinal muscular atrophy the result of defects in motor neuron processes? *Bioessays* **27**, 946-957 (2005).

205. Pearn, J. H., Hudgson, P. & Walton, J. N. A clinical and genetic study of spinal muscular atrophy of adult onset: the autosomal recessive form as a discrete disease entity. *Brain* **101**, 591-606 (1978).

206. Wirth, B., Brichta, L. & Hahnen, E. Spinal muscular atrophy: from gene to therapy. *Semin. Pediatr. Neurol.* **13**, 121-131 (2006).

207. Gilliam, T. C. *et al.* Genetic homogeneity between acute and chronic forms of spinal muscular atrophy. *Nature* **345**, 823-825 (1990).

208. Brzustowicz, L. M. *et al.* Genetic mapping of chronic childhood-onset spinal muscular atrophy to chromosome 5q11.2-13.3. *Nature* **344**, 540-541 (1990).

209. Melki, J. *et al.* Gene for chronic proximal spinal muscular atrophies maps to chromosome 5q. *Nature* **344**, 767-768 (1990).

210. Lefebvre, S. *et al.* Identification and characterization of a spinal muscular atrophy-determining gene. *Cell* **80**, 155-165 (1995).

211. Roy, N. *et al.* The gene for neuronal apoptosis inhibitory protein is partially deleted in individuals with spinal muscular atrophy. *Cell* **80**, 167-178 (1995).

212. Burglen, L. *et al.* The gene encoding p44, a subunit of the transcription factor TFIIH, is involved in large-scale deletions associated with Werdnig-Hoffmann disease. *Am. J. Hum. Genet.* **60**, 72-79 (1997).

213. Carter, T. A. *et al.* A multicopy transcription-repair gene, BTF2p44, maps to the SMA region and demonstrates SMA associated deletions. *Hum. Mol. Genet.* **6**, 229-236 (1997).

214. Scharf, J. M. *et al.* Identification of a candidate modifying gene for spinal muscular atrophy by comparative genomics. *Nat. Genet.* **20**, 83-86 (1998).

215. Wirth, B. An update of the mutation spectrum of the survival motor neuron gene (SMN1) in autosomal recessive spinal muscular atrophy (SMA). *Hum. Mutat.* **15**, 228-237 (2000).

216. Burglen, L. *et al.* Structure and organization of the human survival motor neurone (SMN) gene. *Genomics* **32**, 479-482 (1996).

217. Chen, Q. *et al.* Sequence of a 131-kb region of 5q13.1 containing the spinal muscular atrophy candidate genes SMN and NAIP. *Genomics* **48**, 121-127 (1998).

218. Monani, U. R. *et al.* A single nucleotide difference that alters splicing patterns distinguishes the SMA gene SMN1 from the copy gene SMN2. *Hum. Mol. Genet.* **8**, 1177-1183 (1999).

219. Helmken, C. *et al.* Evidence for a modifying pathway in SMA discordant families: reduced SMN level decreases the amount of its interacting partners and Htra2-beta1. *Hum. Genet.* **114**, 11-21 (2003).

220. Lim, S. R. & Hertel, K. J. Modulation of survival motor neuron pre-mRNA splicing by inhibition of alternative 3' splice site pairing. *J. Biol. Chem.* **276**, 45476-45483 (2001).

221. Cartegni, L., Hastings, M. L., Calarco, J. A., de, S. E. & Krainer, A. R. Determinants of exon 7 splicing in the spinal muscular atrophy genes, SMN1 and SMN2. *Am. J. Hum. Genet.* **78**, 63-77 (2006).

222. Cartegni, L. & Krainer, A. R. Disruption of an SF2/ASF-dependent exonic splicing enhancer in SMN2 causes spinal muscular atrophy in the absence of SMN1. *Nat. Genet.* **30**, 377-384 (2002).

223. Lorson, C. L., Hahnen, E., Androphy, E. J. & Wirth, B. A single nucleotide in the SMN gene regulates splicing and is responsible for spinal muscular atrophy. *Proc. Natl. Acad. Sci. U. S. A* **96**, 6307-6311 (1999).

224. Hofmann, Y., Lorson, C. L., Stamm, S., Androphy, E. J. & Wirth, B. Htra2-beta 1 stimulates an exonic splicing enhancer and can restore full-length SMN expression to survival motor neuron 2 (SMN2). *Proc. Natl. Acad. Sci. U. S. A* **97**, 9618-9623 (2000).

225. Hofmann, Y. & Wirth, B. hnRNP-G promotes exon 7 inclusion of survival motor neuron (SMN) via direct interaction with Htra2-beta1. *Hum. Mol. Genet.* **11**, 2037-2049 (2002).

226. Young, P. J. *et al.* SRp30c-dependent stimulation of survival motor neuron (SMN) exon 7 inclusion is facilitated by a direct interaction with hTra2 beta 1. *Hum. Mol. Genet.* **11**, 577-587 (2002).

227. Schrank, B. *et al.* Inactivation of the survival motor neuron gene, a candidate gene for human spinal muscular atrophy, leads to massive cell death in early mouse embryos. *Proc. Natl. Acad. Sci. U. S. A* **94**, 9920-9925 (1997).

228. Miguel-Aliaga, I., Chan, Y. B., Davies, K. E. & van den, H. M. Disruption of SMN function by ectopic expression of the human SMN gene in Drosophila. *FEBS Lett.* **486**, 99-102 (2000).

229. Miguel-Aliaga, I. *et al.* The Caenorhabditis elegans orthologue of the human gene responsible for spinal muscular atrophy is a maternal product critical for germline maturation and embryonic viability. *Hum. Mol. Genet.* **8**, 2133-2143 (1999).

230. Liu, Q. & Dreyfuss, G. A novel nuclear structure containing the survival of motor neurons protein. *EMBO J.* **15**, 3555-3565 (1996).

231. Burghes, A. H. & Beattie, C. E. Spinal muscular atrophy: why do low levels of survival motor neuron protein make motor neurons sick? *Nat. Rev. Neurosci.* **10**, 597-609 (2009).

232. Carvalho, T. *et al.* The spinal muscular atrophy disease gene product, SMN: A link between snRNP biogenesis and the Cajal (coiled) body. *J. Cell Biol.* **147**, 715-728 (1999).

233. Fischer, U., Liu, Q. & Dreyfuss, G. The SMN-SIP1 complex has an essential role in spliceosomal snRNP biogenesis. *Cell* **90**, 1023-1029 (1997).

234. Young, P. J. *et al.* The exon 2b region of the spinal muscular atrophy protein, SMN, is involved in self-association and SIP1 binding. *Hum. Mol. Genet.* **9**, 2869-2877 (2000).

235. Giesemann, T. *et al.* A role for polyproline motifs in the spinal muscular atrophy protein SMN. Profilins bind to and colocalize with smn in nuclear gems. *J. Biol. Chem.* **274**, 37908-37914 (1999).

236. Talbot, K. *et al.* Missense mutation clustering in the survival motor neuron gene: a role for a conserved tyrosine and glycine rich region of the protein in RNA metabolism? *Hum. Mol. Genet.* **6**, 497-500 (1997).

237. Lorson, C. L. *et al.* SMN oligomerization defect correlates with spinal muscular atrophy severity. *Nat. Genet.* **19**, 63-66 (1998).

238. Burnett, B. G. *et al.* Regulation of SMN protein stability. *Mol. Cell Biol.* **29**, 1107-1115 (2009).

239. Nguyen, t. M. *et al.* A two-site ELISA can quantify upregulation of SMN protein by drugs for spinal muscular atrophy. *Neurology* **71**, 1757-1763 (2008).

240. Liu, Q., Fischer, U., Wang, F. & Dreyfuss, G. The spinal muscular atrophy disease gene product, SMN, and its associated protein SIP1 are in a complex with spliceosomal snRNP proteins. *Cell* **90**, 1013-1021 (1997).

241. Buhler, D., Raker, V., Luhrmann, R. & Fischer, U. Essential role for the tudor domain of SMN in spliceosomal U snRNP assembly: implications for spinal muscular atrophy. *Hum. Mol. Genet.* **8**, 2351-2357 (1999).

242. Pellizzoni, L., Charroux, B. & Dreyfuss, G. SMN mutants of spinal muscular atrophy patients are defective in binding to snRNP proteins. *Proc. Natl. Acad. Sci. U. S. A* **96**, 11167-11172 (1999).

243. Pellizzoni, L. Chaperoning ribonucleoprotein biogenesis in health and disease. *EMBO Rep.* **8**, 340-345 (2007).

244. Raker, V. A., Hartmuth, K., Kastner, B. & Luhrmann, R. Spliceosomal U snRNP core assembly: Sm proteins assemble onto an Sm site RNA nonanucleotide in a specific and thermodynamically stable manner. *Mol. Cell Biol.* **19**, 6554-6565 (1999).

245. Meister, G. *et al.* Methylation of Sm proteins by a complex containing PRMT5 and the putative U snRNP assembly factor pICln. *Curr. Biol.* **11**, 1990-1994 (2001).

246. Lamond, A. I. & Earnshaw, W. C. Structure and function in the nucleus. *Science* **280**, 547-553 (1998).

247. Meister, G., Buhler, D., Pillai, R., Lottspeich, F. & Fischer, U. A multiprotein complex mediates the ATP-dependent assembly of spliceosomal U snRNPs. *Nat. Cell Biol.* **3**, 945-949 (2001).

248. Gall, J. G., Tsvetkov, A., Wu, Z. & Murphy, C. Is the sphere organelle/coiled body a universal nuclear component? *Dev. Genet.* **16**, 25-35 (1995).

249. Coovert, D. D. *et al.* The survival motor neuron protein in spinal muscular atrophy. *Hum. Mol. Genet.* **6**, 1205-1214 (1997).

250. Lefebvre, S. *et al.* Correlation between severity and SMN protein level in spinal muscular atrophy. *Nat. Genet.* **16**, 265-269 (1997).

251. Burlet, P. *et al.* The distribution of SMN protein complex in human fetal tissues and its alteration in spinal muscular atrophy. *Hum. Mol. Genet.* **7**, 1927-1933 (1998).

252. Monani, U. R. Spinal muscular atrophy: a deficiency in a ubiquitous protein; a motor neuron-specific disease. *Neuron* **48**, 885-896 (2005).

253. Rossoll, W. *et al.* Smn, the spinal muscular atrophy-determining gene product, modulates axon growth and localization of beta-actin mRNA in growth cones of motoneurons. *J. Cell Biol.* **163**, 801-812 (2003).

254. Rossoll, W. *et al.* Specific interaction of Smn, the spinal muscular atrophy determining gene product, with hnRNP-R and gry-rbp/hnRNP-Q: a role for Smn in RNA processing in motor axons? *Hum. Mol. Genet.* **11**, 93-105 (2002).

255. Doussau, F. & Augustine, G. J. The actin cytoskeleton and neurotransmitter release: an overview. *Biochimie* **82**, 353-363 (2000).

256. Bloom, O. *et al.* Colocalization of synapsin and actin during synaptic vesicle recycling. *J. Cell Biol.* **161**, 737-747 (2003).

257. Kong, L. *et al.* Impaired synaptic vesicle release and immaturity of neuromuscular junctions in spinal muscular atrophy mice. *J. Neurosci.* **29**, 842-851 (2009).

258. Murray, L. M. *et al.* Selective vulnerability of motor neurons and dissociation of pre- and post-synaptic pathology at the neuromuscular junction in mouse models of spinal muscular atrophy 10. *Hum. Mol. Genet.* **17**, 949-962 (2008).

259. Rochette, C. F., Gilbert, N. & Simard, L. R. SMN gene duplication and the emergence of the SMN2 gene occurred in distinct hominids: SMN2 is unique to Homo sapiens. *Hum. Genet.* **108**, 255-266 (2001).

260. DiDonato, C. J. *et al.* Cloning, characterization, and copy number of the murine survival motor neuron gene: homolog of the spinal muscular atrophy-determining gene. *Genome Res.* **7**, 339-352 (1997).

261. Hsieh-Li, H. M. *et al.* A mouse model for spinal muscular atrophy. *Nat. Genet.* **24**, 66-70 (2000).

262. Monani, U. R. *et al.* The human centromeric survival motor neuron gene (SMN2) rescues embryonic lethality in Smn(-/-) mice and results in a mouse with spinal muscular atrophy. *Hum. Mol. Genet.* **9**, 333-339 (2000).

263. Gavrilina, T. O. *et al.* Neuronal SMN expression corrects spinal muscular atrophy in severe SMA mice while muscle-specific SMN expression has no phenotypic effect. *Hum. Mol. Genet.* **17**, 1063-1075 (2008).

264. Monani, U. R. *et al.* A transgene carrying an A2G missense mutation in the SMN gene modulates phenotypic severity in mice with severe (type I) spinal muscular atrophy. *J. Cell Biol.* **160**, 41-52 (2003).

265. Parsons, D. W. *et al.* Intragenic telSMN mutations: frequency, distribution, evidence of a founder effect, and modification of the spinal muscular atrophy phenotype by cenSMN copy number. *Am. J. Hum. Genet.* **63**, 1712-1723 (1998).

266. Le, T. T. *et al.* SMNDelta7, the major product of the centromeric survival motor neuron (SMN2) gene, extends survival in mice with spinal muscular atrophy and associates with full-length SMN. *Hum. Mol. Genet.* **14**, 845-857 (2005).

267. Butchbach, M. E., Edwards, J. D. & Burghes, A. H. Abnormal motor phenotype in the SMNDelta7 mouse model of spinal muscular atrophy. *Neurobiol. Dis.* **27**, 207-219 (2007).

268. Bromberg, M. B. An approach to the evaluation of peripheral neuropathies
11. *Semin. Neurol.* **30**, 350-355 (2010).

269. Lacomis, D. Small-fiber neuropathy. *Muscle Nerve* **26**, 173-188 (2002).

270. Poncelet, A. N. An algorithm for the evaluation of peripheral neuropathy. *Am. Fam. Physician* **57**, 755-764 (1998).

271. Kanji, J. N., Anglin, R. E., Hunt, D. L. & Panju, A. Does this patient with diabetes have large-fiber peripheral neuropathy?
1. *JAMA* **303**, 1526-1532 (2010).

272. NIH Diabetic Neuropathies: The Nerve Damage of Diabetes. *National Diabetes Information Clearinghouse* **59**, (2009).

273. Vinik, A., Ullal, J., Parson, H. K. & Casellini, C. M. Diabetic neuropathies: clinical manifestations and current treatment options
3. *Nat. Clin. Pract. Endocrinol. Metab* **2**, 269-281 (2006).

274. Goke, B., Parhofer, K. & Otto, C. *Diabetes mellitus*. Urban & Fischer bei Elsevier, (2002).

275. Wild, S., Roglic, G., Green, A., Sicree, R. & King, H. Global prevalence of diabetes: estimates for the year 2000 and projections for 2030. *Diabetes Care* **27**, 1047-1053 (2004).

276. Tillil, H., Nick, O. & Kobberling, J. [Modern diagnosis and classification of diabetes mellitus]. *Z. Arztl. Fortbild. Qualitatssich.* **92**, 456-466 (1998).

277. Thrailkill, K. M. Insulin-like growth factor-I in diabetes mellitus: its physiology, metabolic effects, and potential clinical utility. *Diabetes Technol. Ther.* **2**, 69-80 (2000).

278. Tan, K. & Baxter, R. C. Serum insulin-like growth factor I levels in adult diabetic patients: the effect of age
12. *J. Clin. Endocrinol. Metab* **63**, 651-655 (1986).

279. Wuarin, L., Guertin, D. M. & Ishii, D. N. Early reduction in insulin-like growth factor gene expression in diabetic nerve. *Exp. Neurol.* **130**, 106-114 (1994).

280. Feng, G. *et al.* Imaging neuronal subsets in transgenic mice expressing multiple spectral variants of GFP. *Neuron* **28**, 41-51 (2000).

281. Zierz, S. & Jerusalem, F. *Muskelerkrankungen*
1. (2003).

282. Holtmann, B. *et al.* Triple knock-out of CNTF, LIF, and CT-1 defines cooperative and distinct roles of these neurotrophic factors for motoneuron maintenance and function. *J Neurosci.* **25**, 1778-1787 (2005).

283. Michaelidis, T. M. *et al.* Inactivation of bcl-2 results in progressive degeneration of motoneurons, sympathetic and sensory neurons during early postnatal development. *Neuron* **17**, 75-89 (1996).

284. Schroder, J. M., Bohl, J. & Brodda, K. Changes of the ratio between myelin thickness and axon diameter in the human developing sural nerve. *Acta Neuropathol.* **43**, 169-178 (1978).

285. Nyenwe, E. A., Jerkins, T. W., Umpierrez, G. E. & Kitabchi, A. E. Management of type 2 diabetes: evolving strategies for the treatment of patients with type 2 diabetes
1. *Metabolism* **60**, 1-23 (2011).

286. Hughes, R. *et al.* Randomized controlled trial of intravenous immunoglobulin versus oral prednisolone in chronic inflammatory demyelinating polyradiculoneuropathy
2. *Ann. Neurol.* **50**, 195-201 (2001).

287. Bradford, M. M. A rapid and sensitive method for the quantitation of microgram quantities of protein utilizing the principle of protein-dye binding
9. *Anal. Biochem.* **72**, 248-254 (1976).

288. Bartlett, J. M. & Stirling, D. A short history of the polymerase chain reaction
11. *Methods Mol. Biol.* **226**, 3-6 (2003).

289. Saiki, R. K. *et al.* Enzymatic amplification of beta-globin genomic sequences and restriction site analysis for diagnosis of sickle cell anemia
7. *Science* **230**, 1350-1354 (1985).

290. Simon, C. M., Jablonka, S., Ruiz, R., Tabares, L. & Sendtner, M. Ciliary neurotrophic factor-induced sprouting preserves motor function in a mouse model of mild spinal muscular atrophy
1. *Hum. Mol. Genet.* **19**, 973-986 (2010).

291. McComas, A. J., Sica, R. E., Campbell, M. J. & Upton, A. R. Functional compensation in partially denervated muscles
24. *J. Neurol. Neurosurg. Psychiatry* **34**, 453-460 (1971).

292. Gordon, J. W. *et al.* Regulation of Thy-1 gene expression in transgenic mice
2. *Cell* **50**, 445-452 (1987).

293. Morris, R. Thy-1 in developing nervous tissue
22. *Dev. Neurosci.* **7**, 133-160 (1985).

294. Williams, A. F. & Gagnon, J. Neuronal cell Thy-1 glycoprotein: homology with immunoglobulin. *Science* **216**, 696-703 (1982).

295. Pun, S., Santos, A. F., Saxena, S., Xu, L. & Caroni, P. Selective vulnerability and pruning of phasic motoneuron axons in motoneuron disease alleviated by CNTF
2. *Nat. Neurosci.* **9**, 408-419 (2006).

296. Hoh, J. F. Muscle fiber types and function. *Curr. Opin. Rheumatol.* **4**, 801-808 (1992).

297. Pette, D. & Staron, R. S. Cellular and molecular diversities of mammalian skeletal muscle fibers
7. *Rev. Physiol Biochem. Pharmacol.* **116**, 1-76 (1990).

298. Schmalbruch, H. [Types of fibers in the leg musculature of the mouse]. *Z. Zellforsch. Mikrosk. Anat.* **79**, 64-75 (1967).

299. Chin, E. R. *et al.* A calcineurin-dependent transcriptional pathway controls skeletal muscle fiber type
2. *Genes Dev.* **12**, 2499-2509 (1998).

300. Wu, H. *et al.* MEF2 responds to multiple calcium-regulated signals in the control of skeletal muscle fiber type
1. *EMBO J.* **19**, 1963-1973 (2000).

301. Sagot, Y. *et al.* Polymer encapsulated cell lines genetically engineered to release ciliary neurotrophic factor can slow down progressive motor neuronopathy in the mouse
3. *Eur. J. Neurosci.* **7**, 1313-1322 (1995).

302. Sagot, Y., Rosse, T., Vejsada, R., Perrelet, D. & Kato, A. C. Differential effects of neurotrophic factors on motoneuron retrograde labeling in a murine model of motoneuron disease 1. *J. Neurosci.* **18**, 1132-1141 (1998).

303. Sendtner, M. *et al.* Cryptic physiological trophic support of motoneurons by LIF revealed by double gene targeting of CNTF and LIF 1. *Curr. Biol.* **6**, 686-694 (1996).

304. Murphy, E. H., Brown, J., Iannuzzelli, P. G. & Baker, R. Regeneration and soma size changes following axotomy of the trochlear nerve. *J. Comp Neurol.* **295**, 685-697 (1990).

305. Fressinaud, C., Jean, I. & Dubas, F. Selective decrease in axonal nerve growth factor and insulin-like growth factor I immunoreactivity in axonopathies of unknown etiology 3. *Acta Neuropathol.* **105**, 477-483 (2003).

306. Beattie, J., Allan, G. J., Lochrie, J. D. & Flint, D. J. Insulin-like growth factor-binding protein-5 (IGFBP-5): a critical member of the IGF axis. *Biochem. J.* **395**, 1-19 (2006).

307. Bremer, J. *et al.* Axonal prion protein is required for peripheral myelin maintenance. *Nat. Neurosci.* **13**, 310-318 (2010).

308. Zielasek, J., Martini, R. & Toyka, K. V. Functional abnormalities in P0-deficient mice resemble human hereditary neuropathies linked to P0 gene mutations. *Muscle Nerve* **19**, 946-952 (1996).

309. Liu, J.-P., Baker, J., Perkins, A. S., Robertson, E. J. & Efstratiadis, A. Mice carrying null mutations of the genes encoding insulin-like growth factor I (Igf-1) and type 1 IGF receptor (Igf1r). *Cell* **75**, 59-72 (1993).

310. Schweizer, U. *et al.* Conditional gene ablation of Stat3 reveals differential signaling requirements for survival of motoneurons during development and after nerve injury in the adult. *J. Cell Biol.* **156**, 287-297 (2002).

311. Henderson, C. E. *et al.* GDNF: a potent survival factor for motoneurons present in peripheral nerve and muscle. *Science* **266**, 1062-1064 (1994).

312. Takahashi, R. *et al.* A null mutation in the human CNTF gene is not causally related to neurological diseases. *Nat. Genet.* **7**, 79-84 (1994).

313. Giess, R. *et al.* Potential implications of a ciliary neurotrophic factor gene mutation in a German population of patients with motor neuron disease. *Muscle Nerve* **21**, 236-238 (1998).

314. Giess, R. *et al.* Early onset of severe familial amyotrophic lateral sclerosis with a SOD-1 mutation: potential impact of CNTF as a candidate modifier gene. *Am. J. Hum. Genet.* **70**, 1277-1286 (2002).

315. Keating, G. M. Mecasermin. *BioDrugs.* **22**, 177-188 (2008).

316. McWhorter, M. L., Monani, U. R., Burghes, A. H. & Beattie, C. E. Knockdown of the survival motor neuron (Smn) protein in zebrafish causes defects in motor axon outgrowth and pathfinding. *J Cell Biol.* **162**, 919-931 (2003).

317. Chan, Y. B. *et al.* Neuromuscular defects in a Drosophila survival motor neuron gene mutant. *Hum. Mol. Genet.* **12**, 1367-1376 (2003).

318. Kolb, S. J., Battle, D. J. & Dreyfuss, G. Molecular functions of the SMN complex 1. *J. Child Neurol.* **22**, 990-994 (2007).

319. Jablonka, S., Beck, M., Lechner, B. D., Mayer, C. & Sendtner, M. Defective Ca2+ channel clustering in axon terminals disturbs excitability in motoneurons in spinal muscular atrophy 7. *J. Cell Biol.* **179**, 139-149 (2007).

320. Friesen, W. J. & Dreyfuss, G. Specific sequences of the Sm and Sm-like (Lsm) proteins mediate their interaction with the spinal muscular atrophy disease gene product (SMN)
5. *J. Biol. Chem.* **275**, 26370-26375 (2000).

321. Bouveret, E., Rigaut, G., Shevchenko, A., Wilm, M. & Seraphin, B. A Sm-like protein complex that participates in mRNA degradation
2. *EMBO J.* **19**, 1661-1671 (2000).

322. He, W. & Parker, R. Functions of Lsm proteins in mRNA degradation and splicing
2. *Curr. Opin. Cell Biol.* **12**, 346-350 (2000).

323. Zhang, H. *et al.* Multiprotein complexes of the survival of motor neuron protein SMN with Gemins traffic to neuronal processes and growth cones of motor neurons. *J. Neurosci.* **26**, 8622-8632 (2006).

324. Fallini, C. *et al.* The survival of motor neuron (SMN) protein interacts with the mRNA-binding protein HuD and regulates localization of poly(A) mRNA in primary motor neuron axons
1. *J. Neurosci.* **31**, 3914-3925 (2011).

325. Glinka, M. *et al.* The heterogeneous nuclear ribonucleoprotein-R is necessary for axonal beta-actin mRNA translocation in spinal motor neurons
1. *Hum. Mol. Genet.* **19**, 1951-1966 (2010).

326. Schubert, T. & Akopian, A. Actin filaments regulate voltage-gated ion channels in salamander retinal ganglion cells
1. *Neuroscience* **125**, 583-590 (2004).

327. Robinson, P. *et al.* Formation of N-type (Cav2.2) voltage-gated calcium channel membrane microdomains: Lipid raft association and clustering
2. *Cell Calcium* **48**, 183-194 (2010).

328. Nishimune, H., Sanes, J. R. & Carlson, S. S. A synaptic laminin-calcium channel interaction organizes active zones in motor nerve terminals
4. *Nature* **432**, 580-587 (2004).

329. Nishimune, H. *et al.* Laminins promote postsynaptic maturation by an autocrine mechanism at the neuromuscular junction
2. *J. Cell Biol.* **182**, 1201-1215 (2008).

330. Kariya, S. *et al.* Reduced SMN protein impairs maturation of the neuromuscular junctions in mouse models of spinal muscular atrophy. *Hum. Mol. Genet.* **17**, 2552-2569 (2008).

331. McGovern, V. L., Gavrilina, T. O., Beattie, C. E. & Burghes, A. H. Embryonic motor axon development in the severe SMA mouse. *Hum. Mol. Genet.* **17**, 2900-2909 (2008).

332. Ruiz, R., Casanas, J. J., Torres-Benito, L., Cano, R. & Tabares, L. Altered intracellular Ca2+ homeostasis in nerve terminals of severe spinal muscular atrophy mice
3. *J. Neurosci.* **30**, 849-857 (2010).

333. Oprea, G. E. *et al.* Plastin 3 is a protective modifier of autosomal recessive spinal muscular atrophy
1. *Science* **320**, 524-527 (2008).

334. Bretscher, A. Fimbrin is a cytoskeletal protein that crosslinks F-actin in vitro. *Proc. Natl. Acad. Sci. U. S. A* **78**, 6849-6853 (1981).

335. Funakoshi, H. *et al.* Differential expression of mRNAs for neurotrophins and their receptors after axotomy of the sciatic nerve
1. *J. Cell Biol.* **123**, 455-465 (1993).

336. Kust, B. M., Copray, J. C., Brouwer, N., Troost, D. & Boddeke, H. W. Elevated levels of neurotrophins in human biceps brachii tissue of amyotrophic lateral sclerosis
8. *Exp. Neurol.* **177**, 419-427 (2002).

337. Kobayashi, N. R., Bedard, A. M., Hincke, M. T. & Tetzlaff, W. Increased expression of BDNF and trkB mRNA in rat facial motoneurons after axotomy
2. *Eur. J. Neurosci.* **8**, 1018-1029 (1996).

338. Boyd, J. G. & Gordon, T. A dose-dependent facilitation and inhibition of peripheral nerve regeneration by brain-derived neurotrophic factor
4. *Eur. J. Neurosci.* **15**, 613-626 (2002).

339. Markus, A., Zhong, J. & Snider, W. D. Raf and akt mediate distinct aspects of sensory axon growth. *Neuron* **35**, 65-76 (2002).

340. Wegrzyn, J. *et al.* Function of mitochondrial Stat3 in cellular respiration. *Science* **323**, 793-797 (2009).

341. Tanaka, E. & Sabry, J. Making the connection: cytoskeletal rearrangements during growth cone guidance
2. *Cell* **83**, 171-176 (1995).

342. Ng, D. C. *et al.* Stat3 regulates microtubules by antagonizing the depolymerization activity of stathmin
8. *J. Cell Biol.* **172**, 245-257 (2006).

343. Torres-Benito, L., Neher, M. F., Cano, R., Ruiz, R. & Tabares, L. SMN Requirement for Synaptic Vesicle, Active Zone and Microtubule Postnatal Organization in Motor Nerve Terminals
1. *PLoS. One.* **6**, e26164 (2011).

344. Rende, M. *et al.* Immunolocalization of ciliary neuronotrophic factor in adult rat sciatic nerve. *Glia* **5**, 25-32 (1992).

345. Yokogami, K., Wakisaka, S., Avruch, J. & Reeves, S. A. Serine phosphorylation and maximal activation of STAT3 during CNTF signaling is mediated by the rapamycin target mTOR
1. *Curr. Biol.* **10**, 47-50 (2000).

346. Ning, K. *et al.* PTEN depletion rescues axonal growth defect and improves survival in SMN-deficient motor neurons
3. *Hum. Mol. Genet.* **19**, 3159-3168 (2010).

347. Wu, K. Y. *et al.* Local translation of RhoA regulates growth cone collapse
2. *Nature* **436**, 1020-1024 (2005).

348. Cingolani, L. A. & Goda, Y. Actin in action: the interplay between the actin cytoskeleton and synaptic efficacy
4. *Nat. Rev. Neurosci.* **9**, 344-356 (2008).

349. Zhu, Q., Couillard-Despres, S. & Julien, J. P. Delayed maturation of regenerating myelinated axons in mice lacking neurofilaments
11. *Exp. Neurol.* **148**, 299-316 (1997).

350. Benowitz, L. I. & Routtenberg, A. GAP-43: an intrinsic determinant of neuronal development and plasticity
1. *Trends Neurosci.* **20**, 84-91 (1997).

351. Tsai, L. K. *et al.* IGF-1 delivery to the CNS attenuates motor neuron cell death but does not improve motor function in type III SMA mice
1. *Neurobiol. Dis.* (2011).

352. Duan, C., Liimatta, M. B. & Bottum, O. L. Insulin-like growth factor (IGF)-I regulates IGF-binding protein-5 gene expression through the phosphatidylinositol 3-kinase, protein kinase B/Akt, and p70 S6 kinase signaling pathway
1. *J. Biol. Chem.* **274**, 37147-37153 (1999).

353. Fleming, J. M., Leibowitz, B. J., Kerr, D. E. & Cohick, W. S. IGF-I differentially regulates IGF-binding protein expression in primary mammary fibroblasts and epithelial cells
3. *J. Endocrinol.* **186**, 165-178 (2005).

354. De, W. F. *et al.* The expression of the chemorepellent Semaphorin 3A is selectively induced in terminal Schwann cells of a subset of neuromuscular synapses that display limited anatomical plasticity and enhanced vulnerability in motor neuron disease. *Mol. Cell Neurosci.* **32**, 102-117 (2006).

355. Li, M., Sendtner, M. & Smith, A. Essential function of LIF receptor in motor neurons. *Nature* **378**, 724-727 (1995).

356. Jedrzejowska, M. *et al.* Unaffected patients with a homozygous absence of the SMN1 gene
3. *Eur. J. Hum. Genet.* **16**, 930-934 (2008).

357. Sendtner, M. Therapy development in spinal muscular atrophy
7. *Nat. Neurosci.* **13**, 795-799 (2010).

358. Hua, Y., Vickers, T. A., Baker, B. F., Bennett, C. F. & Krainer, A. R. Enhancement of SMN2 exon 7 inclusion by antisense oligonucleotides targeting the exon
3. *PLoS. Biol.* **5**, e73 (2007).

359. Passini, M. A. *et al.* CNS-targeted gene therapy improves survival and motor function in a mouse model of spinal muscular atrophy
8. *J. Clin. Invest* **120**, 1253-1264 (2010).

360. Zaiss, A. K. & Muruve, D. A. Immunity to adeno-associated virus vectors in animals and humans: a continued challenge
2. *Gene Ther.* **15**, 808-816 (2008).

361. Zhou, H. *et al.* Generation of induced pluripotent stem cells using recombinant proteins
9. *Cell Stem Cell* **4**, 381-384 (2009).

362. Marchetto, M. C. *et al.* A model for neural development and treatment of Rett syndrome using human induced pluripotent stem cells
3. *Cell* **143**, 527-539 (2010).

363. Takahashi, K. *et al.* Induction of pluripotent stem cells from adult human fibroblasts by defined factors
3. *Cell* **131**, 861-872 (2007).

364. Mitne-Neto, M. *et al.* Downregulation of VAPB expression in motor neurons derived from induced pluripotent stem cells of ALS8 patients
1. *Hum. Mol. Genet.* **20**, 3642-3652 (2011).

365. Ebert, A. D. *et al.* Induced pluripotent stem cells from a spinal muscular atrophy patient
21. *Nature* **457**, 277-280 (2009).

366. ALS CNTF Treatment Study [ACTS] Group. Phase II-III double blind, placebo-controlled clinical trial of subcutanleous administration od recombinant human ciliary neurotrophic factor (rHCNTF) in Amyotrophic Lateral Sclerosis. Neurology 45(suppl 4), A448. 1995.
Ref Type: Abstract

367. Dittrich, F., Thoenen, H. & Sendtner, M. Ciliary neurotrophic factor: Pharmakokinetics and acute phase response. *Ann. Neurol.* **35**, 151-163 (1994).

368. Azzouz, M. Gene Therapy for ALS: progress and prospects. *Biochim. Biophys. Acta* **1762**, 1122-1127 (2006).

369. Polydefkis, M., Griffin, J. W. & McArthur, J. New insights into diabetic polyneuropathy. *JAMA* **290**, 1371-1376 (2003).

370. Strotmeyer, E. S. *et al.* The relationship of reduced peripheral nerve function and diabetes with physical performance in older white and black adults: the Health, Aging, and Body Composition (Health ABC) study. *Diabetes Care* **31**, 1767-1772 (2008).

371. Lobsiger, C. S. *et al.* Schwann cells expressing dismutase active mutant SOD1 unexpectedly slow disease progression in ALS mice
1. *Proc. Natl. Acad. Sci. U. S. A* **106**, 4465-4470 (2009).

372. Vincent, A. M., Russell, J. W., Low, P. & Feldman, E. L. Oxidative stress in the pathogenesis of diabetic neuropathy. *Endocr. Rev.* **25**, 612-628 (2004).

373. Fleming, J. M., Brandimarto, J. A. & Cohick, W. S. The mitogen-activated protein kinase pathway tonically inhibits both basal and IGF-I-stimulated IGF-binding protein-5 production in mammary epithelial cells
1. *J. Endocrinol.* **194**, 349-359 (2007).

374. Zeslawski, W. *et al.* The interaction of insulin-like growth factor-I with the N-terminal domain of IGFBP-5. *EMBO J.* **20**, 3638-3644 (2001).

375. Windebank, A. J., Sorenson, E. J., Civil, R. & O'Brien, P. C. Role of insulin-like growth factor-I in the treatment of painful small fiber predominant neuropathy
1. *J. Peripher. Nerv. Syst.* **9**, 183-189 (2004).

6 Appendix

6.1 List of Figures

6.2 List of Tables

6.3 List of Abbreviations

AAV	Adeno-associated virus
ACh	Acetylcholine
AChE	Acetylcholinesterase
AChR	Acetylcholine receptor
ALS	Amyotrophic lateral sclerosis
AON	Antisense oligonucleotide
BNDF	Brain-derived neurotrophic factor
CaM kinases	Ca^{2+}/calmodulin dependent protein kinase II
Cav2.2	Calcium channels
CB	Cajal body
CIDP	Chronic inflammatory demyelinating polyradiculoneuropathy
CMAP	Compound motor action potential
CNS	Central nervous system
CNTF	Ciliary neurotrophic factor
Cre	Cre recombinase
CSF	Cerebrospinal fluid
CT-1	Cardiotrophin-1
DNA	Desoxyribonucleic acid
DCN	Deep cerebellar nucleus
DMD	Duchenne muscular dystrophy
DNP	Diabetic neuropathy
dNTP	Desoxyribonucleotriphosphate
E	Embryonic day
e.g.	Exempli gratia
ECM	Extracellular matrix
EMG	Electromyography
Erk	Extracellular signal-regulated kinase
ESE	Exonic splicing enhancer
ESS	Exonic splicing silencer
FL	Full length
GAP-43	Growth associated protein 43
GBS	Guillain-Barré-Syndrom

GDNF	Glial-derived neurotrophic factor
Gems	Gemini of coiled bodies
GPI	Glycosyl-phosphatidylinositol
HBSS	Hank's balanced salt solution
HE	Haemalum eosin
hiPS	Human induced pluripotent stem
hnRNP	Heterogenous ribonucleoproteins
HSPG	Heparin sulfate proteoglycans
IGF-1	Insulin-like growth factor 1
IGF-1R	Insulin-like growth factor receptor 1
IGFBP-5	Insulin-like growth factor binding protein 5
ISE	Intronic splicing enhancer
ISS	Intronic splicing silencer
JAK	Janus kinase
kb	Kilobases
kDa	KiloDalton
LIF	Leukaemia inhibitory factor
MAPK	Mitogen-activated protein kinase
MND	Motoneuron diseases
mTOR	Mammalian target of rapamycin
NAIP	Neuronal apoptosis inhibitory protein
NCV	Nerve conduction velocity
NF-L	Neurofilament-light
NGF	Nerve growth factor
NMJ	Neuromuscular junction
NRG1-III	Neuregulin 1-Type III
NT-3	Neurotrophin-3
P	Postnatal day
PBS	Phosphate buffered saline
PCR	Polymerase chain reaction
PDGF-BB	Platelet derived growth factor-BB
PFA	Paraformaldehyde
PI-3K	Phosphoinositide 3-kinase
pICln–PRMT5	Protein arginine methyltransferase 5

PNS	Peripheral nervous system
PTEN	Phosphatase and tensin homolog
ROCK	RhoA kinase
RT-PCR	Reverse transcriptase polymerase chain reaction
SDS	Sodium dodecyl sulfate
HSP	Hereditary spastic paraplegia
SMA	Spinal muscular atrophy
SMN	Survival of motoneuron gene
SMUAP	Single motor unit action potentials
STAT-3	Signal Transducer and Activator of Transcription
STZ	Streptozotocin
TrkB	Tropomyosin related kinase B
U snRNP	Small nuclear ribonucleoproteins
UNRIP	UNR-interacting protein
UTR	Untranslated region
°C	Degrees Celsius
µm	Micrometer

6.4 Affidavit/Eidesstattliche Erklärung

Affidavit

I hereby declare that my thesis entitled **Effects of the neurotrophic factors CNTF and IGF-1 in mouse models for spinal muscular atrophy and diabetic neuropathy** is the result of my own work. I did not receive any help or support from commercial consultants. All sources and / or materials applied are listed and specified in the thesis.

Furthermore, I verify that this thesis has not yet been submitted as part of another examination process neither in identical nor in similar form.

Würzburg……
Date Signature

Eidesstattliche Erklärung

Hiermit erkläre ich an Eides statt, die Dissertation **Effekte der neurotrophen Faktoren CNTF und IGF-1 in Mausmodellen für spinale Muskelatrophie und diabetische Neuropathie** eigenständig, d.h. insbesondere selbstständig und ohne Hilfe eines kommerziellen Promotionsberaters, angefertigt und keine anderen als die von mir angegebenen Quellen und Hilfsmittel verwendet zu haben.

Ich erkläre außerdem, dass die Dissertation weder in gleicher noch in ähnlicher Form bereits in einem anderen Prüfungsverfahren vorgelegen hat.

Würzburg……
Datum Unterschrift

6.5 Publication List

Simon, C.M. et al., *Dysregulated Expression of IGFBP-5 Causes Axonal Degeneration and Motoneuron Cell Death in Diabetic Neuropathy* (manuscript under review)

Simon, C.M., Jablonka, S., Ruiz, R., Tabares, L. and Sendtner, M., *Ciliary Neurotrophic Factor-induced Sprouting Preserves Motor Function in a Mouse Model of mild Spinal Muscular Atrophy*, Hum. Mol. Genet., 19 (2010) 973-986.

Fischer, M., Pereira, P.M., Holtmann, B., **Simon, C.M.**, Hanauer, A., Heisenberg, M. and Sendtner, M., *P90 Ribosomal s6 Kinase 2 Negatively Regulates Axon Growth in Motoneurons*, Mol. Cell Neurosci., 42 (2009) 134-141

6.6 Conferences

"**Dysregulated Expression of IGFBP-5 Causes Axonal Degeneration and Motoneuron Cell Death in Diabetic Neuropathy"**
Poster Presentation at the Society for Neuroscience (SFN) Annual Meeting, November 13 – 17 2010, San Diego, California, USA

"Ciliary Neurotrophic Factor-induced Sprouting Preserves Motor Function in a Mouse Model of mild Spinal Muscular Atrophy"
Poster Presentation at the EMBO|EMBL Symposium: Structure and Function of Neural Circuits, September 5 – 8 2010 at EMBL, Heidelberg, Germany

"Ciliary Neurotrophic Factor-induced Sprouting Preserves Motor Function in a Mouse Model of mild Spinal Muscular Atrophy"
Poster Presentation at the Society for Neuroscience (SFN) Annual Meeting, October 17 – 21 2009, Chicago, Illinois, USA

"Increased Single Motor Unit Action Potentials by Enhanced Axonal Sprouting as a Compensatory Mechanism in a Mouse Model for Spinal Muscular Atrophy Type III"
Poster Presentation at the Federation of European Neuroscience Society (FENS), July 12 – 16 2008, Geneva, Switzerland

Danksagung

Mein besonderer Dank gilt an erster Stelle Herrn Prof. Dr. Michael Sendtner, der mir ermöglichte meine Doktorarbeit an dem Institut für klinische Neurobiologie zu absolvieren. Durch eine hervorragende Betreuung, hochinteressante Seminare, wissenschaftliche Diskussionen, Teilnahme an internationalen Kongressen und eine Laborausstattung die seinesgleichen sucht, gewährleistete er eine erfolgreiche Promotion. Ich durfte soviel von Ihnen lernen. Vielen Dank!

Vielen Dank auch an Herrn Professor Dr. Erich Buchner und an Herrn Professor Dr. Rudolf Martini für die Übernahme der Zweitgutachter. Ich erinnere mich noch sehr gut daran, als ich das erste Mal 2004 in Ihren Vorlesungen saß und auf den Geschmack der Neurobiologie gebracht wurde. Herr Buchner ermöglichte mir meine ersten unvergesslichen Laborerfahrungen 2005 in Konrad Zinsmaier‘s Arbeitsgruppe in Tuscon, Arizona. Auch Herr Martini trug maßgeblich dazu bei, dass ich mich für den Weg der klinische Neurobiologie entschieden habe. Dafür Danke ich Ihnen sehr.

Während meiner Promotion habe ich so viele KollegInnen kennenlernen dürfen und einige sind zu sehr guten Freunden geworden. Vorab ein Dankeschön an alle, die mich in den letzten Jahren begleitet haben.

Ein besonderer Dank geht an die „Familie“ der Kopfklinik. Durch sie war das Arbeiten immer ein Vergnügen.

Dirk „der große Bruder“ war seit der ersten Sekunde mein Wegbegleiter und immer der wichtigste Ansprechpartner. Er nahm sich bei jeder Frage, war sie auch noch so trivial, die Zeit und half mir bei der Planung und Ausführung vieler Experimente. Dein sorgfältiges, gewissenhaftes und sauberes Arbeiten mit allen Kontrollen nahm ich mir stets als Vorbild. Neben der beruflichen Zusammenarbeit, bist du auch ein sehr guter Freund geworden. Der Aufenthalt in Chicago und die ewige Tabelle sind nur zwei Höhepunkte einer tollen Zeit. Ich hätte nie gedacht, dass ich mit einem FC-B-Fan so gut befreundet sein könnte. Danke Dir!

Nicole „die kleine Schwester“ ist das gute Elflein im Labor und verhindert mit ihrer Organisation das absolute Chaos. Sie ist nach meinem Abgang die Dienstälteste im

Kopfkliniklabor. Auch Sie ist eine gute Freundin geworden. Vielen Dank dafür und dass ich bei Johannes und Dir des Öfteren einkehren durfte und eure Schoki geplündert habe. In diesem Zusammenhang natürlich auch ein großes Dankeschön an das ehemalige Labormitglied und Tennis Newcomer of the Year Johannes.

Benni ist der jüngere Bruder im Kopfklinik-Team. Ich habe noch nie einen facettenreicheren Menschen getroffen wie dich. Bei Dir weiß man nie was als Nächstes passiert. Wir zwei haben während der letzten zwei Jahre das Labor geteilt, aber es war immer sehr harmonisch und kam nie zu Platzproblemen. Auch Du bist ein guter Freund geworden. Gracias!

Frank ist der Zwillingsbruder, den ich nie hatte. Wir teilen beide die Leidenschaft der Luftfart. Mit deiner ausgeglichenen Art bringst du die perfekte Balance in die Gruppe. Als lokale Estenfelder Berühmtheit hast du immer einen Hauch von Hollywood ins Labor gebracht. Ein Danke reicht bei dir nicht aus, eher ein MÖLDERS!

Jan, unser riesen Nesthäkchen der Familie, ist zwar erst seit acht Monaten bei uns, aber nicht mehr wegzudenken. Nach einer Woche hat man bereits gesehen, dass du als Mediziner Forschung im Blut hast. Außerhalb des Labors bist du auch eine echte Bereicherung und dabei spreche ich nicht nur von ASTRA. Danke, Digga!

Sibylle ist die große Schwester, die alles in der Kopfklinik überschaut und leitet. Du hattest seit Beginn meiner Diplomarbeit immer ein offenes Ohr. Bei forschungsrelevanten oder nicht wissenschaftlichen Problemen hattest du immer einen guten Ratschlag. Danke.

Natürlich darf hier Katrin nicht fehlen. Du hast mir viele Techniken beigebracht und warst meine erste Laborkollegin. Du hast hier organisatorisch alles zu 100% im Griff gehabt und ich freu mich, wenn du ab Januar wieder da bist. Danke.

Selbstverständlich sind mir auch alle im MSZ sehr ans Herz gewachsen.Trotz der räumlichen Trennung war es immer sehr schön, lustig und informativ, wenn ich euch besucht habe. Leider kann ich nicht jeden Einzelnen hier nennen. Besonders möchte ich aber Carsten danken, der mit seiner ausgeglichenen, ruhigen Art mir immer wertvolle wissenschaftliche Tips gegeben hat. Wir haben in verschiedenen Projekten zusammengearbeitet und ich habe viel durch deine Expertise lernen drüfen. Außerdem möchte ich noch Bu und Nici erwähnen.

Wir haben zusammen die komplette Doktorarbeit zusammen durchlebt und unser Trip nach München war legendär. An alle im MSZ vielen Dank.

Auch vielen Dank an Viktor, Regine, Helga, Herrn Horschig und alle Mitarbeiter des Tierstalls. Ihr durftet hautnah miterleben wie ich versucht habe Mäuse per Luftweg nach Spanien zu transportieren. Ohne euch würde kein Experiment laufen!

Urveen und Judita möchte ich auch danken. Ihr habt mich immer super unterstüzt, wenn es um Formulare, Reiseanträge und sonstigen Papierkrieg ging.

Außerdem möchte ich einigen Weggefährten in der Kopfklinik außerhalb unserer Arbeitsgruppe danken: Janos, Dennis, Bene und Topper. Besonders von Dir, Janos, habe ich viele Präparationstricks lernen dürfen. Danke!

Zudem möchte ich Herrn Professor Dr. Klaus Toyka danken. Er gab mir stets wertvolle Tips für meine zukünftige Karriere und zeigte mir, wie faszinierend Elektrophysiologie sein kann.

Besonders möchte ich mich bei meinen zwei besten Freunden Markus und Dikembe bedanken. Markus, deine Arbeitsmoral hat mich begeistert und es war immer motivierend zu wissen, dass auch zu später Stunde in der benachbarten Frauenklinik noch hart gearbeitet wurde. Du hast dir immer Zeit für zahlreiche wissenschaftliche Diskussionen genommen. Außerhalb der Arbeit konnten wir uns durch emotionsgeladene Tennismatches von der Arbeit ablenken. Desweiteren möchte ich mich bei Dikembe bedanken, der eine wirtschaftliche Dissertation bald abschließen wird. Die Telefonate und Besuche in München waren immer Wahnsinn und haben mir neue Kraft für das Labor gegeben. Danke, Jungs!!!

Ausdrücklich möchte ich mich bei meinen Eltern, Inge und Jürgen Simon, bedanken, die mich immer unterstützt und motiviert haben. Egal wie groß die Zweifel und Sorgen auch waren, Ihr habt mir sie alle genommen. Tausend Dank!

Zum Schluss möchte ich noch Dir, Jenny, danken. Du bist das Beste was mir je passiert ist. Obwohl wir seit zwei Jahren durch 6631 Kilometer getrennt sind, wird unsere Liebe immer stärker. Du hast mir immer Mut gemacht und an mich geglaubt. Die größte Motivation für diese Arbeit war, dass ich anschließend wieder bei dir sein werde.